AIR MOVEMENT & VENTILATION CONTROL WITHIN BUILDINGS

12th AIVC Conference, Ottawa, Canada
24-27 September, 1991

POSTER 29

A New Passive Tracer Gas Technique for Ventilation Measurements

Hans Stymne, Anita Eliasson

The National Swedish Institute for Building Research
P.O Box 785
S-801 29 GÄVLE
Sweden

Synopsis

A new passive tracer gas method for ventilation measurements is described. The method utilizes passive tracer gas release from a liquid perfluorocarbon compound contained in a glass vial, equipped with a teflon membrane. Air sampling is also done passively by diffusion through a glass tube containing activated carbon. Quantitative analysis of trapped tracer compound is performed by solvent extraction and gas chromatographic separation using a liquid injection technique. Separation is done with a two-column system and quantitative analysis with an electron capture detector. The paper describes the method and results from the calibration procedure. A short description of a simplified calculation scheme and field measurement technique is also presented.

List of symbols

$\bar{c}$ time averaged tracer concentration [g m^{-3}]

$\dot{m}$ tracer gas release rate [g h^{-1}]

$\dot{m}_A$ release rate of tracer A [g h^{-1}]

m_A totally released amount of tracer [g]

M adsorbed amount of tracer in a sampler [g]

T sampling time [h]

$\tilde{q}$ estimated total effective air flow rate [m^3h^{-1}]

$\tilde{q}_A$ estimated flow rate, calculated from $\frac{\kappa_A}{\beta_A}$ [m^3h^{-1}]

$\tilde{q}_{12}$ estimated flow rate, calculated from $\frac{\kappa_j}{\beta_{1j}}$, where tracer **j** is emitted in zone 2 [m^3h^{-1}]

q_{ij} flow rate of air entering zone **i** from zone **j** [m^3h^{-1}]

α fraction of total flow rate

β_A fraction of the totally released amount of tracer A, that is adsorbed in a sampler

β_{1A} fraction of the totally released amount of tracer A, that is adsorbed in a sampler positioned in zone 1

κ_A equivalent air sampling rate for tracer A [m^3h^{-1}]

1 Background

In the last few years, the interest in the passive tracer gas technique for measuring ventilation flow rates in buildings has grown rapidly. The underlying principles for this technique, which was originally developed at the Brookhaven National Laboratories have been described elsewhere (Dietz & Cote 1982, Dietz *et al.* 1986). Today, there are a few laboratories performing the necessary chemical analysis. The possibilities and limitations of this technique have recently been discussed by several authors (D'Ottavio *et al.* 1988, Dietz 1988, Sherman 1989, Sandberg & Stymne 1989). A state-of-the-art report has recently been published (Säteri (ed.) 1991). However, there are still relatively few field measurements being reported where the passive tracer gas technique is used.

1.1 General principles

The common features of a passive tracer gas technique are the following.

1.1.1 The tracer compound is contained in liquid form in a small closed container, part or whole of which is slightly permeable to the compound. The tracer compound must possess the following characteristics:

- have negligible adsorption by materials occurring in buildings
- be completely harmless to human health at concentrations well above those which might appear inside a building during measurement
- have a high enough volatility to evaporate at the required rate
- not normally appear in indoor air
- be detectable at extremely low concentrations with a GC detector
- be commercially available at a relatively low price

Many fluorinated hydrocarbons of moderate molecular weight fulfill all of the above criteria. Thus, wholly fluorinated (perfluorinated) hydrocarbons have been extensively used. Accordingly, the method is often referred to as the PFT-method (PerFluorocarbon Tracer method).

1.1.2 The sampling of air which contains tracer is done passively using a diffusion tube, containing an adsorbent, which is not easily saturated with the main constituents of the air.

The sampling tube has an opening of accurately reproducible area and length. This may be accomplished with a capillary tube opening. Ideally, the net transport rate of tracer in the air through the opening is diffusion controlled. In this case the net rate of tracer flow is proportional to the area of the opening and to the tracer concentration difference between the air outside the tube and at the surface of the adsorbent. It is also inversely proportional to the distance between the opening and the adsorbant surface. The equivalent net sampling rate of air containing a tracer can be expressed in $g/h \cdot (g/m^3)^{-1}$ which has the dimension $m^3 h^{-1}$. Thus the sampling rate of air can conveniently be expressed in volumetric flow rate units. A typical flow rate is 10 $(ml),h^{-1}$. The sampling flow rates differ for different compounds.

Two main types of adsorbent can be used. One type is based on a heat resistant porous polymer, from which the trapped compounds are preferably desorbed by heat. The other type is based on activated carbon, from which the trapped compounds are either thermally desorbed or extracted by a liquid solvent.

1.1.3 Quantitative analysis of the amount of adsorbed tracer gas.
After sampling for a suitable length of time, the adsorption tubes are sealed and sent to a laboratory for analysis. The analysis is performed using gas chromatography (GC), though other methods might also be suitable.

Depending on the the type of adsorbent used in the sampling, either thermal desorption or liquid extraction is used. The thermal desorption technique has the advantage that 100 % of the trapped tracer is injected into the GC. When using liquid extraction, usually less than 1 % is injected. Thus the thermal desorption technique gives a much higher sensitivity. However, with the types and amounts of tracer gas that are commonly used, sensitivity is not the crucial problem. If sensitivity criteria permit the use of the liquid extraction technique, there are certain advantages. The main ones being that repeated analysis can be performed on the same sample and that standard samples can easily be prepared by dilution.

The detector commonly employed for quantitative analysis of a PFT-compound is the electron capture detector (ECD). With this type of detector, the detectability limit is in the order of 10^{-15}g. Thus an injected amount of 10^{-13}g is clearly enough to make a quantitative analysis. As shown below, this is less than the amount usually injected after liquid extraction.

A typical sampling rate with a capillary opening is 10^{-5} m^3h^{-1}. With a tracer concentration in the air of 0.12 (μg), m^{-3}, the amount of tracer adsorbed in 14 days will be approximately 0.4 ng, which is more than 1000 times the amount needed for a good quantitative analysis. The 0.12 (μg), m^{-3} tracer concentration level, is the level achieved with a tracer release rate of 200 ng, min^{-1} and a diluting ventilation air flow rate of 100 m^3h^{-1}.

Separation from other substances trapped in the adsorption medium and contamination from the extraction solvent, the analysing equipment or the trapping compound itself, are more critical issues than sensitivity.

2 Description of the method

The passive tracer gas method described in this paper (the **SIB** method) has been developed at the **S**wedish **I**nstitute for **B**uilding Research. The basic principles are the same as for the BNL method (Dietz & Cote 1982), while the analysis technique was inspired by the method used by Mailahn *et al.* (1987, 1989). The different steps of the method, i.e. tracer gas release, air sampling and analysis are described below.

2.1 Tracer gas release

At present two different perfluorocarbon compounds can be used on a routine basis. These are hexafluoro-benzene (PB) and octafluoro-methylbenzene (PMB). A tracer compound is contained in an ordinary 2 ml glass vial, sealed with a 1 mm thick teflon membrane. The membrane is kept in place with a crimped on aluminium cap with a 5 mm central opening (fig. 1a). The tracer diffusion rate is determined by intermittently weighing the vial.

2.2 Air sampling

The diffusion samplers are made from standard charcoal sampling tubes (SKC Anasorb) which are cut 17 mm above the level of the charcoal bed (fig. 1b). The inside diameter is 4.3 mm and the diffusion length 17±1 mm. Before and after sampling the tube is protected with a plastic cap. The tubes contain a sorbent layer with appr. 100 mg activated carbon and a backup layer with appr. 50 mg.

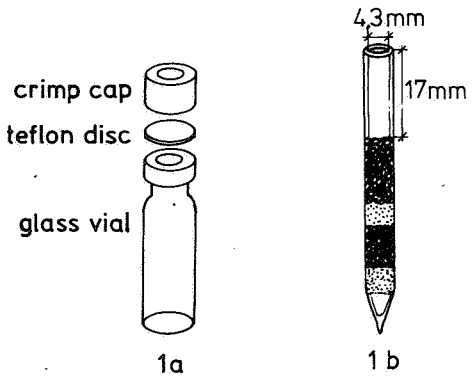


Figure 1a *Tracer gas source arrangement*

Figure 1b *Diffusion sampler arrangement. The glass tube is a standard commercial charcoal sampling tube, which is cut 17 mm above the charcoal bed.*

2.3 Analysis

2.3.1 Desorption

The desorption is done with toluene (Aristar 99.5 %). Prior to use this is further purified from low boiling contaminants by fractionated distillation at a reflux ratio of appr. 100:1. The distillate (1/3) is discarded and the residue is used as the extraction solvent. For extraction, 1 ml of the purified toluene is pipetted into the vial, to which the activated carbon has been transferred. To speed up the extraction the vial is vibrated for 45 minutes in a developing vibrator.

2.3.2 Separation

The analysing equipment is described in more detail below under the heading "GC EQUIPMENT".

1 µl of the toluene solution is injected using a direct injection technique without split, into a precolumn (8 m x 0.53 mm Carbowax fused silica). The helium carrier flow in the precolumn is 10 ml/min. The injector temperature is 140°C and the oven temperature is 60°C, isothermal. An effluent fraction from the precolumn containing the tracers (see fig. 2) is directed to a cold trap (a 0.2 m methyl silicone capillary column, cooled with liquid carbon dioxide). After collection, the trap is flash heated to 100-140°C to inject the trapped compounds into the analytical column (a 25 m x 0.25 mm fused silica column coated with methyl silicone). When reinjection to the analytical column begins, simultaneous backflushing of the precolumn occurs. The flow of helium carrier gas through the analytical column is 1.45 ml/min. When the compounds of interest have left the analytical column, the temperature is raised to 140°C during 5 minutes to clean the columns. Prior to the next injection, the injector compartment is flushed with He for 3 min. The analytical column is equipped with an EC detector.

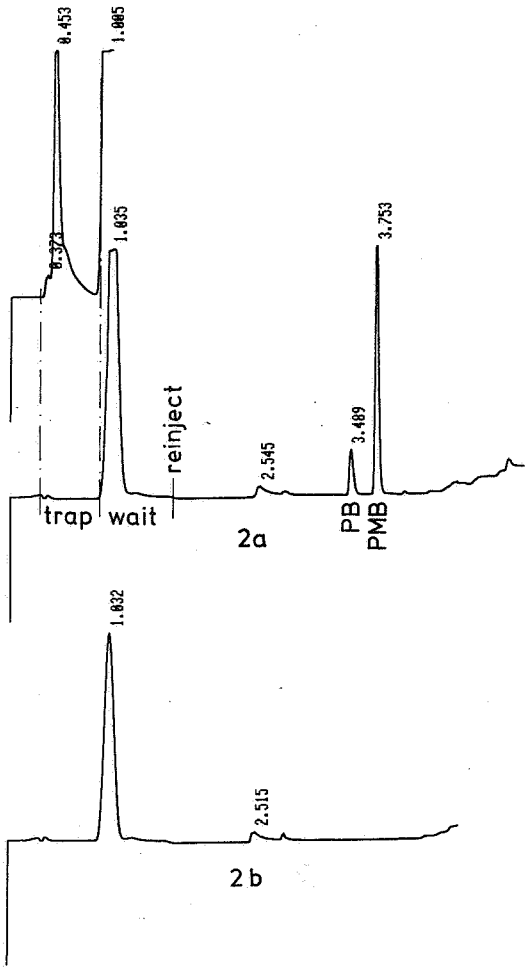


Figure 2a *Chromatogram recorded with an electron capture detector showing the separation of $2.38 \cdot 10^{-12}$ g hexafluorobenzene (PB) and $2.43 \cdot 10^{-12}$ g octafluorotoluene (PMB) in 1 µl toluene solution. The fraction trapped from the precolumn (see insert) is reinjected at 1.6 min into the analytical column.*

2b *Corresponding chromatogram of pure solvent (without tracer compounds), using the same fraction cut as in fig. 2a.*

2.4 GC-equipment

2.4.1 Gas chromatograph: Hewlett-Packard 5890A

Detectors: Electron capture detector (ECD)

Injector: Split/splitless. Autoinjection without split.

2.4.2 Columns:

Precolumn - WCOT fused silica 8 m x 0.53 mm, Chrompack CP- WAX52CB, coating thickness=2 μm

Analytical column - WCOT fused silica 25 m x 0.25 mm, Chrompack CP-SIL 8CB, coating thickness =1.2 μm

2.4.2 Column switching system: Chrompack MUSIC , which essentially is a computerized "Dean" switched system equipped with a cooled trap between the two columns.

2.5 Calibration and quality assurance

The different steps of the analysis process have been tested in the laboratory for reproducibility and accuracy.

The tracer release rate from the sources described earlier have been tested in the laboratory by intermittently weighing the bottles. After 4 weeks of equilibration the release rate from individual sources show a good constancy over time. Unfortunately, there is a variation between different sources which makes individual calibration of sources necessary. The release rate is strongly dependant on temperature - increasing approximately 5 % per degree Kelvin. An alternative (but appreciably more expensive) type of source, based on capillary diffusion shows instanteneous equilibration and a much less variation (S. D. < 3 %) in release rates between individuals.

The sampling rate of the diffusive sampling tubes has been tested in a space with controlled ventilation flow rate. A typical example is given in fig. 3. The sampling rate is shown to be constant with time. The sampling rate is preferentially expressed in cubic meters of sampled air per hour (m^3/h).

This **equivalent air sampling rate** (κ) is dependant on the diffusion coefficient of the tracer in air and is therefore different for different tracer compounds. For our design of diffusive samplers κ_{PB} is found to be $18.5 \cdot 10^{-6}$ m^3/h and κ_{PMB} = 16.5 m^3/h (a small correction, due to the fact that the recovery of the extraction is slightly less than 100 % is introduced in the κ_{PB} - see below).

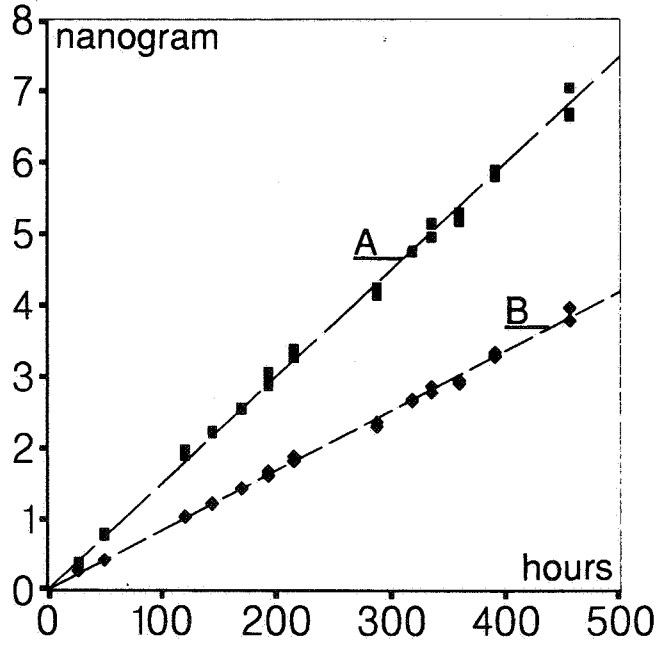


Figure 3 *Result from a diffusion sampling rate test under controlled ventilation rate. Analyzed amount of adsorbed tracer compounds are displayed for duplicate injections of extracts from two sampling tubes per occasion*

The **distribution coefficients** between activated carbon and the extraction solvent (toluene) have been studied. It was found that the presence of activated carbon did not affect the concentration of PMB in the liquid phase. PB, however, was adsorbed slightly stronger than the solvent on the solid phase - yielding only a 96 % concentration recovery in the liquid phase. To avoid computational complications, this deviation from 100 % recovery is not explicitly corrected for. Instead, it is implicitly compensated for, by the use of a lower value of the equivalent sampling rate κ_{PB} than would otherwise have been found.

2.6 Quantitative analysis

Injection to the GC is done automatically from a sampling tray with a capacity of 100 sample vials.

The quantitative analysis of the tracer compounds is performed by the use of the integrated area under the ECD-signals of the compounds after GC-separation as described above.

It is shown (fig. 4) that the integrated signal area is directly proportional to the amount injected to the gas chromatograph.

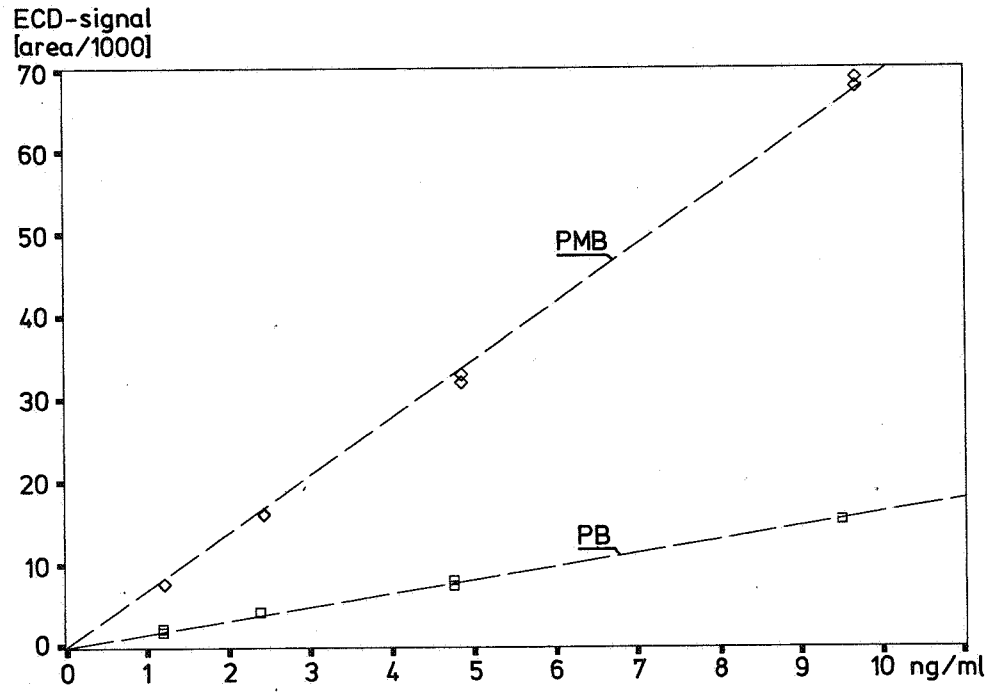


Figure 4 *Integrated ECD-signal of PB and PMB peaks for different concentrations in toluene solution. The injected amount is 1 µl*

The proportionality factors are updated every fourth sample run, by injecting an external standard sample, with accurately known concentrations of PB and PMB in toluene. A new standard solution is made daily by dilution (1:20) from a stock solution. The external standard usually employed has a concentration of appr. 10 ng/ml of PB and 5 ng/ml of PMB.

The standard deviation of the quantitative analysis of repeated injections from the same sample amounts to 1 %.

The standard deviation of the quantitative analysis of the amounts of tracers desorbed from different samplers, which are exposed under equivalent conditions, amounts to 5 %.

Capped samplers can be kept several weeks in room temperature without desorption or adsorption of tracers. However, capped samplers and tracer gas sources should not be kept together in a badly ventilated space, because adsorption has been shown to occur in heavily contaminated environments.

3 Calculation procedure and field measurement technique

The amount (M) of a tracer gas adsorbed in a diffusive charcoal sampling tube, which is exposed during a time period T, in an environment with a time - averaged tracer concentration of $\bar{c}$ is given by

$$M = \kappa \cdot \bar{c} \cdot T \qquad (1)$$

During the same period the amount (m) of tracer released from a tracer gas source in the space is given by:

$$m = \dot{m}T \tag{2}$$

where $\dot{m}$ is the constant emission strength of the source.

1 and 2 yield

$$\beta = \frac{M}{m} = \frac{\kappa \cdot \bar{c}}{\dot{m}} \tag{3}$$

where β is the fraction of the totally emitted amount of tracer in the space, which is adsorbed on a sampler during the exposure time.

Assuming a perfect mixing ventilation system with a constant ventilation flow rate of q (m^3/h), mass conservation of the tracer yields

$$q \cdot \bar{c} = \dot{m} \tag{4}$$

3 and 4 yield

$$q = \frac{\kappa}{\beta} = \frac{\kappa}{(\frac{M}{m})} \tag{5}$$

Thus, in a perfect mixing ventilation system with a constant ventilation flow rate, the flow rate q can easily be calculated from the quotient between the sampling rate (κ) and the sampled fraction β.

The name "effective" ventilation flow rate has earlier been adopted for the flow rate determined this way, even if the ventilation rate is not constant in time (Sherman & Wilson 1986). The effective flow rate is usually smaller than the true time averaged ventilation flow rate, when variation occurs.

The notation $\tilde{q}_A$ is used here to denote the flow, estimated from a tracer gas experiment utilizing tracer of type A, according to equation (5) above, even if the flow varies in time or the mixing is non-uniform.

$$\tilde{q}_A = \frac{\kappa_A}{\beta_A} \tag{6}$$

Therefore, $\tilde{q}_A$ does not usually correspond to the time-averaged total ventilation flow rate.

3.1 Incomplete mixing

A complication which nearly always occurs in real systems is incomplete mixing.

The mathematical tool for dealing with tracer gas experiments in non-uniformly mixed system, is the multicell theory.

In this theory - the space is subdivided into a number of cells (N), each of which is assumed to be uniformly mixed. Mass balances are set up for each cell separately.

The theory leads to a set of N simultaneous equation systems, which can only be solved completely, by an experiment using as many different tracer gases as there are cells.

It is out of the scope of this paper to go any further into the multicell theory. This is discussed in several other papers (e.g. Sandberg 1984).

For field measurements, it is normally out of question to perform complete multicell experiments. Certain simplifications can be made, especially since limited information is often sufficient. A couple of such simplifications, which have been shown to yield satisfactory results, are given below.

3.1.1 One zone approximation

Often the only information requested is the total ventilation rate to the space. To solve the mass balance equation in this case, the only information we need is the concentration of tracer in the extracted air. In mechanically ventilated buildings and in naturally ventilated buildings, which are not too leaky, there are dedicated air extract points. If there is only one extract air terminal, a tracer gas sampler should be positioned in the vicinity of this terminal. It does not matter how the air flows in the building, or how tracer sources are distributed. All entering air and tracer must pass the air terminal.

However, even in small apartments there are normally at least two air terminals - one in the kitchen and one in the bathroom.

In the following we assume that there are two extract points (1 and 2) and that samplers have been positioned close to each of these two points. Only one tracer gas type is employed, who's concentration is C_1 and C_2 respectively at the two extract points.

We further assume that the extract flow rates at the two terminals are respectively $q/2(1+\alpha)$ and $q/2(1-\alpha)$.

where q is the total air flow rate and α can take a value between -1 and +1.

The mass balance equation gives:

$$\begin{aligned} \dot{m} &= q/2\cdot[(1+\alpha)C_1 + (1-\alpha)C_2] \\ &= q/2\cdot[C_1 + C_2 + \alpha(C_1 - C_2)] \end{aligned} \qquad (7)$$

or

$$\frac{\dot{m}\cdot 2}{(C_1 + C_2)} = q[1 + \alpha\cdot\frac{(C_1 - C_2)}{(C_1 + C_2)}] \qquad (8a)$$

In terms of the notations introduced above eq. (8) can be written:

$$\tilde{q} = \frac{2}{\frac{1}{\tilde{q}_{1A}} + \frac{1}{\tilde{q}_{2A}}} = q[1 + \alpha \cdot \frac{\frac{1}{\tilde{q}_{1A}} - \frac{1}{\tilde{q}_{2A}}}{\frac{1}{\tilde{q}_{1A}} + \frac{1}{\tilde{q}_{2A}}}] \qquad (8b)$$

$$\tilde{q} = q + q \cdot \alpha \frac{\frac{1}{\tilde{q}_{1A}} - \frac{1}{\tilde{q}_{2A}}}{\frac{1}{\tilde{q}_{1A}} + \frac{1}{\tilde{q}_{2A}}}; \quad \frac{\tilde{q} - q}{q} = \alpha \frac{\frac{1}{\tilde{q}_{1A}} - \frac{1}{\tilde{q}_{2A}}}{\frac{1}{\tilde{q}_{1A}} + \frac{1}{\tilde{q}_{2A}}} \qquad (9)$$

where the flow rate estimate $\tilde{q}$ is based on the average tracer concentration at the two extract terminals.

From this formula the relative error in the estimate due to uneven tracer distribution can be calculated.

The worst estimate will appear when $\alpha = \pm 1$ i.e. when all air leaves at only one terminal.

The maximum relative error will be $\frac{|C_1 - C_2|}{C_1 + C_2} = \frac{\left|\frac{1}{\tilde{q}_{1A}} - \frac{1}{\tilde{q}_{2A}}\right|}{\frac{1}{\tilde{q}_{1A}} + \frac{1}{\tilde{q}_{2A}}}$ in this case.

Often, it is simple to choose the position of the tracer gas source(s) so that the concentrations are approximately equal at both extract points. Of course one should avoid placing a source closer to one sampler than the other. If the one zone approximation was inadequate, one at least gets an indication of the maximum error introduced.

3.1.2 Two zone approximation

It is not unusual that the extract points are far from each other, and that an appreciable amount of outdoor air is introduced between the extract points. In this case it is often not evident where to place the tracer source or sources so that the tracer concentration can be expected to be similar at the two extracts points.

In this case it is better to divide the space into two zones, each of which contains one main air extract area. It is not necessary to know the zone boundaries or assume uniform mixing within each zone. The two types (A and B) of tracer sources should be positioned one in each zone (1 and 2), preferably in rooms with the most supply air. The samplers shall be positioned in the vicinity of the extract points. The extract flow rates at the two extract points are assumed to be q_1 and q_2 respectively.

The mass balance equations are

$$C_{1A} \cdot q_1 + C_{2A} \cdot q_2 = \dot{m}_A$$
$$C_{1B} \cdot q_2 + C_{2B} \cdot q_2 = \dot{m}_B \qquad (10)$$

where C_{1A} is the concentration of tracer A in the extract area of zone 1 and q_1 is the flow rate of extract air zone 1. The other notations follow the same rule. In terms of the time integrated tracer amounts introduced earlier, this equation system can be written:

$$\frac{\beta_{1A}}{\kappa_A} \cdot q_1 + \frac{\beta_{2A}}{\kappa_A} \cdot q_2 = 1 \quad ; \quad \frac{q_1}{\tilde{q}_{1A}} + \frac{q_2}{\tilde{q}_{2A}} = 1$$
$$\frac{\beta_{1B}}{\kappa_B} \cdot q_1 + \frac{\beta_{2B}}{\kappa_B} \cdot q_2 = 1 \quad ; \quad \frac{q_1}{\tilde{q}_{1B}} + \frac{q_2}{\tilde{q}_{2B}} = 1 \qquad (11)$$

where β_{1A} is the fraction of totally emitted amounts of tracer A that is adsorbed in a sampler in zone 1.

The equation system can easily be solved for q_1 and q_2.

3.1.3 Complete two cell system

In some cases it is desirable to treat the building as a complete two cell system, even if there is not uniform mixing within each zone. This is for example the case in two storey houses. Here, not only the total air flow rate is of interest, but also, for example, the amount of air extracted from the upper floor originating from supply to the ground floor.

Each floor is treated as one zone with its own type of tracer. The treatment is similar to that in the two zone approximation mentioned earlier, but now it is also necessary to sample the air flowing between the two zones. The tracer emission sources are preferably positioned as far as possible away from identifiable extract points and the stairway, in rooms with the most supply air. The air is sampled in the vicinity of the extract points and the stairway.

Without any derivation we can write the so called inverse flow matrix ($\mathbf{Q}^{-1}$) which is directly obtained from the result of the passive tracer gas measurements:

$$\mathbf{Q}^{-1} = \begin{pmatrix} \frac{\beta_{1A}}{\kappa_A} & \frac{\beta_{1B}}{\kappa_B} \\ \frac{\beta_{2A}}{\kappa_A} & \frac{\beta_{2B}}{\kappa_B} \end{pmatrix} = \begin{pmatrix} \frac{1}{\tilde{q}_{1A}} & \frac{1}{\tilde{q}_{1B}} \\ \frac{1}{\tilde{q}_{2A}} & \frac{1}{\tilde{q}_{2B}} \end{pmatrix} \qquad (12)$$

where it is assumed that tracer A has been emitted in zone 1 and tracer B in zone 2. Each β value must be characteristic for all air leaving a zone (both at extract points and at the stairway).

Each term in the inverse flow matrix has its physical interpretation (see for example Sandberg (1984))

In order to be interpreted in terms of air flow rates, it is necessary to invert the matrix, to obtain the flow matrix **Q**, which is easily done with a 2 x 2 -matrix.

$$\mathbf{Q} = (\mathbf{Q}^{-1})^{-1} = \begin{pmatrix} q_{11} & -q_{12} \\ q_{21} & q_{22} \end{pmatrix} \qquad (13)$$

The q_{11} value is interpreted as the total flow rate of air entering zone 1 from all other zones including the ambient. The q_{12} value should be interpreted as the flow rate from zone 2 entering zone 1. The sum of terms in row 1 of the flow matrix is the flow rate of air entering zone 1 directly from outside. Row 2 correspondingly yields the ambient air flow rate entering zone 2. The column row sums yield the corresponding direct outflow of air to the ambient. The sum of all terms yield the total ventilation flow rate to the system.

3.2 Example

Fig. 5 shows the calculated flows according to equation 6 for different types of tracer sources, located in different parts of an apartment with balanced ventilation. The varying results for different sampler locations illustrate the non-uniform mixing of ventilation air.

If the extract air flow rates at extract points **1** and **2** (see fig. 5) are called q_1 and q_2 respectively, the two zone approximation (equation system 11) yields the following results:

$$\frac{q_1}{132} + \frac{q_2}{118} = 1 \qquad \text{for tracer A}$$

and

$$\frac{q_1}{105} + \frac{q_2}{160} = 1 \qquad \text{for tracer B}$$

Solving the equation system yields:

$$q_1 = 58.4 \text{ m}^3/\text{h} \; ; \; q_2 = 66.7 \text{ m}^3/\text{h} \; ; \; q_{tot} = q_1 + q_2 = 125.1 \text{ m}^3/\text{h}$$

By utilizing the one zone approximation, according to equation (8) instead of the two zone approximation, about the same result (125 m^3/h) is obtained for the total ventilation flow. This result is obtained whether the calculation is based on tracer A or B. The satisfactory result from the one-zone approximation is due to the fact that there are approximately equal flows (α=0.07) from the two extract points (see equation 9).

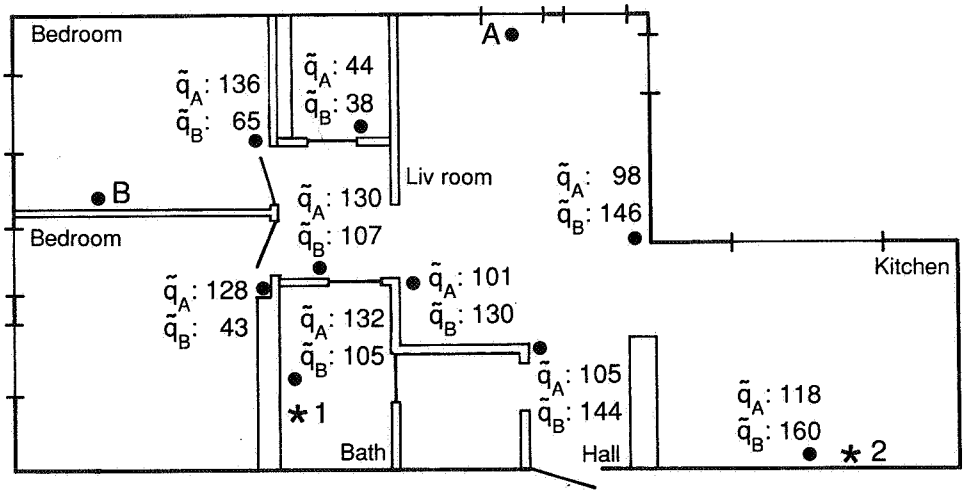


Figure 5 *Result of a passive tracer gas measurement in an apartment with balanced mechanical ventilation. Flow rates* $\tilde{q}_A = (\frac{K_A}{\beta_A})$ *and* $\tilde{q}_B = (\frac{K_B}{\beta_B})$ *(m³/h) are calculated at different samper positions. A and B denote the positions of tracer sources of type A and B respectively. *1 and *2 denote the positions of the air extract points*

3.3 Remarks

When performing a passive tracer gas measurement, we have found it to be a good practice to use two different types of tracers. Furthermore, we normally use a greater number of samplers than are necessary to calculate the total ventilation flow rate. The extra samplers give valuable extra information on the air flow pattern in the investigated space.

The practice we use, is to sample the air leaving the test space. In leaky, naturally ventilated houses, it is usually not possible to identify specific extract and supply points. This strategy is, therefore, not useful in this case. A better strategy might be to distribute several sources in order to obtain as homogenous a concentration as possible over the whole space. Sampling should be performed in many points to get an average concentration of the air leaving the system. In Sweden, however, even naturally ventilated houses are tight and equipped with extract air terminals where most air leaves the house. The practice of sampling close to identifiable extract points must be used with caution. It is not advisable to sample in a closed extract room e.g. a bathroom, where outside air also enters, for example, through a frequently opened window. The air short-circuiting in a bathroom should not be allowed to influence the computation of the ventilation flow rate available for the living space. In this case a better practice is to position the sampler outside the door to that space.

4 Conclusions

A new routine analysis method for two different perfluorocarbons, suitable for passive tracer gas measurements has been developed and extensively tested. The method is based on liquid extraction of the adsorbed tracer gases from active carbon in diffusive sampling tubes, gas chromatographic separation on a two-column system and quantitative analysis by and electron capture detector.

AIR MOVEMENT & VENTILATION CONTROL WITHIN BUILDINGS

12th AIVC Conference, Ottawa, Canada
24-27 September, 1991

POSTER 30

Use of tracergas to determine leakage in domestic heat recovery units (HRV)

Alphonse R. Hanlo

Cauberg-Huygen Raadgevende Ingenieurs B.V.
(consulting engineers)
PO box 1590
8001 BN ZWOLLE, the Netherlands
Fax: + 31 (0)38 223197

1. Introduction. (Abstract)

Tracergases provide a way to determine airflows in different situations. In some cases it is the only way to get quantitative information. This paper presents two cases in which tracergases are used for measuring the internal leakage in heat recovery units.
Internal leakage in heat recovery ventilators (HRV's) for domestic use may cause some problems:

- the real quantity of fresh air entering the building is unknown
- electrical power for the fans is used inefficiently
- smelling air a.g. from the kitchen may re-enter the building due to cross leakage from exhaust air tot supply air
- the efficiency of the HRV seems apparently better.

Most commonly used in domestic buildings in The Netherlands is a cross-stream HRV. The internal leakage in three types of HRV's is measured using N_2O as a tracergas. It is shown that major leakage occurs alongside the heat exchanger blok. Internal leakage in the heat exchanger itself however can not be neglected. The measurements show that an air leakage rate of less than 3 % of the total airflow can be obtained by careful design.

Secondly is shown how internal air leakage in a (rotating valve) back flow heat recovery ventilator is measured. This type of heat recovery ventilator uses an accumulating mass to recover heat. Due to this principle a certain amount of leakage from exhaust air to supply air is unavoidable. The exact amount of air leakage can be measured using a continually sampling infra-red absorption analyser. With the results it was proved that the efficiency of the heat recovery was only minimal influenced by the leakage.

2. Leakages in heat recovery units

All possible leakage flows for a cross flow heat recovery ventilator are give in figure 1.
At first is being noticed that leakage flows I'_{12} and I'_{34} parallel to the head flows I_{12} en I_{34}, can never be determined by measuring on the outside of the heat recovery unit. The effect of this leakage flow is only a decreased efficiency. This could also be caused by a bad K-value (in $W/m^2.K$) of the heat recovery ventilator. Both causes ara disindistinguishable, therefor these leakage flows will be left out of consideration [1].

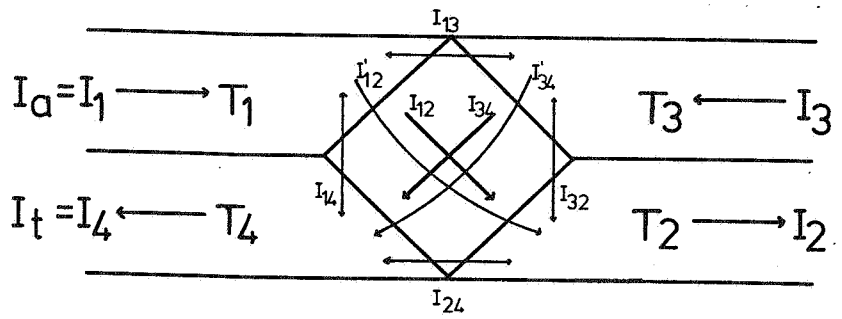


Figure 1. Leakage flow scheme.

The direction of the other 4 leakage flows are caused by the static pressures P_1 up to P_4 of the different compartments of the heat recovery unit.
The relation of these static pressures is dependant of the position of the ventilators in the unit. The pressure distribution of the examined heat recovery units was
$P_3>P_4>P_1>P_2$.

3. Theoretical background of the measuring procedure.

In a practice situation, whereby the behaviour of a unit is examined, the following measure values are known (see figure 2):

- temperatures T_1 up to T_4 in °C
- volume flows I_1, I_4 in m^3/h
- tracergasconcentration C_1, C_2 and C_4 in ppm
- ventilatorcapacity Q_2, Q_4 in W.

From the measured concentrations follow the leakfraction F_t (from exhaust domestic air to supplied fresh air) and F_a (from intake fresh air to exhaust domestic air).

$$F_t = (C_4/C_1) \quad (3.1a)$$
$$F_a = 1 - (C_2/C_1) \quad (3.1b)$$

On the basis of the known leakfractions can now be determined the resulting volume flows in the unit (I_{12}, I_{34}), the resulting leak flows (I_{14}, I_{32}):

$$I_{12} = I_1 - F_t \cdot I_4 \quad (3.2a)$$
$$I_{14} = F_t \cdot I_4 \quad (3.2b)$$
$$I_{34} = (1 - F_t) \cdot I_4 \quad (3.2c)$$
$$I_{32} = F_a \cdot (I_1 - F_t \cdot I_4)/(1 - F_a) \quad (3.2d)$$

and also the still unknown volume flows (I_2, I_3):

$$I_2 = I_{12} + I_{32} \quad (3.3a)$$
$$I_3 = I_{34} + I_{32} \quad (3.3b)$$

On the basis of the now known volume flows and the known electrical power of the ventilators the heating of the air through the ventilators can be known.

$$T_2' = T_2 - Q_2/(\rho \cdot C_p \cdot I_2) \quad (3.4a)$$
$$T_4' = T_4 - Q_4/(\rho \cdot C_p \cdot I_4) \quad (3.4b)$$

With ρ = the density of the air in kg/m^3
C_p = the heat capacity of air in W/kg°C

From these measured temperatures follow the corrected temperature efficiency of the heat recovery unit on exhaust (η'_a) and supply (η'_t)

$$\eta'_a = (T_1 - T_2')/(T_1 - T_3) \quad (3.5a)$$
$$\eta'_t = (T'_4 - T_3)/(T_1 - T_3) \quad (3.5b)$$

These efficiencies can be corrected for the occurring leakages assuming a worst case leakage situation.

$$\eta'_{a,c} = (\eta'_a - F_a)/(1 - F_a) \quad (3.6a)$$
$$\eta'_{t,c} = (\eta'_t - F_t)/(1 - F_t) \quad (3.6b)$$

The largest of both corrected efficiencies is equal to the **energy efficiency** of the heat recovery unit, the smallest of the both corrected efficiencies is equal to the **sensible heat recovery efficiency**.

Theoretical the corrected efficiencies are equal to equal volume flows. In case of unequal volume flows the corrected efficiency can be measured backward to an efficiency for equal design volume flows, assuming that the K-value of the heat recovery block is almost constant. Herefor the ratio of the volume flows will be calculated at first:

$$Y_t = I_{34}/I_{12} \quad (3.7a)$$
$$Y_a = I_{12}/I_{34} \quad (3.7b)$$

and calculating the heat-transfer-number:

$$Z_t = (l_{34}/l_o) \cdot \ln [(Y_t \cdot \eta'_{t,c} - 1)/(\eta'_{t,c} - 1)/(1 - Y_t)] \quad (3.8a)$$

$$Z_a = (l_{12}/l_o) \cdot \ln [(Y_a \cdot \eta'_{a,c} - 1)/(\eta'_{a,c} - 1)/(1 - Y_a)] \quad (3.8a)$$

With l_o as the design volume flow. The efficiency of equal design volume flows is:

$$\eta_{t',g} = Z_t/(1 + Z_t) \quad (3.9a)$$

$$\eta_{a',g} = Z_a/(1 + Z_a) \quad (3.9b)$$

The procedure is theoretical only correct for back flow heat recovery ventilators in a worst case leakage situation but also appears to be good in practice for cross flow heat recovery ventilators.

4. Internal leakage measurement in test set up among working conditions.

4.1. Measure situation.

In figure 2 is given the measure set up for the determination of internal leakage among working conditions. The air supply and air exhaust holes are provided with a rulable airresistance (f.i. a butterfly valve) and with a supply for measuring air volume flows.
The rulable air resistances are being set up so that the real pressure distributions in the canals around the units arise.

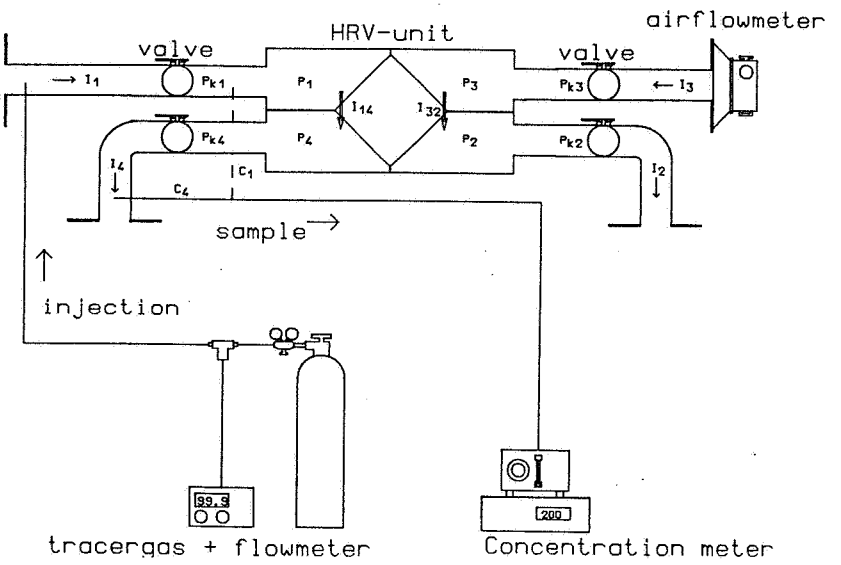


Figure 2. Measure set up

The exhausted volume flow (l_1) and the supplied volume flow (l_4) will be set up on practice values (225 m^3/h). The volume flows l_1 up to l_4 will be measured and also the pressures in the air canals P_{k1} up to P_{k4} and the pressures in the compartments of the heat recovery unit (P_1 up to P_4).
The resulting leakage flow $l_t = l_{14}$ from exhaust to supply will be determined by injection of a tracergas (N_2O) in the exhausted airflow.
After sufficient mixture the tracergasconcentration will be measured in the exhausted airflow (C_1) and in the supplied airstream (C_4).

If the external leakage can be neglected, the following resulting leakage flow will exist:

$$l_{14} = (C_4/C_1) * l_4 \quad (4.1)$$

This expression is only operative if the draw air volume flow I_{32} of draw to exhaust will be determined in the same way according:

$$I_{32} = (C_2/C_3) * I_2 \qquad (4.2)$$

4.2. Measuring results

The internal leakage is measured with 3 units (figure 3 up to 5). The measured resulting leakage flows; from exhaust to supply to the building (I_{14}) and supply from outside to exhaust out of the building (I_{32}) are mentioned for 2 measure situations in table 1.

Unit	measure situation	leakage flow [m^3/h]	
		I_{14}	I_{32}
A (fig. 2)	(regular)	< 2	17
	(modified)	< 2	11
B (fig. 3)	(regular)	< 2	< 2
	(modified)	< 2	< 2
C (fig. 4)	(regular)	3	22
	(modified)	< 2	11

Table 1. Internal leakage on the basis of tracergas measurement.

From table 1 it appears that leakage from exhaust to supply almost doesnot exist. This is accountable in the ground of the occurring pressure distributions in the unit (see figure 2).
Leakage from exhaust to supply can only be measured with unit A and unit B. The rest leakage in the improved situation is ascribed to a part leakage via the heatrecovery block and a part leakage along the sides of the heat recovery block and the cover. The leakage via the heat recovery block will be small. On the basis of measure information these leakage is about 3 to 5 m^3/h in case of 300 Pa pressure difference.

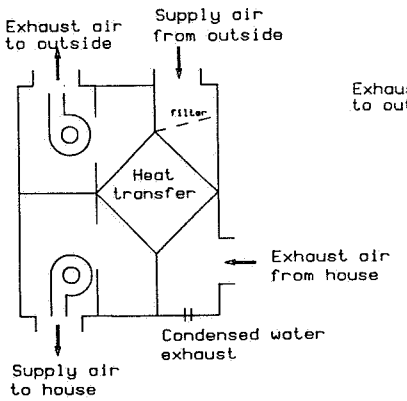


Figure 3: Unit A.

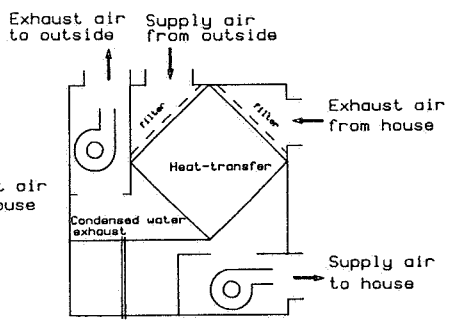


Figure 4: Unit B.

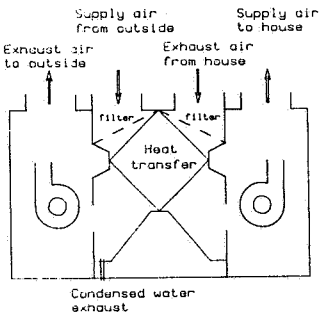


Figure 5: Unit C.

5. Proposal to standardization

From the measure results it appeared that the resulting leakage flow from exhaust to supply (I_{14}) can be reduced to less than 1% of the supplied airflow. As a provisional standard on the basis of the measurement results wil be used in [2]:

- the ventilation air supplied to the dwelling cannot consist of more than 1% exhausted dwelling air, as a result of **internal leakage** in the heat recovery unit.

From smell spreading and the loss of ventilator capacity the resulting internal leakage ($l_{14} + l_{32}$) is of importance. As a provisional standard is mentioned in [2]:
- the **total result internal leakage** among working condition is not allowed to be more than 2,5% of the total air volume flow. In case of a airflow of 2 x 225 m^3/h this is at most 11m^3/h.

6. Back flow heat recovery ventilator

6.1. Working principle and leakages.

Finally the application of leakage measurement with tracergas on the back flow recovery ventilator. The unit is concerning air capacity comparable with other heat recovery units for application in dwellings [3].
The air flow supplied by the unit to the measure dwelling was 149 m^3/h, the exhausted airflow was 184 m^3/h.

On the basis of the working principle (figure 7) of the unit 3 types of leakage can occur (see figure 6):
- leakage during the overturn of the shuttle valve ("short circuit").
- leakage through back flow of exhausted dwelling air from the canals and the accumulation mass.
- leakage between the shuttle valve in the final position ("steady" leakage).

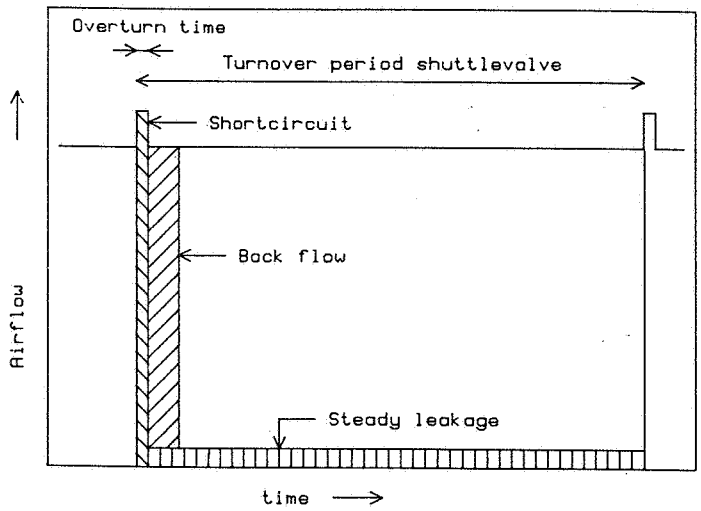


Figure 6: Possible occurring leakages.

The exhausted air from the dwelling will be blowed into the dwelling as a result of all 3 types of leakages. Except smell spreading, apparently these leakages also influence the efficiency of the unit.

6.2. Measurements

The occurring leakages are measured with the help of a tracergas. The tracergas (figure 7) is injected in one of the exhaust canals. The tracergasconcentration in the exhausted air is measured in the canal after the exhaust ventilation. From the relation of the

injected quantity tracergas and the measured tracergasconcentration in the exhausted air, the exhausted quantity is determined. Also the short increasement of the exhausted air quantity during the overturn of the shuttle valve is measured on this manner. Herefrom the occurring leakage is determined.

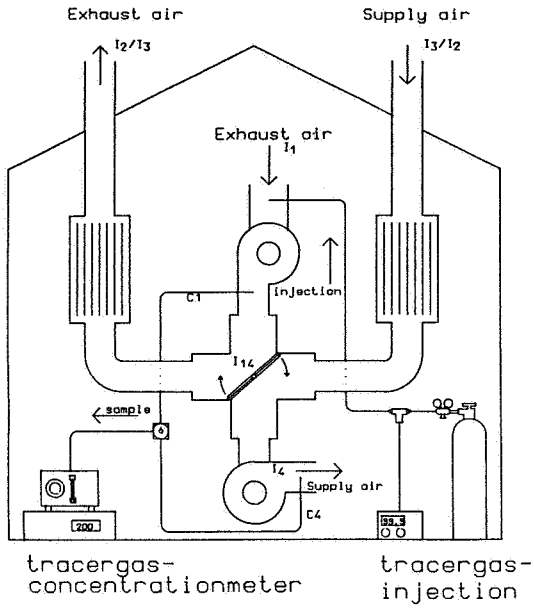


Figure 7: Measure set up.

The tracergasconcentrationmeter has a certain slowness. The rapid concentration changes during and after the turnover of the shuttle valve will be spread over a longer period. This has no influence on the average concentration which eventually is important for the determination of the leakage. Considering the minimal measure reach of the tracergasconcentrationmeter it appeared that less than 1% leakage along the shuttle valve takes place in the end position. The measured average leakage can be calculated back to the real leakage (table 2).

	time [s]	leakage flow [m^3/h]	average percentage [%]
leakage during the turnover of the shuttle valve	0,9	202	1,3 %
leakage through backflow of air from the canals	2,8	184	3,7 %
Stationary leakage via the shuttle valve in the end position	76	< 2	< 1 %

Table 2. The measured air leakage of exhausted inside air to supplied outside air, divided in time and quantity.

6.3. Efficiencies

The measured efficiencies of the heatrecovery unit can be corrected for the leakage. Herewith the following suggestions are made:

1. The measured efficiency can be corrected with the help of an average measured

leakage percentage.

2. The temperature of the leakage air is equal to the temperature of the exhausted inside air.

Both suggestions are justified [3]. Suggestion 2 means that it is assumed that these leakage takes place directly from the exhausted inside air to the supplied air of the dwelling. This is pointed out with the "worst case" situation because the influence of the leakage on the efficiency is at its maximum and therewith the correction on the measured efficiency is the highest.
The efficiency of the unit is measured during a period of 3 weeks. The measured average efficiency is a lineair equation (figure 8). Considering this efficiency as a function of the temperature difference ΔT between inside and outside air and corrected for the leakage and inequal supplied and exhausted volume flow.

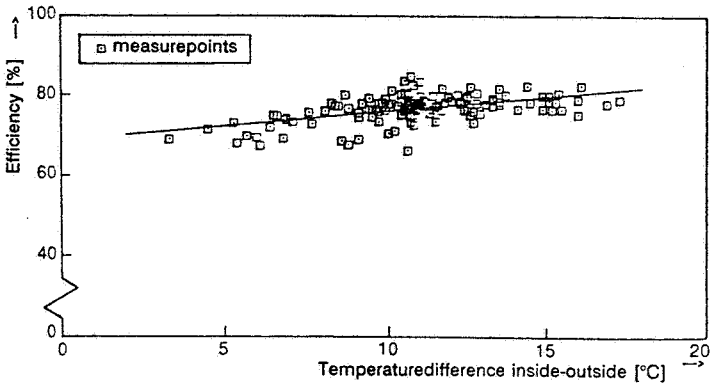


Figure 8: Measured efficiency (corrected for leakage).

6.4. Conclusions

From the measurements appears that the shuttle valve of the unit in the final position closes sufficiently to prevent leakage along this shuttle valve. The leakage during and short after the turn over of the shuttle valve is normal for the heat recovery principle and therewith unavoidable. The measurements have showed that these leakage can be estimated on the basis of the turnover time of the shuttle valve and the volume of the canals between the shuttle valve and outside. The unavoidable leakage percentage is about 2,4% in case of a minimal canal volume and dependent of the volume flows.

7. References

[1] Cauberg, J. and Gerwen, R. van: Detection of leakage in heat recovery units with tracer gas and the influence of leakage on the efficiency. Report 9939-1* Cauberg-Huygen Raadgevende Ingenieurs B.V., 1988 (in Dutch).

[2] Gerwen, R. van and Weevers, C: Leakage in heat recovery units: Field tests and proposal for standardization. Report 890332-1* Cauberg-Huygen Raadgevende Ingenieurs B.V., 1990 (in Dutch).

[3] Gerwen, R. van: Leakage and efficiency measurement on a heat recovery exchanger based on accumulation and shuttle valve. Report 5860-1* Cauberg-Huygen Raadgevende Ingenieurs B.V., 1990 (in Dutch).

* Research reports by order of the Dutch Agency for Energy and the Environment (NOVEM).

Apendix A.

Definitions apply in this paper:

- **Resulting leakage flow** (l_{14}, l_{32})
  The nett volume flow which comes via several ways eventually from the exhausted inside air in the supplied outside air resp. from the exhausted outside air in the supplied inside air.
- **Leakage fraction** (F_1, F_2)
  The part of the supplied outside air, consisting of exhausted inside air resp. the part of the exhausted inside air consisting of exhausted outside air. If the leakage will be mentioned in percents there will be spoken of leakage percentage.
- **Efficiency** (η_a, η_b)
  With efficiently is undoubtedly meant the temperature efficiency. This is the relation of the reached temperature difference and the largest temperature difference. This reached temperature difference can be measured in the exhausted and supplied outside air (η_t) or in the exhausted and supplied inside air (η_a).
- **Measured efficiency**
  The temperature efficiency measured on the basis of the measured temperature of the airflows without the heat recovery unit.
- **Temperature corrected efficiency** (η'_a, η'_b).
  The temperature efficiency measured on the basis of the measured temperature inclusively the effect of heating up through the ventilators.
- **Corrected efficiency** ($\eta'_{a,c}$, $\eta_{t,c}$).
  The temperature efficiency inclusively the effect of heating up through ventilators and the effect of leakage.
- **Energy efficiency**
  The relation of the recycled sensible heat and the maximal to recycle sensible heat considering the fact that the maximal temperature difference can only be covered by the smallest volume flow.
- **Sensible heat recovery efficiency**
  The relation of the recycled sensible heat and the maximal to recycle sensible heat considering the fact that the maximal temperature difference can only be covered by the largest volume flow.

AIR MOVEMENT & VENTILATION CONTROL WITHIN BUILDINGS

12th AIVC Conference, Ottawa, Canada
24-27 September, 1991

POSTER 31

A Novel Infrared Absorption Spectrometer for Use in Ventilation Studies

Phillips, Duncan A., Bragg, Gordon M., & Weckman, Elizabeth, J.,

Department of Mechanical Engineering,
University of Waterloo,
Waterloo, Ontario,
CANADA,
N2L 3G1

Synopsis

This paper reports the design, development, calibration and testing of a fast-response, multi-channel tracer gas concentration measuring instrument. The instrument uses an innovative application of Infrared Absorption techniques to measure Sulphur Hexaflouride (SF_6) concentrations. This approach allows the overall cost of a multi-channel continuous-recording unit to be reduced without sacrificing overall performance. A calibration over the range 5.0 to 50.0 ppmV SF_6 is shown. The current measurement resolution is 0.06 ppmV, and the accuracy is $\pm 5.0\%$. Methods of improving these two parameters are presented, and further enhancements suggested.

1.0 Introduction

This paper reports the design, development, calibration and testing of a fast-response, multi-channel tracer gas concentration measuring instrument. Tracer gas concentration measurement instruments are recognized as valuable tools by building ventilation researchers. Currently, these instruments are used to measure ventilation rates - both infiltration and mechanical - from which contaminant trajectories and histories in buildings may be determined.

Many instrumentation systems and experiments, using either Gas Chromatography (GC) [1,2] or a commercially available Infrared (IR) Absorption device [3], have been reported in the literature. A further instrument reported is based on Quadrupole Mass Spectroscopy [4].

Unfortunately, available gas concentration instruments are only suitable for determination of long term changes in contaminant concentration since they are limited by very slow measurement speeds. They do not allow identification of short term, quickly changing local exposure problems, such as "work place exposure zones"[1]. Furthermore, current instruments do not allow measurement of spatial and time resolved phenomena such as length scales of contaminant concentration. This shortfall is compounded when it is necessary to track contaminant concentrations at more than one location.

Some researchers have attempted to optimize systems using current instruments by combining single analyzers with sophisticated, multi-point, sequential sampling setups [1,6,4]. Unfortunately, these are subject to long time delays between measurements while the instrument is flushed. Other techniques have used a separate analyzer for each sample location [7,2].

---

[1] Defined by Corn & Egmen (1979), to be "areas with a consistent pattern of exposure".

This leads to significant financial investments in equipment.

The Infrared Absorption Spectrometer described in this paper addresses the problems of measurement speed and cost. In addition, it is intended to have the following characteristics:

a) Ease of transportation;
b) *Simultaneous* sampling of multiple locations;
c) Real-time continuous monitoring;
d) High signal to noise ratio;
e) Wide range of concentration detection;
f) Minimum support facilities;
g) Long-term, unattended operation;
h) Unobtrusive sampling; and,
i) Low cost.

An instrument with these properties would be capable of studying contaminant spatial correlations both inside rooms, and between rooms; identifying spatial variations in concentration in the region of fume hoods; and performing investigations on the relationship between personal and area sampling in industrial hygiene applications.

2.0 DESIGN AND DEVELOPMENT

2.1 Conceptual Considerations: The measurement technique used is Infrared Absorption (IRA) with Sulphur HexaFlouride (SF_6) as the tracer gas. This combination was chosen since SF_6 is widely recognized as a suitable tracer gas, and its detectability by IRA is high.

Gas Chromatography (GC) as a measurement technique was not considered to have a sufficiently fast response time. Authors have reported same-zone-successive-measurement times from 30 seconds [2] to 3 minutes [8] using either a single analyzer for each sample location or sequential sampling respectively. Reported measurement times for IRA indicate sampling times better than 30 seconds.

The initial choice of SF_6 as the tracer gas does not exclude the use of other gases. With a broadband light source in the instrument, virtually any gas with strongly accessible absorption bands in the infrared could be used to track concentration distributions in space and time.

2.2 Functional Description: The instrument consists of five main components:

a) Light delivery optics;
b) Gas sample cells;
c) Sampling system;
d) Custom electronics; and,
e) IBM compatible microcomputer.

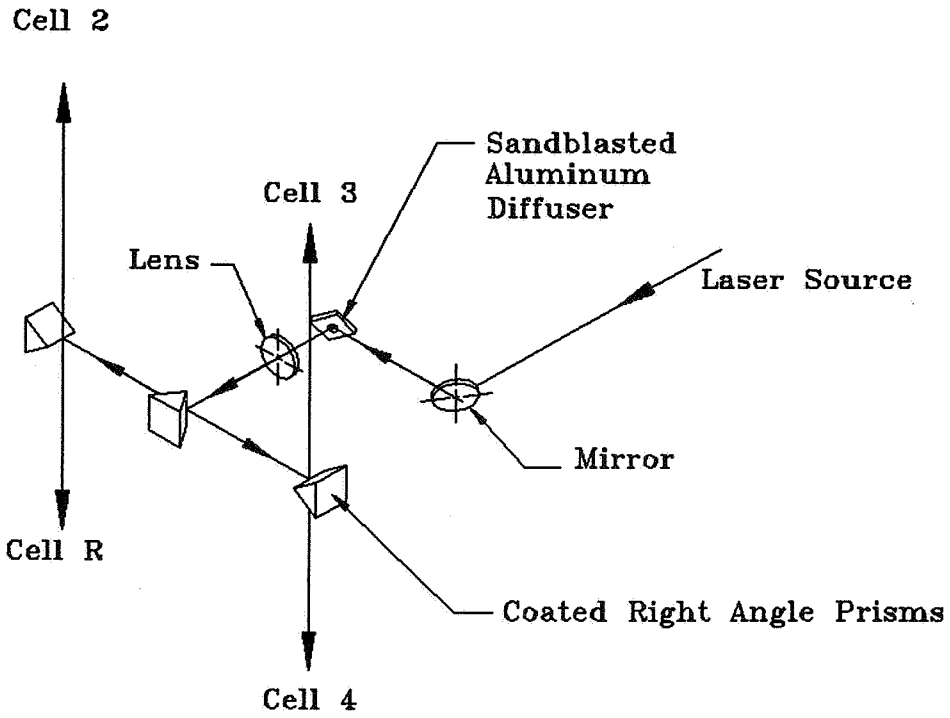


Figure 1 - Light Delivery Optics.

The light delivery optics are shown in Figure 1. The three millimetre beam generated by a 10 Watt Carbon Dioxide laser is reflected from a mirror onto an aluminium diffuser. The light scattered from the diffuser is collimated by a 25 cm lens. This light beam is divided into four smaller beams by a series of prisms. These smaller beams are then reflected into the four gas sampling cells. Of the four cells, three are sample cells, and the fourth is a laser power monitoring cell, for normalization and calibration.

The light beam makes two passes along the length of each gas sample cell before hitting a pyroelectric detector (IR light measuring device). The total path length is approximately two meters in each cell.

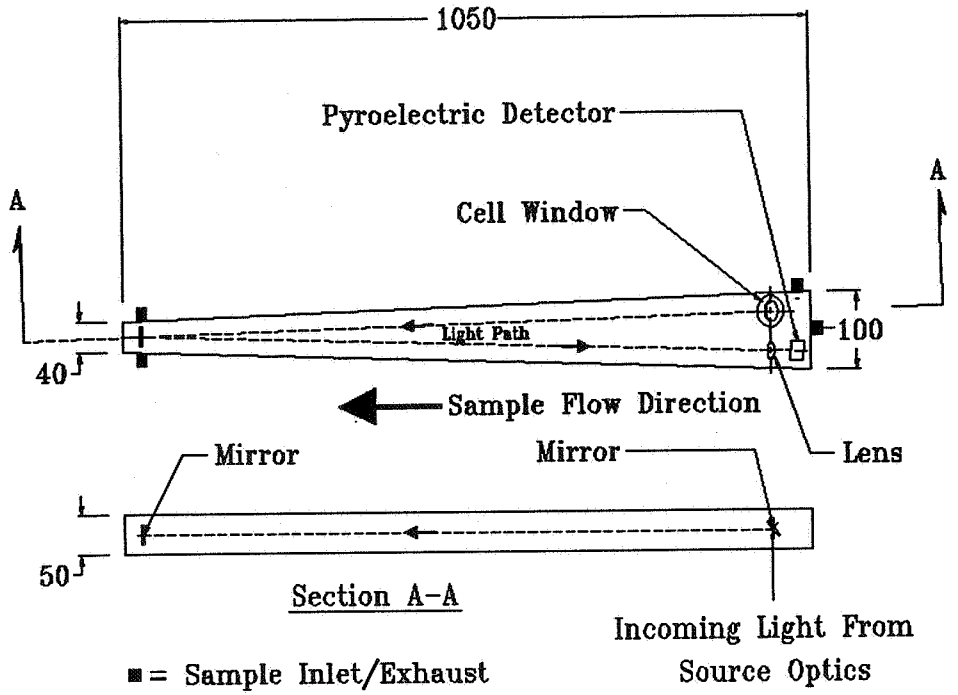


Figure 2 - Gas Sample Cells, Top View.

Gas samples are continuously delivered to the wide end of each cell, drawn out by a vacuum pump through the narrow end and released to the ambient air (See Figure 2). The sample flow rate is set for each cell using a high precision rotameter and valve. The cell volume is 4.0ℓ.

The custom electronics consist of two parts. Digital elements control the laser triggering and operating condition, the tracer gas delivery system, and the timing of sample readings by the computer. Analog electronics use lock-in amplification techniques to resolve small signals from the pyroelectric detectors, and computer controlled gain switching to extend the operating range of the instrument.

An IBM compatible computer provides the overall control of all functions and logs the data for subsequent processing. Post experiment digital filtering [3] allows high resolution concentration measurements in time *without* waiting for the sample cell to be flushed.

For mobility, the instrument is mounted on a trolley, and a hand cart is used to carry the SF_6 tank and associated gas handling hardware.

3.0 CALIBRATION AND TESTING

3.1 Calibration: Calibration is done using a recirculation system with a 32 litre mixing chamber to ensure uniform test sample mixing. A precise quantity of tracer gas is injected into the mixing chamber, and the signal from the pyroelectric detector in the sample cell is monitored until steady state is reached. At this point a reading is taken. Repeated over the calibration range a calibration curve is developed for the sample cell (See Figure 3).

To reduce the effect of the laser instabilities, a relative laser power value is monitored at all times and is used to normalize the signal from the sample cell. To ensure day to day calibration continuity a zeroing value is taken at the beginning of a calibration. The governing equation/calibration curves follow the relationship:

$$c_i(t)=\frac{1}{K_{1i}}\ln\left[\frac{1}{K_{2i}}\frac{S_i(t)}{S_r(t)}\frac{S_r(c_i=0)}{S_i(c_i=0)}\right] \qquad (1)$$

In the above expression $c(t)$ is the SF_6 concentration measured in time, S is the signal from the pyroelectric detectors, and K_1 and K_2 are calibration constants. The subscripts r and i refer to the reference cell, and any of the sample cells respectively.

Figure 3 illustrates a typical calibration curve obtained for mid range concentrations of SF_6 in a sample cell. Points are shown for concentration increments of approximately 3 ppmV. Each data point on the graph is the average value of at least two blocks of data taken at different times. Each data block is in turn the average of 1500 consecutive measurements of SF_6 concentration. Within each data block (1500 points) the repeatability was $\pm 1\%$, giving a limiting sensitivity/resolution of 0.06 ppmV for the lowest measured concentration. The current accuracy of the instrument is $\pm 5.0\%$.

Block to block repeatability was not as good - typically 3.2% (average) - due to problems with the stability of the laser mode as well as uncertainties in the normalization procedure. These problems are currently being investigated, but should be solved using a combination of water cooling of the laser, and digital filtering of the detector signals. These improvements are expected to improve both the resolution and sensitivity of the instrument.

3.2 Testing: Figure 4 illustrates the typical concentration decay of a single gas cell from a uniform concentration to zero. In this test, the flow rate of

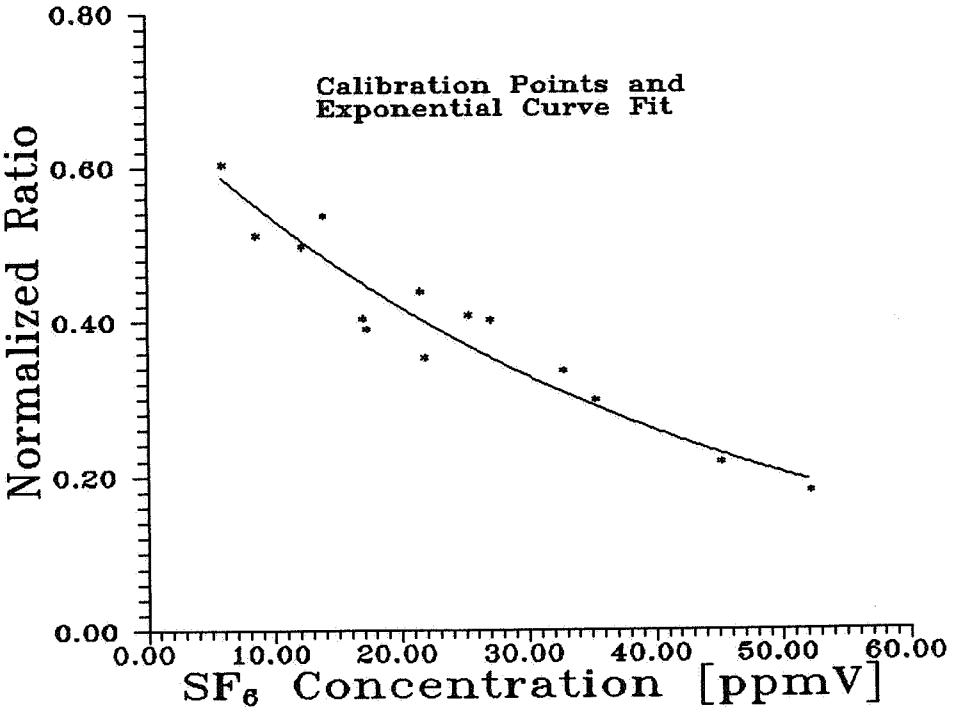


Figure 3 - Calibration Curve, Normalized Signal versus Concentration.

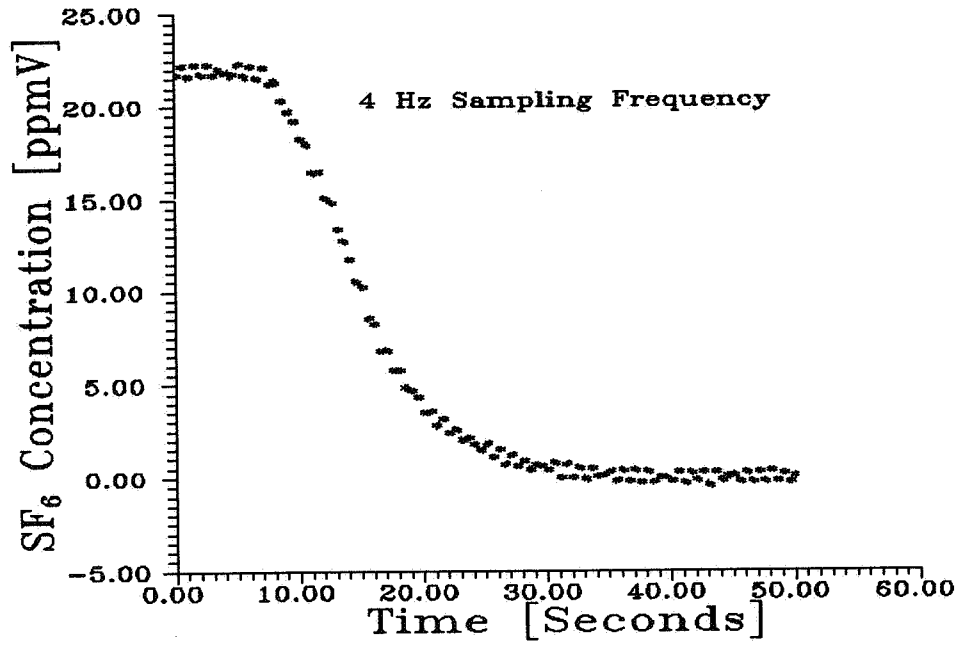


Figure 4 - Concentration Decay Curve from 21.9 to 0.0 ppmV SF_6.

fresh air into the SF_6 "contaminated" cell was set at 16.0 ℓ/min, and the cell volume was 4.0 ℓ. The starting concentration was 21.9 ppmV and the cell was well mixed. Full evacuation of the cell took 28.5 seconds or

approximately two times the minimum expected evacuated time (4.0 [ℓ]/16.0[ℓ/min]). As a result, a time resolution of 5 times 15 seconds, or 75 seconds may be expected to be accurately recorded. This sampling time may be reduced by increasing the flow rate.

4.0 SUMMARY AND CONCLUSIONS

Currently, the accuracy of this instrument is ±5%. The resolution is 0.06 ppmV, and the maximum time required between samples is 75.0 sec. Water cooling of the laser, and further digital filtering of the output signal should improve the overall system performance.

5.0 FURTHER ENHANCEMENTS

The current measurement system consists of three sample cells/channels, however, one advantage to this system is the ease with which additional sample cells may be added to allow the measurement of concentrations in more zones.

In addition, since the IRA system works on the principle that different gases absorb different wavelengths of light, the instrument can, with the addition of a broadband light source, test for a variety of gases at numerous locations simultaneously. In practice this would mean that a continuous variable light filter, with computer control of its setting would be switched back and forth between the absorption wavelengths of the various gases of interest. The speed of switching and accuracy would depend on the speed of the measurement electronics and repeatability of the computer controlled filter.

With these enhancements the instrument is capable of performing *near-simultaneous*, *multi-zone*, *multi-tracer gas* concentration measurements from the same gas sample, should a broadband light source be provided. This feature would be a clear advantage for researchers using multi-zone and multi-gas analytic/experiment methods.

Acknowledgements

The financial support of the Natural Sciences and Engineering Research Council (NSERC) of Canada is gratefully acknowledged.

REFERENCES

[1] Alevantis, L.E., (1989),
A Computer-Controlled System for Measuring Ventilation Rates of Buildings Using Sulphur Hexaflouride as a Tracer Gas, *Design and Protocol for Monitoring Indoor Air Quality, ASTM STP 1002*, N.L. Nagda & J.P. Harper, Editors, American Society for Testing and Materials, Philadelphia, 1989, pages 257-265.

[2] Roussel, C., Garnier, G., & Faivre-Pierret, R., (1985),
A Tracer-Gas System to Evaluate the Efficiency of Ventilation Systems or Simulate the Consequences of an Accident, *Ventilation 85, Proceedings of the 1st International Symposium on Ventilation for Contaminant Control*, H.D. Goodfellow, Editor, Toronto, 1985, pages 291-295.

[3] Skotte, J., Bruem, N.O., & Schneiser, T., (1990),
Improving an IR Tracer Gas Analyzer by Digital Filtering, *Building and Environment*,Vol. 25, No. 2, Pages 151-154.

[4] Sherman, Max, (1990),
A Multitracer System for Multizone Ventilation Measurement, *Review of Scientific Instruments*, Vol. 61, No. 9, pages 2457-2461.

[5] Corn, M., & Egmen (1979),
Workplace Exposure Zones for Classification of Employee Exposures to Physical and Chemical Agents, *American Industrial Hygiene Association Journal*, Vol. 40, pages 47-57.

[6] Perera, M.D.A.E.S., Walker, R.R., & Oglesby, O.D., (1985),
Infiltration Measurements in Naturally Ventilated Large Multi-Celled Buildings, *Ventilation 85, Proceedings of the 1st International Symposium on Ventilation for Contaminant Control*, H.D. Goodfellow, Editor, Toronto, 1985, pages 807-825.

[7] Waters, J.R., Lawrence, G.V., & Jones, N., (1989),
A Tracer Gas Decay System for Monitoring Air Infiltration and Air Movement in Large Single Cell Buildings, *Design and Protocol for Monitoring Indoor Air Quality, ASTM STP 1002*, N.L. Nagda & J.P. Harper, Editors, American Society for Testing and Materials, Philadelphia, 1989, pages 266-286.

[8] Fortmann, Roy C., Rector, Harry E., & Nagda, Niren L., (1989), **A Multiple Tracer System for Real Time Measurement of Interzonal Airflows in Residences,** *Design and Protocol for Monitoring Indoor Air Quality, ASTM STP 1002*, N.L. Nagda & J.P. Harper, Editors, American Society for Testing and Materials, Philadelphia, 1989, pages 287-297.

AIR MOVEMENT & VENTILATION CONTROL WITHIN BUILDINGS

12th AIVC Conference, Ottawa, Canada
24-27 September, 1991

POSTER 32

An Integral Mass Balance Formulation of the Constant Concentration Tracer Technique

James W. Axley

Building Technology Program
Massachusetts Institute of Technology
Cambridge, Massachusetts
U. S. A.

Synopsis

Three basic tracer gas techniques for measuring air flow rates in building systems have been developed over the past several decades – the *decay*, *constant injection*, and *constant concentration* techniques. These techniques were originally formulated using differential mass balance equations, or solutions to these equations, that describe the dispersal of tracer in building air flow systems. In recent years alternate formulations of the decay and constant injection techniques based on integral mass balance equations have been considered [1, 2]. These integral formulations have led to new variants of these traditional techniques and have provided means to improve the accuracy of these methods.

This paper extends the integral mass balance approach to the remaining constant concentration technique. An integral formulation of the constant concentration problem is presented that accounts for the possibility of variation of tracer concentration. This approach leads, in principle, to data reduction strategies that may be expected to improve the accuracy of the constant concentration technique and that may be used to isolate those portions of a given constant concentration data set that are likely to be most reliable. The method is applied to the reduction of constant concentration data sets measured at the National Swedish Institute for Building Research and the results of this application are reviewed.

List of Symbols

C_i concentration in zone i expressed in terms of mass fraction (mass-tracer/mass-air)
C_t target concentration
δC_i the variation of concentration about the target concentration in zone i
$\Delta C_i = C_i(t_2) - C_i(t_1)$ the change of concentration from time t_1 to t_2 in zone i
G_i the mass rate of release of tracer in zone i (mass-tracer/time)
M_i the mass of air within zone i (mass-air)
$[M] = \text{diag}\{M_1, M_2, \ldots\}$ the system capacitance matrix
t time
$\Delta t \equiv t_2 - t_1$ time interval from t_1 to t_2
Tol acceptance tolerance
W_{oi} total outdoor air flow rate into zone i, the diagonal elements of [W] (mass-air/time)
[W] the system transport matrix assembled from unknown system air flows
{ } vector quantities
[ ] matrix quantities

1. Introduction

The movement of air into, out of, and through out building systems determines, to a great extent, the quality of air indoors and the energy requirements needed to condition this air to realize thermal comfort. Ironically, in spite of the importance of air movement in buildings, building designers, operators, and occupants seldom have detailed knowledge of the nature of air flow in building systems and have no practical means to measure these air flows directly. As a consequence, the design and control of building air flow systems leaves much to be desired. To address this problem two indirect approaches to determine air flows in building systems have evolved over the past four decades – building *pressurization*

techniques and *tracer gas techniques* – following the seminal work of Dick [3]. Building pressurization tests are devised to measure building leakage characteristics that may be used to estimate fresh air infiltration [4, 5].

Tracer gas techniques attempt to deduce the building air flows that disperse one or more tracer gases released within a building system by measuring the concentration variations of tracer and attempting to solve associated equations that describe the conservation of tracer mass. In principle, tracer techniques are relatively straightforward but difficulties arise because the requisite mass conservation relations may only be formulated for relatively idealized circumstances (e.g., steady air flow and perfectly-mixed conditions in hypothetical building zones) and often lead to mathematically *ill-conditioned* problems that are especially sensitive to measurement error.

Tracer gas techniques may be classified by a) the tracer injection strategy, b) the data measurement method, and c) mass conservation formulation used. Three tracer injection strategies are commonly used a) an initial injection to establish an initial tracer concentration for the *decay technique*, b) a constant injection of tracer that is the basis of the *constant injection techniques*, and c) an injection of tracer controlled to maintain constant concentrations of tracers within the building system that is the basis of the *constant concentration techniques*. When applied to buildings that may reasonably be idealized as multiple, well-mixed zones, the decay and constant injection techniques have the potential to determine infiltration, exfiltration, and zone-to-zone air flow rates, but the associated mass conservation equations tend to be ill-conditioned.

The constant concentration technique, on the other hand, can only determine fresh air infiltration into each of the idealized building zones but yields mass conservation equations that are well-conditioned and, as a result, provides the most accurate determination of these air flows [6, 7]. Given this potential, researchers in the field have focused on development of control strategies and instrumentation needed to maintain the constant concentration conditions that are the basis of the method and yield well-conditioned problems [6, 8, 9]. This paper presents an alternative, and complementary, strategy to realize the potential of the constant concentration method.

2. Integral Formulation of the Constant Concentration Equations

The constant concentration method provides a means to determine the total flow rate of outside air into each zone of buildings that may be idealized as well-mixed, multi-zone systems. This is achieved by injecting a tracer gas into each zone in a carefully controlled manner with the objective of maintaining a constant concentration, the so-called target concentration C_t, throughout the entire building system. If this objective is achieved then the zonal concentrations may be expressed as:

$$\{\mathbf{C}\} = C_t\{1, 1, \ldots 1\}^T = C_t\{1\} \tag{1}$$

and the time rate of change of these concentrations will vanish:

$$\frac{d\{\mathbf{C}\}}{dt} = 0 \tag{2}$$

where each element of the system *concentration vector* **{C}** corresponds to the concentration within each zone. (Vector quantities will be identified by both bold fonts and braces, { }, and matrix quantities by bold fonts and square brackets, [ ].)

At these constant conditions, then, the instantaneous mass balance equations for the tracer assume the particularly simple form:

$$[\mathbf{W}]\, C_t \{1\} = \{\mathbf{G}\} \tag{3a}$$

where **[W]** is the system *transport matrix*, a square matrix containing terms *assembled* from the unknown system air flows [10], and $\{\mathbf{G}\} = \{G_1, G_2, \ldots\}$ with G_i the mass rate of release of tracer in zone i. As C_t is a scalar this equation may be rewritten as:

$$[\mathbf{W}]\{1\} = \frac{1}{C_t}\{\mathbf{G}\} \tag{3b}$$

The quantity on the left hand side of this equation is a vector of the row sums of the system mass transport matrix which is simply equal to the total outdoor air flow rate into each of the zones (i.e., if the tracer is an passive contaminant, outdoor tracer concentrations are negligible, and each zone is well-mixed [10]). Designating the total outdoor air flow rate into zone i by W_{oi} we may rewrite Equation 3b as:

$$W_{oi} = \frac{G_i}{C_t} \tag{3c}$$

That is to say, by employing the constant concentration strategy the coupled system of mass conservation equations is transformed into a system of simple scalar equations – equations that are inherently well-conditioned.

In the practical application of the constant concentration technique zone concentrations are controlled with periodic injections of tracer so that the time variation of G_i typically varies discontinuously between zero and relatively large pulses. It is not, therefore, reasonable to apply this equation directly using instantaneous values of G_i, instead a mean value over a reasonable averaging time period is used:

$$W_{oi} \approx \frac{\int_{t_1}^{t_2} G_i \, dt \Big/ \Delta t}{C_t} \quad ; \quad \Delta t \equiv t_2 - t_1 \tag{3d}$$

This simple result is the basis of the constant concentration technique. Although this technique is particularly simple in concept it is somewhat difficult to apply due to the instrumental control problems one encounters in attempting to maintain constant concentrations within the building system. Nevertheless, the technique has proven to be reliable and accurate [8, 11], especially when each of the individual zones is well-mixed and when the requisite constant concentration conditions are, in fact, maintained, and provides the only means available, at this time, to make nearly instantaneous determinations of these crucial fresh air flow rates.

It is useful to reconsider the constant concentration technique using an integral, rather than instantaneous, formulation of the tracer mass balance relation. To this end we shall assume that tracer concentrations within each zone of the multi-zone system vary by an amount, $\{\delta\mathbf{C}(t)\}$, about the target concentration, or:

$$\{\mathbf{C}(t)\} = C_t\{1\} + \{\delta\mathbf{C}(t)\} \tag{4}$$

Again, for simplicity, we assume negligible tracer concentrations out-of-doors and substitute this expression for the controlled zonal concentrations into the governing mass balance relation, using, now, an integral form:

$$\int_{t_1}^{t_2} [\mathbf{W}]\{C_t\{1\} + \{\delta\mathbf{C}(t)\}\}\,dt + [\mathbf{M}]\{\Delta\mathbf{C}\} = \int_{t_1}^{t_2} \{\mathbf{G}\}\,dt \tag{5}$$

where $<t_1, t_2>$ is an arbitrary time interval, $\{\Delta\mathbf{C}\} = \{\mathbf{C}(t_2)\} - \{\mathbf{C}(t_1)\}$, and $[\mathbf{M}] = \text{diag}\{M_1, M_2, \ldots\}$, with M_i the mass of air in zone i.

Although the time interval, $<t_1, t_2>$, is, in principle, arbitrary we prefer to select it so that it is small enough to assure that during this interval the system air flows and, hence, $[\mathbf{W}]$ remain practically constant allowing Equation 5 to be rewritten as;

$$[\mathbf{W}]\int_{t_1}^{t_2} \{C_t\{1\} + \{\delta\mathbf{C}(t)\}\}\,dt + [\mathbf{M}]\{\Delta\mathbf{C}\} = \int_{t_1}^{t_2} \{\mathbf{G}\}\,dt \tag{6}$$

If, then, the time interval is chosen so that:

$$\int_{t_1}^{t_2} \{\delta\mathbf{C}(t)\}\,dt = \{0\} \tag{7}$$

then Equation 6 simplifies to yield:

$$[\mathbf{W}]\{1\} = \frac{\int_{t_1}^{t_2} \{\mathbf{G}\}\,dt - [\mathbf{M}]\{\Delta\mathbf{C}\}}{C_t\,(t_2 - t_1)} \tag{8a}$$

Recognizing $[\mathbf{M}]$ is a diagonal matrix we obtain the final result:

$$W_{oi} = \frac{\int_{t_1}^{t_2} G_i\,dt - M_i\,(C_i(t_2) - C_i(t_1))}{C_t\,(t_2 - t_1)} \tag{8b}$$

(Compare to Equation 3c.)

The practical application of the constant concentration technique involves the periodic measuring of zonal tracer concentrations followed by a burst injection of tracer, when necessary, to maintain the desired target concentration. The time period between concentration measurement and burst injections is typically on the order of one or two minutes although shorter sampling times may be possible [8]. During a sampling time interval the integral $\int G_i dt$ is simply equal to the amount of tracer released to zone i.

To account for the variation of tracer concentration about the target concentration one could, then, monitor both the zone concentrations and the integral of their variation about the target value during the test. If during a given time period of, say, five or more sampling intervals the integral of the variation is observed to be negligibly small then one may apply Equation 8b directly to the data to obtain an estimate of the total outdoor air flow into each zone, W_{oi}, whether the zonal concentrations remain on target or not as the MΔC term provides an appropriate correction. If the integral of the variation is not observed to be negligibly small then one may either note this inadequacy in the data and make no attempt to determine air flows during the time period or, perhaps, search the time period for an interval when the integral of variation is, in fact, negligibly small, and compute air flows using Equation 8b. When tracer concentrations are well-controlled the integral of the variation and the MΔC correction will be negligibly small, as a result, Equation 8b will simplify to the conventional form, Equation 3c.

What criteria may be used to determine if the integral of the variation is negligibly small? Clearly, if the integral of the zone concentrations, over the time interval chosen, is well-approximated by the integral of the target concentration:

$$\int_{t_1}^{t_2} \{C_t\{1\} + \{\delta \mathbf{C}(t)\}\}\, dt \approx \int_{t_1}^{t_2} C_t\{1\}\, dt = C_t \Delta t\{1\} \tag{9a}$$

the objective will be met and Equation 6 will simplify to the desired form. Rearranging Equation 9 we obtain a more convenient relative form:

$$\frac{\int_{t_1}^{t_2} \{\delta \mathbf{C}(t)\}\, dt}{C_t \Delta t} \approx \{0\} \tag{9b}$$

For computational purposes it is proposed that an acceptance criteria or *tolerance* be based on an maximum norm of the absolute value of each term of this criteria:

$$\mathrm{Tol} \equiv \left\| \mathrm{Abs}\left\{ \int_{t_1}^{t_2} \{\delta \mathbf{C}(t)\}\, dt \Big/ C_t \Delta t \right\} \right\|_{max} \tag{10}$$

3. Application

Sandberg and Blomqvist conducted a number of tests, using an indoor test house contained within their laboratory at the National Swedish Institute for Building Research, to

investigate the ability of the constant concentration technique to follow sudden changes in air flow and to identify optimal control algorithms for the constant concentration test equipment used [6]. Total fresh air flow into the test house was mechanically controlled to vary in a step-wise manner while tracers were injected into each of five different rooms in an attempt to maintain a target concentration in all rooms. A total of eight different control algorithms were considered, identified as ALGO1 through ALGO8. We shall consider result obtained for a poorly-controlled case, ALGO5, and a well-controlled case, ALGO6. The results obtained using the six other cases were similar.

All tests were conducted in a similar manner. Tracer concentrations were measured in each of the five rooms at 15 second intervals, pulse injections of tracer were then applied to each room in an attempt to control concentrations at the target value of 50 ppm and, after a 60 second delay, the procedure was repeated. As a result, concentrations were measured in each of the five rooms on a 120 second interval. The measured concentration histories for two representative rooms, identified as room 1 and 5, for the cases discussed here are plotted below, Figures 1 and 2. The relative success of control algorithm ALGO6 is evident from these results.

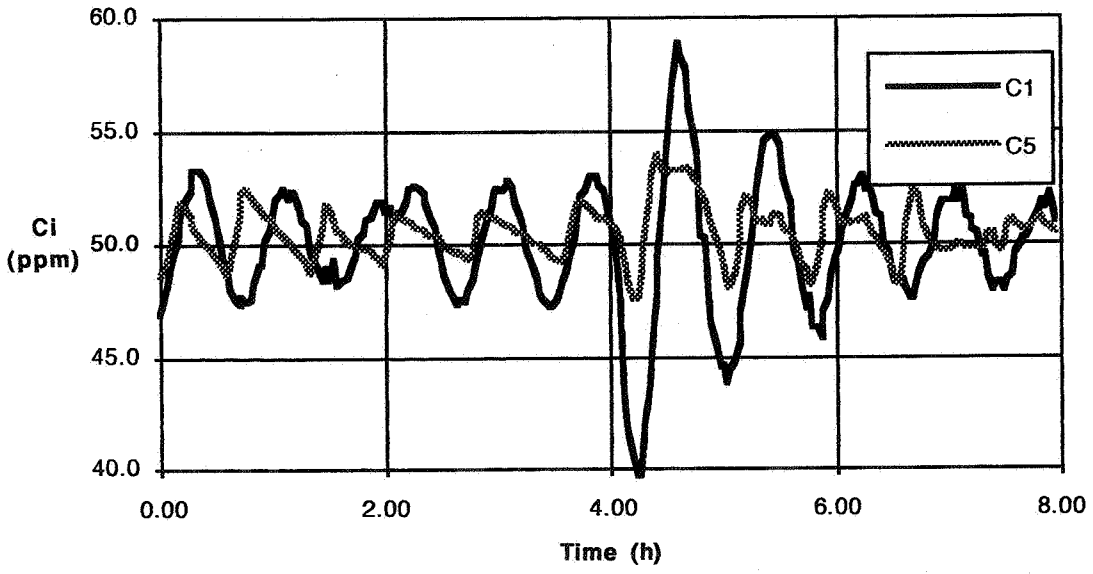


Figure 1 Representative Concentration Time Histories for Test ALGO5

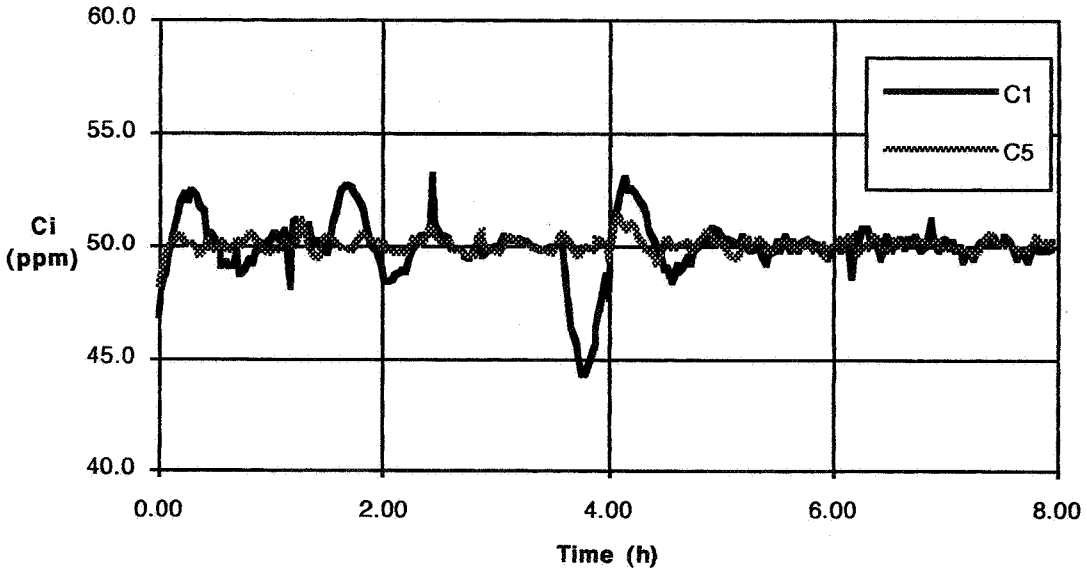


Figure 2 Representative Concentration Time Histories for Test ALGO6

The integral form of the constant concentration theory, Equation 8b, was applied to this, and all other, data using an integration time interval of 30 minutes (i.e., numerically integrating the discrete measured concentration data using 15 data values for each room). This resulted in a *30-minute moving estimate* of fresh air flow into each room (i.e., W_{oi}, i = 1, 2, ... 5) at 2 minute intervals. Summing these results, an estimate of the total fresh air flow into the house was determined and, using the target concentration of 50 ppm, the acceptance criteria was computed, Equation 10, at each of the 2 minute intervals. The results are compared below to the mechanically controlled total fresh air flow for two acceptance tolerances, 1% Tol and 2% Tol, Figures 3 and 4. The total fresh air flow reported by Sandberg and Blomqvist is also plotted using + markers labeled as ALGO5 and ALGO6, respectively.

Regrettably, while tracer was injected at 120 second intervals in controlled pulses, the amount of tracer injected was not recorded. The recorded data provided only values for the integral of the total tracer injected in each of several consecutive 30 minute intervals. Consequently, to apply Equation 8b the integral of amount of tracer injected:

$$\int_{t_1}^{t_2} G_i \, dt$$

was estimated by linear interpolation between these 30 minute values.

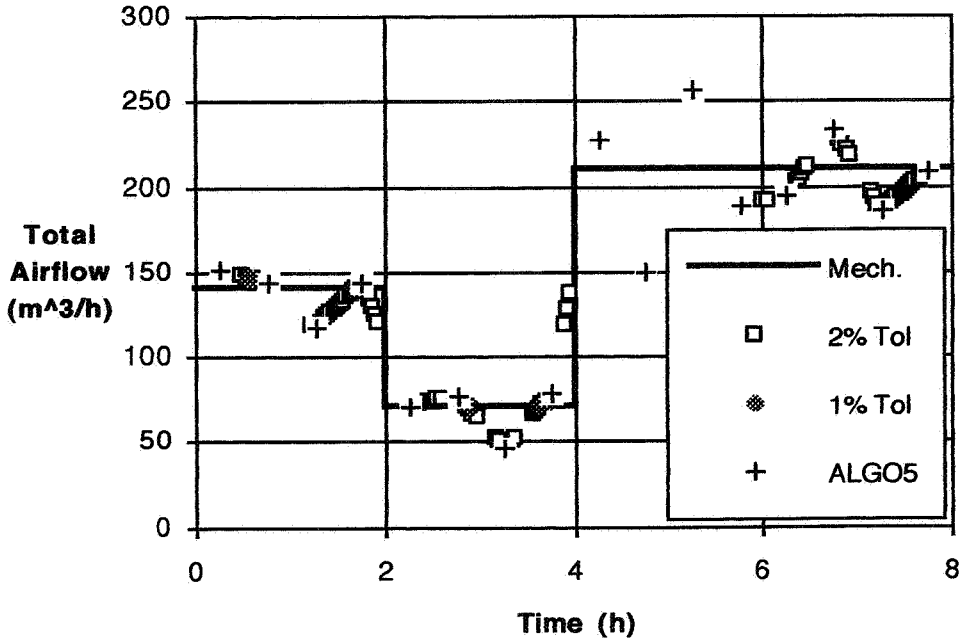


Figure 3 Comparison of Air Flow Estimates with Mechanically Controlled Values for ALGO5

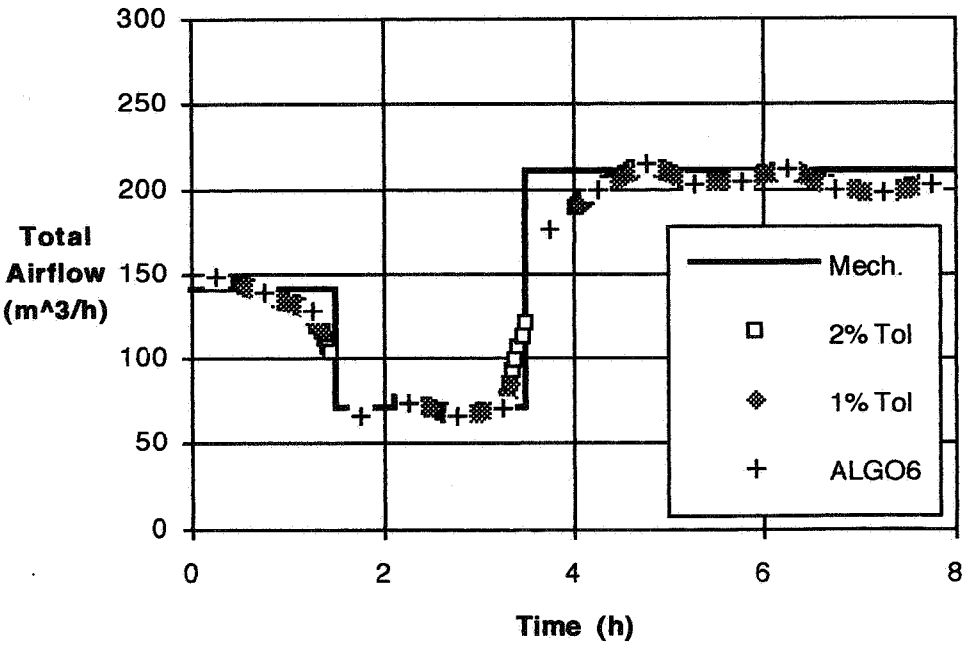


Figure 4 Comparison of Air Flow Estimates with Mechanically Controlled Values for ALGO6

Figures 3 and 4 may be somewhat difficult to read at first. The solid line presents the variation of total airflow as controlled by the mechanical system. Each of the markers

represents an estimate of the total air flow during the 30 minute time period centered on the marker. The + markers indicate the estimates based upon the conventional constant concentration approach, Equation 3d, as reported by Sandberg and Blomqvist. The □ markers indicate the estimates based upon the integral approach, Equation 8b, having an acceptance tolerance, Equation 10, less than or equal to 2% and the ◈ markers an acceptance tolerance of less than or equal to 1%.

As expected from the theory, the smaller acceptance tolerance of 1% yields better estimates of total airflow but also results in the rejection of much of the data. In the case with poor control of the zone concentrations, Figure 3, nearly all of the data is rejected when the 1% criteria is enforced. For the well-controlled case, on the other hand, most of the data passes the 1% tolerance test. The results obtained for the six other tests not reported here are similar – a 1% tolerance consistently results in accurate estimates of total air flow and, for these test involving sudden changes of airflow, a rejection of much of the recorded data as unacceptable – although the results from two test, ALGO7 and ALGO8, revealed consistent underestimations of air flows for both conventional and integral approaches indicating a systematic source of error. Accepting integral constant concentration results passing the 2% tolerance test generally provides better estimates of airflow than those reported by Sandberg and Blomqvist and results in the rejection of some of the data as unacceptable (e.g., those + values between the 4th and 6th hours of Figure 3) but overall the success is not as consistent as provided by the 1% acceptance tolerance.

4. Conclusion

An integral formulation of the theory underlying the constant concentration tracer technique has been presented that leads to data reduction strategies that appear to improve the accuracy of the technique and provides the means to isolate those portions of a given constant concentration data set that are likely to be most reliable. When applied to eight data sets provided by the National Swedish Institute for Building Research (NSIBR) the proposed data reduction method lead to consistently better accuracy than that provided by the conventional approach when a data acceptance criteria demanding the integral of variation of zone concentrations remain within a 1% tolerance of the corresponding integral of the target concentration was enforced. While a 2% tolerance generally provided better accuracy than the conventional approach tolerances larger than 2% offer no significant advantage. Finally, it should be noted that the proposed approach offers no remedy for systematic errors that, apparently, resulted in consistent under-predictions of air flows for two of the data sets analyzed.

The application of the proposed data reduction strategy to the NSIBR data sets was compromised by insufficient detail in the record of tracer injection time histories. Presumably, a more complete record of tracer injection – easily obtained using available instrumentation – would have improved results.

The proposed approach involves numerically evaluating integrals of the variation of zone concentrations about the target concentration and integrals of the tracer injection time history. The integration time interval is, in principle, arbitrary although, from a practical point of view, an interval small enough to assure that system air flows remain relatively constant and yet large enough to provide sufficient measured data to realize an accurate numerical integration should be used. A time interval of 30 minutes was used in the present study to yield results that could be compared to those results reported by the investigators at

NSIBR but in other circumstances one may consider searching the data for time periods that result in satisfaction of the acceptance criteria. Following a similar argument, the target concentration may also be considered to be arbitrary and one may search the data set, using a variety of candidate target concentrations, to find combinations of target concentrations and integration time intervals that result in satisfaction of the acceptance criteria.

A formal error analysis of the proposed approach was not considered in the present study. It is believed that such an analysis would be relatively straightforward and could establish the quantitative link between the accuracy of computed fresh air flows and the acceptance tolerance imposed.

Acknowledgement

This study was made possible through the generous contribution by Mats Sandberg and his colleagues of measured data collected at the National Swedish Institute of Building Research.

References

1. AXLEY, J. AND A. PERSILY. "Integral Mass Balances and Pulse Injection Tracer Techniques." in Proceedings of the 9th AIVC Conference: Effective Ventilation. 1988. Gent, Belgium: AIVC.
2. PERSILY, A. AND J. AXLEY. "Measuring Airflow Rates with Pulse Tracer Techniques." in ASTM Symposium Air Change Rates and Air Tightness in Buildings. 1989. Atlanta: ASTM.
3. DICK, J.B., "Experimental Studies in Natural Ventilation of Houses." Journal of the Institution of Heating and Ventilating Engineers, 1949. (December, 1949): pp. 420-466.
4. CHARLESWORTH, P., "Technical Note AIVC 24: AIVC Measurement Techniques Workshop Proceedings and Bibliography. 1988", Air Infiltration and Ventilation Centre:
5. LIDDAMENT, M. AND C. THOMPSON, "Technical Note AIVC 10: Techniques and Instrumentation for the Measurement of Air Infiltration in Buildings – A Brief Review and Annotated Bibliography." 1983, Air Infiltration and Ventilation Centre:
6. SANDBERG, M. AND C. BLOMQVIST. "A Quantitative Estimate of the Accuracy of Tracer Gas Methods for the Determination of the Ventilation Flow Rate in Buildings." Building and Environment. 1985. Great Britain: Pergamon Press, Ltd. pp. 139-150
7. SANDBERG, M.G. "Predicting a Time-Varying Flow Rate Using the Constant Concentration and Decay Technique." ASHRAE Transactions. V. 93, Pt. 1, 1987.
8. BOHAC, D., D.T. HARRJE, AND G.S. HORNER. "Field Study Comparisons of Constant Concentration and PFT Infiltration Measurements." Proceedings 8th AIVC Conf., Uberlingen, Germany, Sept. 1987. Great Britain: AIVC.
9. SHERMAN, M.H. AND D.J. DICKERHOFF. "A Multigas Tracer System for Multizone Air Flow Measurements." Proceedings of BTECC IV: Thermal Performance of Exterior Envelope. 1989. Atlanta: ASHRAE.
10. AXLEY, J.W., "Multi-Zone Dispersal Analysis by Element Assembly." Building and Environment, 1989. Vol. 24, No. 2: pp. 113-130.
11. SANDBERG, M. "Ventilation Efficiency as a Guide to Design." in ASHRAE Transactions. 1983.

AIR MOVEMENT & VENTILATION CONTROL WITHIN BUILDINGS

12th AIVC Conference, Ottawa, Canada
24-27 September, 1991

POSTER 33

A New Approach for the Numerical Identification of Interzonal Airflows from Tracer Gas Measurements

Simone GuitiZad[1] † Helmut Jarausch[1] Willigert Raatschen[2]

[1] Institut für Geometrie und Praktische Mathematik
Technische Hochschule RWTH Aachen
Templergraben 55
D–W–5100 Aachen

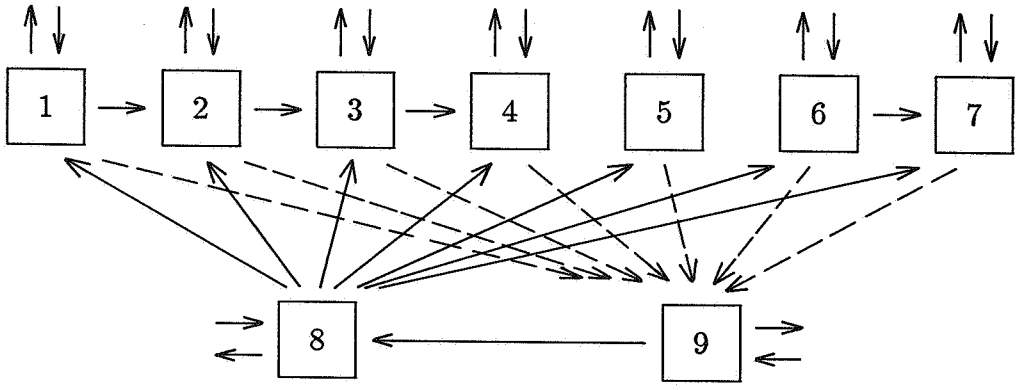
[2] DORNIER GmbH
Postfach 1420
D–W–7990 Friederichshafen 1

0. Synopsis

This paper presents a new approach to determine the interzonal airflows of a multizone system using tracer gas measurements. In contrast to methods proposed earlier, the presented method does not use the mass balance as basis for the least squares problem but identifies the interzonal airflows as coefficients of the evolution equations for the concentrations. Therefore estimating the derivatives with respect to the time from measured data is avoided. Furthermore the concentration can be calculated arbitrary points in time. In addition, if exact intervals bounding the sampling error are available, interval arithmetic can be used to determine bounds for the interzonal airflows.

1. Introduction

For determining the unknown interzonal airflows of a multizone enclosure, it is modelled as an multizone system. To illustrate this, consider the following example, for which we want to thank J. B. Mattson, Lund University, Sweden. This model consists of 9 zones, where the zones 8 and 9 correspond to a main air supply and exhaust air ducts.



Later the method presented in this paper will be demonstrated on this example.

Using the mass–balance for each zone we get

$$V_i \dot{\tilde{c}}_i = \sum_{j=0,\, j\neq i}^{n} \tilde{q}_{ij}\, \tilde{c}_j \;-\; \sum_{j=0,\, j\neq i}^{n} \tilde{q}_{ji}\, \tilde{c}_i \;+\; \tilde{g}_i \quad , \qquad i = 1, \cdots, n$$

where n is the number of zones, $\tilde{q}_{ij}$ the interzonal airflow from zone j into zone i (index 0 for outdoor air), V_i the volume of zone i, $\tilde{c}_j$ the concentration in zone j and $\tilde{g}_i$ the injection (constant) into zone i.

With $c_i \equiv \tilde{c}_i - \tilde{c}_0$ we get

$$(1.1) \qquad V_i \, \dot{c}_i = \sum_{j=1,\, j\neq i}^{n} \tilde{q}_{ij} \, c_j \; - \sum_{j=1,\, j\neq i}^{n} \tilde{q}_{ji} \, c_i \; + \; \tilde{g}_i \quad , \qquad i = 1, \cdots, n$$

The system (1.1) will be used to compute the modelled concentrations at time t .

The problem of determining the interzonal airflows now leads to a nonlinear least squares problem, which is solved using the Gauss-Newton-method.

Having identified the unknown parameters, one can get information about the quality of these approximations using statistical considerations, i.e. the á–posteriori–covariance matrix.

It may be possible that the structure of the multizone system does not allow us to identify all parameters. In this case only certain fixed linear combinations are identifiable. We use a heuristic algorithm to find 'smallest' sets of dependent parameters.

Last, interval arithmetic is used to get bounds for the true values of the interzonal airflows.

2. The Identification Problem

Now we have to determine the interzonal airflows from the measured tracer gas concentrations. Let m be the number of sampling intervals, M the number of samples, $\bar{c}_i \in \mathbb{R}^n$ the measured concentrations and $c(t_i, Q) \in \mathbb{R}^n$ the modelled concentrations at time t_i $(0 \leq i \leq m)$, where the parameter–vector Q contains the unknown interzonal airflows. Thus the interzonal airflows can be determined by the requirements

$$c(t_i, Q) \approx \bar{c}_i \quad , \qquad i = 0, \cdots, m$$

Under the assumption that the measurement errors and model uncertainties can be described by a Gaussian statistics, the least squares method gives an optimal estimator

$$(2.1) \qquad Q = \arg\min_{Q} \sum_{i=0}^{m} \| c(t_i, Q) - \bar{c}_i \|_2$$

According to (1.1) the time evolution of the concentrations $c(t, Q)$ can be modelled by

$$(2.2) \qquad V \, \dot{c}(t, Q) \; = \; Q \, c(t, Q) + \tilde{g} \quad , \qquad c(t_0, Q) = c_0$$

With $V = diag(V_1, \cdots, V_n)$, $\tilde{g} = (\tilde{g}_1, \cdots, \tilde{g}_n)^T$, $g \equiv V^{-1}\tilde{g}$ and

$$Q = (q_{ij}) \qquad q_{ij} = \begin{cases} \tilde{q}_{ij} & \text{if } i \neq j \\ \sum_{z=0,\, z\neq i}^{n} \tilde{q}_{zi} & \text{if } i = j \end{cases}$$

we get

$$\dot{c}(t,Q) = V^{-1}\, Q\, c(t,Q) + g \;\equiv\; f(t,c,Q) \quad , \qquad c(t_0,Q) = c_0 \tag{2.3}$$

There exist several methods to solve the linear differential equation (2.3), e.g.

i) a closed formula for the exact solution
ii) solving (2.3) with a numerical scheme

With the aid of the variation of constants formula we obtain the solution of (2.3) with $A \equiv V^{-1}Q$

$$c(t,Q) = \exp(At)\, c(t_0,Q) \;+\; A^{-1}\,(\exp(At) - I)\, g \tag{2.4}$$

where I is the identity–matrix in $\mathbb{R}^{n\times n}$. The concentrations can now be approximated using a Padé–Approximation to the exponential function. But this method needs $\mathcal{O}(n^3)$ operations to compute the solution and is therefore not efficient.

To integrate (2.3) numerically, we can use

- an explicit method of Runge–Kutta type, e.g. as given by Dormand and Prince (1980) with automatic step size control (see [1] page 171).
- an implicit method like the extrapolated lineary implicit Euler method combined with a dense output formula and automatic step size control. The advantage of this method is, that it is well suited for the (mildly) stiff equations (2.3) and with the aid of the dense output formula we can obtain the solution at each point of time within each integration step (see [2]).

Each of the proposed methods is able to approximate the solution of (2.3) at arbitrary points in time. Notice that $c(t,Q)$ is piecewise continously differentiable with respect to time.

Since the initial values c_0 are not known we have to identify them as well. Putting $P = \begin{pmatrix} c_0 \\ Q \end{pmatrix} \in \mathbb{R}^n$, now (2.3) is replaced by

$$\begin{aligned} \dot{c}(t,P) &= V^{-1}\, Q\, c(t,P) + g & c(t_0,Q) &= c_0 \\ \dot{Q} &= 0 & Q(t_0) &= Q \end{aligned} \tag{2.5}$$

Problem (2.1) now reads

$$P = \arg\min_P \sum_{i=0}^{m} \|c(t_i, P) - \bar{c}_i\|_2 \quad . \tag{2.1'}$$

For this nonlinear least squares problem we have to evaluate $c(t_i, P)$, i.e. solve (2.5), so the whole technique is similar to the shooting technique for boundary value problems. Moreover, the nonlinear problem (2.1') is solved by iterating with the linearized problem — this technique is called the Gauss–Newton–Method. We linearize $c(t, P)$ at $\tilde{P}$. We get with $c_p \equiv \partial c / \partial P$

$$c(t, P) \approx c(t, \tilde{P}) + c_p(t, \tilde{P})(P - \tilde{P}) \tag{2.6}$$

Inserting (2.6) into (2.1') we get

$$\min_P \sum_{i=0}^{m} \left\| c_p(t_i, \tilde{P})(P - \tilde{P}) - (\bar{c}_i - c(t_i, \tilde{P})) \right\|_2$$

With $\Delta P = (P - \tilde{P}) \in \mathbb{R}^N$ and

$$J = \begin{pmatrix} c_p(t_0, \tilde{P}) \\ \vdots \\ c_p(t_m, \tilde{P}) \end{pmatrix} \in \mathbb{R}^{M \times N}, \qquad b = \begin{pmatrix} c(t_0, P) - \bar{c}_0 \\ \vdots \\ c(t_m, P) - \bar{c}_m \end{pmatrix} \in \mathbb{R}^M$$

where M is the number of samples and N is the number of the unknown parameters, we get the linearized least squares problem

$$\min_{\Delta P} \|J \Delta P - b\|_2 \tag{2.7}$$

The solution P of (2.1') is now obtained with the aid of ΔP by iteration

$$P^{k+1} = P^k + \Delta P \tag{2.8}$$

which terminates when $\|\Delta P\|_2$ is small enough. For this iteration we have to compute the Jacobian J .

Theorem 1 Suppose that the partial derivatives of f in (2.3) with respect to c exist and are continous. Let $C \equiv \begin{pmatrix} c \\ Q \end{pmatrix}$.

Then the solution $C(t, P)$ is differentiable with respect to P and the derivative is given by the matrix $\partial C / \partial P \equiv R(t, t_0)$, where R is the solution of the so called 'variational equation'

$$\dot{R}(t) = \begin{pmatrix} f_c(t, c, Q) \\ f_Q(t, c, Q) \end{pmatrix} \cdot R(t, t_0) \quad , \qquad R(t_0) = E_n \tag{2.9}$$

where E_n is the identity-matrix in $\mathbb{R}^{n\times n}$ (see [1], pp 97). Notice that here we have $f_c(t,c,Q) = A$.

In our case, theorem 1 is not directly applicable since the right hand side of (2.3) is discontinous at those points in time, where the injection $\tilde{g}$ (a step function) has jumps. But one can show that the conclusion of theorem 1 stays valid.

The solution R of (2.9) can now be obtained by the same methods as the solution of (2.3). It is also possible to compute J by divided differences, but in this case it is necessary to freeze the step sizes, that means the step sizes used during the computation with the initial value $\tilde{c}$ are memorized and reused during the computation with the initial value $\tilde{c} + \delta c$.

Differentiating the solution given by (2.4) one can give a closed form solution of the variational equation (2.9) by theorem 2.

Theorem 2 Let $A = (a_{ij}) \in \mathbb{R}^{n\times n}$ be regular and $t \geq 0$

Then

$$\frac{\partial}{\partial a_{ij}} exp(At) = \sum_{k=1}^{\infty} \frac{1}{k!} \sum_{z=0}^{k-1} A^k B^{(ij)} A^{k-z-1}\, t^k$$

$$\frac{\partial}{\partial a_{ij}} A^{-1}(exp(At) - I) = \sum_{k=1}^{\infty} \frac{1}{(k+1)!} \sum_{z=0}^{k-1} A^z B^{(ij)} A^{k-z-1} t^{k+1}$$

where $B^{(ij)} = (b_{ls}^{ij})$ with $b_{ls}^{ij} = \begin{cases} 1 & \text{for } l = i \text{ and } s = j \\ 0 & \text{otherwise} \end{cases}$

To solve the linear least squares problem (2.7) we first compute the QR - factorization of J such that $J = QR$, where $Q \in \mathbb{R}^{M\times M}$ is an orthogonal matrix and $R = (R_1, 0)^T \in \mathbb{R}^{M\times N}$ is a triangular matrix. Then we have

$$\|J\,\Delta P - b\|_2^2 = \|Q\,R\,\Delta P - b\|_2^2 = \|R_1\,\Delta P - b_1\|_2^2 + \|b_2\|_2^2$$

$$\text{with} \quad Q^T b = \begin{pmatrix} b_1 \\ b_2 \end{pmatrix} \quad \text{and} \quad b_1 \in \mathbb{R}^N$$

Thus (2.7) is reduced to the much smaller problem

$$\min_{\Delta P} \|R_1\,\Delta P - b_1\|_2 \tag{2.10}$$

which can be tackled by the singular value decomposition. For this one computes orthogonal matrices $U, \mathcal{V} \in \mathbb{R}^{N\times N}$ and a diagonal matrix $\Sigma = \text{diag}(\sigma_1, \cdots, \sigma_N)$ such that $R_1 = U\,\Sigma\,\mathcal{V}^T$.

Using this factorization, the solution of (2.10) can be expressed as:

$$\Delta P = \mathcal{V}\ \Sigma_r^+\ U^T b_1 \tag{2.11}$$

The pseudo inverse Σ_r^+ of Σ is given by $\Sigma_r^+ = \mathrm{diag}(\sigma_1^{-1}, \cdots, \sigma_r^{-1}, 0, \cdots)$, where r denotes the numerical rank of R_1, which is equal to the numerical rank of J (see [3], p. 242). Thus the use of the singular value decomposition aids in determining the numerical rank of R_1. This is combined with a trust region algorithm for the nonlinear problem (2.1) (see [9]). In principle the numerical rank is determined such that the solution ΔP of (2.10) is bounded by R_T – the trust region radius. For more difficult problems — characterized by a given amount of nonlinearity *in relation to* the minimal value in (2.1) — we have to include a Levenberg–Marquardt regularization technique, as well (see [9], pp 218–228). The relation of the numerical rank r to the size of the step ΔP follows from (2.11)

$$\|\Delta P\| = \sum_{i=1}^{r} (U_i^T\, b_1)/\sigma_i$$

3. Statistical Considerations

Once one has calculated the solution of (2.1) by iterating (2.7), it is desirable to give error estimates for the solution. For this we consider the the last iteration.
The vector b_1 of (2.7) coincides with the measured data $\bar{c}$ up to the bias $c(\cdot, P)$. Therefore the components b_1^i $(1 \le i \le N)$ of the vector b_1 can be viewed as statistical independent random variables with mean value $\tilde{b}_1^i$ and variance σ, which equals the variance of the measured data $\bar{c}_i$.
Then one gets for the expected value :

$$E(b_1^i) = \tilde{b}_1^i \quad , \qquad i = 1, \cdots, N$$

and for the covariances of b_1^i

$$cov(b_1^i, b_1^j) \;=\; E\big((b_1^i - \tilde{b}_1^i)(b_1^j - \tilde{b}_1^j)\big) \;=\; \begin{cases} \sigma^2 & \text{if } i = j \\ 0 & \text{otherwise} \end{cases}$$

Under these assumptions the solution ΔP of (2.7) can be viewed as random variable too and because ΔP is given by $\mathcal{V}\ \Sigma_r^+\ U^T b_1$ we obtain the expected value of ΔP

$$E(\Delta P) = \mathcal{V}\ \Sigma_r^+\ U^T \tilde{b}_1$$

Thus we have for the covariance matrix (see [10], p 182)

$$E(\ (\Delta P - E(\Delta P))\ (\Delta P - E(\Delta P))^T) \;=\; \sigma^2\ \mathcal{V}\ (\Sigma_r^+)^2\ \mathcal{V}^T \;\equiv \mathcal{C}$$

From this we also get the correlation coefficients $cor(\Delta P_i, \Delta P_j)$ for the solution, which indicate how much the computed parameter ΔP_i depends on the computed parameter ΔP_j. We have

$$cor(\Delta P_i, \Delta P_j) = \frac{C_{i,j}}{\sqrt{C_{i,i}C_{j,j}}} \quad , \qquad i,j = 1,\cdots,N$$

4. Singular Jacobian

Sometimes it is known in advance or detected in previous runs that the Jacobian J in (2.7) is singular. This may have different reasons

- there exists no connexion between some zones
- some combinations of parameters cannot be identified numerically because some zones are hardly influenced by the given injections into other zones.

In this case it is interesting to know which parameters or combinations of parameters lie in the kernel of J and thus cannot be identified. We get the (numerical) null space from the singular value decomposition of R_1

$$\text{null}\, J = \text{span}\{V_{r+1}, \ldots, V_N\} \tag{3.1}$$

But, to draw conclusions on which parameters are identifiable and on the experimental settings, we need a special type of basis for the kernel where each basis vector has as many zero components as possible. The remaining (hopefully) few nonzero components can be interpreted as coefficients of those linear combinations of parameters that cannot be identified — at least by the current experimental settings.

It is well known that computing a 'sparsest null space basis' cannot be done efficiently. Therefore one has to resort to heuristic algorithms which compute a nearly optimal basis. In our case we propose the following simple algorithm. Let k denote the dimension of the null space (here $k = N - r$), and $z^1, \ldots, z^k$ a basis for it. We start with $z^j = V_{r+j}$, $1 \le i \le k$. We now try to replace each of these basis vectors z^j by a vector with fewer nonzero components. We describe the first step only, the same technique is applied to the remaining vectors — theoretically by renumbering the vectors z^j. For ease of presentation let us rename z^1 to z.

We need some more notation. Let us define the 'indicator vector' χ

$$\chi_i = \begin{cases} 1 & \text{if } z_i = 0 \text{ (or should be 0)} \\ 0 & \text{if } z_i \text{ may be nonzero} \end{cases}$$

and

$$Z = (z^2, z^3, \ldots, z^k)$$

$$\alpha = \begin{pmatrix} \alpha_2 \\ \vdots \\ \alpha_k \end{pmatrix} \qquad \alpha_j \in \mathbb{R}$$

$$X = \mathrm{diag}(\chi_1, \ldots, \chi_N)$$

Note that in this notation the new basis vector $\tilde{z}$ has the representation $z + Z\alpha$.

We now proceed as follows

Loop over the following steps and the inner loop until we escape the inner loop because the maximum number of iterations is exceeded.

- Increase the number of components in z , that should equal 0 , by 1. For this select an index l at random for which $\chi_l = 0$ and set $\chi_l = 1$, i.e. z_l should become 0 , now.
- $\star$ Solve the least squares problem
  $e = \min_{\alpha} \|X(z + Z\alpha)\|_2$.
  Note that multiplication by X is 'shooting operator' which kills all components which are allowed to take nonzero values. If e is tiny, we have succeeded in finding the replacement vector $\tilde{z} = z + Z\alpha$ with just that vector α for which the minimum is attained.
- Set $e_o = e$.

Iterate the following step until we escape or the maximum number of iterations is exceeded.

- (Exchange step)
  Select indices i and j for which $\chi_i = 0$, $\chi_j = 1$ and set $\chi_i = 1$, $\chi_j = 0$. Perform step ($\star$) and escape if e is tiny. Otherwise proceed as in 'simulated annealing' (see [12] for an introduction).
  Accept this exchange if $e^{(e_o - e)/T} > \gamma$.
  Here γ is some constant $\gamma < 1$, $\gamma \approx 1$ and $T > 0$ is the simulated temperature which is driven to 0 gradually. Note that a step with $e < e_o$ is always accepted. Set $e_o = e$.
  Otherwise undo this exchange step.

5. Calculation of Intervals for the Parameters

Interval arithmetic gives a possibility of computing bounds for the parameters, if there exist bounds for the measurements. Analogous to calculating with real numbers, one can calculate with intervals using the following arithmetic

Let $\star \in \{ +, -, *, / \}$, $I_1 = [a,b]$ and $I_2 = [c,d]$ then we define $I_1 \star I_2 = \{x \star y \mid x \in I_1 \ \wedge \ y \in I_2\}$ where I_1/I_2 is defined only if $0 \notin I_2$.

This can be extended to vectors and matrices (see [4,6]).

Now we want to compute intervals bounding all parameters. For this the solution of the interval version of (2.3) is needed

$$\dot{c}(t,P) = A\,c(t,P) + g \quad , \qquad c(t_0,P) = c_0 \tag{5.1}$$

where now A is an interval matrix, $c(t,p)$ and c_0 are interval vectors. The interval differential equation (5.1) can now be solved by an algorithm due to R. Lohner[7]. This gives the interval solution $c(t,P)$ for a given parameter interval P. The parameter interval has again to be determined by solving (now an interval) nonlinear least squares problem. Similarly as in (2.1), given an interval vector $\bar{c}_i$ of measurements, an interval vector P containing all solutions of

$$\arg\min_{\tilde{P}} \sum_{i=0}^{m} \|c(t_i,\tilde{P}) - \tilde{c}_i\|_2 \qquad \text{for all} \qquad \tilde{c}_i \in \bar{c}_i \tag{5.2}$$

has to be determined. This can again be reduced to a sequence of linear interval least squares problems. Let ΔP be the interval vector containing all solutions of

$$\arg\min_{\widetilde{\Delta P}} \ \|J\,\widetilde{\Delta P} - b\|_2 \tag{5.3}$$

where J is an interval extension of the Jacobian in (2.7) and b is an ordinary vector given by

$$b = \begin{pmatrix} c(t_0,\breve{P}) - \breve{\bar{c}}_0 \\ \vdots \\ c(t_m,\breve{P}) - \breve{\bar{c}}_m \end{pmatrix}$$

where $\breve{P}$ denotes the midpoint of the interval vector P and $\breve{\bar{c}}_i$ denote the midpoints of the interval vectors $\bar{c}_i$, $0 \le i \le m$. Therefore the solution ΔP of (5.3) is an interval vector and can be obtained using an algorithm due to Neumaier[5].

The solution of (5.2) is again obtained by iteration

$$P^{k+1} = P^k + \Delta P^k$$

and this iteration terminates when $P^{k+1} \subset P^k$.

Numerical Example

We used the experimental setting of [11]. We were able to get the same results as quoted in [11] using 8 iterations. The results agreed within 3% in most cases and up to 12% in a few cases.
In addition we computed the correlation coefficients and variances. All initial values could be identified with a variance of about 1%. The variances of the interzonal airflows differ widely. We got the following results (the notation $i \rightarrow i$ denotes the sum of all outflows from zone i)

interzonal airflow between zones	variance[%]
1→9, 2→9, 3→9, 4→9, 5→9, 6→9, 7→9, 8→8, 9→8, 9→9	0 – 0.7
1→1	1.7
1→2, 2→2, 2→3, 3→3, 3→4, 4→4, 5→5, 6→6	2.5 – 9
6→7, 7→7, 8→7	14 – 18
8→1	86
8→2, 8→4, 8→5, 8→6	109 – 280
8→3	550

Furthermore the correlation coefficients between the initial concentrations and all the other parameters are quite small (about 10^{-3}) except the correlations of initial concentrations of connected zones which amount to 0.1 (approximately). Quite high correlations were found for the the following pairs of airflows $(9\rightarrow 8, 1\rightarrow 9)$, $(1\rightarrow 9, 2\rightarrow 9)$, $(4\rightarrow 9, 9\rightarrow 9)$ which amount to 0.914 , 0.956 , 0.916 , respectively.

Summary and Conclusions

We have presented a new technique for estimating the interzonal airflows from tracer gas measurements. We set up a system of differential equations for the time evolution of the concentrations in each zone. The interzonal airflows enter these differential equations as coefficients. These unknown coefficients as well as the unknown initial concentrations are numerically identified by solving a (nonlinear) least squares problem where one function evaluation amounts to solving these differential equations with given initial values and coefficients. With the aid of the Jacobian of this 'function' we are able to estimate variances for and correlations between the unknown quantities. Furthermore, studying the (numerical) null space of this Jacobian shows unidentifiable interzonal airflows (or combinations) and gives hints on possible optimizations of the experimental settings. If rigorous bounds (intervals) for the measured data are available there is also a technique for computing rigorous bounds for the interzonal airflows (intervals), provided the applicability of the underlying model is out of question.

References

[1] Hairer,E., Nørsett,S.P. and Wanner,G. *Solving ordinary differential equations I, Nonstiff problems* Springer, Berlin 1987

[2] Hairer,E. and Ostermann,A. *Dense output for extrapolation methods* report Universitè de Genéve, 1988

[3] Golub,G.H. und van Loan,Ch.F. *Matrix computations, second edition*
The John Hopkins University Press, Baltimore and London 1990

[4] Moore,R. *Intervallanalyse*
R. Oldenbourg Verlag, München, Wien 1969

[5] Neumaier,A. *Solving linear least squares problems by interval arithmetic* Freiburger Intervallberichte, 1987

[6] Neumaier,A. *Intervalmethods for systems of equations*
Cambridge University Press, Cambridge, 1990

[7] Lohner,R. *Enclosing the solution of ordinary initial and boundary value problems*
in E. Kaucher, U.Kulisch and Ch. Ullrich (eds) 'Computerarithmetic', Teubner, Stuttgart, 1987

[8] Louis,A.K. *Inverse und schlecht gestellte Probleme*
Teubner Studienbücher Mathematik, Stuttgart 1989

[9] Dennis,J.E.jr. and Schnabel,R.B. *Numerical methods for unconstrained optimization and nonlinear equations*
Prentice Hall Series in Computational Mathematics, Englewood Cliffs 1983

[10] Stoer,J. and Bulirsch,R. *Einführung in die Numerische Mathematik Band I und II* Springer Verlag, Heidelberg, Berlin, 1983

[11] Mattson,J.B. *An Experiment for Airflow determination by Quadratic Programming* Air Infiltration Review, Vol 11(4), 1990

[12] Press,W.H., Flannery,B.P., Teukolsky,S.A. and Vetterling,W.T. *Numerical Recipes*
Cambridge University Press, Cambridge, 1986

[13] GuitiZad,S. *Zur numerischen Identifizierung von Luftaustauschraten in Gebäuden*
Diplomarbeit am Institut für Geometrie und Praktische Mathematik, RWTH Aachen, 1991

AIR MOVEMENT & VENTILATION CONTROL WITHIN BUILDINGS

12th AIVC Conference, Ottawa, Canada
24-27 September, 1991

POSTER 34

Ventilation Effectiveness - The AIVC Guide

J R Waters , C E Brouns

Coventry Polytechnic
Department of Civil Engineering and Building
Priory Street
Coventry CV1 5FB
Great Britain

Fax: +44 (0)203-258597

1. SYNOPSIS

Sandberg and Skåret differentiate between the terms air change efficiency and ventilation effectiveness. Air change efficiency is a measure of how effectively the air present in a room is replaced by fresh air from the ventilation system whereas ventilation effectiveness is a measure of how quickly an air-borne contaminant is removed from the room. The AIVC guide covers ventilation effectiveness and related concepts. It shows the origins of the concepts used, provides proofs of essential formulae, and suggests standard symbols and definitions. It also recommends methods of measurement, and discusses the range of application of the concepts.

2. LIST OF SYMBOLS

Symbols		Units
t	time	s
τ_n	nominal time constant for the ventilation air	s
τ_n^c	nominal time constant for the contaminant	s
$\bar{\tau}_e^c$	local mean age of contaminant at the exhaust duct	s
$\bar{\tau}_p^c$	local mean age of contaminant at point p	s
$<\bar{\tau}^c>$	room mean age of contaminant	s
D_p	total dosage index	s
T_{pn}	transfer index	s/m^3
U_p	local purging flow rate	m^3/s
ε^c	ventilation effectiveness	
η^c	contaminant removal efficiency	
ε_p^c	local air quality index	
$C_p(t)$	concentration of contaminant at point p at time t	
$C_e(t)$	concentration of contaminant at exhaust duct at time t	
C_s	concentration of contaminant in supply duct	
$C(0)$	initial concentration of contaminant in the room	
$<C(t)>$	room mean concentration of contaminant	
C_i	concentration of contaminant in zone i	
V	room volume	m^3
V_c	equivalent volume of contaminant in the room	m^3
V_{ci}	equivalent volume of contaminant in zone i	m^3
Q	airflow rate from the supply duct	m^3/s
q_i	injection rate of contaminant in zone i	m^3/s
F_{ij}	air flow rate from zone i to zone j	m^3/s

3. INTRODUCTION AND OBJECTIVES

The concept of ventilation effectiveness is now well established in research literature as an index of the removal of contaminants from a ventilated space.

The theoretical background has been fully described by Sandberg [1,2,3], Skåret [4] and others, and many examples of its application have been described. The purpose of the AIVC guide on ventilation effectiveness is to encourage the use of the concepts outside the research field in the area of general practice, both as a design tool and as a means of measurement. In fulfilling this purpose, three objectives were identified. The first is the standardisation of the definitions and symbols used for the various indices which fall within the overall concept of ventilation effectiveness. The second is to provide examples of the application of the concept to the idealised cases of fully mixed flow and piston (or displacement) flow in a single zone, with further examples showing the effect of extending the representation of a ventilated space to more than one zone. The third is to give guidance on the interpretation of the values obtained, especially for ventilation effectiveness itself.

In preparing the guide, it was assumed that the principal readership would be practitioners who were wishing to use the concept for the first time, and that experts would wish to consult the document in order to use standardised definitions and symbols. Consequently, the only section of the guide which is in any way new is the section on the interpretation of ventilation effectiveness values, where it has been found that there is as yet insufficient evidence to suggest a common approach.

4. SELECTION AND DEFINITION OF VENTILATION EFFECTIVENESS INDICES

The two most fundamental indices are ventilation effectiveness and local air quality index. In addition to those, it was decided to include some other indices which provide a measure of the effect of a contaminant within a ventilated space, even though they may not be in general use at the present time. For example, the local purging flow rate has been included on the grounds that it is closely related to the local air quality index, and because it forms a link to the more important dosage index. Also, in forming the definitions, it was decided to use net contaminant concentration values rather than absolute values. In other words, the existing contaminant concentration in the outside or air supply is taken as zero, and concentration levels within the ventilated space are measured above this. This provides clearer and simpler definitions without any loss of generality. It was also considered important to choose the simplest and most obvious definitions. The definitions which have been included therefore are as follows.

Nominal Time Constant for the Contaminant (τ_n^c)

The ratio between the equivalent volume of contaminant in the room and the contaminant injection rate:

$$\tau_n^c = \frac{V_c}{q} = \frac{V.\langle C(\infty)\rangle}{q}$$

Ventilation Effectiveness (ε^c)

The ratio between the steady state concentration of contaminant at the exhaust duct and the steady state mean concentration of contaminant in the room:

$$\varepsilon^c = \frac{C_e(\infty)}{\langle C(\infty) \rangle}$$

Contaminant Removal Efficiency (η^c)

$$\eta^c = \frac{\varepsilon^c}{\varepsilon^c + 1}$$

Local Air Quality Index (ε_p^c)

The ratio between the steady state concentration of contaminant at the exhaust duct and the steady state concentration of contaminant at a point p in the room:

$$\varepsilon_p^c = \frac{C_e(\infty)}{C_p(\infty)}$$

Local Purging Flow Rate (U_p)

The ratio between the contaminant injection rate at a point p and the steady state contaminant concentration at that point:

$$U_p = \frac{q_p}{C_p(\infty)}$$

The Dosage Index (D_p)

The time integral of the contaminant concentration at a point p. If the integral is over all time, it is called the total dosage index:

$$D_p = \int_0^\tau C_p(t).dt$$

Transfer Index (T_{pn})

The transfer index at point p due to a sudden release of contaminant at point n is the total dosage index at p per unit volume of contaminant released at n:

$$T_{pn} = \frac{D_{pn}}{V_{cn}}$$

The defining equations for some of the indices can be cast in alternative forms, and the most useful alternatives are included alongside the original definitions. Provided certain conditions are met, it is also possible to write equations linking some of the indices, and these too have been included.

5. IDEALISED EXAMPLES

The value of the ventilation effectiveness, ε^c, has been evaluated for a series of idealised examples. There were three reasons for doing this. Firstly, it provides a simple demonstration of the evaluation process; secondly, it shows how the ventilation effectiveness depends on the distribution of contaminant injection; and thirdly, it provides a base of idealised values which can be used for comparison with ventilation effectiveness values in real situations. The strategy in presenting this in the guide has been to start by treating the ventilated space in the simplest possible way as a single zone. This is analysed in fully mixed flow and then in piston flow. Then the effect of improving the representation of the space, first as two zones (a model which appears frequently in the literature [1,4]), and then four zones is considered. Between them, the single zone, the two zone and the four zone models provide a useful indication of the range and pattern of values that may be expected for ventilation effectiveness. The possibility of using one of the CFD models which are now available is also mentioned but not described in detail; models of this type are reviewed in AIVC technical note 33. In evaluating these idealised cases, it has also been assumed that the contaminant is "passive", that is, it mixes immediately with the air without any momentum of its own. Although the indices are also valid for "active" contaminants, it is difficult to find a generalised way of dealing with them.

6. RESULTS OF THE IDEALISED EXAMPLES

Piston (displacement) flow is of particular interest because it is often considered to be the most efficient method of removing contaminants from a space. Figure 1 shows the results for true piston flow in a single zone for four different patterns of contaminant injection. The four patterns correspond to:

(i) uniform injection throughout the whole space,
(ii) localised injection accross a plane,
(iii) uniform injection in a region close to the inlet duct, and
(iv) uniform injection in a region close to the exhaust duct.

The results show the extent to which the ventilation effectiveness depends on the injection pattern; all values between unity and infinity are possible.

The results for the two zone model are shown in Figure 2, which is the well known plot of ventilation effectiveness versus recirculation factor. An interesting feature of this model is that it is capable of showing the effect of short-circuiting of ventilation effectiveness between the inlet and outlet ducts, a phenomenon which gives ventilation effectiveness values below unity. Also, as the recirculation factor increases, the properties associated with the fully mixed model become more dominant. When the recirculation factor exceeds approximately 4.5, the ventilation regime is essentially fully mixed.

The results for a four zone model have been included as an example of multizone modelling, and to illustrate the effect of greater model detail. The results, shown in Figures 3 and 4 are not very different from the two zone model, except for the case of an impermeable partition between two of the zones. Again, the model is similar to the fully mixed case when the recirculation factor is greater than about 4.5.

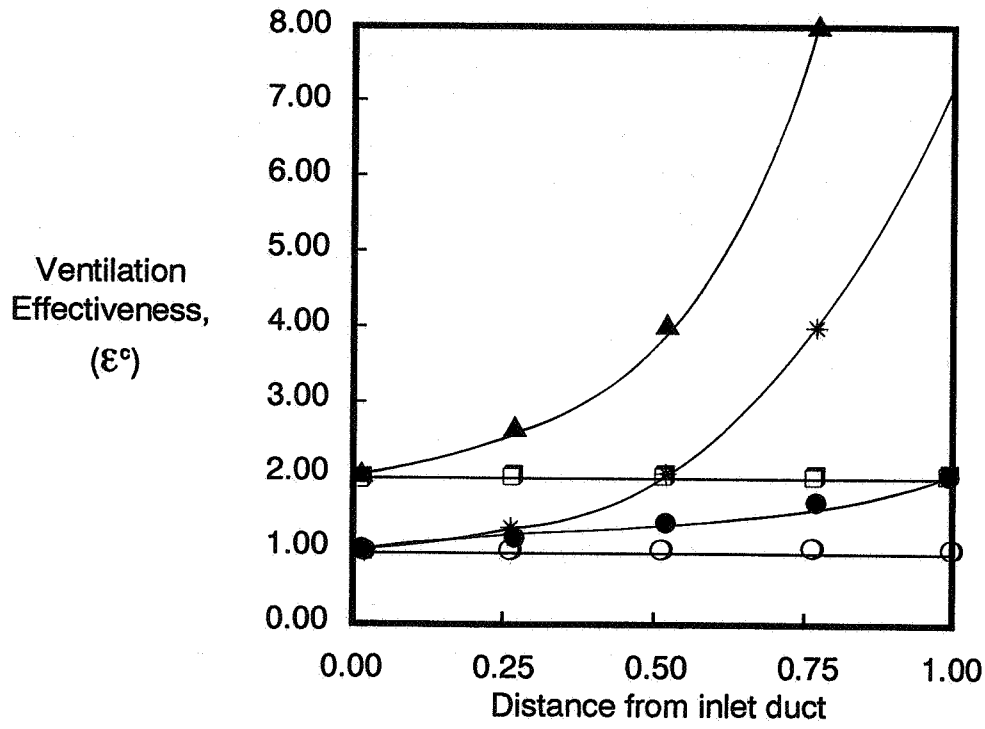


Figure 1 - Ventilation Effectiveness versus distance of contaminant source from inlet duct.

Key:

- Fully mixed flow
- Uniform injection throughout the whole space
- Localised injection accross a plane
- Localised injection in a region close to the inlet duct
- Localised injection in a region close to the outlet duct

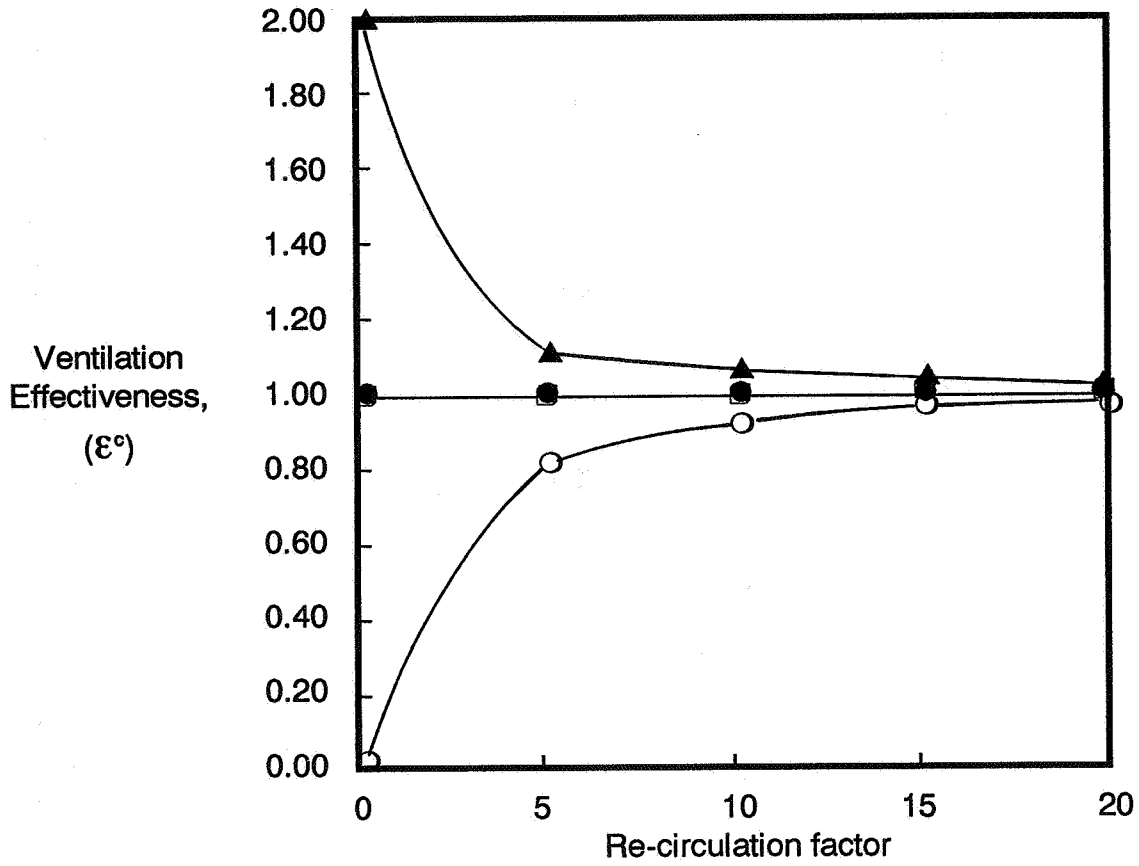


Figure 2 - Ventilation Effectiveness versus Re-circulation factor for a two zone model.

Key:

- Injection in the unoccupied zone for a short-circuiting flow
- Injection in the unoccupied zone for a piston flow
- Injection in the occupied zone for a short-circuiting flow
- Injection in the occupied zone for a piston flow

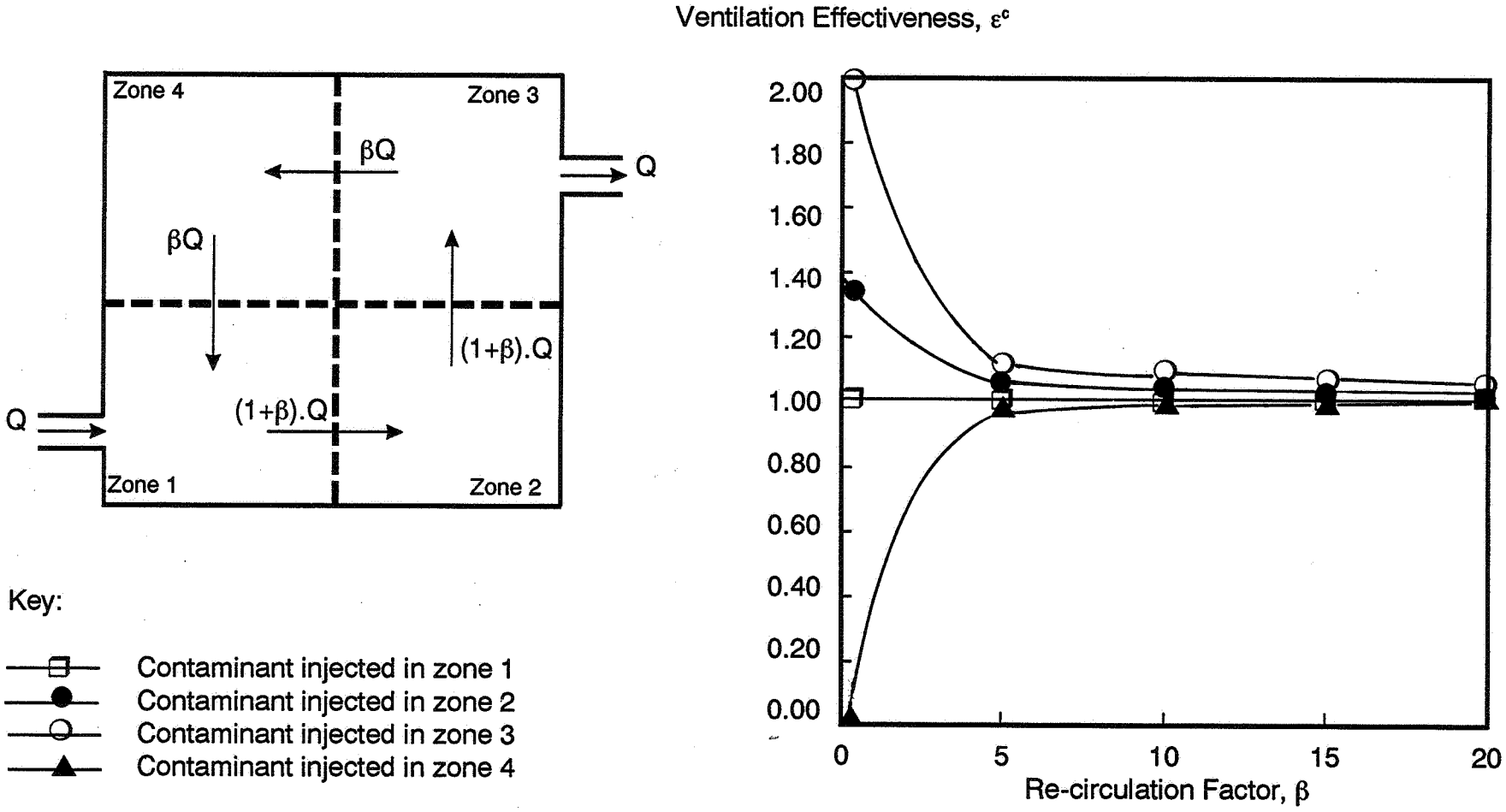
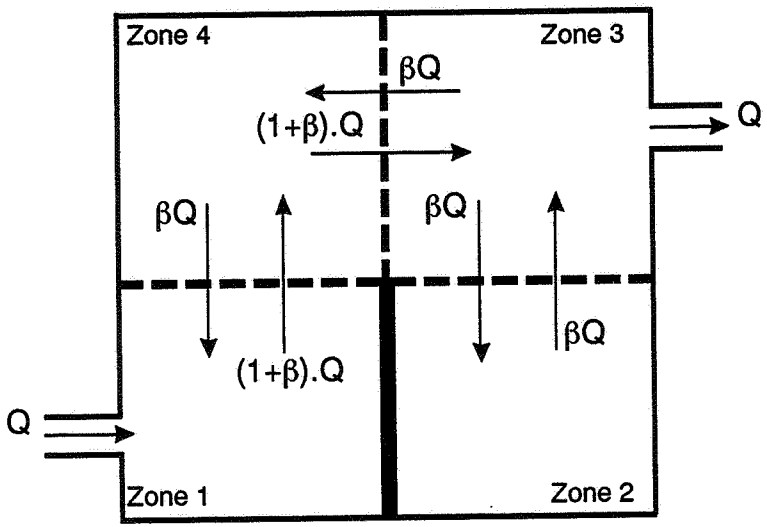


Figure 3 - Ventilation Effectiveness versus Re-circulation factor for a four zone partitioned model.



Key:

Contaminant injected in zone 1
Contaminant injected in zone 2
Contaminant injected in zone 3
Contaminant injected in zone 4

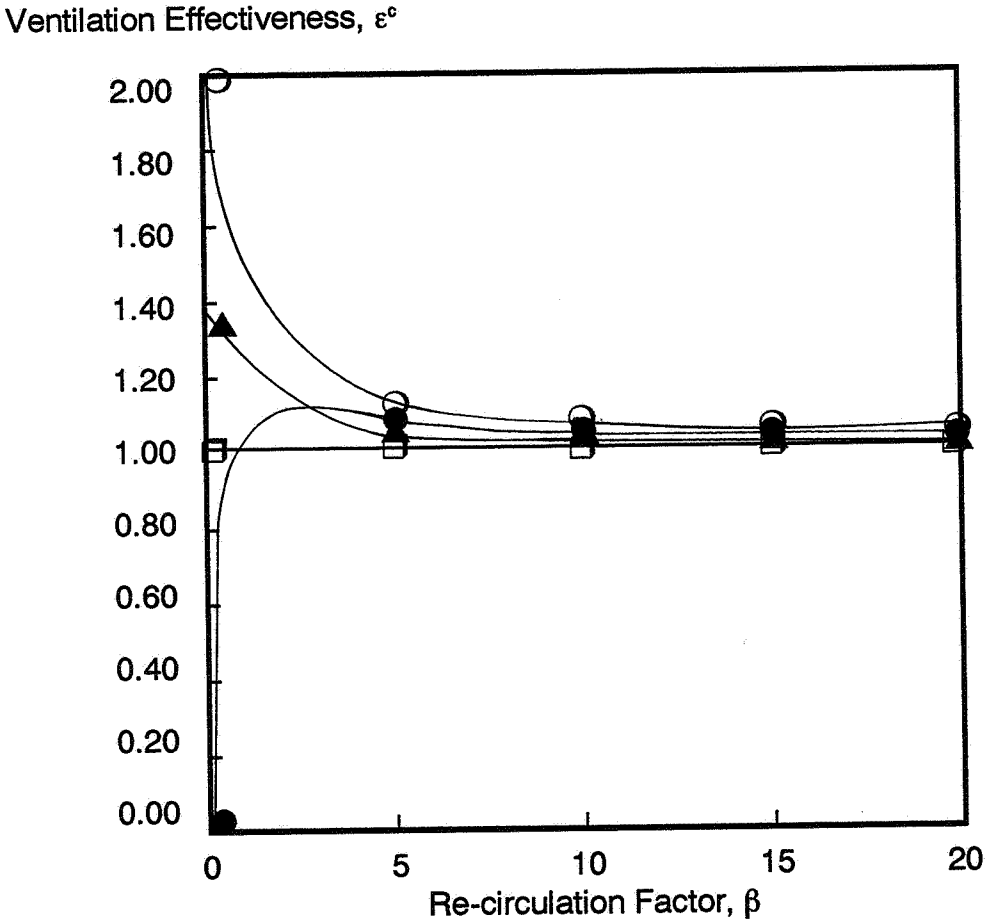


Figure 4 - Ventilation Effectiveness versus Re-circulation factor for a four zone re-circulation model.

7. METHODS OF MEASUREMENT

In order to determine any of the indices, it is necessary to measure the concentration of the contaminant at the appropriate points in the room. If it is not possible to use the contaminant itself, a tracer which imitates the behaviour of the contaminant may be used. All of the indices defined in paragraph 4 may be determined by direct measurement of the appropriate equilibrium contaminant concentration. However, there are two difficulties in using this method. Firstly, in some cases it is necessary to find the room average concentration, $\langle C(\infty) \rangle$, which may require measurements to be made at a large number of positions within the space. Secondly, if the time constant of the system is long, it may be necessary to continue measurements for an unacceptably long time in order to achieve equilibrium. Consequently, the guide suggests that it is often better to derive the required index from measurements of the time evolution of contaminant concentration.

8. INTERPRETATION AND APPLICATION

The indices fall in two groups. On the one hand, τ_n^c, ε^c, and η_c are indices of the whole space. On the other hand, ε_p^c, U_p, D_p, D_{pn}, T_{pn} all refer to a specific point. In the case of the whole space, it is a matter of choice whether to use ε^c or η^c. The former is immediately meaningful in terms of contaminant concentration ratios, whereas the latter has the advantage of always being within the range zero to unity. No recommendation is made as to which should be used.

The biggest problem with the ventilation effectiveness index is the interpretation of particular values. The results for the idealised examples showed that, except for fully mixed flow, the value is highly sensitive to the position and distribution of the contaminant source. Consequently, the value of the ventilation effectiveness taken on its own is not sufficient to make a judgement on the success of a ventilation system in removing a contaminant. There are several possible solutions to this problem. For example, if it is accepted that piston flow is the most efficient type of ventilation system, a value for ε^c could be compared with the value that would have been obtained if a piston flow had been installed. The comparison could be made with one of the four cases described above, presumably taking the idealised case whose contaminant distribution is most similar to the real case. One could then define a ventilation effectiveness ratio, r^c, such that:

$$r^c = \frac{\varepsilon^c(\text{real})}{\varepsilon^c(\text{piston})}$$

The value of r^c, which must lie in the range 0 to 1 (and could therefore be expressed as a percentage), gives a single figure indication of the performance of the system as a proportion of the best possible performance for the given contaminant distribution. It has also been suggested [5] that a critical feature of any ventilation system is its ability to sweep out a contaminant after injection has ceased. The nominal time constant of the contaminant is a measure of this, and again one could take the ratio between τ_n^c for the real system and τ_n^c for an idealised piston flow system in the same space. However, this leads to the same result as before, provided the nominal time constant for the ventilating air is the same in both the real and idealised cases, because:

$$r^c = \frac{\varepsilon^c(\text{real})}{\varepsilon^c(\text{piston})}$$

$$= \frac{\tau_n^c}{\tau_n}(\text{real}).\frac{\tau_n}{\tau_n^c}(\text{piston})$$

$$= \frac{\tau_n^c(\text{real})}{\tau_n^c(\text{piston})}$$

An alternative approach is to produce a simple parametric model. Most ventilation systems fall between the two extremes of fully mixed flow and piston flow. Indeed, whereas piston flow may be the ideal way of removing contaminants, mixing is necessary in order to provide uniform temperature and humidity. A simple three parameter model can be constructed by combining them, so that the parameters are the nominal time constant of the ventilating air for both types of flow, and the proportions in which they are mixed. The poster display gives some examples of the properties of such a model. The interpretation of the local indices follow directly from their definition. The local air quality index is the local equivalent of the ventilation effectiveness; the local purging flow rate is essentially measuring the same thing but in units of flow.

REFERENCES:

1. Sandberg, M.: 'What is ventilation efficiency?'. Building and Environment, Vol.16, Part 2, 1981, pp123-135.
2. Sandberg, M.: 'Ventilation efficiency as a guide to design'. Ashrae Transactions'83, Vol.89, Part II.
3. Sandberg, M.; Skåret, E. and Mathisen, H.M.: 'Air change and ventilation efficiency - New aids for hvac designers'. A report from the Nordic Ventilation Group, The National Swedish Building Research Institute, 1988.
4. Skåret, E.: 'Ventilation efficiency - A survey of concepts of ventilation effectiveness'. Sintef report STF15 - A84057, 1984.
5. Shaw, C.Y.: Private communication, May 1991.

AIR MOVEMENT & VENTILATION CONTROL WITHIN BUILDINGS

12th AIVC Conference, Ottawa, Canada
24-27 September, 1991

POSTER 35

Investigation of a combined ventilation and heating system for resedential buildings

Prof. Dr.-Ing. F. Steimle, Dipl.-Ing. B.Mengede, Dipl.-Ing. J. Röben

Universität Essen
Angewandte Thermodynamik und Klimatechnik
Universitätsstr.15, W-4300 Essen 1, Federal Republic of Germany

Telephone 49 (0)201/183-2600
Telefax 49 (0)201/183-2584

Investigation of a combined ventilation and heating system for resedential buildings

Synopsis

Combined ventilation and heating systems in floors demand extensive investigations about the heat transfer before they could be installed in residential buildings. For basic investigation about the heat transfer two experimental plants with different duct geometries are build in a laboratory of the University of Essen. Especially the measurements of temperature on different places of the plants are taken to determine the heat transfer at the two floors. The evaluation of the test data show that a floor with a cavity which is built with cones is unqualified for a combined ventilation and heating system. The difference of the temperature between the air inlet and the room is too low, because the heat loss at the floor surface is too high. A good combination is the air duct system which is ending in an area of 1000 mm lenght containing a cavity which is built with cones. This system guarantees sufficient high temperature at the air inlet to obtain a comfortable room temperature.

List of symbols

k	coefficient of heat transmission [W/m^2K]
L	lenght [m]
q	heat flux [W/m^2]
Q	heat flow [W]
t	temperature [°C]
$\triangle T$	difference of temperature [K]

Subscrips

c	convective
log	logarithm
RL	indoor air
tot	total
0	reference level

1. Introduction

Residential buildings are now better insulated than ever before because of the energy saving issues. Consequently the tightness of the buildings is increasing, but this requires the application of mechanical ventilation systems. On the European market today a lot of ventilation systems combined with conventional heating systems are already available. Another possibility is the use of a warm air heating system which combines ventilation and heating in the building. Basic investigations about the heat transfer of these systems are accomplished on two experimental plants with a great variation of working parameters. Hereby floors with different duct geometries are put in operation. To assess the working quality the splitting of heat flows into a part which release heat through the floor surface and a part which is transported by air is of particular interest.

2. Description of testing plants

The testing plants (Fig. 1) consist of two materials, the lower layer is heat insulating polyurethan and the upper layer is finish floor.

The difference between the two plants is the intermediate layer, which is in plant 1 a cavity built with cones and in plant 2 ducts which are cut in an additional layer of polyurethan. One of the ducts is also equipped with cones. Both ducts are ending in a cavity of one meter length built with cones and the supply air flows through the air inlet into the room. The outlet grilles should be installed in front of the external wall.

The supply air is heated up by a water/air heat exchanger which is admitted with electrical heated water. The temperature of the supply air at the entrance of the testing area variies between 29°C and 39°C. The range of variation of the supply air temperature during one serie of experiments was always lower than 3K. The difference between the supply air and the internal temperature was only 10K because of an insufficient cooling of the room.

The temperature sensors are installed at the entrance in the floor, the beginnig (axis A) and the end (axis B) of the testing area and also at the

inlet grille, see Fig. 1. For the determination of the air volume flow a device basing on the thermoanemometrical principle is installed over the inlet grilles.

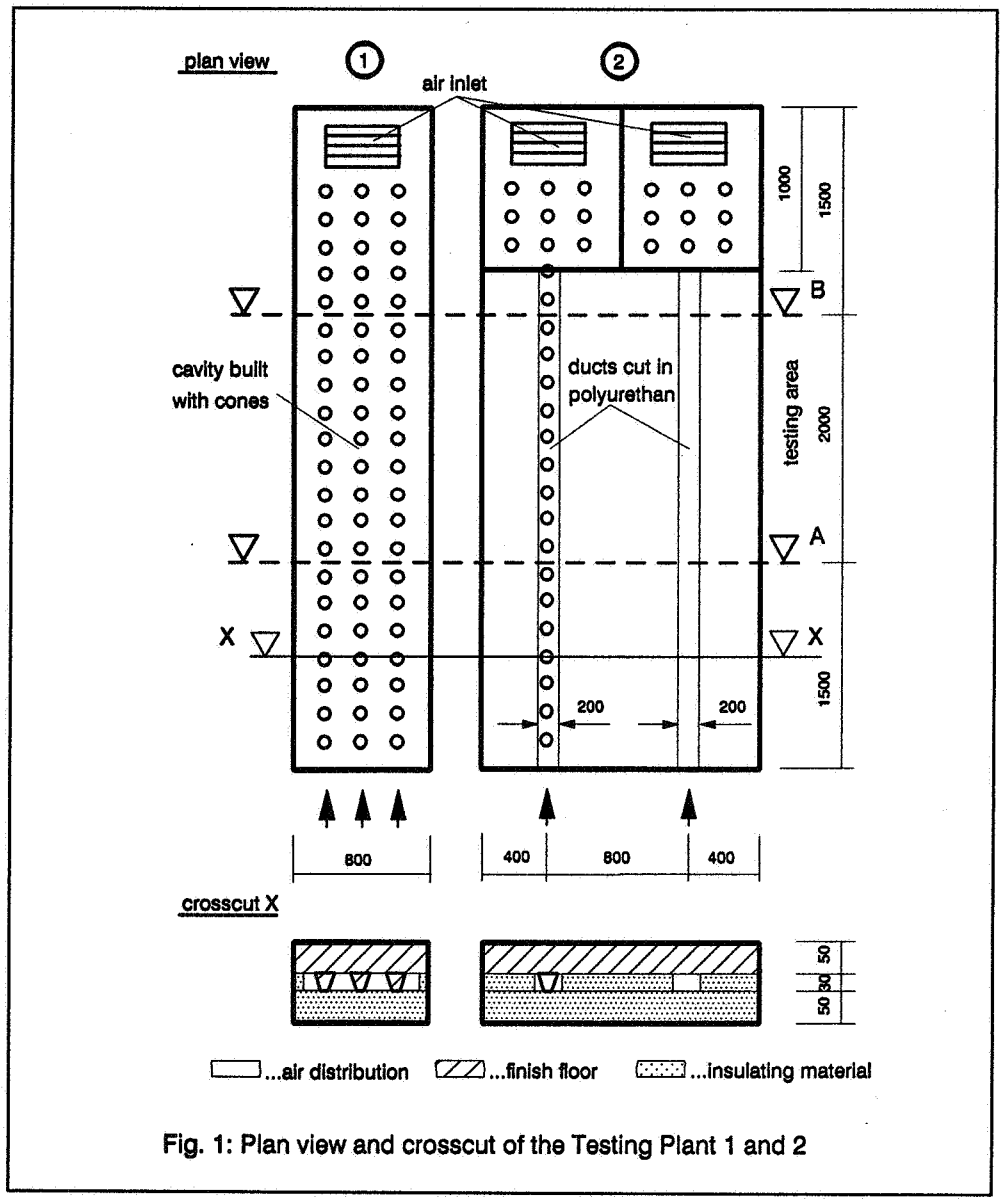


Fig. 1: Plan view and crosscut of the Testing Plant 1 and 2

3. Measurements and results

For a better understanding the results of the testing plant 1 and 2 are directly compared.

Fig. 2 and 3 show the temperature difference between the axis A and B as well as the convective heat loss related to the air flow rate. The

temperature difference is standardized by the relation to the length of the testing area. As convective heat loss is considered from the supply air in the duct respectively the cavity to the floor surface. For the testing plant 1 the convective heat loss is related to the whole testing area (W/m^2), whereas for the plant 2 it is relative to the length of the ducts (W/m). The convective heat loss of the duct system depends only on the air flow rate and the temperature difference; for the cavity system also the width takes influence on the heat loss.

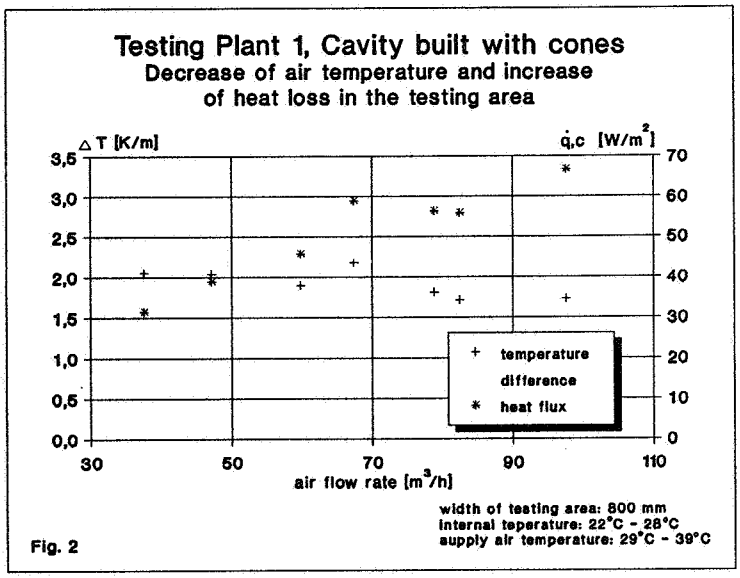


Fig. 2

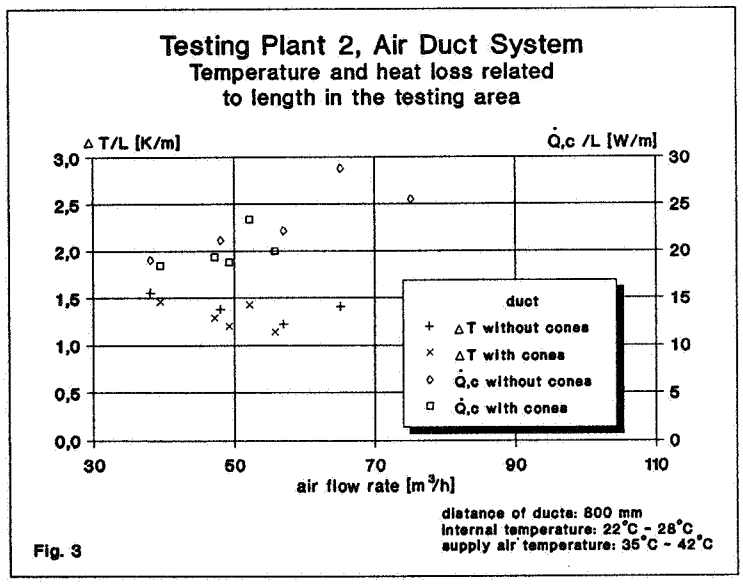


Fig. 3

It is evident that for both systems the temperature difference decreases slightly, whereas the convective heat loss rises strongly with increasing air flow rate. Considering an air flow rate of 50 m^3/h the temperature difference of plant 1 is 2K, of plant 2 only 1,3K.

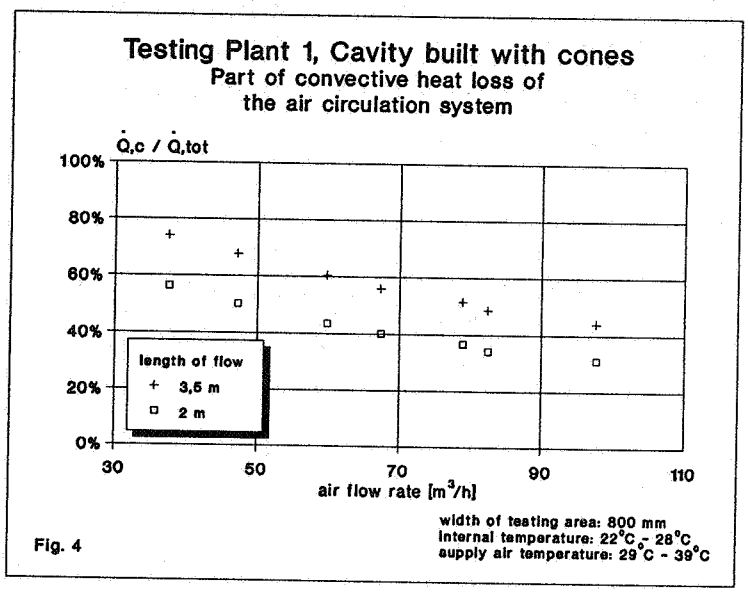


Fig. 4

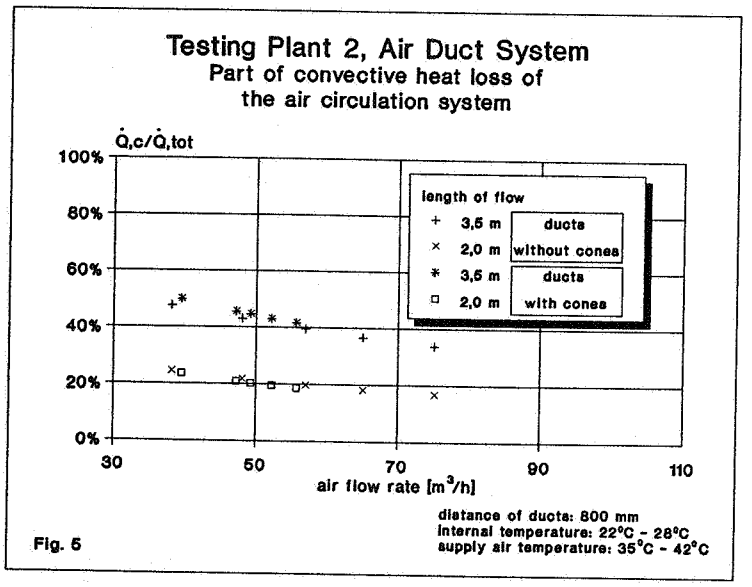


Fig. 5

Fig. 4 and 5 show the part of convective heat loss of the air circulation system related to the air flow rate. For an air flow rate like in practice of 40 m^3/h the part of the surface heating in the testing plant 2 is 40%, whereas in plant 1 it's greater than 70% because of the great storing capacity of the floor. This effects low temperatures at the air inlet so that

the system 1 is not qualified for the transport of warm air over a long way. On the other hand the temperature at the air inlet of the system 2 is high enough to guarantee a good performance of the combined ventilation and heating system. The controllability is also better as in system 1.

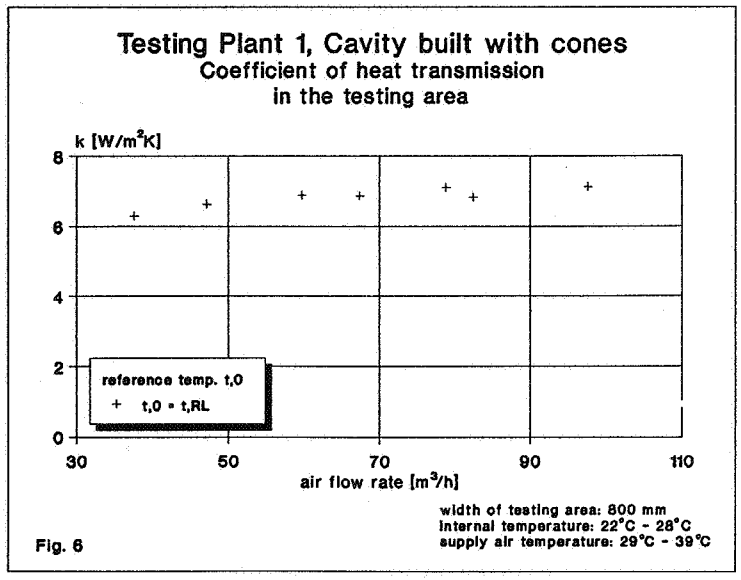


Fig. 6

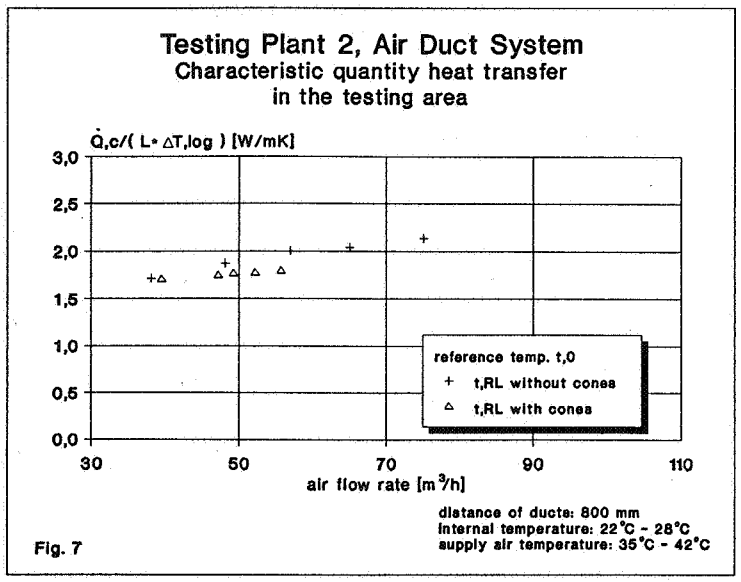


Fig. 7

The coefficient of heat transmission related to the air flow rate is shown in Fig. 6 and the characteristic quantity heat transfer in Fig. 7. These two figures are compared directly, because the distance of the ducts is the same as the width of the testing area (800 mm). Only for a distance lower than 500 mm the characteristic quantity is depending on the distance of

the ducts. The coefficient of heat transmission in Fig. 6 with approximately 7 W/m^2K is too high for a combined ventilation and heating system (see also Fig. 2). Fig. 7 shows evidently lower values.

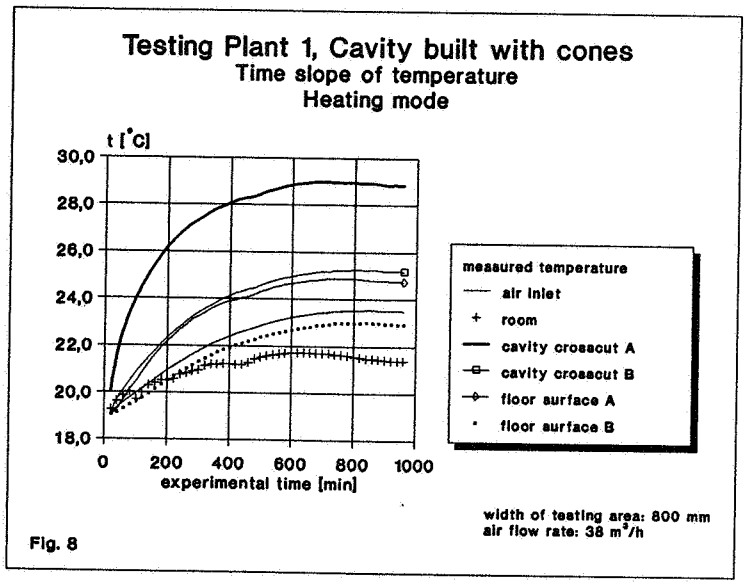


Fig. 8

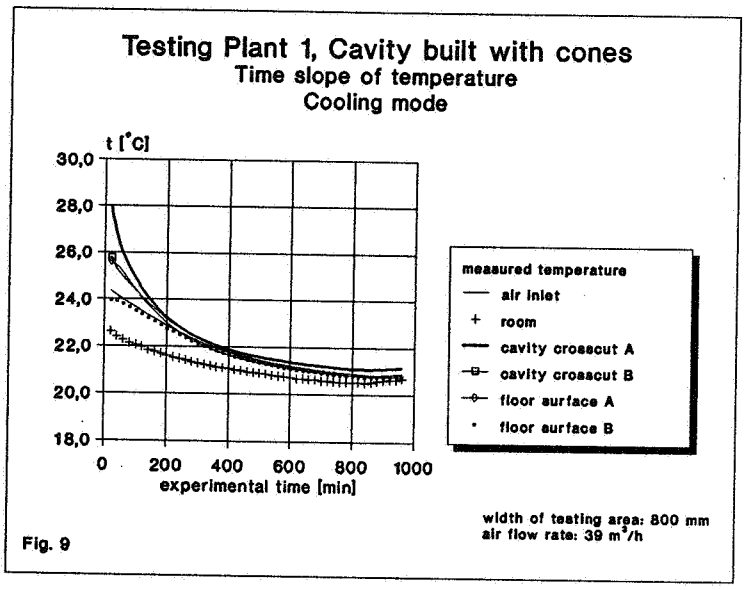


Fig. 9

The influence of the thermal inertia of the cavity floor construction for the heating respectively the cooling mode is recognizable in Fig. 8 and 9. Only after 10h working time the storage process in the floor was finished and the difference between the temperature at the air inlet and the room temperature is too low. Fig. 10 and 11 show a lower thermal inertia because the storing capacity is not so high. At the air inlet of the cavity

floor built with cones the temperature increase about 2K after 300 min whereas the temperature at the air duct system increase about 2K after 30 min.

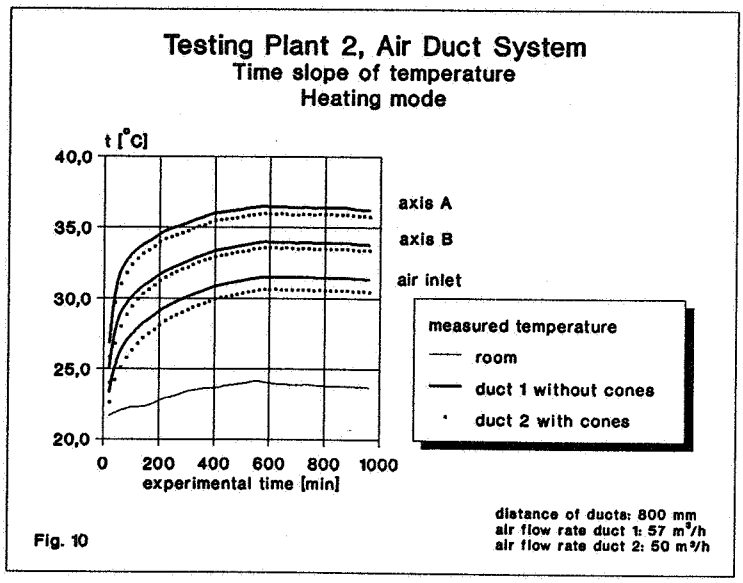


Fig. 10

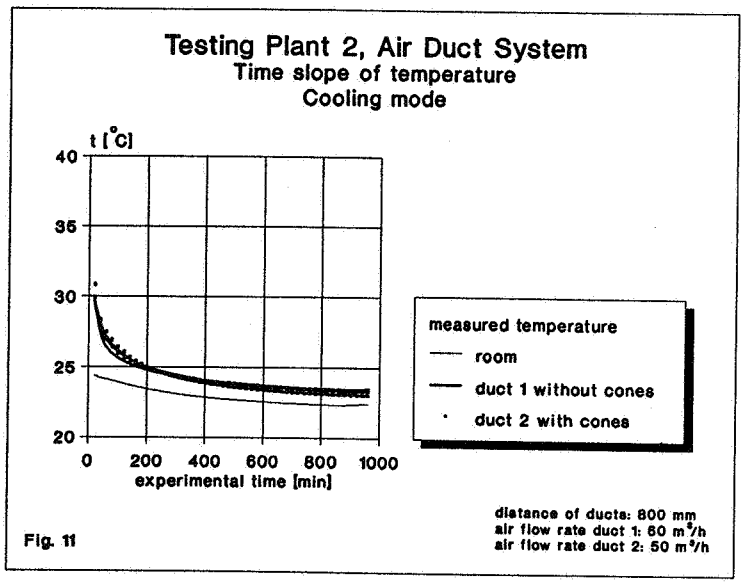


Fig. 11

The investigation showed that the pressure drop of the duct equipped with cones is much to high for practical applications. For this reasons this construction is not further considered.

4. Summary

The results of the measurements have shown that the floor with a cavity built with cones is unsuitable for a combined ventilation and heating system. The heat loss at the floor surface is too high so that the supply air temperature at the air inlet is not sufficient for room heating. There is, therefore, also a risk of air draughts in the occupied zone.

The advantages of the air duct system with a cavity area at the end are the compensation of the low temperature at the cold external walls or windows by the veil of warm air. Because of the high temperatures at the inlet grille the system guarantees a good performance combined with a controllability.

5. References

[1] GLIMPEL, TH.
"Stationäre Wärmeleitung und Temperaturverteilung in warmluftdurchströmten Fußbodenkonstruktionen"
Dissertation Universität Essen (1990)

[2] IHLE, C.
"Hinweise zur Planung von Lüftungs- und Luftheizungsanlagen"
sbz 22, 1983, pp1498-1506 (Part 1) and sbz 23, 1983, pp1549-1558 (Part 2)

[3] MADAUS, C.
"Warmluft-Zentralheizungen"
TAB No.6, 1987, pp505 f.

[4] SCHLAPMANN, D.
"Konvektiver Wärmeübergang an beheiztenFußböden"
Diss. VDI Berichte Reihe 6, No.97, Düsseldorf 1982

AIR MOVEMENT & VENTILATION CONTROL WITHIN BUILDINGS

12th AIVC Conference, Ottawa, Canada
24-27 September, 1991

POSTER 36

THERMAL COUPLING OF LEAKAGE AIRFLOWS AND HEATING LOAD IN BUILDING COMPONENTS AND BUILDINGS

MARKKU VIRTANEN

Laboratory of Heating and Ventilation
Technical Research Centre of Finland
Lämpömiehenkuja 3
SF-02150 Espoo 15
Finland

SYNOPSIS

Simulation models basing on 2-dimensional finite-difference approach were developed for the steady-state and dynamic analyses of the thermal coupling of leakage airflows and building components. The considered types of leakage flows were crack flow and filtration through porous materials. At building level analyses a static flow network approach was applied in order to calculate airflow balance of a building, while for the thermal coupling of convective heat flows of air leakages and transmission heat flows of leaky structures a 2-dimensional modified transfer-function approach was applied.

It is suggested in the paper that the value of transmission heat losses should be corrected by a factor, modified Nusselt number, in order to take into account the heat recovery effect of leakage airflows. Depending on leakage airflow rate, thermal properties and dimensions of the structure as well as the leakage route, the correction factor of transmission heat losses can be as low as 0.60. The correction factor of total heat losses can be 0.86, respectively. According to measurements the correction factor of transmission heat losses was 0.35-0.85, while it for total heat losses was 0.86-0.96. The heat recovery effect is approximately the same for both infiltration and exfiltration.

At the building level, the correlation between airtightness, leakage distribution, air change rates and thermal performance of a single family house was analyzed. The house was supplied with mechanical exhaust ventilation system and the supply air was taken in as leakages through building envelope. The calculated annual heating energy consumption of the building was 6-9 % less compared with the calculation results where the heat recovery effect was not taken into account. If the heat recovery effect was taken into account in calculation of transmission heat losses, the average correction factor was 0.85-0.90. Actual values depend on airtightness and leakage distribution of building envelope.

1. INTRODUCTION

The actual heating load of a building often differs from the designed load. One reason for this is the uncontrolled ventilation through a building envelope. Differences in calculated and measured heating loads have usually been explained with the uncontrolled ventilation using the leakage ventilation rate as a correction parameter of heating load analyses. Hydraulic properties of different leakage routes have been studied widely and leakage flow rates can nowadays be predicted rather well. The thermal coupling of leakage flows and heating load has not, however, been studied and therefore the heating load of leakage ventilation has been calculated according to the leakage flow rate and the temperature difference of inside and outside air.

The thermal coupling of leakage airflows and conduction heat flows of structures has been omitted. Nevertheless, if we consider for example through a structure infiltrating air, the cold outside air is heated by conduction heat flows inside a structure before it

enters the room space. Due to infiltrating airflow also the conduction heat flow at the interior surface is increased. If we consider the interior surface as control surface of the system, the total heating load due to convection heat losses of infiltrating air and conduction heat losses of a structure is less compared with the case where pure conduction of a structure occurs and infiltrating air is assumed to flow in at outside temperature. The difference in the total heating load is due to the heat recovery effect of infiltrating air.

In this paper the effect of both infiltrating and exfiltrating airflows on thermal behavior of structures are considered. The considered flow cases are crack flow and filtrating airflow through porous materials. The interaction of airflows and heat transfer in structures is analyzed by computer simulation using the finite difference approach. Some results of experiments will also be shown.

In building simulation the correlation between airtightness, leakage distribution, air change rates and thermal performance will be considered. In analyses a static flow network approach was applied in order to calculate the airflow balance of a building, while for heating load calculation of leaky wall structures a 2-dimensional modified transfer-function approximation was applied.

2. INFLUENCES OF LEAKAGE AIRFLOWS ON THERMAL BEHAVIOR OF A STRUCTURE

2.1 Basic model equations

In general, the types of leakage flows are crack flow, crack flow and infiltration, and pure infiltration.

In case of pure infiltration the continuity, momentum and energy equations are /1/

$$\frac{\partial}{\partial t}\langle\rho_f\rangle = -\nabla \cdot \langle q_{m,f}\rangle \tag{1}$$

$$\frac{\partial}{\partial t}\langle\rho_f \vec{v}_f\rangle = \frac{K_{v,f}}{\eta_f}\left(\nabla^2 \langle p_f\rangle^{(f)} + \beta \langle\rho_{f,ref}\rangle^{(f)}\vec{g} \cdot \nabla \langle T\rangle\right) \tag{2}$$

$$\frac{\partial}{\partial t}\sum_{\alpha=sf}\langle\rho_\alpha h_\alpha\rangle = -\nabla \sum_{\alpha=sf}\langle\vec{q}_\alpha\rangle - \nabla \cdot \langle h_f \vec{q}_{m,f}\rangle \tag{3}$$

When deriving the momentum equation it is assumed that the airflow is a Darcy-type flow. In energy equation it is assumed that the air and the solid matrix (structure) have equal temperatures locally. In building physics applications, the capasity terms of Eqs 1 and 2 can be assumed zero.

In a building structure there may occur internal convection allthough there are no cracks through it. Analysis of the influences of natural convection on transmission heat losses is given by /2/. In examples which will be considered in this paper the effect of gravity forces is not taken into account, ie. the second term of the righthand side in Eq. 2 is omitted.

In the case of crack flow the energy equation of the flowing component can be written in the form (flowing component as control volume)

$$\frac{\partial}{\partial t}(\rho_f h_f) = - \nabla \cdot \vec{q}_f - \nabla \cdot (h_f \vec{q}_{m,i}) - \frac{1}{V}\int_{\partial v_{fs}} \vec{q}_f \cdot \vec{n}_{fs}\, dA \qquad (4)$$

Correspondingly, for the stagnant component (stagnant component as control volume)

$$\frac{\partial}{\partial t}(\rho_s h_s) = - \nabla \cdot \vec{q}_s - \frac{1}{V}\int_{\partial v_{fs}} \vec{q}_s \cdot \vec{n}_{sf}\, dA \qquad (5)$$

The thermal coupling between the flowing and stagnant component can be given by Eq. 6.

$$\int_{\partial v_{fs}} \vec{q}_s \cdot \vec{n}_{sf}\, dA = \int_{\partial v_{fs}} \alpha_{sf} (T_s - T_f) \cdot \vec{n}_{sf}\, dA \qquad (6)$$

According to previous model equations computer codes for 2-dimensional cases basing on finite difference method have been developed. Boundary condition of the first kind for solving the airflow balance of structure in pure infiltration case was used. When solving the thermal balance of a structure boundary condition of the third kind was used. In a case of crack flow, the thermal balance of flowing component was solved applying the boundary condition of the first kind. In the entrance of leakage route the leakage air temperature is either outdoor or indoor temperature, in case of infiltration it is outdoor temperature and in case of exfiltration indoor temperature, respectively /3/.

Let us define a modified Nusselt number Nu_c to characterize the heat recovery effect of leakage air. With this definition the heat recovery effect is taken into account as a correction factor for transmission heat losses. If we consider interior surface of a structure as control surface, the modified Nusselt number is defined as

infiltration:
$$Nu_c = \frac{(\int_A q\, dA + \phi_{conv}) - \phi_{conv,\,o}}{\int_A q_0\, dA} \qquad (7.1)$$

exfiltration:
$$Nu_c = \frac{\int_A q\, dA}{\int_A q_0\, dA} \qquad (7.2)$$

where

q is conduction heat flux with the effect of airflow,
q_0 conduction heat flux without the effect of airflow,
Φ_{conv} convection heat flow with the effect of thermal coupling,
$\Phi_{conv,0}$ convection heat flow without the effect of thermal coupling
A control surface area.

2.2 Computer simulations of structures

Figure 1 shows the heating of leakage air as a function of leakage route length, heat flux profiles at the outer surface, and the modified Nusselt number with different leakage flow rates on some typical leakage routes. The calculations have been carried out for steady-state conditions where the outside and inside temperatures are -10° C and +20° C, respectively.

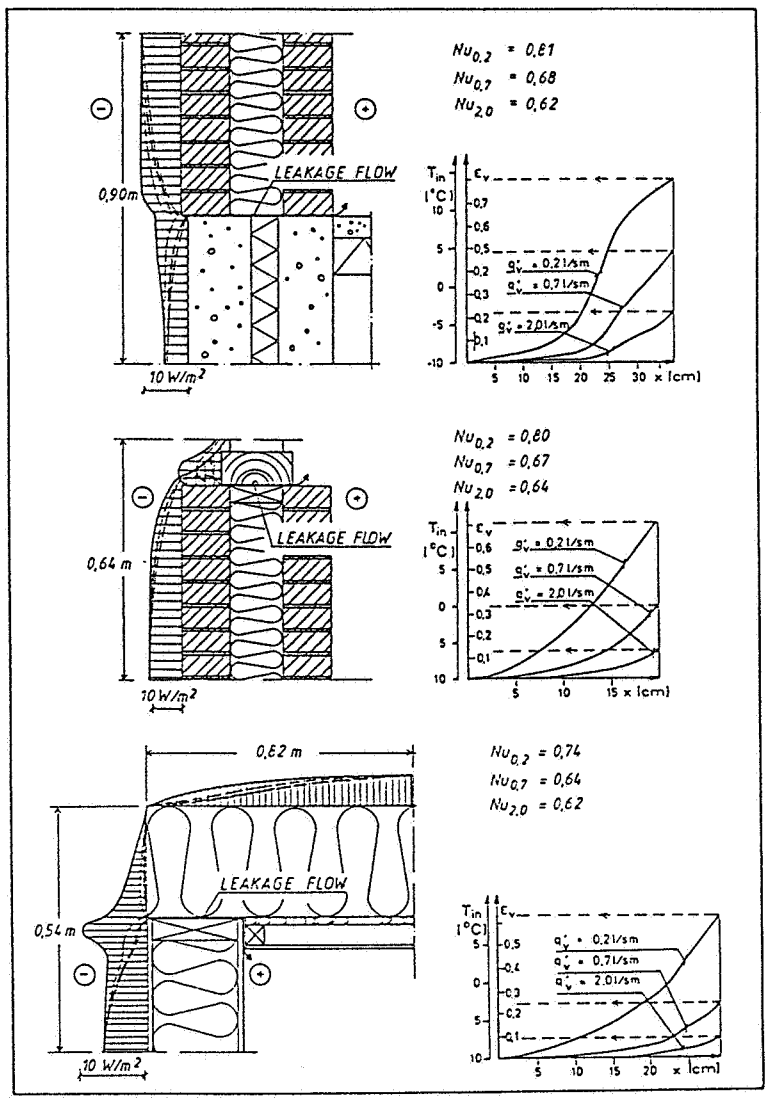


Figure 1. Warming up of leakage airflow and modified Nusselt numbers for some typical wall structures /4/.

In Fig. 1 the outer surface of the structure is cooled as the leakage air in outside air temperature flows into the crack and is heated there by conduction heat flow. As a result, heat flux at the outer surface is decreased (constant heat transfer coefficient at surface). Heat losses at the outer surface decrease more effectively the higher leakage flow rates are. Heat flux profiles drawed with a solid line

represent pure conduction. The dash lines take the effect of leakage airflow into account. In this case the modified Nusselt numbers have been calculated considering exterior surface of a structure as control surface and applying Eg. 7.2.

The dimensions of control surfaces are also shown in Fig. 1.

In practical cases there are difficulties to determine the actual leakage route inside a structure. Usually only the location of inflowing air is known. Let us now consider a structure shown in Fig. 2 and ,in addition, we assume four different leakage routes inside the structure. The considered leakage airflow rate is 0.34 dm^3/sm and the flow direction is from outside to inside as well as from inside to outside. In steady-state conditions 0° C outside temperature and +20° C inside temperature are assumed. Table 1 summarizes the calculation results.

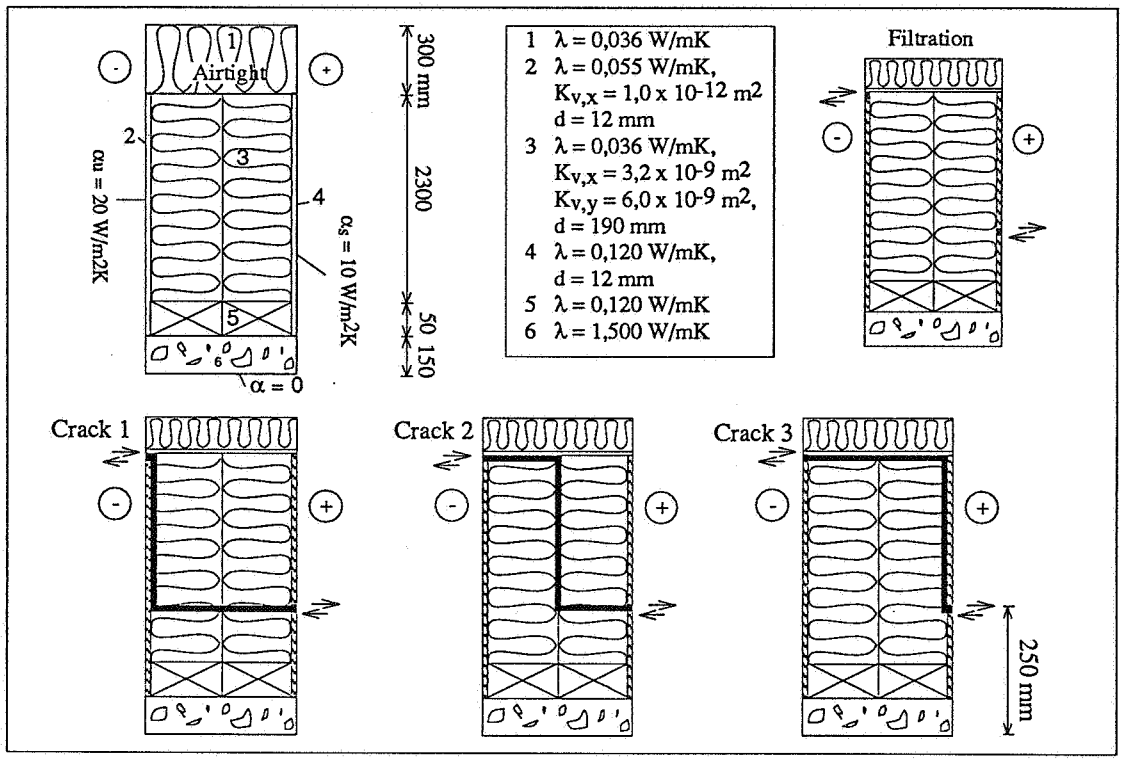


Figure 2. Example structure and four possible leakage routes.

It can first be concluded that the airflow direction does not influence the heat recovery effect. It should, nevertheless, be noticed that the thermal properties of leakage air have been determined according to the average of inside and outside air temperature. The heat recovery is the most effective in a case of pure filtration. Crack cases 1 and 3 have similar heat recovery effect, although the warming up of incoming leakage air is more effective in crack case 3 than in crack case 1.

Table 1. Transmission and convection heat flows at interior surface of a structure, and heat recovery effect in different leakage route and flow direction cases /3/.

Calculation cases	Φ_c	Φ_{conv}	Φ_{tot}	Nu_c
	W/m	W/m	W/m	-
No thermal coupling	21.6	8.2	29.8	1.00
Infiltration	25.4	1.2	26.6	0.85
Crack 1 (inflow)	24.6	4.2	28.8	0.95
Crack 2 (inflow)	25.0	2.5	27.5	0.90
Crack 3 (inflow)	28.4	0.4	28.8	0.95
Exfiltration	18.4	8.2	26.6	0.85
Crack 1 (outflow)	20.6	8.2	28.8	0.95
Crack 2 (outflow)	19.3	8.2	27.5	0.90
Crack 3 (outflow)	20.6	8.2	28.8	0.95

It also been found out that, if the leakage route (crack) is directly across the structure, the increasing of insulation thickness decreases the modified Nusselt number, ie. the heat recovery effect is improved. If the thermal conductivity of the insulation material is of the magnitude .04 W/mK, the increasing of insulation thickness has only a slight influence on the temperature of incoming leakage air /3/.

The leakage airflows influence also the thermodynamic behavior of wall structures. It has been found out that by increasing the leakage airflow rate from outside to inside, the thermodynamic delay of a wall structure will be decreased /3/. Also convective heat flows of leakage ventilation should be considered dynamic. In this paper the dynamic behavior of leaky wall structures will be taken into account by applying the modified transfer-function approximation in the calculation of conductive and convective heat flows.

2.3 Experiments

Measurements concerning thermal effects of leakage flows have been done in laboratory conditions. Fig. 3 shows the measured and calculated heating of leakage air in a crack, heat flux and temperature profiles at the inside surface of the structure as well as the temperature profile at the outside surface of the structure. The outside temperature was -2.8 °C and the inside temperature was 22.7 °C, respectively. The measured airflow rate was 2.7 dm^3/sm.

In Fig. 3 the temperature gradient of leakage air is very high at inside surface of the structure. Therefore, the temperature measurement of incoming air is relatively inaccurate. The measured modified Nusselt number (correction factor for transmission heat losses) was Nu_c =0.35, while the calculated value was Nu_c =0.43. The measured and calculated correction factors for the total heat loss (transmission and convection) were 0.94 and 0.95, respectively.

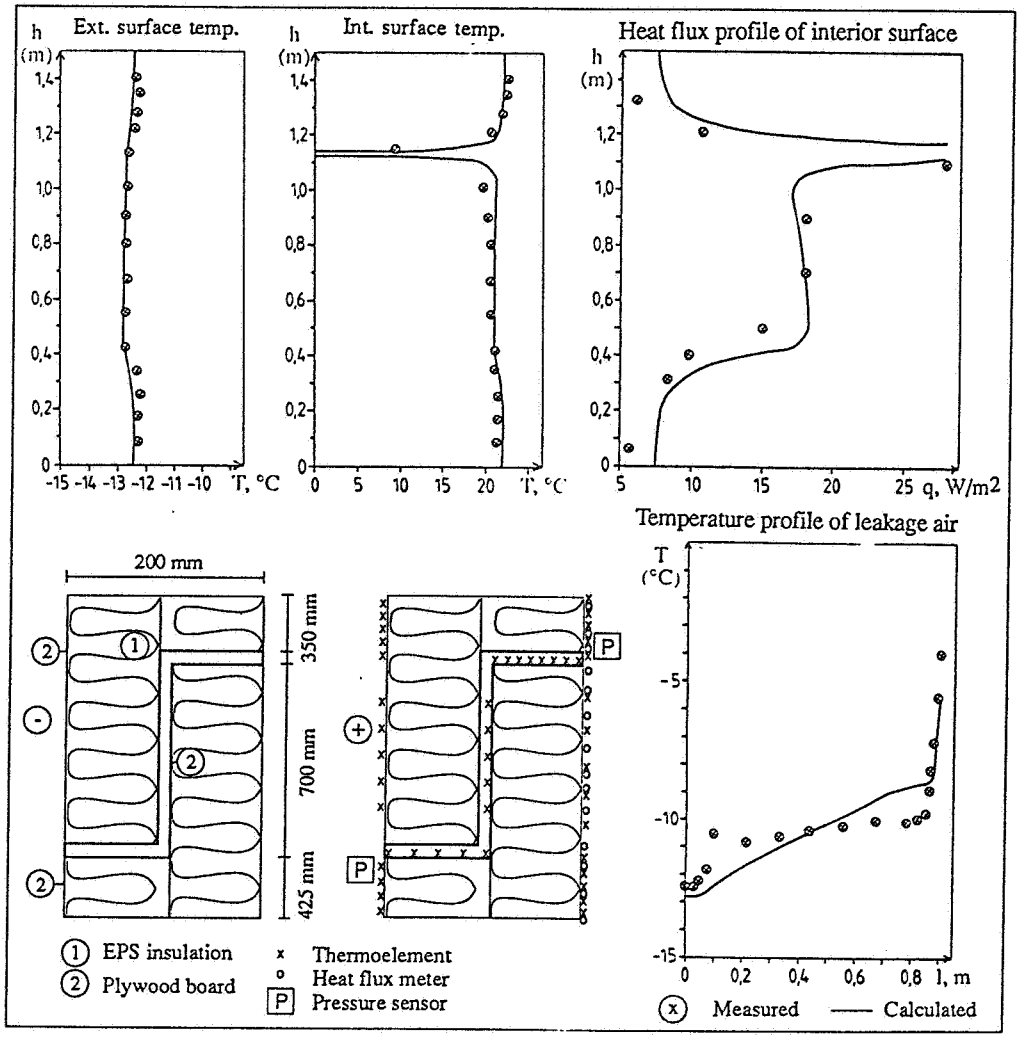


Figure 3. Measured and calculated heating of leakage air, heat flux and temperature profiles at inside surface, and temperature profile at outside surface of structure. Steady-state condition.

In Fig. 4 the measured and calculated results for one wall section are shown. The outside temperature was 4.5 °C and inside temperature was 21.0 °C, respectively. The measured pressure difference over the wall was 27 Pa and the corresponding airflow rate was 0.87 dm^3/sm. The inside surface was absolutely airtight, except one crack through which the air flows in. The airflow field, shown in Fig. 4, is calculated. Also the temperature isotherms are calculated. The calculated

modified Nusselt number for this case was Nu_c=0.83, while it according to measurements was Nu_c=0.50-0.85. The calculated correction factor for the total heat loss was 0.95 and the measured value was in the limits 0.86-0.96, respectively. The measured values include the horizontal deviation of temperatures.

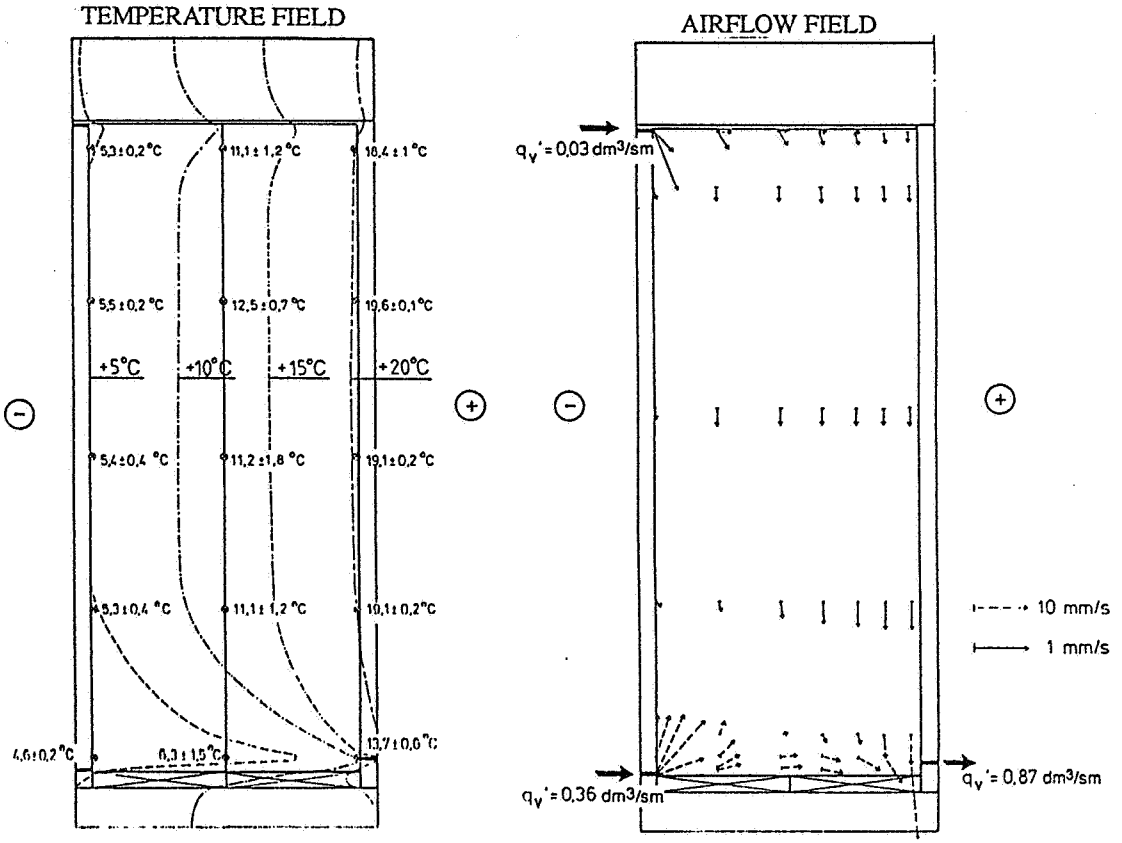


Figure 4. The calculated airflow field, and the measured and calculated temperature field of a structure.

3. HEAT BALANCE OF A BUILDING

3.1 Heating load of ventilation and transmission losses

In Fig. 5 heat balance of a building in general is shown. In our considerations certain terms of the heat balance have been omitted in order to find out the thermal coupling of leakage airflows and the heating load clearly. The solar heat gain and heat gain from people, devices etc. have been omitted. The control system of heating is assumed ideal, ie. the room air temperature stays constant at the desired value. In addition, the heat flow through floor is assumed to depend on the temperature difference of inside and outside air.

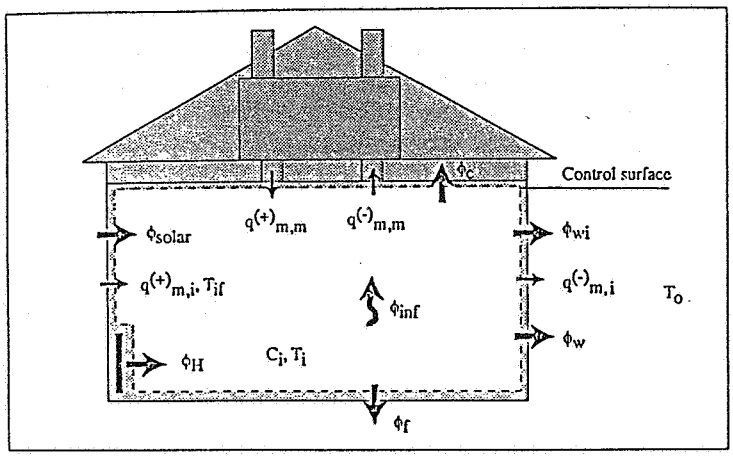


Figure 5. Heat balance of a building.

According to simplifications and assumptions made above, the heat balance of a building takes the form

$$\phi_h(t) = \phi_c(t) + (1 - \varepsilon_i(t))q^{(+)}_{m,i}(t)\, c_p\, (T_i - T_o(t)) \qquad (8)$$

where

$$\varepsilon_i = (T_{if} - T_o)/(T_i - T_o) \qquad (9)$$

It should be noticed that transmission heat loss term in Eq. 8 includes transmission heat losses of both airtight and leaky wall structures.

When evaluating the effect of leakage airflows on the heating load of a building in a dynamic condition, the heat balance and the airflow balance have to be solved simultaneosly. In our case the computer code MOVECOMP /5/ to calculate the airflow balance of a building was applied. MOVECOMP is based on a static flow network approach. For heating load calculation of leaky wall structures a 2-dimensional modified transfer-function approximation was applied and for airtight structures 1-dimensional approach was applied, respectively. The simultaneous solving procedure of airflow and heat balance of a building is described more detailed in /3/.

3.2 Transfer-function approach for airtight and leaky wall structures

Transmission heat flows of a building are solved using 1- and 2-dimensional response factors. For airtight wall structures 1-dimensional response factors are applied /6/, and for leaky wall structures (crack flow) modified 2-dimensional response factors are applied /3/, respectively.

In a case of airtight wall structures the only time-dependent variable is the outside temperature, because inside temperature was assumed constant. If, in addition, convective heat transfer coefficients of exterior and interior surfaces of a structure are assumed constant, the heat flux at interior surface can be written as follows

$$q_t = \sum_{k=0}^{\infty} X_i \, (T_i - T_{o,t-k}) \tag{10}$$

where X_i are response factors of heat flux (1-dimensional) at interior surface against unit triangular pulse of outside temperature excitation.

Taking a more practical form for Eg. 10 (/7/), we get the total transmission heat loss for airtight wall structures

$$\phi_{c,t} = \sum_{n=1}^{N1} A_n \left[c_n \, q_{n,t-1} + \sum_{k=0}^{K} X'_{n,k} (T_i - T_{o,t-k}) \right] \tag{11}$$

$$X'_o = X_o, \; k = 0$$
$$X'_k = X_k - cX_{k-1}, \; k \geq 1$$

In Eg. 11 A_n is the inside surface area of airtight wall structures, N1 is the number of different airtight structures and c_n is the common ratio, respectively.

In a case of leaky wall structures the wall system is similarly linear as in a case of airtight wall structures, if constant leakage airflow rate and constant thermal properties of air are assumed. Nevertheless, airflow rate is varying with time and, therefore, an approximation for the calculation of transmission and convection heat losses is made. The transmission heat flow at interior surface of a leaky wall structure is approximated as follows (approximation is illustrated in Fig. 6)

$$\phi'_{c,t} = \sum_{k=0}^{\infty} Y_{k,t-k} \, (T_i - T_{o,t-k}) \tag{12}$$

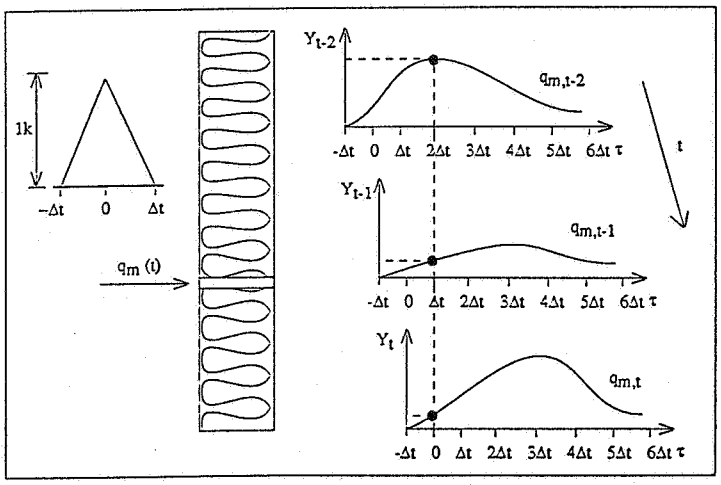


Figure 6. Response of heat flow at interior surface of structure against a unit triangular pulse of outside temperature excitation. The leakage airflow rate is variable, /3/.

The airflow rate is kept as a parameter value in the calculation of response factors. Response factors corresponding to other leakage flow rates than parameter values are obtained by linear interpolation. In addition, the common ratio reaches a nearly constant value with different airflow rates. The total transmission heat loss of leaky wall structures is thus written as

$$\phi'_{c,t} = \sum_{n=1}^{N2} L_n \left[c_n \phi'_{c,n,t-1} + \sum_{k=0}^{K} Y'_{n,k,t-k} (T_i - T_{o,t-k}) \right] \qquad (13)$$

$$Y'_{o,t} = Y_{o,t}, \; k = 0$$
$$Y'_{k,t-k} = Y_{k,t-k} - cY_{k-1,t-k-1}, \; k \geq 1$$

In Eg. 13 L_n is the inside width of a structure for horizontal cracks and inside hight of a structure for vertical cracks, respectively. Y_k are 2-dimensional response factors and N2 is the number of leaky wall structures.

In a case of convection heat losses the common ratio representation is not necessary. The total convection heat loss of a building can thus be written as

$$\phi'_{conv,t} = \sum_{k=0}^{K} Z_{k,t-k} (T_i - T_{o,t-k}), \; (q'_{m,i})_t > 0 \qquad (14)$$

$$(Z_{k,t-k})_{k=0,1\ldots,K} = 0, \; (q'_{m,i})_t \leq 0$$

In Eg. 14 Z_k are 2-dimensional response factors. The total heat loss of a building can be achieved by the superposition of Egs 11, 12 and 14. The comparisions have shown that the results calculated with the present approximation agree very well with the results calculated with finite-difference method /3/.

3.3 Computer simulations of a building

The aim of building level calculations was to analyze the correlation between airtightness, leakage distribution, air change rate and thermal performance. A small house (see Fig. 7) supplied with mechanical exhaust ventilation system was considered. The mechanical exhaust airflow rate was assumed constant corresponding to ventilation rate 0.41 1/h. The supply air was assumed to be taken in as leakages (cracks) through building envelope. In addition, constant inside air temperature was assumed and real measured weather data (outside air temperature, wind velocity and direction) was used.

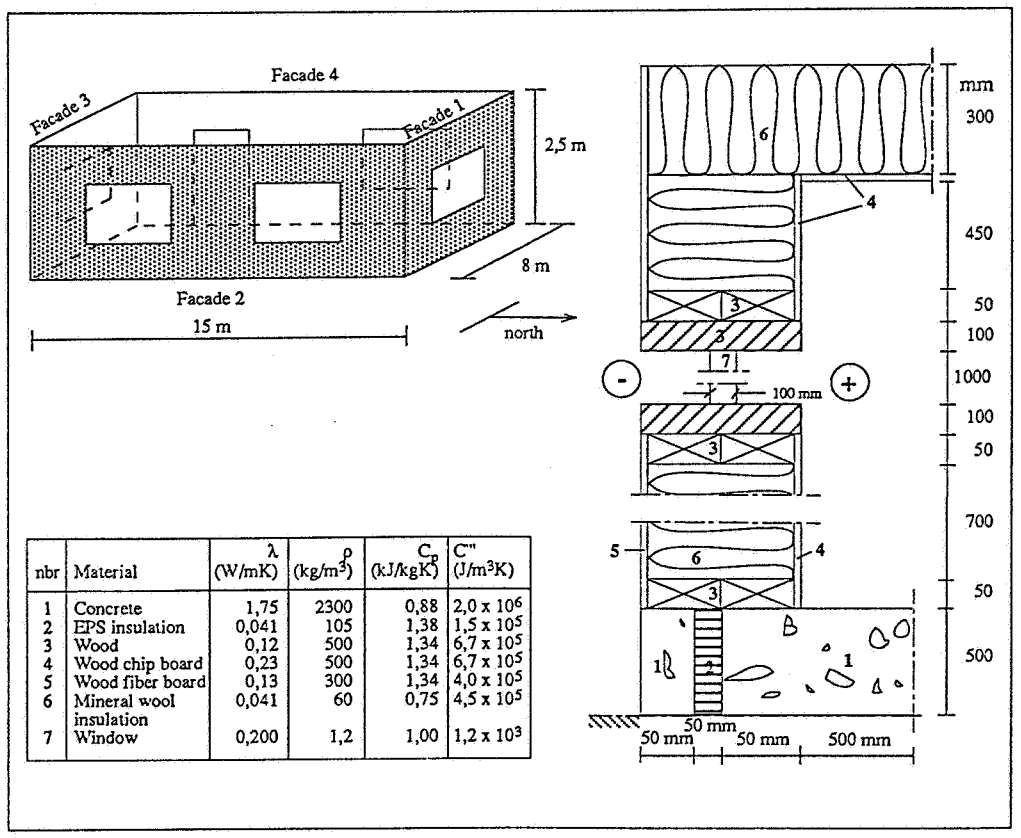
Calculations were carried out for one year period using one hour time step. In analyses two leakage route distributions (case 1 and case 2) and several airtightnesses of a building envelope (n_{50} number) were considered. In case 1 it was assumed that the relative airflow distribution through different leakage routes under 50 Pa pressure difference over the building envelope was as follows

* cracks between window frame and wall structure 30 %,
* cracks between outdoor frame and wall structure 20 %,
* cracks between ceiling and wall structure 20 %,
* cracks between floor and wall structure 20 %,
* cracks between wall structures (corners) 10 %.

Correspondingly in case 2, the considered relative airflow distribution was

* cracks between window frame and wall structure 40 %,
* cracks between outdoor frame and wall structure 20 %,
* cracks between ceiling and wall structure 40 %.

The airtightness of the building envelope was varied by changing the flow resistances of leakage routes so that above conditions could be achieved.



nbr	Material	λ (W/mK)	ρ (kg/m³)	C_p (kJ/kgK)	C'' (J/m³K)
1	Concrete	1,75	2300	0,88	2,0 x 10⁶
2	EPS insulation	0,041	105	1,38	1,5 x 10⁵
3	Wood	0,12	500	1,34	6,7 x 10⁵
4	Wood chip board	0,23	500	1,34	6,7 x 10⁵
5	Wood fiber board	0,13	300	1,34	4,0 x 10⁵
6	Mineral wool insulation	0,041	60	0,75	4,5 x 10⁵
7	Window	0,200	1,2	1,00	1,2 x 10³

Figure 7. Inside dimensions of example building and thermal properties of wall structures. Dimensions of windows and door are 1.8x1.2 m^2 and 1.0x2.0 m^2, respectively.

In Fig. 8 the effect of building envelope airtightness in calculation case 1 on the total airchange rate of the building is shown. Curves in Fig. 8 are minimum and maximum airchange rates for 24 hour periods. It can be seen that airchange rate is constant when the airtightness is n_{50} = 1.0 1/h. Already in conditions where the airtight-

ness is 3.0 1/h, the ventilation rate is occasionally doubled in relation to the desired ventilation rate. If we consider long-term averages, for example one year, the proportion of uncontrolled ventilation of the total ventilation is only 2.5 % in our simulation case, where the building envelope airtightness is 3.0 1/h. As the airtightness is 5.0 and 10.0 1/h, the proportion of uncontrolled ventilation is 13 % and 38 %, respectively.

Simulations have shown (comparisons of cases 1 and 2) that the leakage route distribution has no significant influence on the airchange rate if buildings with similar airtightness and long-term averages are considered. Short-term differences may, however, be remarkable in a way that the less leakage routes there are, the higher occasional uncontrolled ventilation rates appear.

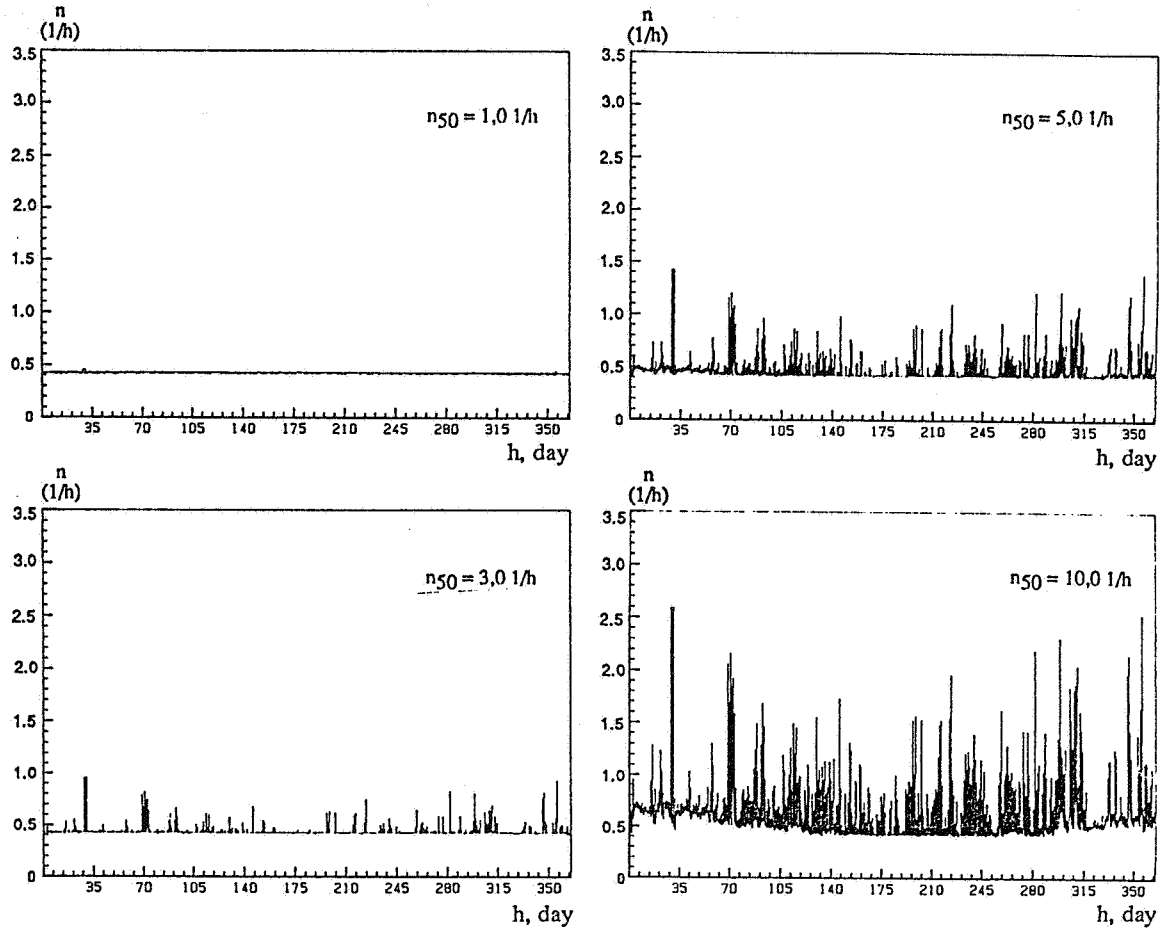


Figure 8. The correlation between the airtightness of building envelope and airchange rate. Minimum and maximum values for 24 h periods.

Table 2 summarizes the results of heat balance analyses. It can be seen that the annual heating energy consumption is in the considered cases roughly 6 - 9 % less compared with the calculation results where the thermal coupling of leakage airflows and conduction heat flows is not taken into account. To take the heat recovery effect into ac-

count, it is suggested that traditionally calculated heating energy corresponding to conduction heat losses should be multiplied with a correction factor. Heating energy due to ventilation could be calculated traditionally. In this case the mean modified Nusselt number is defined as

$$\overline{Nu_c} = \frac{\int_t(\phi_c + \phi_{conv})dt - \int_t(\phi_{conv,\,o})dt}{\int_t(\phi_{c,\,o})dt} \qquad (15)$$

where Φ_c is conduction heat flow with thermal coupling,
Φ_{conv} convection heat flow with thermal coupling,
$\Phi_{c,0}$ conduction heat flow without thermal coupling,
$\Phi_{conv,0}$ convection heat flow without thermal coupling.

It should be noticed that control surface is assumed to be at interior surface of building envelope.

Table 2. The annual heating energy consumption and the mean modified Nusselt number in example cases.

$Q_{tot,o}$ is heating energy consumption as the heat recovery effect is not taken into account,
Q_{tot} heating energy consumption with the heat recovery effect,
$\overline{Nu_c}$ mean modified Nusselt number.

Leakage distribution case	n_{50} (1/h)	$Q_{tot,o}$ (kWh)	Q_{tot} (kWh)	ΔQ_s (%)	$\overline{Nu_c}$ (-)
1	1.0	17754.2	16557.0	- 6.7	0.90
1	3.0	17939.7	16651.1	- 7.2	0.89
1	5.0	18676.9	17296.4	- 7.4	0.88
1	10.0	21511.6	19969.9	- 7.2	0.87
2	1.0	17760.4	16736.1	- 5.8	0.91
2	5.0	18599.8	17228.7	- 7.4	0.88
2	10.0	21330.2	19522.1	- 8.5	0.84

4. CONCLUSIONS

It is suggested in the paper that the value of transmission heat losses should be corrected by a factor, modified Nusselt number, in order to take into account the heat recovery effect of leakage airflows. Depending on leakage airflow rate, thermal properties and dimensions of the structure as well as the leakage route, the correction factor of transmission heat losses can be as low as 0,60. The correction factor of total heat losses can be 0,86, respectively.

According to measurements the correction factor of transmission heat losses was 0,35-0,85, while it for the total heat losses was 0,86-0,96. The heat recovery effect is approximately the same for both infiltration and exfiltration.

At the building level, the correlation between airtightness, leakage distribution, air change rates and thermal performance of a single family house was analyzed. The house was supplied with mechanical exhaust ventilation system and the supply air was taken in as leakages through building envelope. The calculated annual heating energy consumption of the building was 6-9 % less compared with the calculation results where the heat recovery effect was not taken into account. If the heat recovery effect was taken into account in calculation of transmission heat losses, the average correction factor was 0,85-0,90. The actual values depend on airtightness and leakage distribution of building envelope.

REFERENCES

/1/ Kohonen, R., Kokko, E., Ojanen, T., Virtanen, M. Thermal effects of airflows in building structures. Espoo 1985. Technical Research Centre of Finland, Research Reports 367.

/2/ Ojanen, T., Kohonen, R., The effect of airflows on the hygrothermal behavior of building structures. Espoo 1989. Technical Research Centre of Finland, Research Reports 590. In Finnish.

/3/ Virtanen, M., Thermal effects of leakage airflows in buildings. Espoo 1990. Helsinki University of Technology, Faculty of Mechanical Engineering. Licentiate's thesis. In Finnish.

/4/ Kohonen, R., Ojanen, T., Virtanen, M., Thermal coupling of leakage flows and heating load of buildings. Ventilation Technology - Research and application. 8th AIVC conference. Uberlingen, FRG, 21-24 September 1987. England 1987. AIVC, 8th AIVC Conf. Proc., 21 p.

/5/ Herrlin, M., K., MOVECOMP: A static multicell airflow model. ASHRAE Transactions, Vol. 91, Part 2, 1985.

/6/ Mitalas, G., P., Stephenson, D., G., Room thermal response factors. ASHRAE Transactions, Vol. 73, Part 1, 1967.

/7/ Kimura, K., Scientific basis of airconditioning. Applied Science Publishers, London 1977.

AIR MOVEMENT & VENTILATION CONTROL WITHIN BUILDINGS

12th AIVC Conference, Ottawa, Canada
24-27 September, 1991

POSTER 37

SIMULTANEOUS CALCULATION OF AIRFLOWS, TEMPERATURES AND CONTAMINANT CONCENTRATIONS IN MULTI-ZONE BUILDINGS

K. Klobut, P. Tuomaala, K. Sirén, O. Seppänen

Helsinki University of Technology
Laboratory of Heating, Ventilating and Air Conditioning
Otakaari 4
02150 Espoo, Finland

SYNOPSIS

The computer programs published so far have enabled the calculation of airflows at constant temperatures or of air temperatures at constant airflows.

The first version of a new microcomputer program has now been developed in which the airflows and temperatures are calculated simultaneously. The time-dependency of temperatures, airflows and contaminant concentrations is considered in the calculation method. The source strength of contaminants, outdoor air temperature, wind velocity and direction, convection and radiation loads can all be freely scheduled. The supply air temperature in mechanical ventilation can be selected as: (1) constant (and scheduled), (2) equal to that of the outdoor air, (3) calculated as the temperature of the mixture of outdoor air and return air.

Constant-temperature cases were simulated with the program and the results compared with those obtained from more sophisticated programs. Other cases, with variable temperatures, were compared with the measurements. Good agreement of the results was obtained in all cases.

The paper describes the main features of the new program and gives some simulation results.

NOMENCLATURE

A = area of opening, (m^2),
A = flow coefficient, (m^3/s at 1 Pa),
A_w = surface area of wall, (m^2),
A_{ij} = section area of flow path from node i to node j, (m^2),
A_{ww} = surface area of window, (m^2),
a = dummy variable,
B = flow exponent,
C_1 = constant,
C_2 = constant,
C_d = discharge coefficient, (-),
C_i = concentration of contaminant in space associated with node i, (kg/m^3) or (pol) or (vol. ppm),
C_i = thermal capacity of air in zone i, (J/K),
C_{iw} = thermal capacity of wall w in zone i, (J/K),
c_p = specific thermal capacity of air, (J/kgK),
D = equivalent diameter of duct, (m),
F' = function,
F'' = nonlinear function,
f_1 = friction loss factor, (-),

f_2 = local pressure loss factor, (-),
G_i^2 = constant strength of contaminant source placed at node i, (kg/s) or (olf) or (L/h),
H = height of opening, (m),
K_{ij} = general coefficient of pressure loss,(-),
L_{ij} = length of flow path from node i to node j, (m),
L = length of duct, (m),
m_{ij} = mass flow of air from node i to node j, (kg/s),
p_i = absolute pressure at node i, (Pa),
p_u = pressure difference that accounts for the effect of turbulence, (Pa),
p_x = pressure difference that generates the net flow through large opening, (Pa),
Δp = pressure difference, (Pa),
Q_c = thermal load by convection, (W),
Q_r = thermal load by radiation, (W),
q = volume airflow, (m^3/s),
q_1 = air inflow, (m^3/s),
q_2 = air outflow, (m^3/s),
q_{ij} = volume flow of air from node i to node j, (m^3/s),
S_{ij} = stack effect in flow path from node i to node j; head generated by fan, (Pa),
T_i = temperature of air in zone i, (°C),
T^{iw} = surface temperature of wall w in zone i, (°C),
T^{o}_{iwx} = outdoor air temperature, (°C),
T = temperature of air in zone on opposite side of wall w in zone i, (e.g. outdoor air temperature for external wall), (°C),
T^w = temperature of surface of wall, (°C),
ΔT^{wr} = temperature of surface of hemisphere, (°C),
t = temperature difference, (K),
U_{iw} = time, (s),
U_{ww} = overall heat transfer coefficient of wall w in zone i, (W/m^2K),
V_i = overall heat transfer coefficient of window, (W/m^2K),
v = volume of space associated with node i, (m^3),
v_x = velocity of airflow, (m/s),
W = mean air velocity corresponding to net flow rate through large opening, (m/s),
= width of the opening, (m),

α_c = film heat transfer coefficient by convection, (W/m^2K),
α_r = film heat transfer coefficient by radiation, (W/m^2K),
ϱ = air density, (kg/m^3),
ϱ_m = mean air density, (kg/m^3),

1. INTRODUCTION

A number of programs have been developed recently for predicting contaminant concentrations, e.g. [2, 13], for the thermal simulation of buildings, mainly with respect to energy analysis, e.g. [1], and for calculating the airflows in a building, e.g. [16]. The state of the art is to the best of the authors' knowledge represented by: CONTAM [2] for concentration prediction, AIRNET [16] combining infiltration, airflows and ventilation ducting, and DTFAM [3] considering coupled airflow and thermal analysis (not yet released).

The thermal capacity of the building structure has an effect on the indoor air temperature. There is a link between the air temperature and air flows. Airflows are the major distribution routes by which contaminants spread throughout the building. Therefore, the airflows and air temperatures should be taken into consideration in predicting contaminant concentrations in the building.

None of the available programs is alone capable of simultaneously calculating contaminant concentrations, airflows and air temperatures. This fact provided the main stimulus for the research work presented here. The aim of the study was to develop the first version of a computer program for predicting contaminant concentrations in buildings making simultaneous allowance for airflows and the thermal behaviour of the building structure in dynamically changing conditions. The program was intended for microcomputer to enable simulations covering a period of one or two days.

The following is a brief report of the fundamentals of the models used in the program and some simulation results.

2. GENERAL

The program is called TFCD. The letters in the abbreviation contain information on what the program does - it calculates Temperatures, air Flows, Concentrations of contaminant and air quality in terms of Predicted Percentage of Dissatisfied (PPD) due to contaminant concentration.

The source code of the program, listed in [8], is written in Fortran 77. Figure 1 depicts the sequence in which the computations are performed by the program.

The simulated building is modelled by a network whose branches represent airflow routes and its nodes refer

to the volumes (zones). The program is at present capable of simulating a system consisting of at most 40 nodes.

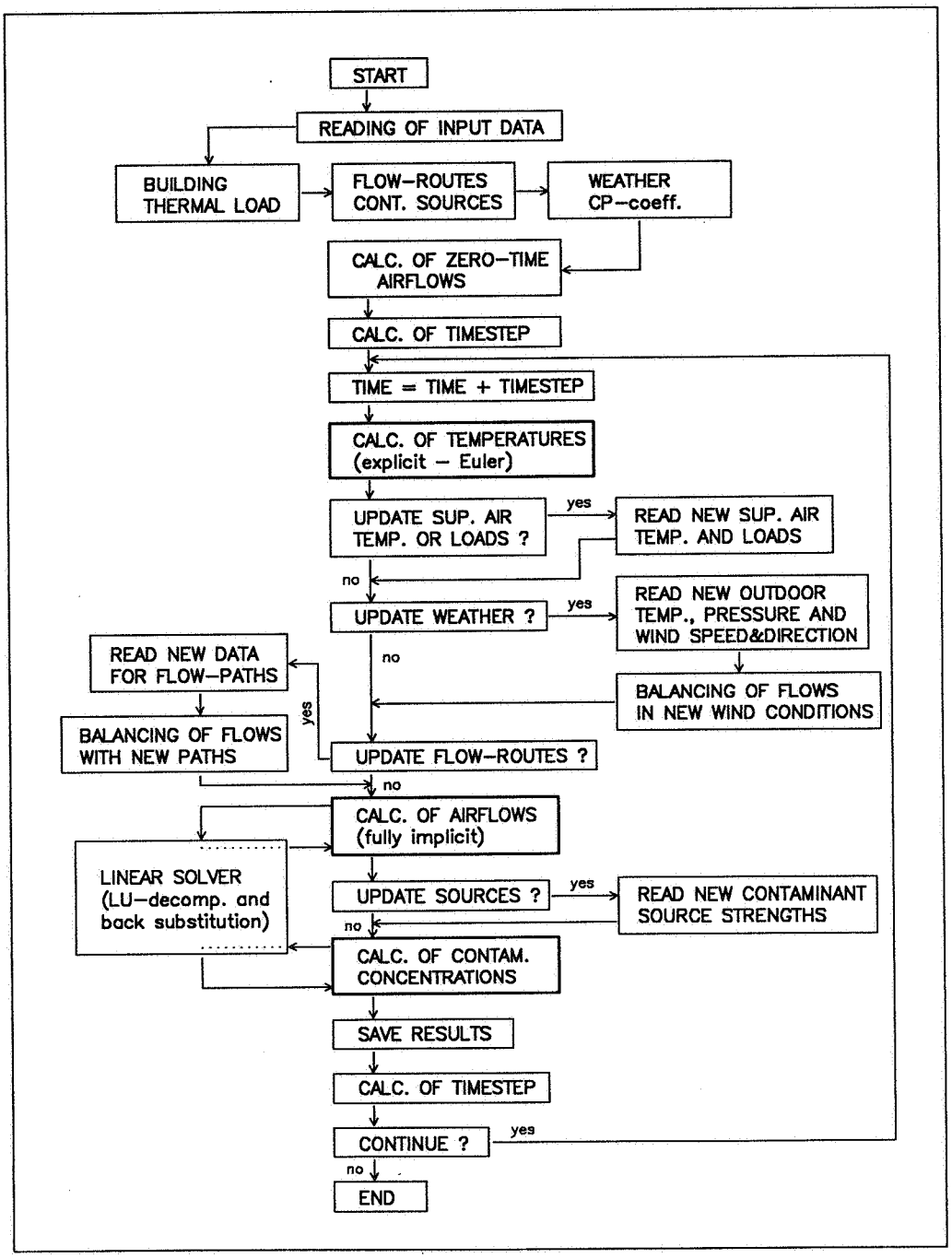


Figure 1. A simplified block diagram of the program.

In order to enable the simulation of cases resembling reality as well as possible, the following options are provided for use in the program :

- outdoor air temperature - constant, changing according to sine function in 24 hour period, changing stepwise with a free schedule;
- barometric pressure, wind speed and direction - constant, changing with a free schedule;
- supply air temperature of mechanical ventilation - constant, changing stepwise with a free schedule, equal to outdoor air temperature, equal to the temperature of a mixture of outdoor air and return air (if such is used);
- thermal loads by convection and radiation - constant, changing stepwise with a free schedule;
- strengths of contaminant sources - constant, changing stepwise with a free schedule;
- type and pressure-flow characteristics of airflow routes - constant, changing with a free schedule (change of type limited, see Appendix 2 in [8]).

3. CALCULATION OF TEMPERATURES

An extended version of the thermal model presented in [5] was applied for calculation of the air temperatures at the indoor nodes of building network. Each room in the building was considered as one or more zones vertically stacked. One network node was placed in each zone. It was assumed that the air inside the zone is instantly and perfectly mixed. The set of differential equations was written for each zone :

$$\frac{dT_i}{dt} C_i = \sum_j m_{ji} c_p (T_j - T_i) + \sum_{iw} \alpha_c A_{iw} (T_{iw} - T_i) + \sum_{ww} U_{ww} A_{ww} (T_o - T_i) + Q_c \qquad (1)$$

$$\frac{dT_{iw}}{dt} C_{iw} = A_{iw} (T_{iwx} - T_{iw}) \left[\frac{1}{U_{iw}} - \frac{1}{\alpha_c + \alpha_r} \right]^{-1} + Q_r + \alpha_c A_{iw} (T_i - T_{iw}) + \alpha_r A_{iw} (T_{iwr} - T_{iw}) \qquad (2)$$

The set for a node has one equation (1) and as many equations (2) as there are walls (10=max.) associated with the node in question.

Whereas the thermal capacity of the zone air is calculated at each time step, the thermal capacity of the wall is approximated by one constant. Since it is related to the duration of the simulation, the wall capacity will obtain different values depending on the application.

The Euler method was chosen for solving the temperatures. Advantages of this are the minimal computational effort required to find temperatures and the fact that there is no need for iterations between temperatures and airflows. The stability analysis is then inevitable. However, the cost is ultimately an advantage because the upper limit for the time step emerges automatically from stability analysis. Thus the user of the program is not faced with the cumbersome task of deciding the length of the time step to be used in simulation.

4. CALCULATION OF AIRFLOWS

4.1. Numerical model of building network

The building is considered as a set of nodes connected by the branches of the network. Network nodes are placed at the external envelope, at both ends of the flow paths in the ducting, and in the indoor zones of the building.
The wind pressure acting on the external nodes, fans in the air handling system and buoyancy create pressure differences between the nodes of the network.

For each network node in the ventilation ducting and indoor zones of the building, the following differential equations are written [7]

$$V_i \frac{d\varrho_i}{dt} + \sum_j m_{ij} = 0 \qquad (3)$$

$$\frac{L_{ij}}{A_{ij}} \frac{dm_{ij}}{dt} - p_i + p_j + \frac{1}{2} K_{ij} |m_{ij}| m_{ij} = S_{ij} \qquad (4)$$

Equations (3) and (4) must both be fulfilled for all the nodes simultaneously. This model was first adapted for calculating the airflows in the building in

computer code SMOV [15].

The model based on eqs. (3) and (4) predicts the airflows as one-way flows. A separate model is used in the program for calculating two-way flows through large openings.

In order to obtain the solution, the differential eqs. (3) and (4) must be discretized. Fully implicit discretization avoids potential stability problems. Equations (3) and (4) are discretized and linearized as shown in [7]. The linear matrix equation is created and solved in the program by means of standard LU-decomposition and the back substitution method [10].

The general coefficient of pressure loss, K_{ij} in model eq. (4), is calculated from the equation

$$0.5\ K_{ij}\ m_{ij}^2 = \Delta p_{ij} \qquad (5)$$

The coefficient K_{ij} is calculated in a different way depending on the pressure-flow characteristics of the flow path. At present the program is able to handle nine types of flow paths. Their characteristics are provided in the appendix.

4.2. Calculation of two-way flows

The model [13] used in the program to calculate the two-way airflows through large openings consists of a large number of equations that may be written in general form as :

$$q_1 = C_1\ C_d\ W\ H \cdot F'\{a,H\} \cdot F_1''\{p_x, p_u, \varrho_m, a, H\} \qquad (6)$$

$$q_2 = C_2\ C_d\ W\ H \cdot F'\{a,H\} \cdot F_2''\{p_x, p_u, \varrho_m, a, H\} \qquad (7)$$

The difference between the outlow q_2 and the inflow q_1 is the net flow

$$q_2 - q_1 = q_{net} \qquad (8)$$

The discharge coefficient, C_d, is calculated from the formula

$$C_d = 3.7v_x + 6.4v_x e^{-\Delta T} - 0.9e^{-\Delta T} + 0.96 \qquad (9)$$

where :

$$v_x = q_{net} / (H\ W) \quad . \tag{10}$$

Equation (9) was derived from the results of tracer gas measurements and is valid for [13]

$0 \leq v_x \leq 0.05$ m/s and $0 \leq \Delta T \leq 3.0$ K .

The values for constants C_1, C_2 and the forms of functions F' and F'' in eqs. (6) and (7) are obtained in the program by selecting applicable equations from the model set, see [13] for precise formulation of the equations. Appropriate equations are identified depending on the position of neutral levels, the temperature difference between the spaces and the values of the pressure differences.

5. CALCULATION OF CONTAMINANT CONCENTRATIONS

5.1. Numerical model and solution method

The numerical model for calculating contaminant concentrations is based on a simple differential equation of contaminant mass balance similar to eq. (3) for air. It was assumed that the contaminant is instantly and perfectly mixed with the air and is passive.

Once the airflows have been determined, the balance equation of the mass for contaminant may be written for each node of the building network. It is discretized as [12] :

$$\frac{C_i^{(t)} - C_i^{(t-\Delta t)}}{\Delta t} V_i = G_i + \sum_{j=i} q_{ji} C_j^{(t)} - \sum_{j=i} q_{ij} C_i^{(t)} \tag{11}$$

The superscript $(t-\Delta t)$ refers to the value at the previous time step and (t) refers to the value at the present time step.

Equation (11) is rearranged to obtain a linear matrix equation that is solved for the vector of concentrations by means of the same solver (standard LU-decomposition and back substitution method) as was previously used to determine the airflows.

5.2. Evaluation of air quality

Three units may be used in the program for calculating the contaminant concentrations (kg/m^3, ppm, pol).

The perceived air quality may be quantified in terms of Predicted Percentage Dissatisfied [6] as :

$$PPD = 395 \exp(-3.25\ C^{-0.25}) \quad \text{for} \quad C \leq 31.3 \text{ decipol}$$

$$PPD = 100\ \% \quad \text{for} \quad C > 31.3 \text{ decipol} \qquad (12)$$

where C is the perceived air pollution expressed in decipols.

The air quality at each node of the network is evaluated in the program by means of eq. (12) whenever the source strengths are expressed in olfs and the concentrations in pols.

6. RELIABILITY CONSTRAINTS OF THE MODELS

The reliability of the numerical methods applied in the program was proved by means of validation cases [8]. However, comprehensive verification by means of measurements must still be conducted in order to gain general confidence in the simulation results.

At this stage, it should be pointed out that the models used in the program contain several simplifications. Some of them were necessary in order to reduce the computer memory requirements and thus to meet the aim that the program should run on a microcomputer.

The most important simplification of the thermal model is the requirement of the thermal capacity of each wall to be provided in input data, i.e. it is not calculated within the program. Advanced methods exist, involving response factors, for determining the dynamical behaviour of multi-layer walls. These methods are applicable to long-term simulations, e.g. aiming at evaluation of energy consumption in buildings, and require large memory space and computational effort. In short-term simulations only the dynamics of the active part of the wall has an impact on the space air temperature [5]. If this active part consists of one layer, its capacity may be approximated [8]. In future versions of the program some improvement allowing for the simulation of multi-layer walls should be considered.

The reliability of the model for calculating airflows

is affected by the quality of the input data. For example, in spite of the fact that considerable effort has already been made to collect the wind pressure coefficients [9, 4], generally applicable data are still not available. The values of the parameters for the leakage characteristics of elements in a modelled building required by the program as input data are uncertain as long as they are not measured in situ.

Airflows between vertically stacked spaces were modelled as one-way flows. This is a rough simplification and should be updated as soon as a more advanced model is available.

The assumption of the instantaneous and perfect mixing of air and contaminant within the zone is the fundamental simplification applied in the model for calculating the contaminant concentrations in the building. It was inevitable since it is not yet known how to deal with nonuniform distribution of concentration. Due to this simplification, the choice of zones has a decisive effect on the calculated results. Usually it is correct to simulate one zone in one room. However, in some cases, particularily when the doorway is large in proportion to the size of the room, it may be useful to combine several rooms into one zone, see e.g. [14]. The only way to confirm the correctness of the choice of zones is by measurement.

The simplifications used in the models should be kept in mind since they affect the results of the simulations performed with the program.

7. EXAMPLE OF A PROGRAM APPLICATION

Part of a fictive office building was used in the simulations. The system consists of four rooms (each 4x4x3m) and a corridor, fig. 2. The corridor was divided into two equal zones (8x2x3m) with a large opening (height 3m, width 2m) between them. All the doors are 2m high and 1m wide. Convective thermal loads ranging from 7.5 W/m^2 to 30 W/m^2 are imposed on each of the rooms 13 through 16. A contaminant source of 25 olfs is placed only in room 13. The mechanical ventilation, fig. 2, aimed to represent a typical design solution.

Ventilation air is supplied to and exhausted from the rooms so that the air exchange rates in the rooms are approx. 1.85 $(m^3/h)/m^3$. The rooms are maintained at approx. 20 Pa underpressure with respect to outdoors. The corridor spaces are served only by an extract fan that maintains the corridor at approx. 0.5 Pa underpressure with respect to the rooms.

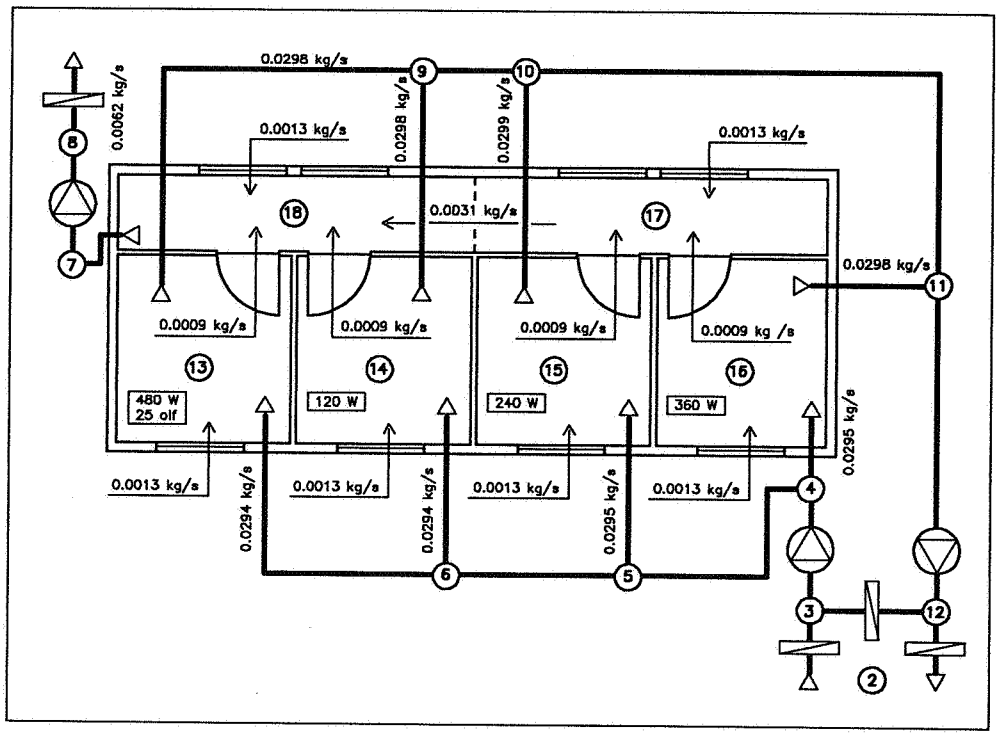


Figure 2. Layout of the simulated building.

The air enters the corridor as infiltration from outdoors and as leakages from the rooms. The doors are assumed to be of poor tightness and the windows are assumed to be relatively tight. Due to the small pressure drop across the closed door, opening the door has little effect on the balance of flows in the system.

A number of simulations were performed to determine the spread of contaminant from room 13, where it is generated, to other spaces of the system in different setups of door positions and with or without the return air. Regardless of whether the return air was used or not, the air flow rates were as shown in fig. 2. The duration of the simulations, 8 hours, depicts the length of the working day in an office building. The building was assumed to be of medium-weight construction, the temperature of the air supplied to all rooms was 17°C, the outdoor air temperature was a constant 20°C and the wind velocity was 0 m/s in all the simulations. In these conditions the airflows, air temperatures and contaminant concentrations were calculated in each zone of the simulated building. The results of the simulations are presented in figs. 3 and 4. The concentrations are

expressed in terms of PPD (eq. (12)) in order to evaluate simultaneously the air quality.

7.1. First simulation

The arrangement in which all the doors were closed was used in the first simulation. The courses of the temperatures, fig. 3a, are in accordance with the thermal loads in the rooms.

A steady state of contaminant concentration in room 13 is achieved after approx. 2 hours when no return air is used, see fig. 3b. The air quality in room 13 is very poor due to the very high strength of the contaminant source. Contaminant penetrates the corridor spaces, where the steady state is not achieved and the air quality remains within the range of acceptability. Due to the design of the airflows, the other rooms remain free from contaminant.

The plot in fig. 3c shows histories of the air qualities in a simulation using 57.2% return air. Steady state concentrations in the rooms are achieved after approx. 4 hours.
It is interesting to note that the use of as much as 57.2% return air does not greatly change the concentration in room 13 compared with full-fresh air ventilation, figs. 3b and 3c. Contaminant re-entering the system with return air spreads not only to room 13 but also to other rooms, i.e. the capacity of the entire system has an impact on the concentration in room 13. Due to the use of return air, the contaminant concentrations are shifted in all spaces of the system and the resulting air qualities are not acceptable. The concentrations in rooms grow faster than those in corridors, due to the high supply air flow rates in the rooms.

7.2. Second simulation

A study was made of the effect of changing the position of the doors on the spread of contaminant throughout the system. The door of room 13, where contaminant was generated, remained open during the simulation. Other doors were simulated to be opened and closed according to the schedule shown at the bottom of fig. 4.

As long as the door of the room remains closed, the temperature grows at a rate proportional to the thermal load and the contaminant does not enter the room when return air is not used, see figs. 4a and 4c. The moment the door is opened, a relatively high temperature difference exists across the opening and powerful two-way airflows through the opening are established, see fig. 4b, where major flows are plotted.

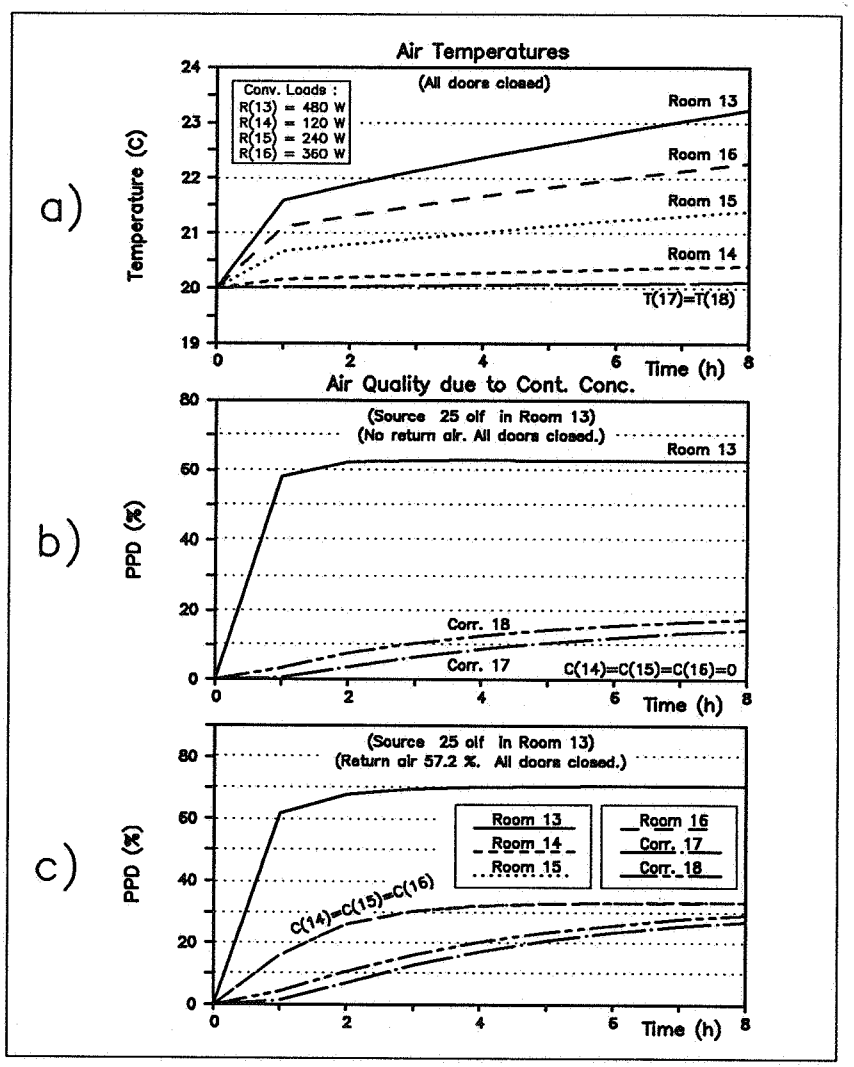
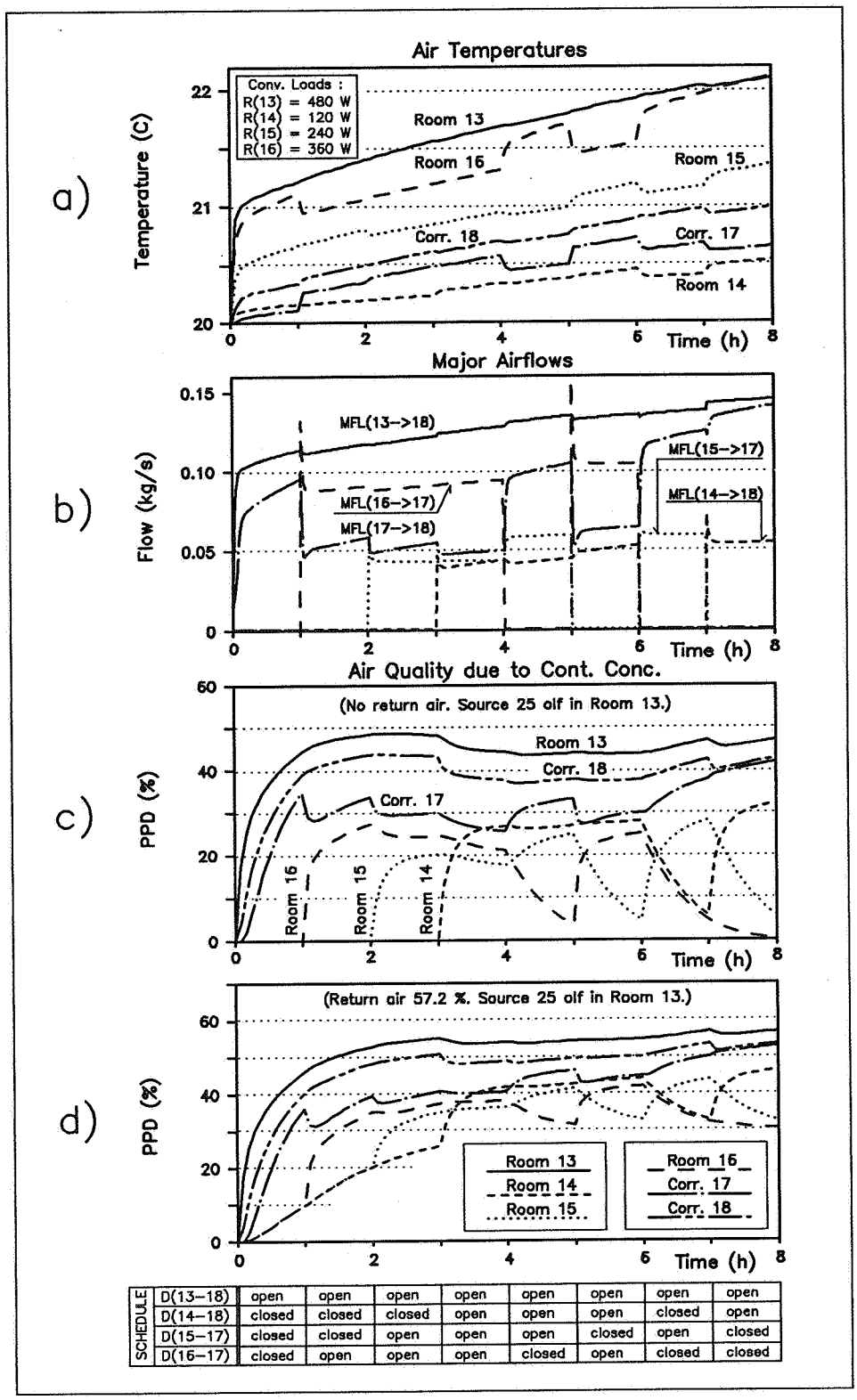


Figure 3. Air temperatures and air qualities in simulated building. All doors closed.

This generates a rapid increase in concentration in the room, since the concentrations in the corridoors are high due to the fact that the door of room 13 is open. Whereas very high concentrations, and thus low air qualities, are obtained within minutes of opening the door, it takes approx. 2 hours for the contaminant to be completely removed from the room after the door has been closed, see fig. 4c.

The use of return air attenuates the changes in concentrations imposed by changes in the position of the doors, evens out the distribution of concentration throughout the building and shifts all the concentrations to a higher level, see fig. 4d.



SCHEDULE									
	D(13-18)	open	open	open	open	open	open	open	open
	D(14-18)	closed	closed	closed	open	open	open	closed	open
	D(15-17)	closed	closed	open	open	open	closed	open	closed
	D(16-17)	closed	open	open	open	closed	open	closed	closed

Figure 4. Air temperatures, major airflows and air qualities in simulated building. Scheduled position of the doors.

7.3. Conclusions

The simulations showed that the air temperatures in a building do not remain constant, see figs. 3a and 4a. The phenomenon of two-way airflows through large openings is very sensitive to temperature, fig. 4b, and has a major influence on the contaminant transport from room to room. Thus the inclusion of thermal analysis in calculating contaminant concentrations considerably improved the reliability of the simulations.

The spread of contaminant in a building is affected by several factors and it seems to be difficult to protect a certain room from contaminant generated elsewhere in the system. Several conditions must be fulfilled to achieve it. First, the room must be maintained at a higher pressure than the rest of the system. Second, 100% fresh air ventilation must be used. Third, the door of the room must be kept closed. If any of the conditions is not fulfilled the contaminant will penetrate the room.

When air recirculation is used, the position of the door is of minor importance since the contaminant will find its way into the room through the air distribution system.
The door of the room where the contaminant is generated should be kept closed. This is the first measure to suppress the spread of contaminant to other spaces in the system.

8. SUMMARY

The computer program was developed for simultaneous dynamic simulation of contaminant concentrations, airflows and temperatures in multi-zone buildings. The theoretical foundations for the computer program were presented. A physical coupling was assumed as existing between the thermal behaviour of the building structure and the interzonal air movements. Thus its impact on the distribution of contaminants in the building was considered. This is a considerable improvement on other hitherto published programs in the same field.

An example building was used in a number of simulations. The dynamic distributions of contaminant concentrations in the building were determined with several door positions, with and without return air. The importance of simultaneous calculation of temperatures and airflows was evident, particularily in simulations including changes in the positions of doors.
The air qualities due to contaminant concentrations were evaluated in different parts of the building.

It was concluded that the first measure to suppress the spread of contaminant throughout the building is to keep the door of the room where it is generated closed. The airflows through the slots around the closed doors are unidirectional; therefore it is important to maintain rooms at a higher pressure than corridors. When the doors of the rooms are open, two-way flows through the door openings are established. The magnitude of two-way airflows through a large opening depends strongly on the temperature difference and is many times that of a one-way flow through a slot. Hence, the contaminant was efficiently distributed to all spaces when the doors were open. When air was recirculated, the contaminant penetrated all spaces in the system regardless of the position of the doors. Higher concentrations were obtained when the doors were open.

The basic simplification used in the program was the assumption of perfect mixing of air and contaminant within the zone. The thermal capacity of each partition in a building structure was roughly modelled as one value to be provided in input data. The outdoor air temperature was assumed to be equal at all outdoor nodes. The airflow through the large opening between vertically stacked spaces was simplified to a one-way flow.

The present version of the program works well and may readily be used for research purposes. Extensive validation by means of measurements should be carried out before it can be applied for design purposes.

APPENDIX

The following are the pressure-flow characteristics of nine types of airflow paths used in the program :

- Pressure loss in duct

$$\Delta p = 0.5 \, \rho \, v^2 \left(\frac{f_1 L}{D} + f_2 \right) \qquad (13)$$

where the pressure loss factor due to friction, f_1, is a function of duct diameter, roughness and Reynolds number.

- Power law for leakage equation

$$q = A \, (\Delta p)^B \qquad (14)$$

- **Quadratic leakage equation**

$$\Delta p = A\,q + B\,q^2 \qquad (15)$$

where coefficients A and B are constants and may be obtained from measurements [11].

- **Logarithmic element**

$$\Delta p = 10^A\,q^B \qquad (16)$$

where A and B are constants obtained from regression analysis.

- **Polynomial approximation**

$$\Delta p = s_0 + s_1 v + s_2 v^2 \qquad (17)$$

where coefficients s are constants.

- **Pressure loss across the damper**

$$\Delta p = 0.5 \cdot v^2 \cdot 2000 \cdot 10^{(e^{-A/4} - 0.0436\,A)} \qquad (18)$$

where A is the angle of the blades, (°); A=0° for closed damper and A=90° for fully open damper.

- **Pressure difference across the fan**

The velocity head generated by the fan is approximated by the second-degree polynomial

$$S_{ij} = s_0 + s_1 q + s_2 q^2 \qquad (19)$$

where q is the volume airflow (m^3/s), s_0, s_1, s_2 are constants and S_{ij} (Pa) is the velocity head. Equation (19) expresses the source term S_{ij} in eq. (4).

The general pressure loss coefficient K_{ij} for the path containing the fan refers to the pressure loss occurring in the part of the ducting included in the path.

- Large opening between vertically adjacent spaces

$$q = C_d A (2/\rho)^{0.5} (\Delta p)^B \quad (20)$$

where C_d is the discharge coefficient.

- Large opening between horizontally adjacent spaces

$$q_{net} = 0.65 H W (2/\rho)^{0.5} (\Delta p)^B \quad (21)$$

ACKNOWLEDGEMENT

This study was part of a project financed by the Ministry of Trade and Industry of Finland. This financial support is gratefully acknowledged.

REFERENCES

[1] - Axley J.: A discrete thermal analysis method for building energy simulation. Report Part 1 Linear thermal systems. Cornell University, New York, March 1986.

[2] - Axley J.: Progress toward a general analytical method for predicting indoor air pollution in buildings. Phase III Report NBSIR 88-3814 National Bureau of Standards, Gaithesburg, USA, July 1988.

[3] - Axley J., Grot R.: The coupled airflow and thermal analysis problem in building airflow system simulation. Preprint of the paper for inclusion in ASHRAE Transactions 1989.

[4] - Balazs K.: A wind pressure database from Hungary for ventilation and infiltration calculations. Air Infiltration Review, Vol. 10, No. 4, Sept. 1989

[5] - Borresen B.A.: Thermal room models for control analysis. ASHRAE Transactions 1981, Tech. Paper No. 2649.

[6] - Fanger P.O.: Introduction of the olf- and the decipol-unit to quantify air pollution perceived by humans indoors and outdoors. Energy and Buildings, Vol.12, 1988.

[7] - Juslin K., Siikonen T.: Solution methods for pipe network analysis. Preprint of the paper for IAEA/NPPCI Specialists Meeting on Nuclear Power Plant Training Simulators, Finland, Sept. 1983.

[8] - Klobut K.: Calculation of Airflows, Temperatures and Contaminant Concentrations in Multi-Zone Buildings. Licentiate's Thesis, Helsinki University of Technology, Faculty of Mechanical Engineering, April 1991.

[9] - Liddament M.: Air infiltration calculation techniques - an application guide. Air Infiltration and Ventilation Centre, Great Britain, 1986.

[10] - Press W.H., et al.: Numerical Recipes; the Art of Scientific Computing. Cambridge University Press & Numerical Recipes Software, USA 1988.

[11] - Saarnio P.: Calculation model for airtightness and natural ventilation of buildings. (In Finnish). Research report No. 242, 1983. Technical Research Centre of Finland.

[12] - Siikonen T.: Solutions method for pipe flow. (In Finnish). Technical Report LVT-6/84. Technical Research Centre of Finland.

[13] - Sirén K.: A computer program to calculate the concentration histories and some air quality related quantities in a multi-chamber system. Helsinki University of Technology, Institute of Energy Engineering, Nov. 1986.

[14] - Sirén K., Helenius T.: The estimation of concentration histories in dwellings in unsteady conditions. Paper at the Conference ROOMVENT-90, Oslo, Norway, June 1990.

[15] - Tuomaala P.: Numerical simulation model for building airflows and indoor air quality. Licentiate's Thesis (in Finnish), Helsinki University of Technology, Faculty of Mechanical Engineering, April 1990.

[16] - Walton G.: AIRNET - a computer program for building airflow network modelling. NISTIR 89-4072 Report, Gaithesburg, USA, April 1989.

AIR MOVEMENT & VENTILATION CONTROL WITHIN BUILDINGS

12th AIVC Conference, Ottawa, Canada
24-27 September, 1991

POSTER 38

An Evaluation of a Computer Code for Predicting Indoor Airflow and Heat Transfer

Yuguo Li and Laszlo Fuchs
Dept. of Gasdynamics
Royal Institute of Technology
S–100 44 Stockholm
SWEDEN

Sture Holmberg
Ventilation Division
Institute of Occupational Health
S–171 84 Solna
SWEDEN

Synopsis

The evaluation of a code can be done by investigating two items: solving the correct equations and solving equations correctly and efficiently. An indoor airflow code VentAirI has been developed and is evaluated here. An evaluating procedure is suggested. The code is characterized by the standard high–Reynolds–number k–ε model with wall function, the two–band radiation model and the SIMPLE algorithm. Test examples are: 1. A three–dimensional forced convection problem (Re=5000), 2. A natural convection problem ($Ra=5*10^{10}$), 3. A natural convection–radiation interaction problem ($Ra=1.45*10^{9}$). All calculations are compared with experimental results and published numerical solutions. Grid refinements are used to improve the accuracy of the predictions. The applicability of the Boussinesq approximation is confirmed. The prediction of heat flux through the boundaries are, however, less accurate. The code exhibits a relatively low convergence rate; the finer the grid, the slower the convergence. A fast multi–grid solver combined with local grid refinements is suggested. Consequently, another indoor airflow code VentAirII is developed.

1. Introduction

One crucial and frequently asked question about the numerical simulation of indoor airflow is: are the accuracy and efficiency of the simulation acceptable? A good indoor airflow code should have: 1) acceptable accuracy for the predicted velocity vector, its fluctuations, the temperature fields (including radiant temperature), contaminant concentration fields and heat transfer rates through the boundaries; 2) acceptable computational cost. Not all of these features are required in all situations. The overall accuracy of the simulation can be influenced by the applicability of the turbulence model, the assumption of Boussinesq approximation, the representation of geometry, the truncation errors, and so on. The dimension of the problem and the numerical algorithm determine the computational cost. In general, confidence in the accuracy of the predictions produced by a code is obtained by investigating two items: 1) solving the correct equations, i.e. evaluating the accuracy of the physical model equations that are being used. 2) Solving these equations correctly and efficiently, i.e. evaluating the accuracy and efficiency of the numerical solution procedure for the given set of governing equations. Numerical algorithms produce only an approximate solution to the governing system of partial differential equations. Errors arise from two components of the numerical methods: discretization errors and iterative (convergence) errors .

The question of model accuracy (e.g. there exists currently no generally valid turbulence closure models) should be kept separate from the one of numerical accuracy. Thus, the various turbulence models cannot be evaluated unless the numerical accuracy is first established. The first requirement is to reduce the numerical error to an acceptable level. For any consistent numerical approximation, the error is reduced as the grid is refined. Therefore, grid refinement is a natural means of improving accuracy. In addition to grid refinement, one may also use higher order discrete approximation. However, higher order approximation can be applied only

when the grid resolution is fine enough to represent the smallest length scales. Here, we shall primarily discuss the spatial resolution aspects.

For evaluating the accuracy of a numerical solution, one may resort to the following: 1). *Code to experiment comparison.* Ideally, the accuracy and limitations of the experimental data should be known and be thoroughly understood. Such kind of experimental data are rather rare, and also it should be noted that agreement with the experiment does not imply universally. A comparison between the experiment and a single shot calculation should be avoided[1]. 2). *Code to exact solution comparison.* For assessing the accuracy of a numerical method, comparison with an exact solution of the problem is the best. However, exact solutions to flow problems are known only in some simple, degenerated cases. Good accuracy in these cases does not imply similar accuracy in other general situations. 3). *Code to code comparison.* It helps to quantify numerical errors between algorithms when identical physical models are solved with different methods. But a comparison of different codes for solving the same governing equations and the same physical problem does not necessarily establish confidence, unless one of the codes has been validated for different parameter values by other means. 4) *Convergence history and spatial resolution analysis.* Slow convergence rate may mask iteration (convergence) errors. Obtaining solutions on successively finer grids reduces the truncation errors and will quantify the effect of grid resolution errors on flow quantities of interest. With Richardson extrapolation, grid refinement can be used to obtain a more accurate result, and then the accuracy of the results can be determined. Richardson extrapolation is applicable only once the asymptotic behavior of the solution is established.

The purpose of this paper is to evaluate the accuracy and efficiency of a computer code. A fast multi–grid solver combined with local grid refinements is suggested for ventilation problems. Three well–known turbulent–flow problems are selected, and computational results of the code on these problems are compared with experimental data and published numerical solutions.

2. Indoor airflow code VentAirI

2.1 Governing equations and Boundary conditions

The indoor airflow code VentAirI, which is under development by the authors, solves the unsteady, Reynolds–averaged Navier–Stokes equations along with the closure k–ϵ model. The equations can be written in the following conservative form:

$$\frac{\partial \varrho u_i}{\partial x_i} = 0 \tag{1}$$

$$\frac{\partial \varrho u_i}{\partial t} + \frac{\partial \varrho u_i u_j}{\partial x_j} = -\frac{\partial p}{\partial x_j} + \frac{\partial}{\partial x_j}[\mu_{eff}(\frac{\partial u_i}{\partial x_j} + \frac{\partial u_j}{\partial x_i})] - \varrho g_i \tag{2}$$

$$\frac{\partial \varrho k}{\partial t} + \frac{\partial \varrho k u_j}{\partial x_j} = \frac{\partial}{\partial x_i}[\frac{\mu_{eff}}{\sigma_k}(\frac{\partial k}{\partial x_i})] + P + G - \varrho\epsilon \tag{3}$$

$$\frac{\partial \rho \epsilon}{\partial t}+\frac{\partial \rho \epsilon u_j}{\partial x_j}=\frac{\partial}{\partial x_i}[\frac{\mu_{eff}}{\sigma_\epsilon}(\frac{\partial \epsilon}{\partial x_i})]+C_{1\epsilon}\frac{\epsilon}{k}(P+G)-C_{2\epsilon}\frac{\rho \epsilon^2}{k} \quad (4)$$

$$\frac{\partial \rho \theta}{\partial t}+\frac{\partial \rho \theta u_j}{\partial x_j}=\frac{\partial}{\partial x_i}[\frac{\mu_{eff}}{\sigma_\theta}(\frac{\partial \theta}{\partial x_i})]+S_\theta \quad (5)$$

with,

$$\mu_{eff}=\mu+f_\mu C_\mu \rho \frac{k^2}{\epsilon}=\mu+\mu_t \qquad P=\mu_t(\frac{\partial u_i}{\partial x_j}+\frac{\partial u_j}{\partial x_i})\frac{\partial u_i}{\partial x_j} \qquad G=\beta g_i \frac{\mu_t}{\sigma_\theta}\frac{\partial \theta}{\partial x_i} \qquad S_\theta=\frac{Q}{C_p}$$

$$C_{1\varepsilon}=1.44,\ C_{2\varepsilon}=1.92,\ \sigma_K=1.0,\ \sigma_\varepsilon=1.3,\ \sigma_\mu=0.09,\ \sigma_\theta=0.9 \quad (6)$$

where *u,v and w* are the velocity components, *p* is the pressure, *k* is the turbulent kinetic energy, ε is the dissipation rate of turbulence, μ_{eff} is the sum of the kinematic laminar viscosity μ and kinematic turbulent viscosity μ_t, C_p is the heat capacity of constant pressure, *Q* is the internal heat generation rate, g_i is the gravitational acceleration in direction x_i, θ is the temperature, ρ is the density (in general $\rho = \rho(\theta)$, when the Boussinesq approximation is used $\rho=\rho_{ref}$, and the buoyancy term in the momentum equation is replaced by $(\rho-\rho_{ref})g_i$, where ρ_{ref} if the reference density).

All variables are given at the supply inlets. The *k* and ε values are determined either by measurement or from the equations given by Awbi[2]. A zero–gradient condition applies to the exhaust outlets. At planes of symmetry, the normal gradient is zero for all quantities, and also the normal velocity components and scalar fluxes are zero. At a wall boundary, Dirichlet boundary conditions are used which are based on the wall functions for velocity, *k* and ε [3] and for θ [4]. For the thermal radiation, the temperature at inside surface is obtained from the energy balance equation of the surface. The radiation calculation considers both long– and short–wave radiation by a two–band radiation model[5]. The indoor air is transparent, the surfaces are grey and all energy is emitted and reflected diffusely.

2.2 Solution procedure

The equations are expressed in time–implicit and conservative finite difference form on a staggered grid. The hybrid upwind/central differencing scheme is used to discretize the advection terms. The finite difference equations are solved by the SIMPLE procedure[6]. The continuity equation is rewritten into an equation for the pressure correction. The resulting algebraic equations are solved by TDMA (Tri–Diagonal Matrix Algorithm) line–by–line method. The solutions presented here are obtained from a four to six order of magnitude reduction in the L2–norm of the residual from its maximum value. The L2–norm of the residual R is defined as:

$$R^* = [\frac{1}{6N}\sum_{i=1}^{N}(R^2_{ui}+R^2_{vi}+R^2_{wi}+R^2_{mi}+R^2_{ki}+R^2_{\epsilon i})]^{\frac{1}{2}} \quad (7)$$

The convergence rate is defined as $(R^*_{final}/R^*_{max})^{(1/Ni)}$, where N is the total number of grid points in the domain, N_i is the iteration number, R_{ui}, R_{vi}, R_{wi}, R_{mi}, R_{ki}, $R_{\varepsilon i}$ are the residuals of the three momentum equations, continuity equation and k– and ε– equations.

3. Evaluation of VentAirI

Test 1. Forced Convection

The evaluation is first carried out for a three–dimensional isothermally ventilated room for which detailed velocity field measurements are available[7]. The practical relevance of the test problem relates to mixing ventilation systems, in which air is often supplied through a small opening near the ceiling, and removed through a return opening close to the floor. The ventilated room is shown in Fig.1. The height of the room is 89 mm. Other dimensions are: is L/H=3.0; W/H=1.0; h/H=0.1; w/H=0.1. The Reynolds number, based on the inlet velocity U_{in} and the height of the inlet, is 5000. The air velocity was measured by a Laser–Doppler Anemometer. The plane y=0 is a symmetry plane. The flow is thus calculated in one half of the room only. Two grids (18*20*20 and 36*40*40) are used. The calculated profiles of longitudinal velocity u at two different z–planes (z/w=0.1 and 0.4), and corresponding measured results are given in Fig.2. The computed velocity profiles are in good agreement with the measurement. A grid–dependent solution is observed and the grid refinement improves the solution in the recirculation region.

One of the advantages of using the wall function method is that it is computationally convenient, i.e. the near–wall region is excluded from the flow domain. This does not mean that a coarse grid is adequate. It is shown here that the accuracy of the predicted velocity field can be improved by a grid refinement. The convergence rate of VentAirI is rather poor for this problem. With under–relaxation, convergence rates of only 0.986 for 18*20*20 and 0.990 for 36*40*40 can be reached. It has been observed that the convergence performance becomes even worse when the grid is finer.

Test 2. Natural Convection

The distribution of indoor air temperature is mostly non–uniform. For example, with displacement ventilation, the flow is generally driven by buoyancy forces. The buoyancy–driven flow in a cavity with differently heated vertical sides is considered here, as suggested by others[8,9]. A full–scale air–filled cavity with dimensions corresponding to the experimental results[16] is chosen here. The cavity is 2.5m high and 0.5m wide, see Fig.3. The two horizontal walls are insulated. The vertical walls are isothermal with temperatures T_h = 80°C and Tc = 34.2°C. The corresponding Rayleigh number based on the cavity height is $5*10^{10}$. The air velocities were measured by a Laser–Doppler Anemometer system. In our numerical calculation, four different uniform grids, 20*20, 40*40, 80*80 and 111*111, are used. In addition, a non–uniform grid, 53*53, is used to produce a very fine grid near the boundary and a

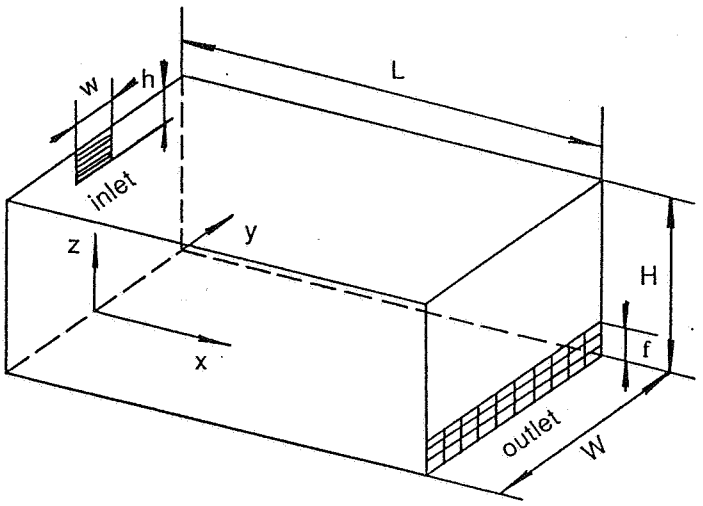


Fig.1 The experimental room for test 1.

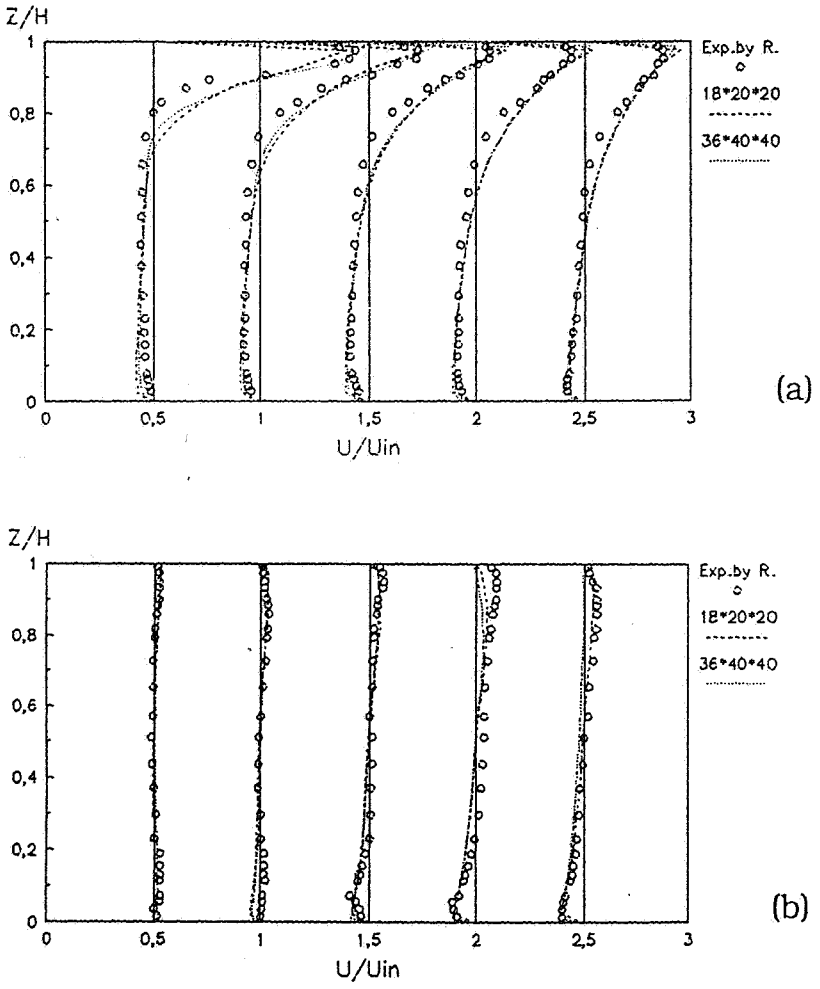


Fig.2 The calculated profiles of u–velocity component at two z–planes (a) z/w=0.1; (b) z/w=0.4.

coarse grid in the central region of the flow field. The convergence rate is in the range of 0.985–0.999.

Fig.4 compares the measured velocity profiles mid–way up the room with the ones computed by the five different grid scales. The vertical temperature profiles in the central section are given in Fig.5. Fig.6 shows the relationship between the local Rayleigh and the local Nusselt numbers. A number of observations can be made, which confirm the conclusions of Chen et al[8]: 1), a good agreement is obtained between the experiment and calculations for mid–height velocity; 2), The measured temperature of cavity in the central section is lower than the computed one. The computed one is symmetric, but not the measured. This is possibly due to the heat loss through the ceiling. There are also a number of points which emerge from a further analysis of the effects of the grid refinements. 1), Fine grid can improve the accuracy of the predicted velocity. 2), the coarse grid near the wall (20*20) gives a too–low convective heat transfer coefficient, and the fine one gives a too–high coefficient (grid 80*80 and 53*53); 3), the uniform grid 111*111 and nonuniform grid 53*53 give two almost equivalent solutions, because they use same mesh space near walls. The importance of the near wall region explains the importance of the model "wall functions" that are used.

Test 3. Natural Convection and Surface Radiation Interactions

There is more energy exchange by radiation at room temperature than is commonly realized[10], particularly when dealing with heating systems with heated surfaces and with displacement ventilation[11]. Radiation exchange between people and their surroundings is an important factor in determining thermal comfort. So the study is extended to include the interaction between natural convection and surface radiation in a square enclosure, for which the calculated results by Fugesi and Farouk[12] are used for comparison.

The geometry of the problem is shown in Fig.7. The opposing walls are maintained at two different constant temperatures, the temperature of left wall being higher than that of right wall. The floor and ceiling are thermally insulated. The surfaces of the entire enclosure are black for radiation, i.e. the wall emissivity is unity. The Prandtl number of the fluid is fixed at 0.686(CO_2). The calculation is performed for Grashof number $1.45*10^9$ and overheat ratio τ of unity (i.e. $T_h = 832.5K$, $T_c = 277.5K$). The calculations and comparison with the results of Fugesi and Farouk[12] for Grashof number $6.55*10^6$ were reported by Li and Fuchs[5]. The Boussinesq approximation is used. Gebhart's absorption method is used to calculate the radiation exchange. The present calculation is performed with a 56*56 non–uniform grid for a turbulent regime. It is impossible to get a converged solution for this problem if the number of grid points is too small and/or the grid points are not properly distributed. This is due to the bad resolution near the wall boundaries. Fig. 8 shows the temperature and flow fields with and without surface radiation. When the radiation is totally neglected, the fields are symmetric. When the surface radiation is considered, the symmetry completely disappears. The core of the fluid becomes warmer when compared to the pure natural convection case. The low–velocity region is moved from the core region to the lower part of the room, leaning toward the cold wall.

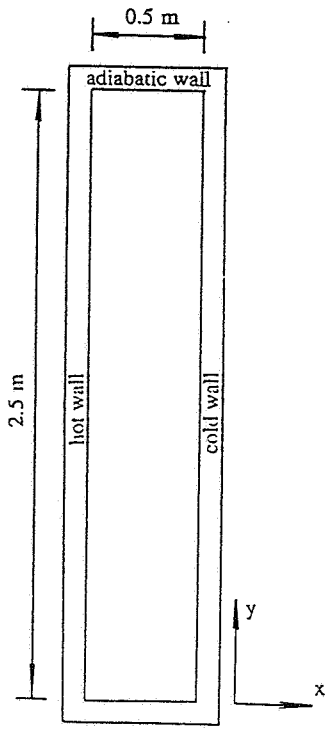


Fig.3 The full–scale air–filled cavity.

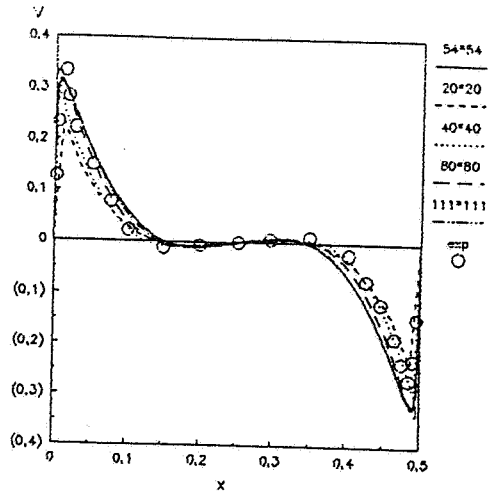


Fig.4 The measured and calculated velocity profiles mid–way up the room with five different grid spacings.

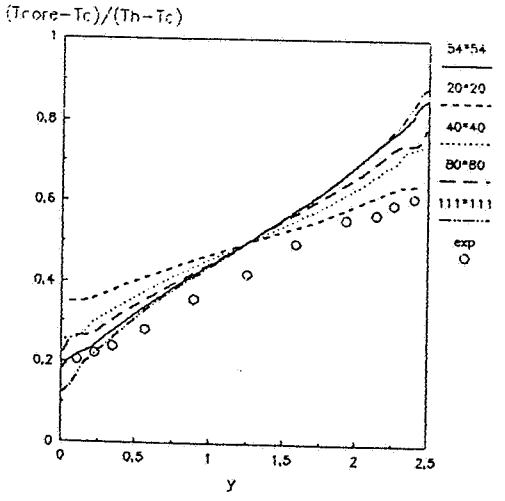


Fig.5 The measured and calculated vertical temperature profiles mid–way up the room by five different grid scales.

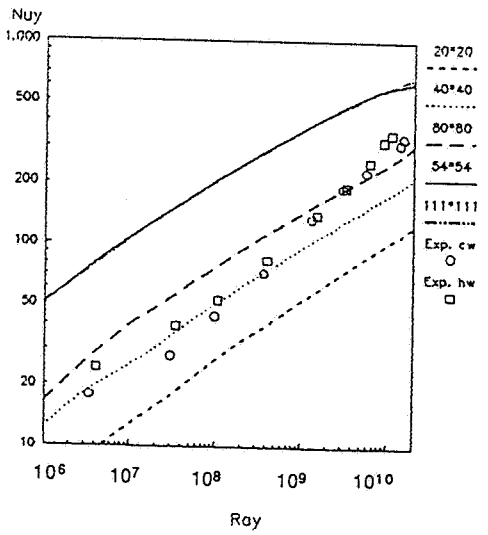


Fig.6 The relationship between local Rayleigh and local Nusselt numbers.

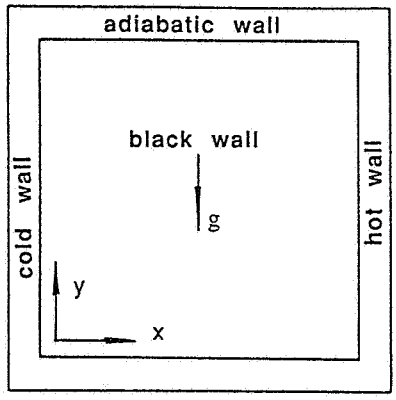


Fig.7 A square enclosure.

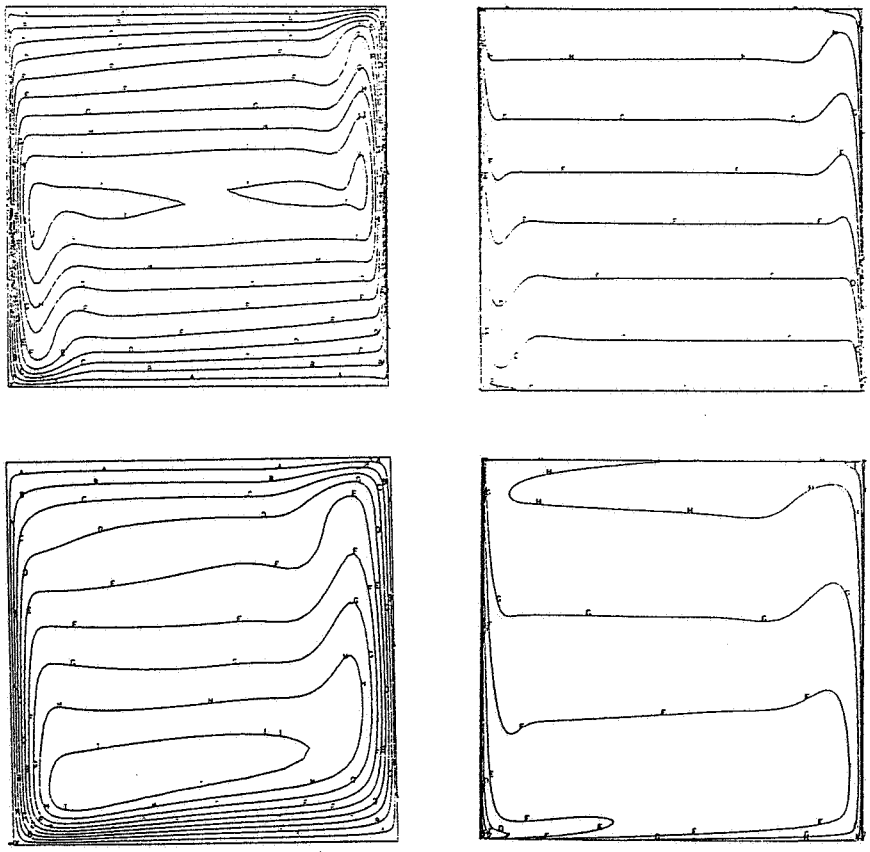


Fig.8 The flow fields (left) and temperature fields (right), with (lower) and without (upper) surface radiation.

Fig.8 is graphically identical to those of Fusegi and Farouk[12]. The velocity profiles along the midplanes of the enclosure are shown in Fig.9. The figure indicates that intense flows are induced near the insulated surfaces when radiation is taken into account. The thickness of the boundary layer in the case of turbulent regime is thinner than in the case of laminar regime[5]. The agreement between our results and the results of Fusegi and Farouk[12] is very good. The discrepancy may be due to the Boussinesq approximation in VentAirI, since the temperature difference is very large.

To further confirm the applicability of the Boussinesq approximation, the calculation is also performed without the Boussinesq approximation. The density variation due to the temperature difference is considered. The results are presented in Fig.10 for overheat ratios of 1.0 (i.e. T_h = 832.5K and T_c = 277.5K)and 0.1 (i.e. T_h = 582.75K and T_c = 527.25K). Grashof number is $6.55*10^6$.The error caused by the Boussinesq approximation is shown in the figure. When the overheat ratio is 0.1, the result considering the density variation is almost identical to the one with the Boussinesq approximation[5]. Our results with the density variation are almost identical to those of Fusegi and Farouk[12,5]. When the temperature difference is less than 50°C, the result with Boussinesq approximation is very good. So it can be concluded that for airflow simulations in ventilated rooms, the Boussinesq approximation is reasonable, since the temperature differences are very small.

4. Overview of Indoor Airflow Code VentAirII

One major numerical disadvantage of VentAirI is its slow convergence rate; the finer the grid, the slower the convergence rate. A second code VentAirII that uses the same governing equations as in VentAirI has been developed. The multi–grid (MG) procedure by Bai and Fuchs[13] and the local grid refinement procedure by Fuchs[14]and Bai and Fuchs[13] are used. The MG method is an iterative procedure which ideally exhibits a grid–independent convergence rate. The local grid refinements make it possible to resolve large gradients in the flow field without influencing the convergence rate of the MG scheme. In this new code (VentAirII), the physical domain is discretized with a global uniform rectangular mesh. In regions of high gradients, e.g. at near wall regions and at inlet/outlet regions, the locally refined mesh is added. The diffusive term is approximated by the central difference scheme. The convective term is discretized by the hybrid central/upwind differencing scheme[6]. The wall function of Launder and Spalding[15] that is used by Bai and Fuchs[13] is replaced by the wall function of Rodi[3], which means that the boundary conditions for k is changed from $dk/dn = 0$ to $k=f(u_t)$. After these modifications, it is found that the convergence performance is improved when the code is applied to the flow in an isothermal box model[13]. The Reynolds number based on the inlet width is 7000 for the isothermal flow in this box. Fig.11 shows the multigrid convergence history using a coarser grid (22*14*14*14) and a finer grid (42*26*26) with the original MG code[13] and VentAirII, respectively. The work unit is defined as the computational effort for one relaxation sweep on the finest level. The residuals are reduced 5 orders of magnitude within 35 work units with VentAirII compared 55 work units with the original MG code. The single grid results with VentAirII is also shown in the figure for comparison. The

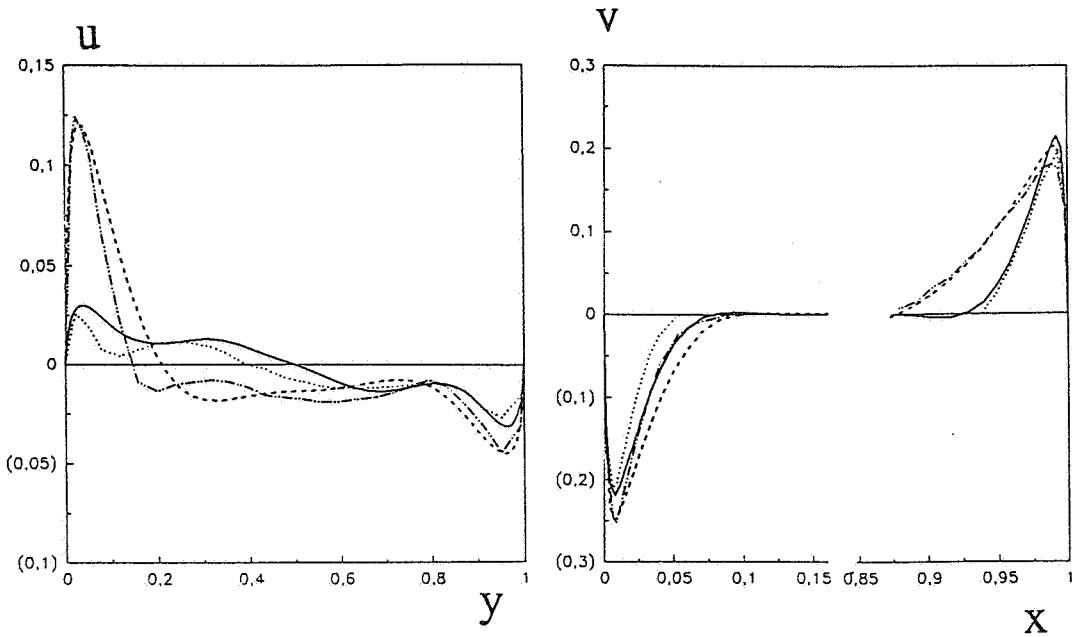


Fig.9 The velocity profiles along the mid–planes of the enclosure. —— *, no radiation;* ------ *, surface radiation;* ..... *, no radiation*[12]*;* —.— *, surface radiation* [12].

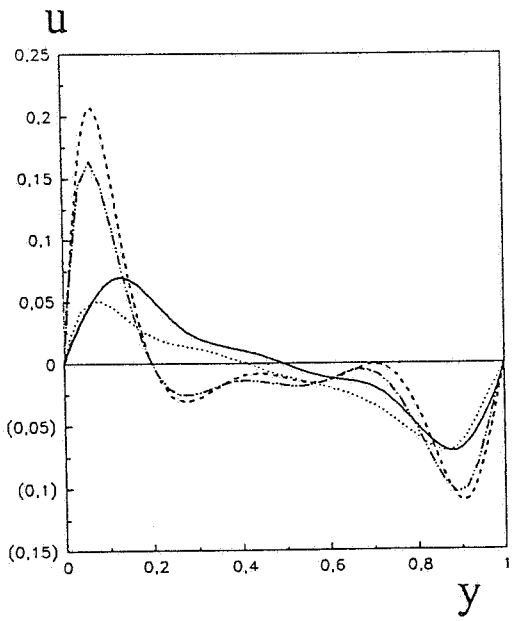


Fig.10 The velocity profiles along the mid–planes of the enclosure with (B) and without (NB) Boussinesq approximation. —— *, no radiation,* τ*=0.1, NB;* ..... *, no radiation,* τ*=1., NB;* ------ *, surface radiation,* τ*=0.1, NB;* —.— *, surface radiation,* τ*=1., NB;* —— *, no radiation,* τ*=1, B*[5].

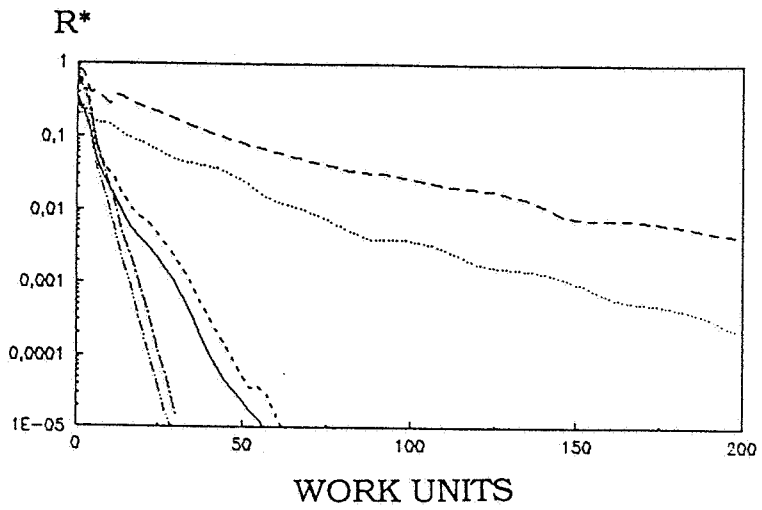


Fig.11 The convergence history of the isothermal box using single–(SG) and 3 levels multi–grid (MG) methods; results of VentAirII*:* ——— *, coarser grid, MG;* –·–·– *, finer grid, MG;* ····· *, coarser grid, SG;* – – – *, finer grid, SG;* results of Bai and Fuchs[13]*:* —— *, coarser grid, MG;* ------ *, finer grid, MG.*

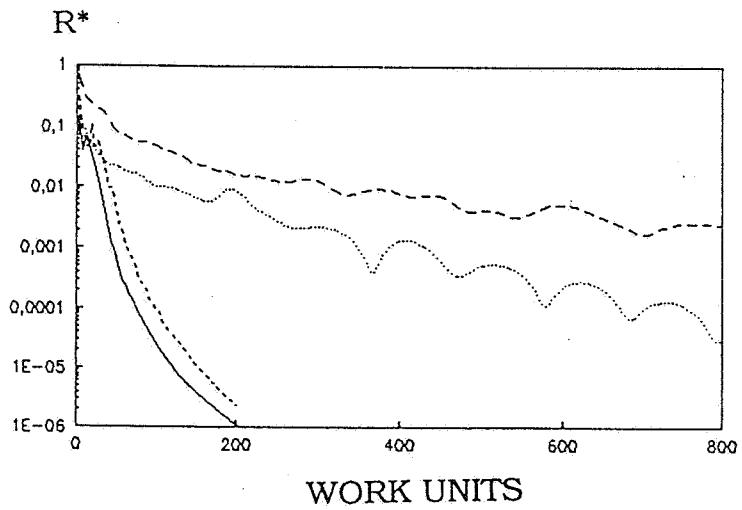


Fig.12 The convergence history of the problem in test 1 using single–(SG) and 3 levles multi–grid (MG) methods; —— *, coarser grid, MG;* ------ *, finer grid, MG;* ····· *, coarser grid, SG;* – – – *, finer grid, SG.*

problem in test 1 is also solved by VentAirII. The VentAirI and VentAirII give identical predictions when using the same finest grid. The convergence history by VentAirII is shown in Fig.12. The coarser grid (22*14*22) and the finer grid (42*26*42) are used. The advantage of the MG method over single grid method with respect to computational speed is displayed. The computational speed with MG is a factor of 6 faster than that of the single grid for the coarser grid and a factor of 50–60 for the finer grid. The main advantage of the MG method is that the computational time is linearly increased with the number of nodes. Local refinements for the problem in test 1 can be found in Li and Fuchs[16].

5. Conclusions

Three turbulent incompressible fluid flows (forced convection, natural convection and convection–radiation interactions) have been tested to evaluate the accuracy and efficiency of the computer code VentAirI.

Solving governing equations correctly and efficiently. The grid refinement studies here indicate that grid fineness can improve the accuracy of the predicted velocity and temperature fields. Grid refinement is also expected to reduce the numerical diffusion. Fine grids and a proper distribution of the grid points are required to get an accurate numerical solution. The usage of a large number of computational elements requires faster convergence. The convergence test shows that VentAirI exhibits a low convergence rate; and the finer the grid the slower the convergence. The problem can be overcome by the MG method together with local grid refinements. This has been demonstrated by VentAirII. A nearly grid–independent convergence has been achieved for the test problems with more than an factor 50 reduction in CPU time for the finer grid. Thus the fast MG solver combined with local grid refinements is very appropriate for ventilation problems

Solving correct governing equations: The applicability of the Boussinesq approximation is confirmed. The results from the various grid scales differ most for quantities that are determined in the inner layer of the boundary layer, for example, the wall heat transfer. This implies that the high–Reynolds–number model with wall functions is not suitable for simulating indoor air flow from the heating and cooling load point of view. HAVC engineers are interested in heat loss and heat gain through the boundaries. Possible improvements to the turbulent model may include improving the wall function treatment or rather eliminating the need for a too coarse scale modelling (using Large Eddy Simulation). Experiments should also be designed properly, so that the produced data are relevant and accurate for code validation.

6. Acknowledgement

This work was financially supported by the Swedish Council for Building Research (BFR). We would like to thank deeply Dr. X.S. Bai for his help in adapting the 3D MG code into VentAirII.

7. References

1. ROACHE, P. J. "Need for control of numerical accuracy", Journal of Spacecraft and Rockets, vol. 27, no. 2, pp. 98–102, 1990.

2. AWBI, H. B. "Application of computational fluid dynamics in room ventilation", Building and Environment, vol.24 no.1, pp.73–84, 1989.

3. RODI, W. "Turbulence models and their application in hydraulics", International Association of Hydraulic Research, Monograph, Delft, 1980.

4. JAYATILLIAKA, C. L. V. Progr. in Heat Mass Transfer, vol.1 pp. 193, 1969.

5. LI, Y., FUCHS, L. "A two–band radiation model for calculating room wall temperature", 1st Baltic Heat Transfer Conference, Göteborg, Sweden, 26th–31st, August, 1991.

6. PATANKAR, S. K. "Numerical Heat Transfer and Fluid Flow", Hemisphere Publishing Corp., Washington, D.C., 1980.

7. RESTIVO, A. "Turbulent flows in ventilated rooms". PhD thesis, Dept. of Mech. Eng., Imperial College, London, 1979.

8. CHEN, Q.Y., MOSER, A., HUBER, A. "Prediction of buoyant, turbulent flow by a low Reynolds number k–e model", ASHRAE Transactions, 1990.

9. BAKER, A. J., KELSO, R.M. "On validation of computational fluid dynamics procedure for room air motion prediction. ASHRAE Transactions, vol.96, part1, 1990.

10. MCINTYRE, D. A. "The thermal radiation field", Building Science, vol.9, pp.247–262, 1974.

11. HEISEILBERG, P., SANDBERG, M. "Convection from a slender cylinder in a ventilated room", Proceedings of Roomvent'90, Oslo, Norway, June 13–15, 1990.

12. FUGESI, T., FAROUK, B. "Laminar and turbulent convection–radiation interactions in a square enclosure filled with a monger gas", Numerical Heat Transfer, part A, vol.15, pp.303–322, 1989.

13. BAI, X. S., FUCHS, L. "A fast multi–grid method for 3–D turbulent incompressible flows", 7th International Conference on Numerical Methods in Laminar and Turbulent Flow, Stanford, California, 15th–19th July, 1991.

14. FUCHS, L. "A local mesh–refinement technique for incompressible flows", Computers & Fluids, vol. 14, no.1, pp.69–81, 1986.

15. LAUNDER, B.E., SPALDING, D.B. "The numerical computation of turbulent flows", Comp. Math. in Appl. Mech. & Engi. 3, pp.269–289, 1974.

16. LI, Y., FUCHS, L., BAI, X.S."Accurate numerical simulation of air flows in ventilated multi–rooms", Building Simulation'91, Nice, Sophia–Antipolis, France, 20th–22nd, August, 1991.

17. CHEESEWRIGHT, R., KING, K.J., ZIAI, S. "Experimental data for the validation of computer codes for the prediction of two–dimensional buoyant cavity flows", Significant Questions in Buoyancy Affected Enclosure or Cavity Flows. ed. Humphrey, J.A.C. et al, pp.75–81, New York, ASME, 1986.

AIR MOVEMENT & VENTILATION CONTROL WITHIN BUILDINGS

12th AIVC Conference, Ottawa, Canada
24-27 September, 1991

POSTER 39

Turbulent Modelling of Airflow Patterns and Ventilation Effectiveness In a Half Scale Office Building.

H.Han, T.H. Kuehn, J.W. Ramsey

Dept of Mechanical Engineering
University of Minnesota
111 Church St, S.E.
Minneapolis, MN 55455
USA

ABSTRACT

The concentrations of indoor pollutants should be maintained below recommended values at all occupied locations at any time. A design method based on minimal air change rates may not be satisfactory, since the ventilation effectiveness is determined not only by the nominal air exchange rate but also many other factors, such as the airflow pattern the space, location of contaminant sources, and properties of the contaminants. It is the objective of the present study to investigate numerically the effect of airflow patterns due to the various factors of ventilation effectiveness.

The control volume based finite difference scheme is utilized to solve steady state flow field. a low Reynolds number k-e turbulent model is implemented to calculate turbulent quantities. The mass conservation equation for a contaminant is solved to calculate transient solutions in the concentration field under the steady state flow field obtained. From the transient concentration field, ventilation effectiveness is calculated using two different methods; 1) Local decay rate of concentration: Slope of Log (concentration) v.s. Time curve, and 2) Local mean age: Equivalent to area under Concentration v.s. Time curve.

The simulations are carried out for several different values of air exchange rates and several different intake and exhaust locations in a two-dimensional model of a half scale office room of 57" high x 77" wide. The distributions of local ventilation effectiveness are presented along with the velocity vectors and concentration distributions in the ventilated space. The results show that the ventilation effectiveness around various locations within the room could vary significantly. It suggests that the design method based on nominal air exchange rate may overestimate the ventilation efficiency and thus underestimate the concentration of contaminants in some locations within the ventilated space, especially regions with large recirculations.

AIR MOVEMENT & VENTILATION CONTROL WITHIN BUILDINGS

12th AIVC Conference, Ottawa, Canada
24-27 September, 1991

POSTER 40

A MULTI-ZONE MODEL TO FACILITATE PREDICTING NATURAL VENTILATION THROUGH BUILDINGS

A.J. FIELD, W.J. BATTY and S.D. PROBERT

DEPARTMENT OF APPLIED ENERGY
CRANFIELD INSTITUTE OF TECHNOLOGY
CRANFIELD
BEDFORD
UNITED KINGDOM

A multi-zone model to facilitate predicting natural ventilation through buildings.

Abstract.

A mathematical model has been developed which will facilitate the prediction of infiltration rates within multi-zone buildings. The aim was to cater for:

(i) significantly different temperatures in different parts of the building;
(ii) flow paths at any height, including vertical connections between zones; and
(iii) flow paths extending over large vertical distances.

These aims led to to the requirement in the associated computer program that the variation of pressure with height be accounted for independently within each zone of the building.

In order to achieve these aims, the flows between zones were modelled by considering pressure differences and flow resistances. The neutral pressure level approach was found to introduce unnecessary complications. If the pressure in each zone varies with height, and at a rate which depends on the zone temperature, it is necessary to determine the the pressure in each zone at a reference height. The floor level of each zone was chosen as the reference height. The total building pressures are solved simultaneously to give these reference pressures.

Predictions obtained from the developed computer program have been compared with analytical solutions for simple systems as well as experimental data.

Notation.

A	Area (m^2).
C	Flow coefficient ($m.s^{-1}Pa^n$).
c	Flow coefficient ($m^3s^{-1}Pa^n$).
g	Acceleration due to gravity (9.81 m s^{-2}).
H	Total building height (m).
h	height (m).
N	Ratio of the calculation height to the total building height.
n	Flow exponent which characterises the flow regime for openings in the building structure. e.g. large openings - n = 0.5, cracks around doors - n = 0.66.
p	Air pressure (Pa).
Q	Air flow rate (m^3s^{-1}).
T	Temperature (°C or K).
λ	Ratio of the height of the neutral pressure level to the building height.
ρ	density (kg m^{-3}).
Ω	Thermal draught coefficient to account for the vertical resistance to flow between the floors of a building.

Subscripts

b	Barometric.
e	Exterior.
f	at floor level.
i	Interior.
h	At a specific height.
o	At a datum position.
st	Due to stack effect.
x	Height up an opening above the floor level.

1. Introduction.

1.1 Aim of the project.

This was to develop a computer model which would permit infiltration rates in buildings to be predicted accurately. Air infiltration arising from wind and stack effects often need to be estimated, as well as the effects of mechanical ventilation.

1.2 Need for air exchange in buildings.

Adequate rates of air change in buildings are needed for several reasons. Ventilation is required to maintain the quality of air in a building by replacing indoor air with fresh outside air. This supply of fresh air is is essential for the support of human metabolism, and to dilute and remove internal air pollutions.

Buildings which are designed to use passive solar heating or cooling may rely on ventilation and air movement as the mechanism for heat transfer. If the system is truly passive, then natural physical processes are used as the sole driving force. In hot conditions, a supply of fresh air can also help to increase heat loss from the body and thus aid in preventing discomfort.

However, excessive ventilation is often responsible for significant energy losses from buildings, and can cause cold and draughty conditions. An optimal level of ventilation should therefore be aimed at during the design of a building. Particular requirements must be met if air movement is used for heating or cooling as well as ventilation [1].

Awareness of infiltration as a major factor in the overall conditioning load of a building has led to tighter construction and integrity of the building enclosure. Consequently, infiltration rates, and their related ventilation rates of heat loss have been reduced. However, this has sometimes created other problems with regard to indoor air quality [2].

It is therefore important to be aware of the air flow pattern in a building when estimating indoor air quality, calculating space conditioning rates of energy consumption, or investigating the potential for using passive solar heating and cooling techniques.

1.3 Causes of air infiltration.

The air flow through a building is caused by natural air infiltration and by the use of mechanical ventilation systems. Natural infiltration occurs because of pressure differences across the openings in the building fabric. These arise due to wind, and thermal buoyancy effects (i.e. *the stack effect).* The wind pressure distribution around a building depends upon the building shape, the velocity and direction of the wind, and the nature of the surrounding terrain. The stack effect is caused by differences in air density resulting from the difference in temperature in the building. The rate of infiltration is a function of the pressure differences and the distribution and dimensions of openings within the building structure.

Natural air infiltration is a haphazard process which gives widely varying rates of ventilation and little control of the pattern of air movement within buildings. However it plays a dominant role in the ventilation of many types of building.

Ventilation needs may also be satisfied by the use of mechanical systems. These allow greater control over the air distribution but they do incur penalties both in terms of capital and running costs. Consequently it may be more cost effective to provide the required ventilation solely through natural means.

Where mechanical ventilation systems are used, the interaction of these systems with the natural air infiltration must be considered in order to achieve optimal performance.

2. Modelling air infiltration.

2.1 Previous work.

In spite of its importance, the analysis of inter-zonal airflows has lagged behind the modelling of other building features [3]. This is largely due to the complexity of the problem. Also the dearth of reliable measured data concerning infiltration characteristics of building components has hindered development. Nevertheless, various infiltration models have been developed over the last two decades. These tend to fall into two groups: single-zone models and multi-zone models [4]. A zone is defined as a fully mixed volume with a constant concentration level of the enclosed gas mixture. Single-zone models may be used where the condition within a building approximates to this limit, for example in small buildings with no internal partitions or at least open internal doors. Unfortunately the limits of single-zone models are often violated by attempting to use such models for multi-zone applications.

Where there are internal partitions in a building or there is an inhomogeneous air concentration in the space, a multi-zone model is required for more accurate predictions to be achieved. This allows the user to divide the building into a number of zones, each at a different pressure, and these are connected by flow paths. A review by Feustel [2] shows that although several models have been developed, there has been little dissemination of the results.

There is a requirement for air infiltration and inter-zonal air movement calculations to be included within thermal building simulation models, in order that predicted air infiltration rates can easily and accurately be assessed during the early stages of a building design.

2.2 The FLOW program.

One computer program called FLOW, developed by Melo and Hammond [5] at Cranfield Institute of Technology, was an attempt to model infiltration arising from wind, stack effect and mechanical ventilation in single and multi-zone applications. The wind pressure coefficients were determined internally, using different empirical correlations for exposed and sheltered sites. However, the treatment of of the stack pressure and internal resistances was relatively crude. Nevertheless FLOW was considered to be a good base from which to develop a more sophisticated model of these parameters.

2.3 Limitations of FLOW.

When FLOW is run in the single-zone mode, the interior is assumed to be at a uniform temperature with a corresponding pressure profile. A number of flow paths may be specified connecting the inside of the building to the outside. The multi-zone model allows the building to be divided into zones, each of which has a different pressure. The following limitations occur with the multi-zone model in FLOW:

(i) The height of each zone must be an integer of the height of a single floor.
(ii) All paths connecting zones must be at the mid-height of a zone.
(iii) A single temperature must be specified to cover all zones in the building.
(iv) Zones may not be connected vertically. The resistance to flows between floors is accounted for by the use of a thermal draught coefficient.
(v) A consequence of (ii) is that the pressure on each floor of a zone is effectively assumed to be constant, as the stack pressure is always calculated at the mid height of the floor.
(vi) A further consequence of (ii) is that all openings which constitute flow paths are assumed to have a bottom and top height which is neglible when compared with the the variation in pressure differences with height. In practice, for tall openings, the pressure difference and hence the air flow can vary with height.

As a result of these factors, FLOW was limited in application to the following cases:

(i) Buildings having a uniform temperature and no partitions.
(ii Buildings which have a uniform internal temperature, and zones which are separated by variable resistances in the horizontal plane together with a constant resistance to flow between floors throughout the building.

2.4 Changes required to improve FLOW.

In order to model inter-zonal air movements in buildings which do not approximate to the conditions just stated, the following improvements were needed:

(i) It should be possible to specify a different temperature for each zone in the building This would allow the modelling of buildings which have significantly different temperatures in adjacent zones.
(ii) Flow paths should be allowed at any height, including connections which join zones vertically.
(iii) Modelling flow paths which cover large vertical heights should be allowed.
(iv) The three previous requirements lead to a fourth condition; i.e. that the variation of pressure with height in each zone should be accounted for. The reason for this is illustrated in figure 1.

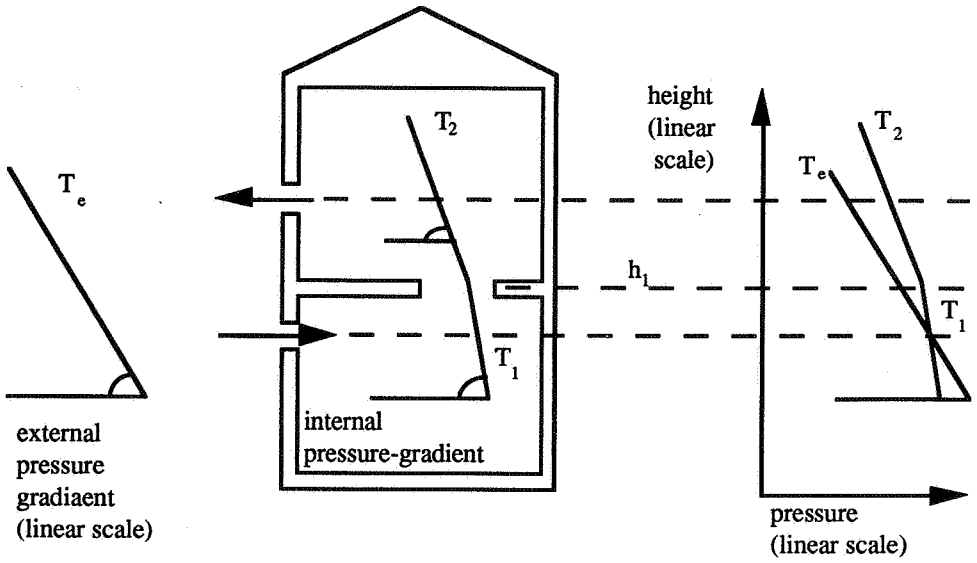


Figure 1: Stack-pressure induced air movements for vertically placed zones at different temperatures.

The figure shows the pressure profiles for a hypothetical case in which flow occurs between two adjacent columns, one of which is split into two zones at different temperatures. The flow between the zones depends on the pressure at the height of each path, which in turn depends upon the temperature in each zone.

2.5 Implications of the required changes.

If the different zones of the building are to have different temperatures, then the pressure profile in a column of the building may vary with height as illustrated in figure 1. For the example shown the pressure profile in the lower zone is given by:

$$p_h = p_1 - 273\ \rho_0\ g\ \frac{h}{T_1} \qquad \ldots(1)$$

where p_1 is the floor-level pressure for the lower floor zone. The pressure profile in the upper zone is given by:

$$p_h = p_2 - 273\ \rho_0\ g\ \frac{h}{T_2} \qquad \ldots(2)$$

where p_2 is the pressure at the base of the upper floor zone. Combining equations (1) and (2) gives the pressure profile in the upper zone as:

$$p_h = p_1 - 273\ \rho_0\ g \left[\frac{h_1}{T_2} + \frac{(h - h_1)}{T_2} \right] \qquad \ldots(3)$$

The stack pressure difference between the inside and outside in the upper zone thus varies with height, and is also a function of the pressure in the lower zone.

If a building has more than one column of zones, each with a different temperature profile, then the stack pressure difference between each column will be a function of the pressure and temperature profile in each adjacent column. The pressure profiles for a building with two distinct air columns may be as shown in figure 2.

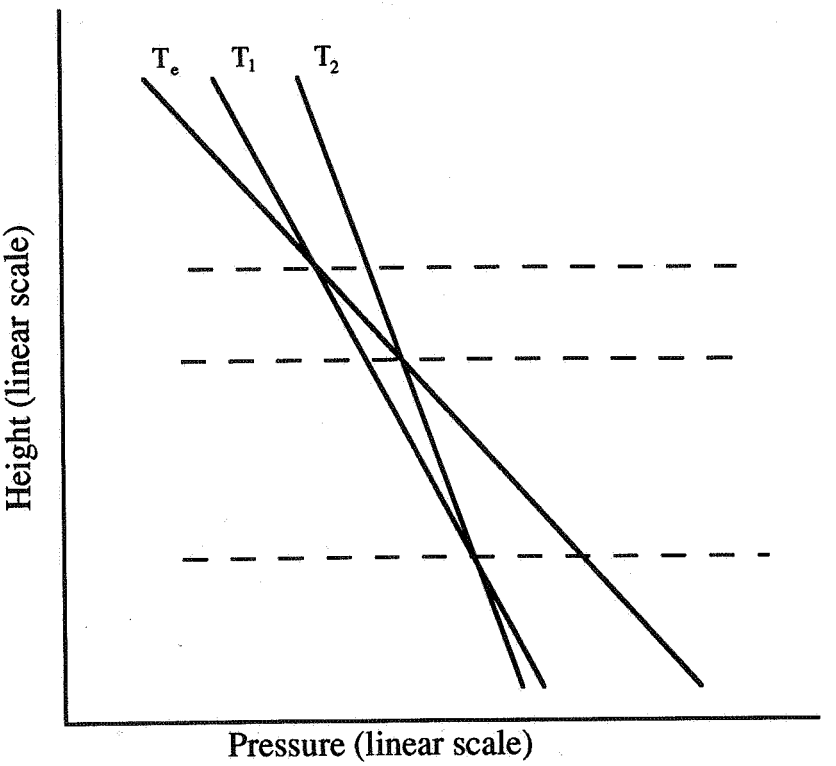


Figure 2: Pressure gradients in a building with separate columns of air at temperatures T_1 and T_2

The problem complexity is increased when resistances are considered in the horizontal plane between zones. At each point where there is a resistance, a discontinuity occurs in the plot of pressure against height, as illustrated in figure 3. FLOW dealt with vertical resistances by using the thermal draught coefficient, which is effectively used to alter the slope of the internal pressure profile. This adjusts the overall stack pressure difference. If variable resistances are to be modelled more accurately, it is necessary to be able to specify each resistance separately.

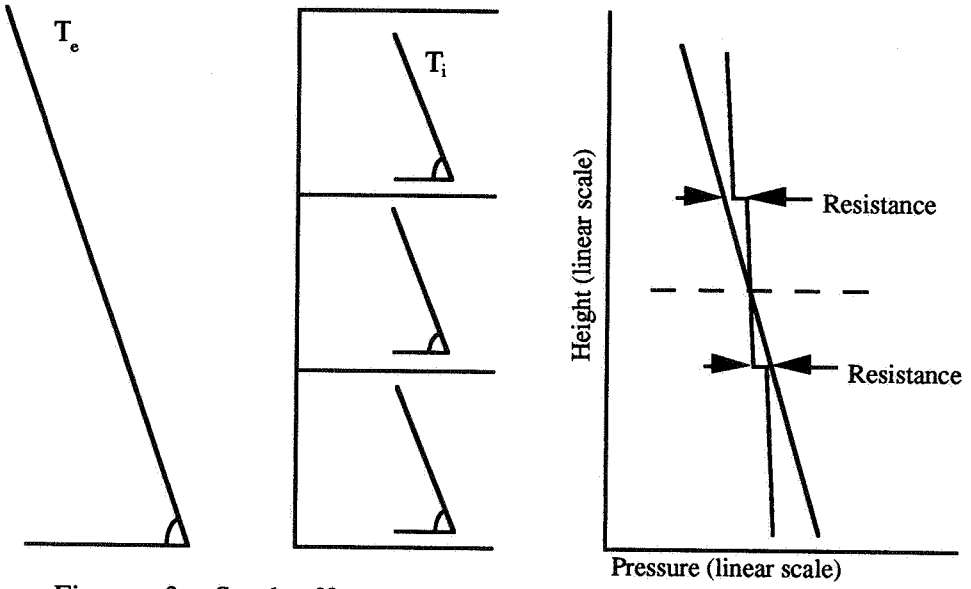


Figure 3: Stack-effect pressure distribution with resistances between floors.

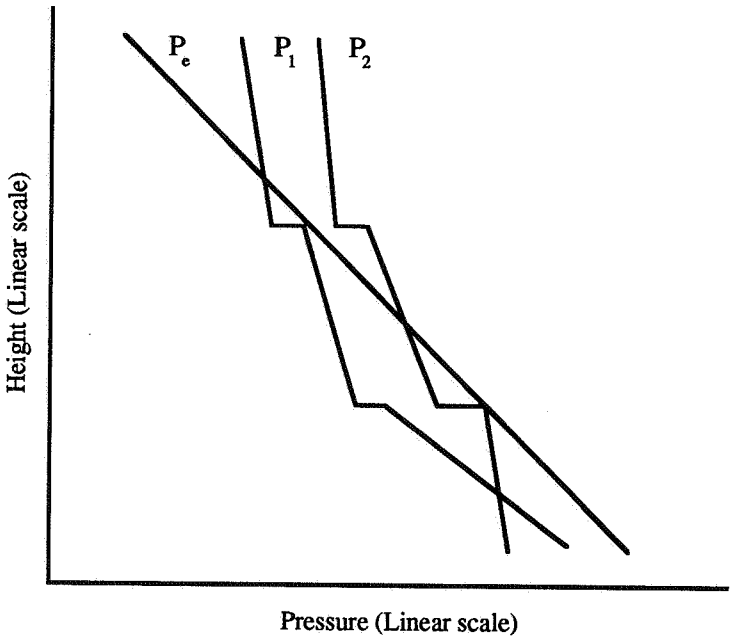


Figure 4: Possible pressure distribution in a building with two separated columns of air, each having zones at different temperatures and separated by varying resistances.

A model should be able to deal with all of the situations previously described, for any building configuration. A possible profile for a building with two air columns, and varying temperatures and resistances, is shown in figure 4.

2.6 Description of the FLOW model.

In FLOW a mass balance of the air entering and leaving each zone is determined. The solution to a problem is found by determining the pressure in each zone at which the set of pressure difference equations for each zone is satisfied, i.e:

$$\sum_{i=1}^{m} Q_{i,j} = 0 \qquad \ldots(4)$$

where m represents the total number of air flow paths connecting to zone i and $Q_{i,j}$ is the flow between zones i and j, and is given by:

$$Q_{i,j} = c_{i,j} (p_i - p_j)^{n_{i,j}} \qquad \ldots(5)$$

where $c_{i,j}$ and $n_{i,j}$ are the flow coefficient and the flow exponent for the flow between zones i and j.

Strictly speaking, this is a volume flow balance rather than a mass balance, as the air density is not included. This introduces an error for flow across the building's external walls, if the internal and external temperatures are different. However, for a flow between internal zones there is no additional error as the zone temperatures are all assumed to be identical.

The effect of mechanical ventilation is accounted for by adding, or subtracting, the net amount of air supplied to, or removed from, each zone to equation (4). Thus the pressurisation caused by the mechanical ventilation system is added to the natural pressure effects.

An iterative technique is needed to solve the sets of non-linear equations. For the single-zone model, the Newton-Raphson method is used. A Taylor expansion is used for multi-zone models and the resulting set of linear equations is solved by Gaussian elimination. Iteration continues until equation (4) is satisfied to within a specified error limit for each zone.

In order to determine the stack pressure differences up the height of the building, an initial estimate is used for the height of the neutral pressure. The user enters this value as one of the input parameters. A previously modified version of FLOW called XFLOW, attempts to improve the estimate of the neutral pressure when an initial solution has been reached for the flows.

3. Strategies for improving FLOW.

In order to improve FLOW so that it meets the criteria suggested in section 2.4, it is necessary to make its operation more flexible.

3.1 Use of the neutral pressure level.

FLOW determined the stack pressure differences on each wall of the building by using the concept of the neutral pressure level. The stack pressure differences were calculated using the expression:

$$p_{st} = 0.0342\ p_b(N-\lambda)H\ \Omega\left[\frac{1}{T_e} + \frac{1}{T_i}\right] \quad ...(5)$$

where N is the ratio of the height at which the pressure p is calculated to the total building height; λ is the ratio of the height of the neutral pressure level to the building height; and Ω is the thermal draught coefficient.

The concept of the neutral pressure level could be extended to be used to find the pressure differences between each adjacent column of air in a building. If there are varying resistances between floors, then there may be more than one neutral pressure level for two adjacent air columns. In the limit, where each floor of a building is sealed from the others, there is a neutral pressure level on each floor, as illustrated in figure 5.

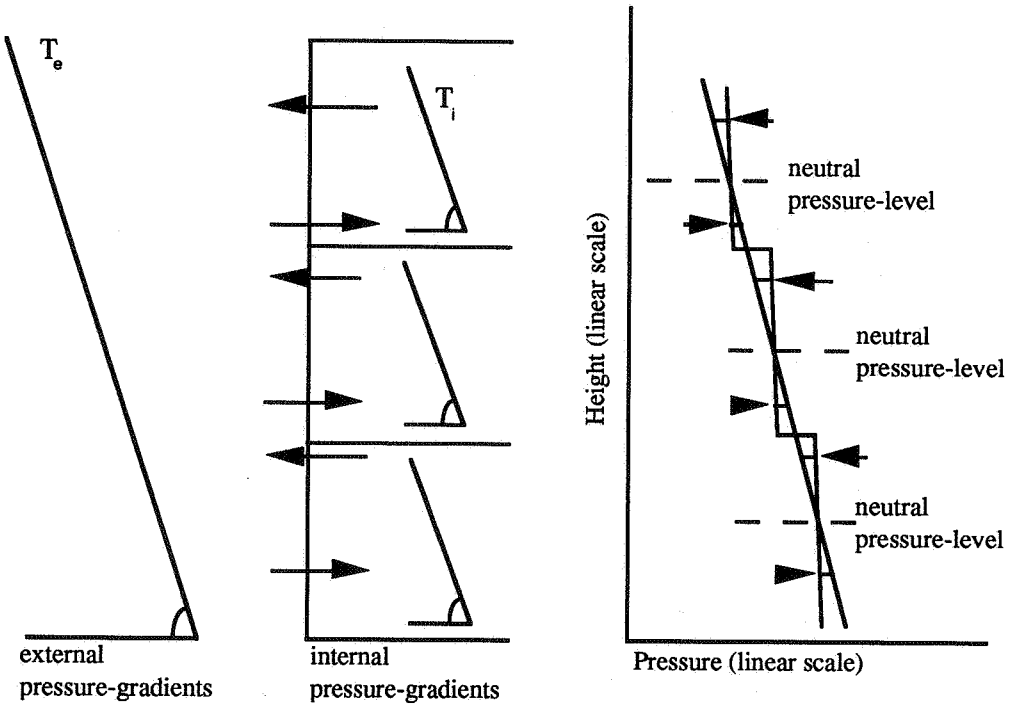


Figure 5: Stack pressure distribution in a multi-storey building with isolated floors.

Because of these complexities, the continued development of FLOW using the concept of the neutral pressure level did not appear to be profitable.

3.2 Consideration of resistances between zones.

Instead of making use of the neutral pressure, it is possible to model the flow between zones by considering pressure differences which act as a driving potential difference across resistances to the flow. An illustrative example is shown in figure 6.

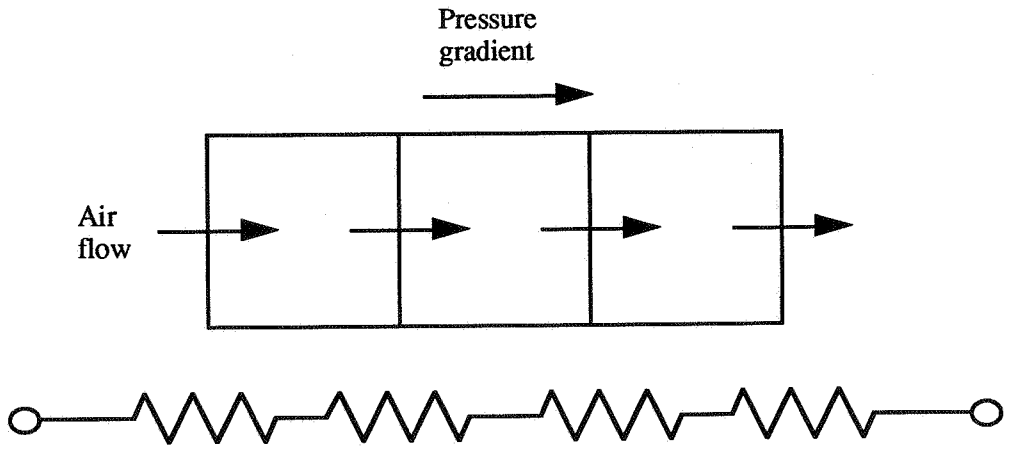


Figure 6: Use of resistances and driving forces to model flow

The pressure in each zone varies with height, and varies at a rate which depends on the zone temperature. Thus if a path joins two zones, which are at different temperatures, the driving force depends upon the height of the path. It is therefore necessary to find the pressure in each zone at a reference height and take account of the variation of pressure with height. The best choice for each reference height was considered to be the floor level of each zone. Some possible pressure profiles for several connected zones are illustrated in figure 7.

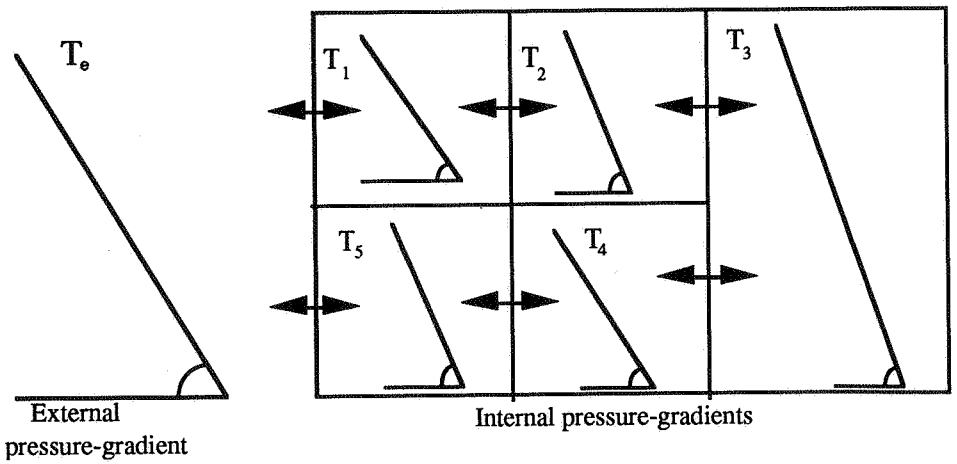


Figure 7: Qualitative indications of representative pressure gradients in some of the various zones.

In order to find the pressure in each zone, a solution must be found which satisfies the boundary conditions (i.e. known outside pressures) and the mass balance for flow into and out of each zone. This can be achieved by estimating the floor level pressure in each zone and taking

account of the pressure variations with height, and then using an iterative technique to solve the set of equations. Using this method means that there is no need to determine any neutral pressure levels.

In view of the apparent simplicity of this method, it was adopted to improve the FLOW model.

3.3 Description of the new model.

The new infiltration model was called VARYFLOW. No changes were made to the existing code which calculated the wind pressure coefficients.

The stack pressure effect for each path is calculated using the resistance method described in the previous section (3.2). A flow path may be at any height, so the wind pressure effects are also determined as a function of height, rather than at the mid-height of each floor only. Paths may connect zones vertically as well as horizontally, so there is no need to specify a thermal draught coefficient.

In order to obtain a starting estimate for the floor level pressure in each zone, the following procedure was adopted.

(i) Order the zones by the number of flow paths connecting each one, starting with that containing the lowest number of paths.

(ii) Select the zones which are connected to the outside.

(iii) Estimate the pressure in each of the selected zones, working through the zones in the order determined by step (i). The pressure is estimated to be an average of the pressure in connecting zones (if already estimated) and the outside pressure for paths to the exterior. Each pressure is adjusted for height.

(iv) Find all zones which are connected to the zones whose pressure has now been estimated

(v) Return to step (iii) until the pressures have been estimated in all zones.

Figure 8 shows an example of the order in which zone pressures would be estimated for a 3 by 3 network of zones.

In order to obtain the best estimate for the floor level pressure, p_f, in a zone, a best fit straight line needs to be applied to the pressures in the connected surrounding zones (see figure 9). In the figure, p_i and h_i are the estimated pressures and path heights for the surrounding zones connected to the zone in question.

A mass balance is performed for each zone to obtain a set of equations which may be solved. In performing the mass balance, the density of the air flowing between zones is assumed to be the average density of the air on either side of the path. The set of equations is then solved using Gaussian elimination, as described in section 2.6 .

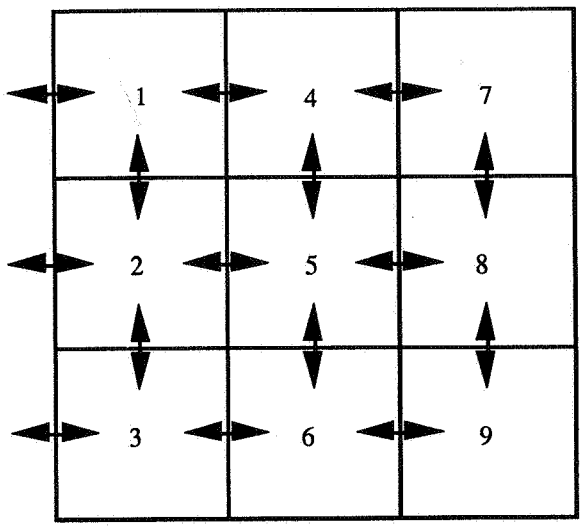


Figure 8: Order of the estimation of pressure in a number of connected zones.

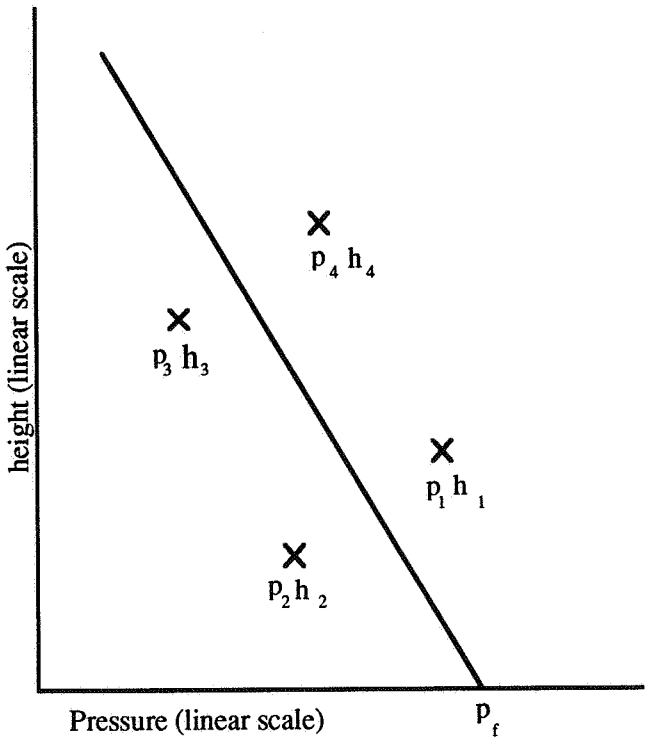


Figure 9: Estimation of p_f from pressures in surrounding zones

The volumetric air flow rate into and out of each zone through each path is reported, using the air density in the zone. Thus the flow rate on either side of a path will be different if the two zones are at different temperatures.

3.4 Large openings.

One further requirement of the new model is that it should be able to predict accurately the flow through large openings. To do this, it was necessary to integrate the flow up the height of the opening in steps such that:

$$Q_x = CA_x(\Delta p_x)^n \qquad ...(6)$$

where subscript x indicates the value is taken at height x. Note that, in this case, the value of the flow coefficient C is different from that used in equation 5 as it does not include the area of the opening.

When entering the data for each flow path, the user may specify those that should be treated as large openings by entering its height and width separately from the value of the flow coefficient, instead of including the path area within the flow coefficient value.

The initial estimate of the flow via each large opening is calculated at the path mid-height. The flow through each path is then calculated in height steps of 0.1m from the bottom to the top, using the pressure difference at each step to get the flow across that particular sub-area. The flows in each direction are summed and reported separately.

The time taken by the program to reach a solution is increased when large openings are used, but the number of iterations taken to reach a solution does not appear to be altered.

3.5 Assumptions made in developing the model.

These were as follows:

(i) Wind pressure coefficients may be used as previously described. the wind speed can be adjusted for height using a power law equation with the magnitudes of the coefficients dictated by the terrain.

(ii) The air in each zone is assumed to be well mixed, and at a single zone temperature.

(iii) Resistance to flow between zones can be modelled using the generalised equation $Q = c.(\Delta p)^n$ where c is the flow coefficient , n is the flow exponent and Δp is the pressure difference across the opening.

(iv) The pressure arising from wind and stack effects may be added together to determine the resulting flow. Air flows arising from mechanical ventilation may be added to the result.

(v) The effect of moisture content on air density may be ignored.

(vi) The density of air passing through a flow path may be taken to be the average of the density on either side of the path.

(vii) The variation of pressure with height is assumed to be linear. In fact, it falls exponentially, but near to the ground the difference is neglible.

3.6 Description of the model code.

The computer program is described below using a pseudo-code representation, in which a formalised language is used to describe the program operation.

3.6.1 Pseudo-code representation of VARYFLOW.

Read input data
Validate data and order zones by the number of connections
Write data to output.

DO for each set of weather data.

IF wind required **THEN**
Calculate wind angle
IF exposed site **THEN**
Calculate c values for an exposed site
ELSE
Calculate the c values for a sheltered site
ENDIF
ENDIF

DO while the pressure is not estimated in all zones.
Estimate pressures in zones next to known pressures.
Find zones now next to known pressures
ENDDO

Solve the set of flow equations
Calculate the air flow into each zone
Determine the infiltration rates

ENDDO

To solve the set of equations.

DO While the sum of flows into each zone is not zero
Calculate the sum of the flow into each zone due to pressures (including mechanical ventilation).
Calculate derivatives with respect to each zone pressure.
IF single zone **THEN**
Solve the equation using the Newton-Raphson method
ELSE
Solve the equation by Gaussian elimination.
ENDIF
Calculate improved estimates for zone pressures
ENDDO

4. Testing and validation of the model.

4.1 Model testing.

The aim of the first phase of the model testing was to discover whether the model could converge to a result for any given problem which lies within the program's data limits, and to ascertain whether the resulting solution makes physical sense.

The model was initially used to simulate the behaviour of a 2-storey building , shown in figure 10, with no wind effects present. The predicted air flow rate for all paths was 16.2 m^3h^{-1}. This solution was achieved in 3 iterations and agreed with the expected behaviour.

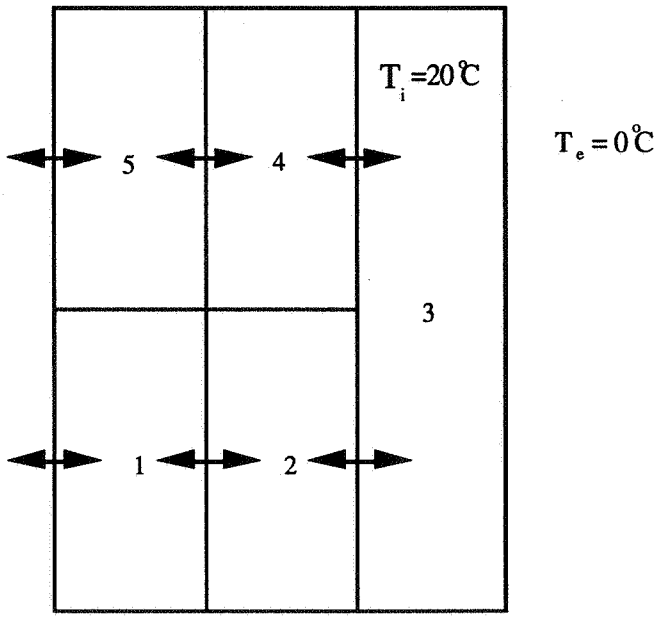


Figure 10: Designation of the zones in the building model to test VARYFLOW

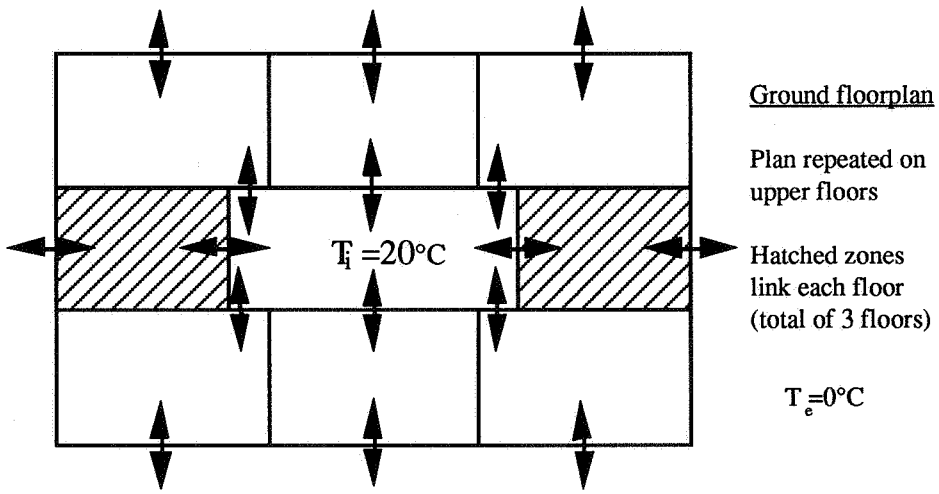


Figure 11: Plan of 48 path building to test VARYFLOW: representative air currents are indicated by the arrows

VARYFLOW was used subsequently to develop models for any configuration of building. It was tested for a variety of problems, one of the most complex being shown by figure 11. Convergence to a solution occurred in 6 iterations. Again, the results agreed with values expected for the problem as formulated by the building model.

4.2 Model validation.

Having produced a model, it is important to determine whether it may be used to obtain accurate predictions of real behaviour. The validation tests performed on the model were in two groups.

First it was necessary to ensure that the program produced results which could be checked by simple calculation. This was achieved by verifying that the results produced by the program were the same as those calculated analytically for simple situations.

The second part of the validation procedure was to compare the predictions of the model with measurements obtained from real buildings. The results of these validation tests are only as reliable as the measured data used for comparison purposes, but they do provide useful information on the model's performance.

4.3 Analytical verification.

For this level of testing, the results produced by the program are compared with analytical solutions for some simple problems, as recommended by Furbringer et al [6]. Each type of infiltration mechanism was tested in order to ensure that the individual parts of the code were examined [7].

The program was tested on a single zone building in which, one flow path was set up on the windward side and another on the leeward side. The model results are compared with those for the analytical solution in Tables 1 and 2.

FLOW MECHANISM	Flow rate, m^3h^{-1}	
	Analytical solution	VARYFLOW solution
Infiltration due to wind	92.4	92.3
Infiltration due to stack effect	2.6	2.6

Table 1. Comparison of infiltration rates for the analytical and VARYFLOW solutions.

FLOW MECHANISM	Over-pressure above atmospheric, Pa	
	Analytical solution	VARYFLOW solution
Mechanical ventilation	411	412

Table 2. Comparison of the calculated over-pressure resulting from mechanical ventilation for the analytical and VARYFLOW solutions.

4.4 Empirical validation.

It is necessary to know the potential accuracy achievable with the model when applied to real situations. In order to determine this, the model was tested using measured infiltration data from real buildings.

4.5 Runcorn House.

Melo [8] tested the original FLOW program against a set of infiltration data which were collected for a house in Runcorn, England. The data available include the flow coefficient and exponent leakage paths between the inside and outside of the building. However, no information was available regarding restrictions to flow between zones within the building. When the measurements were made, all the internal doors were open, so it was assumed that there were no internal resistances to the flows.
The data could thus be used to test the model assuming that the interior of the building could be modelled as a single zone. The temperature was assumed to be constant throughout the building. The house was subject to a high degree of shielding from the wind, so the wind pressure coefficients were calculated using the algorithm for sheltered sites.

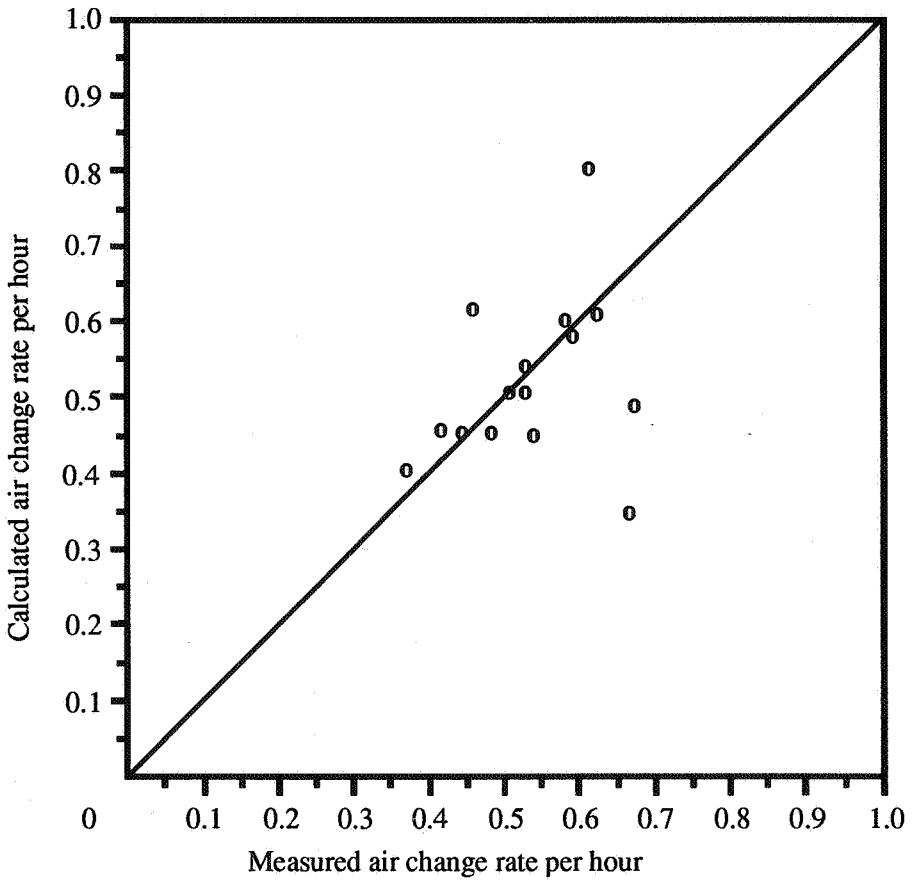


Figure 12: Comparison of the measured and predicted air infiltration rates for Runcorn considered house.

The calculated air infiltration rates are shown in comparison with the measured values in figure 12. Reasonable corroboration ensues, with 11 of the 15 values falling within plus or minus 25% of the perfect correlation line.

4.6 British Gas measurements.

The performance of the model, when used to predict ventilation in a building with zones at different temperatures, was also assessed, using data collected by British Gas [9]. The data available consist of measured air change rates in the rooms of a house, together with measurements of the temperature in each room and the outside weather conditions.

The flow paths and resistance values for each room were not available. However, it was assumed that a flow path existed for each window and door. Values for the flow resistances were estimated using data given by Liddament [4]. During the tests, the toilet and bathroom doors were open, so that these rooms were treated as as being part of the landing. For comparison of the results, the hall was also modelled as being in the same zone.

The values of the measured and predicted air change rates for each room are given in Tables 3 and 4 . The results do not show a high degree of correlation. However, there were probably some considerable errors in the estimates made for the flow coefficients. In particular, there is probably a specific cause for the discrepancy between the predicted and actual values for the flows into the kitchen and bedroom 2 for the predicted values to be so much lower than those measured. The kitchen is downstairs on the leeward side of the building, so it would not be expected to have a high air change rate without good reason.

Data set 1

Wind speed 1.33 ms^{-1}, direction 238°

Outside air temperature = 22.460°C

Room	Temperature (°C)	Measured air change rate (ac/h)	Calculated air change rate (ac/h)
Lounge	24.63	0.26	0.27
Dining	27.47	0.15	0.13
Bed 1	23.82	0.10	0.23
Bed 2	24.59	0.94	0.34
Bed 3	24.89	0.32	0.26
Bed 4	24.62	0.05	0.28
Kitchen	23.78	1.63	0.34
Hall/bath/toilet	23.52	0.88	0.75
AVERAGE		0.53	0.35

Table 3. Comparison of the British Gas measured air change rates with predicted values for "Data set 1".

Data set 2

Wind speed = 2.0 ms^{-1}, direction 276°

Outside air temperature = 22.47°C

Room	Temperature (°C)	Measured air change rate (ac/h)	Calculated air change rate (ac/h)
Lounge	25.32	0.36	0.58
Dining	27.84	0.17	0.36
Bed 1	24.31	0.21	0.51
Bed 2	25.11	1.24	0.76
Bed 3	25.79	0.48	0.59
Bed 4	24.72	0.09	0.39
Kitchen	23.87	1.79	1.39
Hall/Bath/Toilet	23.50	0.98	1.66
AVERAGE		0.64	0.83

Table 4: Comparison of the British Gas measured air change rates with predicted values for "Data set 2".

5. Conclusions.

The VARYFLOW model allowed a sophisticated and flexible approach to the modelling of infiltration in buildings. In particular, the modelling of stack effect pressures allowed the use of different temperatures in each zone. Also, the more flexible approach to the modelling of flow resistances between zones and particularly between floors now allows the modelling of buildings which do not have a uniform resistance to vertical flow throughout the building.

Simple analytical tests suggest the physical modelling is correct. Comparison of the model's predictions against experimental data have shown that predicted flow rates are in approximate agreement with data.

When the problems involved in obtaining accurate flow measurements are considered, together with the difficulty in making good estimates for the flow resistances of openings within building structures, the predicted and measured results were in remarkably good agreement.

References

1. LIDDAMENT, M.W.
"Aspects of natural ventilation in passively heated buildings"
Proceedings of the 2nd UK-ISES Conference, "The efficient use of energy in buildings", Cranfield Institute of Technology, Bedford,UK September 1986.

2. FEUSTEL, H.E.
"Mathematical Modelling of infiltration and ventilation"
10th AIVC Conference Proceedings, Volume 1, Dipoli, Finland, 1989.

3. WALTON, G.N.
"Airflow network models for element based building airflow modelling"
Preprint, ASHRAE Trans, Volume 95, Pt. 2, 1989

4. LIDDAMENT M.W.
"Air infiltration calculation techniques - An applications guide"
Air Infiltration and Ventilation centre, 1985.

5. MELO, C.
"FLOW - An algorithm for calculating air infiltration into buildings"
Proceedings ICBEM'87 International Conference on Building Energy Management, Lausanne, Switzerland, 1987.

6. FURBRINGER J.M., COMPAGNON R., ROULET C.A., GADILHE A.
"Wind and pressure requirements for the validation of a multi-zone air infiltration program."
10th AIVC Conference, Dipoli, Finland, 1989.

7. FEILD A.J.
"The development of a model to predict natural ventilation of buildings."
M.Sc. Thesis Cranfield Institute of Technology, Bedford, UK, 1990.

8. MELO C.
"Improved convective heat transfer and air infiltration models for building thermal simulation."
Ph.D. Thesis Cranfield Institute of Technology, Bedford, UK, 1985.

9. LILLEY J.
(British Gas, Watson House Research Station, London, UK.)
Private communication, 1990.

AIR MOVEMENT & VENTILATION CONTROL WITHIN BUILDINGS

12th AIVC Conference, Ottawa, Canada
24-27 September, 1991

POSTER 41

AIRFLOW AND THERMAL COMFORT IN NATURALLY VENTILATED CLASSROOMS

G. Gan, H.B. Awbi and D.J. Croome

Department of Construction Management & Engineering
University of Reading
Whiteknights, PO Box 219
Reading, RG6 2BU
U.K.

SYNOPSIS

The airflow pattern and thermal comfort in a naturally ventilated classroom were predicted using CFD techniques. The CFD model for turbulent flow consists of equations for the conservation of mass, momentum and thermal energy and the equations for the k-ϵ turbulence model, taking account of the effects of buoyancy and obstacles in the room. The thermal comfort was assessed according to the predicted mean vote (PMV) and predicted percentage of dissatisfied (PPD). The mean radiant temperature for each grid point was calculated from the radiant heat balance for the classroom and the shape factor of the point. The predicted velocity and temperature distributions were compared with experimental results and reasonable agreement was achieved. It was found that occupants in the room have great influence on the airflow pattern and temperature distribution.

1. INTRODUCTION

Modern technology and high living standards make it possible for people to have better comfort whether at home or in offices. Indoor thermal comfort is influenced by air velocity, air temperature, mean radiant temperature and air humidity in addition to the personal parameters such as metabolic rate and clothing. Natural ventilation, in combination with heating when required, is still the main means to achieve adequate thermal comfort for most buildings in the U.K. The airflow in naturally ventilated buildings depends much on the arrangement of doors and windows for given external conditions. In order to achieve a comfortable thermal environment there is a need for defining details of the airflow patterns especially at head and foot levels when designing an effective ventilation system[1]. Difficulties may be encountered however in field tests of naturally ventilated systems because of the uncertainty of various factors that affect their performance. Mathematical modelling as a potential alternative can be used for predicting the performance of these systems.

Computational fluid dynamics (CFD) has for many years been applied in the simulation of room air movement in airconditioned spaces[2]. The simulation of airflow in spaces or cavities dominated by buoyancy has been carried out by a number of investigators[3,4]. These and other investigations were largely performed using reduced-scale models or numerical experiments. In contrast, there is not enough validation of CFD programs using field measurements, especially in naturally ventilated buildings.

Moreover, in most of the available CFD programs the radiant heat transfer is simplified or not accounted for when dealing with thermal comfort. Fanger[5] demonstrated

how to evaluate thermal comfort by taking into account the radiant heat transfer process between the person and the internal surfaces of a room. Kaizuka and Iwamoto[6] calculated the distribution of thermal comfort index caused by radiation interaction in a heated room under the assumptions of uniform air temperature and given air velocity. In this paper the air movement and thermal comfort in a naturally ventilated classroom are predicted using the CFD program ARIA-R. The predictions are compared with measurements in an occupied and unoccupied classroom.

2. MODEL EQUATIONS AND SOLUTION

2.1 Flow equations

The airflow model is based on the continuity equation, Navier-Stokes equation and thermal energy equation together with the k-ϵ turbulence model equations. For a steady incompressible flow the time-average equations are represented by

$$\frac{\partial}{\partial x_i}(\rho U_i \phi) = \frac{\partial}{\partial x_i}(\Gamma_\phi \frac{\partial \phi}{\partial x_i}) + S_\phi \qquad (1)$$

where S_ϕ = source terms of dependent variable ϕ
U_i = mean velocity component in x_i direction
Γ_ϕ = diffusion coefficient for dependent variable ϕ
ρ = fluid density

The flow equations are solved for the 3-D cartesian system using the SIMPLE algorithm[7] with the boundary conditions described elsewhere[8].

2.2 Thermal comfort equations

Thermal comfort is evaluated in terms of predicted mean vote (PMV) and predicted percentage of dissatisfied (PPD) proposed by Fanger[5]. These comfort indices take account of the combined effect of environmental conditions such as air velocity, air temperature, mean radiant temperature and partial water vapour pressure of air and occupant conditions such as clothing and activity levels. In the present evaluation the air velocity and temperature are given by the flow equations. The mean radiant temperature, T_{mrt}, is a function of several parameters such as the temperature and thermal properties of room surfaces and the shape factors between the surfaces. Other parameters, e.g. vapour pressure of air, are given a single value for the whole field.

In the calculation of mean radiant temperature at a grid point in the field, the grid cell is considered as a rectangular parallelepiped. The plane radiant temperature, T_{prt} (K), at each face of the cell is obtained

from[5]:

$$T_{prt}^4 = \frac{1}{\sigma} \sum_{i}^{N} F_{pi} \left[\epsilon_i \sigma T_i^4 + (1 - \epsilon_i) \sum_{j}^{N} F_{ij} J_j\right] \quad (2)$$

where σ is the Stefan-Boltzmann constant ($\sigma = 5.669 \times 10^{-8}$ W/m^2K^4); N is the number of room surfaces; F_{pi} is the shape factor for radiation from face p of the grid cell to the visible room surface i (i = 1 to N); F_{ij} is the shape factor for room surface i and surface j; T_i is the absolute temperature of room surface i; ϵ_i is the emissivity of surface i and J_j is the radiosity for surface j, which is defined as the total radiation that leaves a surface per unit time and per unit area (W/m^2).

The radiosity J_i for surface i is calculated using the following equation, for a specified surface temperature[5]:

$$J_i = \epsilon_i \sigma T_i^4 + (1 - \epsilon_i) \sum_{j}^{N} F_{ij} J_j \quad (3)$$

The mean radiant temperature, T_{mrt}, for the grid cell is then taken as the weighted average of the six plane radiant temperatures for each face of the rectangular parallelepiped based on the face areas.

The predicted mean vote, PMV, and predicted percentage of dissatisfied, PPD (%), are given by[5,9]

$$\begin{aligned} PMV = {} & [0.303\exp(-0.036M) + 0.028] \{(M - W) - 3.05 \times 10^{-3} \\ & \times [5733 - 6.99(M - W) - p_a] - 0.42 [(M - W) - 58.15] \\ & - 1.7 \times 10^{-5} M (5867 - p_a) - 0.0014 M (34 - T_a) \\ & - 3.96 \times 10^{-8} f_{cl} [(T_{cl} + 273)^4 - (T_{mrt} + 273)^4] \\ & - f_{cl} h_c (T_{cl} - T_a)\} \end{aligned} \quad (4)$$

and

$$PPD = 100 - 95 \exp(-(0.03353\ PMV^4 + 0.2179\ PMV^2)) \quad (5)$$

where

$$\begin{aligned} T_{cl} = {} & 35.7 - 0.028(M - W) - I_{cl} \{3.96 \times 10^{-8} f_{cl} \\ & \times [(T_{cl} + 273)^4 - (T_{mrt} + 273)^4] + f_{cl} h_c (T_{cl} - T_a)\} \end{aligned} \quad (6)$$

$$h_c = 2.38(T_{cl} - T_a)^{0.25} \quad \text{for } 2.38(T_{cl} - T_a)^{0.25} > 12.1\sqrt{V_r} \quad (7)$$

$$h_c = 12.1\sqrt{V_r} \quad \text{for } 2.38(T_{cl} - T_a)^{0.25} < 12.1\sqrt{V_r} \quad (8)$$

$$f_{cl} = 1.00 + 1.290\ I_{cl} \quad \text{for } I_{cl} \leq 0.078\ m^2K/W \quad (9)$$

$$f_{cl} = 1.05 + 0.645\ I_{cl} \quad \text{for } I_{cl} > 0.078\ m^2K/W \quad (10)$$

M is the metabolic rate; W is the external work (taken zero here); p_a is the partial water vapour pressure of

air; T_a is the mean air temperature; f_{cl} is the ratio of man's surface area while clothed to the area while nude; T_{cl} is the surface temperature of clothing; h_c is the convective heat transfer coefficient; I_{cl} is the thermal resistance of clothing and V_r is the relative air velocity.

3. RESULTS AND DISCUSSION

The predictions of airflow and thermal comfort were carried out for a naturally ventilated classroom for the summer season. Figure 1 shows a schematic diagram of the classroom at the University of Reading. The room has the dimensions 10.9 x 11 x 3.05 m (length x width x height), with east-west direction along the length. The west side of the room is linked to a main entrance door via a corridor. Part of the south and north faces of the room are glazed, each with six openable windows. Various combinations and positions of window openings have been used during the experiments to investigate the variation in the ventilation characteristics of the room. Air velocities and temperatures were measured at one level, 0.9 m above the floor (head level when seated), with omnidirectional hot wire anemometers. Air flow rates were determined using the concentration decay method with iso-butane as the tracer gas. Besides, indoor air quality was assessed on the basis of the carbon dioxide levels during the occupancy periods and a subjective survey of the occupants was undertaken by means of vote on their sensations of thermal environment and impressions of odour. Tests were conducted both with and without occupancy[10-12].

The following assumptions were made in the CFD prediction:

1. **Heat sources.** The solar heat gain through the glazed area facing south and the heat generation due to equipment in the room were considered to be distributed uniformly over the floor. Heat production by artificial lights near the ceiling was taken as a uniformly-distributed heat source over the ceiling.

2. **Obstacles.** Tables and columns in the room were simulated as obstacles. Occupants were treated as obstacles with heat production (each person 100 W).

3. **Supply air.** The air velocity at the supply openings was calculated from the measured air flow rate and was assumed normal and uniformly distributed across the openings.

A total of ten computer simulations, of which five with occupancy, were performed. The predicted and measured average air velocities and temperatures at the level 0.9 m above the floor are shown in the table below.

Predicted and measured average air velocities and air temperatures in the classroom 0.9 m above the floor

No.	Air change rate (1/hr)	Velocity (m/s)		Temperature (°C)	
		Predicted	Measured	Predicted	Measured
1	3.62	0.090	0.112	23.85	23.03*
2	5.64	0.135	0.160	29.41	28.39
3	5.88	0.124	0.110	26.13	24.80
4	1.68	0.062	0.096	25.23	23.21
5	5.76	0.122	0.097	24.23	23.03
Mean of 1 to 5		**0.107**	**0.117**	**25.77**	**24.49**
6	7.73	0.113	0.092	21.89	21.98*
7	10.20	0.123	0.110	23.69	24.43
8	14.34	0.161	0.107	27.86	27.52
9	2.98	0.079	0.094	23.07	20.88
10	8.76	0.133	0.114	25.29	25.31
Mean of 6 to 10		**0.122**	**0.103**	**24.36**	**24.02**
Mean of 1 to 10		**0.115**	**0.110**	**25.07**	**24.26**

Notes: number 1 - 5 with occupancy and number 6 - 10 without occupancy; the combination and position of window openings varied from one to another.
* discussed in the text.

It can be seen from the table that the simulation gives fairly good predictions of the average values of the velocity and temperature. The mean difference between the predictions and measurements is less than 5% for velocity and 1 K in temperature.

Figures 2 and 3 show the predicted velocity and temperature distributions for the two cases to be discussed hereafter, one with occupancy (case 1), and the other without (case 6). A comparison of predicted velocities and temperatures with the measured values for the corresponding two cases are shown in Figures 4 and 5 whereas the predicted comfort indices are shown in Figures 6 and 7. The air flow rates for case 1 and case 6 are 3.62 and 7.73 air changes per hour respectively (The corresponding supply velocities are 0.356 and 0.76 m/s). In case 1, six windows were half open. Air flowed into the room through four windows in the north face and flowed out from two windows in the south face. In case 6, there were six windows in fully open position in the south wall. However, the direction of wind flow into or out of these windows was not known and it has been assumed that the wind was flowing into the room via the two windows close to the east wall and out from the other four. It can be seen from Figures 4 and 5 that, in general, the predictions are in reasonable agreement with the measurements except that the predicted values near the supply openings are somewhat higher for velocity and

lower for temperature in the air jets. This is mainly attributed to the assumption about the velocity direction at the supply opening. The actual supply velocity might not be perpendicular to the opening area as assumed in the prediction. In fact, during the time of the experiments, the wind directions were north-westerly for case 1 and south-westerly for case 6. Due to the channelling effect of windows open outwards, the incoming air could have been inclined and there might have been vortices formed, which would have interfered with the air jet at the opening.

Figure 4 also indicates that for the case with occupancy the predicted air temperatures vary from the lowest near the supply opening to the highest close to the occupants, whereas the measured values are nearly uniform. This is because of a relatively large difference between the supply air and room bulk temperatures, especially the body temperature, used in the prediction. The measurement was made at some discrete points and therefore could not reflect the full picture of the variations. The variation in the predicted air temperature for the unoccupied room is small (Figure 5), and gives better agreement with measurement in comparison with that for the occupied room. Similarly, the velocity decreases from the supply jet value to a negligible magnitude as the air jet diffuses into the room. Again the variation of predicted velocities is larger than that obtained from measurement. These discrepancies may be attributed to the uncertainties and assumptions in key parameters such as the magnitude and direction of supply air velocity and distribution of heat sources in the space. Nevertheless, in view of the fact that the prediction has been compared with field measurements which are much more complex and, most of all, less controllable than those in, for example, scale or laboratory models, the predictions may be considered satisfactory.

Figures 6 and 7 indicate that the predicted percentage of dissatisfied for the two cases is generally below 10%, well within the acceptable range of 20%[9]. In fact, the average PPDs in the occupied zone (from floor to 1.8 m height) for case 1 and case 6 are about 8% and 7% respectively, both being between neutral and slightly warm. These tests were, however, conducted under a mild environmental temperature (about 20°C). The inference is that the indoor environment may be beyond the acceptable level for thermal comfort when the outdoor temperature is much higher unless it is compensated for by a higher air flow rate. Therefore, in a hot climate some measure may have to be taken to provide sufficient and preferably cool air without causing excessive draught if discomfort in the space is to be avoided. In a cold season, heat needs to be provided to maintain indoor thermal comfort which conforms with normal practice.

To investigate the effect of occupants on the airflow and thermal comfort, an additional prediction was made for the conditions represented by case one but without occupancy. The air flow pattern and temperature distribution for this case are shown in Figure 8. By comparing Figure 2 with Figure 8 it can be seen that the occupants have a great influence on the air flow patterns and temperature distributions within a space. As pointed out above, the presence of an occupant increases the air temperature close to the body and in the wake of the air plume rising about the head due to body heat. The occupant, like other obstacles, influences and diverts air movement. The diversion occurs not only as a result of air separation when flowing over the body but also through the buoyancy force due to the temperature difference between the body and the surrounding air. Exposed skin surfaces are at about 33°C and clothing surfaces can be 24 - 28°C. Consequently, in the absence of the occupants, the velocity in the occupied zone was reduced by 8% and the temperature by 1 K compared to those with occupancy. The occupants naturally affect the distribution of comfort indices as they bring about the change of the indoor environment. However, because of the decrease in the velocity and temperature in the space simultaneously, the overall effect of occupancy on the predicted thermal comfort is small. For example, the average value of the predicted percentage of dissatisfied in the occupied zone decreased from 8% with occupancy to 7% without occupancy. This change, of course, may be quite substantial at certain spots, particularly in and around the area where occupants were originally situated.

4. CONCLUSIONS

The 3-D CFD program ARIA-R, that has been specifically developed to predict the indoor environment, can be used to predict the airflow and thermal comfort in naturally ventilated rooms given knowledge of key parameters such as supply air velocity and temperature. The program can also be used for the prediction of the performance of mechanical ventilation systems.

In a mild climate adequate thermal comfort can be achieved by appropriate arrangement of doors or windows. There may be some difficulties however in maintaining a comfortable environment in a hot climate through natural ventilation alone, depending on the layout of the spaces, the occupancy density and the supply-exit configuration. In this circumstance, cooling may also be required.

In a naturally ventilated room, the airflow patterns and temperature distribution are greatly influenced by the occupants and their distribution in the space. This is also true for mechanical ventilated or airconditioned spaces when the occupancy density is high such as in auditoria[13].

REFERENCES

1. Croome, D.J. "A comparison of upward and downward air distribution systems", in **Ventilation '88: Proceedings of the Second International Symposium on Ventilation for Contaminant Control**, 20-23 September 1988, London, UK, Edited by J.H. Vincent, Pergamon Press, Oxford, 1989, pp433-438.
2. Awbi, H.B. "Ventilation of Buildings", Spon, London, 1991.
3. Ideriah, F.J.K. "Prediction of turbulent cavity flow driven by buoyancy and shear", **J. Mech. Engng Sci., 22**, 1980, pp287-295.
4. Nielsen, P.V., Restivo, A. and Whitelaw, J.H. "Buoyancy-affected flows in ventilated rooms", **Numerical heat transfer, 2**, 1979, pp115-127.
5. Fanger , P.O. "Thermal Comfort -- Analysis and Applications in Environmental Engineering", Robert E. Krieger Publishing Company, Florida, 1982.
6. Kaizuka, M. and Iwamoto, S. "A numerical calculation on the distribution of surface temperature and thermal comfort index caused by radiation interaction in a heated room", **Trans. ASHRAE, 33**, 1987, pp103-113.
7. Patankar, S.V. "Numerical Heat Transfer and Fluid Flow", Hemisphere Publishing Co., Washington, 1980.
8. Gan, G, Awbi, H.B. and Croome, D.J. "Simulation of air flow in naturally ventilated buildings", **Building Simulation '91**. Nice, Sophia-antipolis, France, 1991.
9. ISO 7730 "Moderate thermal environments -- Determination of the PMV and PPD indices and specification of the conditions for thermal comfort", International Organisation for Standardisation, 1984.
10. Zainal, M. and Croome, D.J. "Building planning and ventilation: The effects of natural ventilation via windows and doors linked by corridor/passage-way", **Roomvent '90: Proceedings of the Second International Conference on Engineering Aero- and Thermodynamics of Ventilated Room**, June 13-15, 1990, Oslo, Norway.
11. Zainal, M. and Croome, D.J. "Ventilation characteristics for buildings", **Indoor Air '90: Proceedings of the 5th International Indoor Air Quality and Climate**, July 29 - August 3, 1990, Toronto, Canada.
12. Zainal, M. and Croome, D.J. "Ventilation characteristics of selected type of buildings and indoor climate", **Proceedings of the 11th AIVC Conference**, September 20-23, 1990, Belgirate, Italy.
13. Croome, D.J. and Roberts, B.M. "Airconditioning and Ventilation of Buildings", Chapter 11, Pergamon Press, Oxford, 1981.

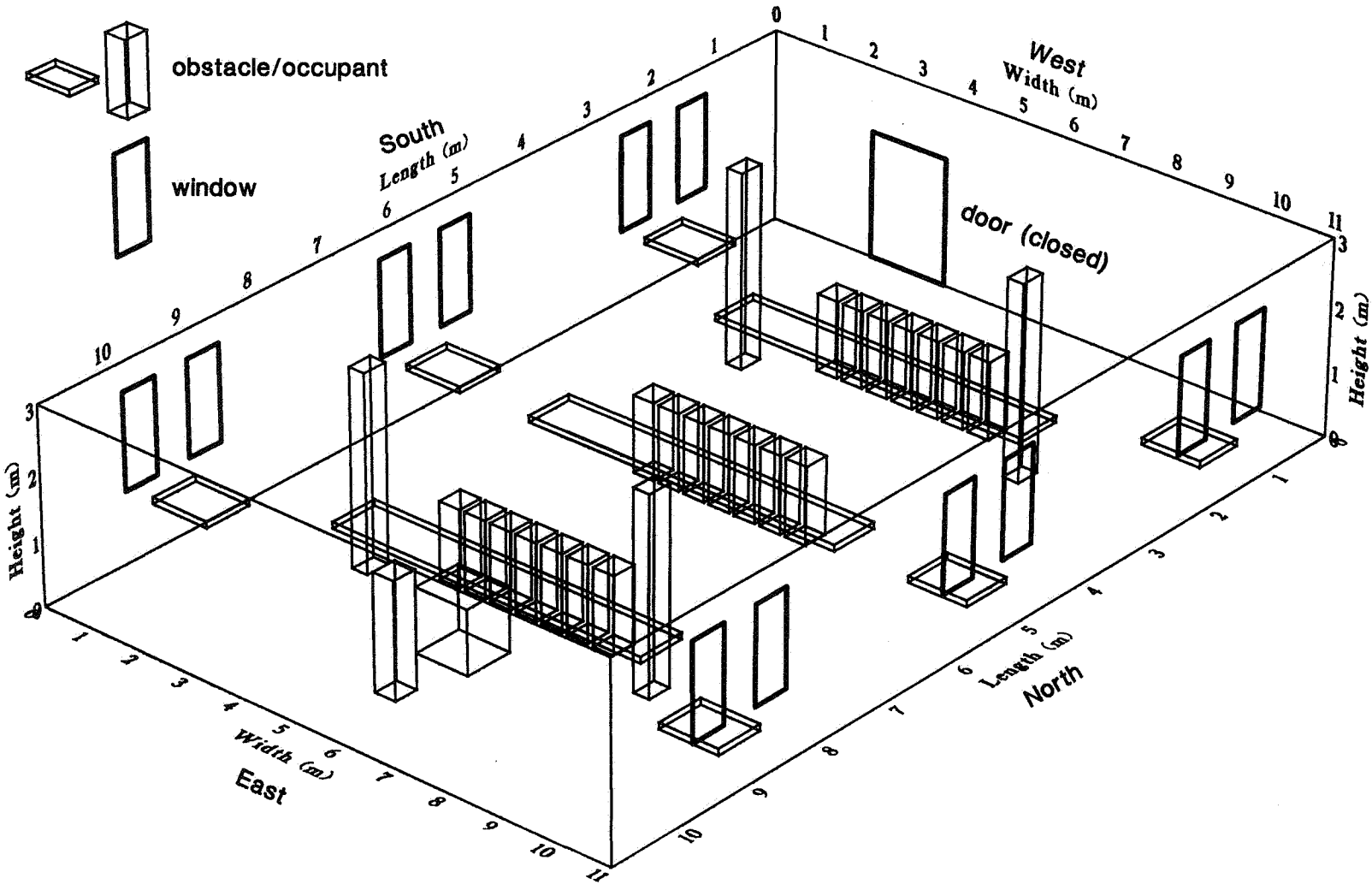
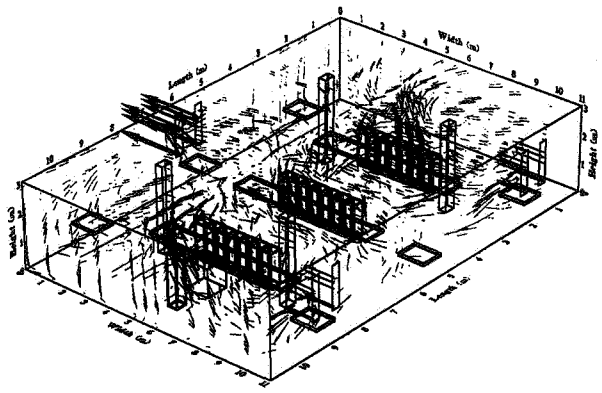
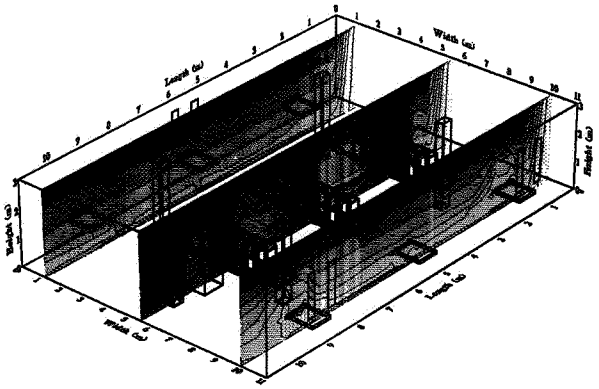


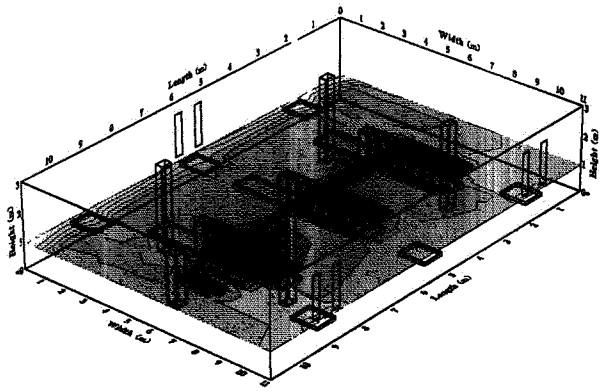
Fig. 1 Schematic diagram of the classroom



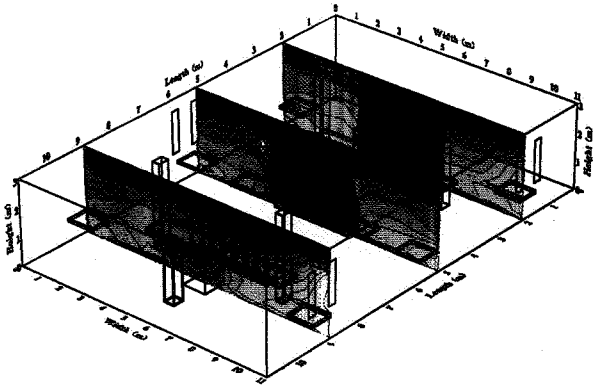
(a) Velocity vectors



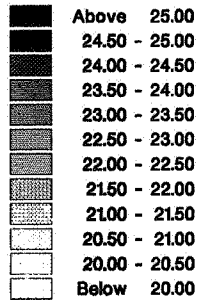
(b) Isotherms on vertical planes



(c) Isotherms on a horizontal plane

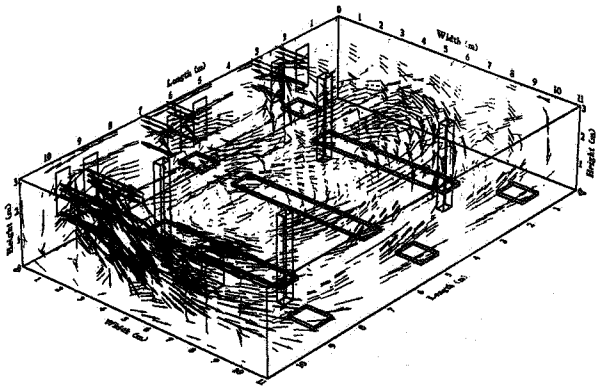


(d) Isotherms on vertical planes

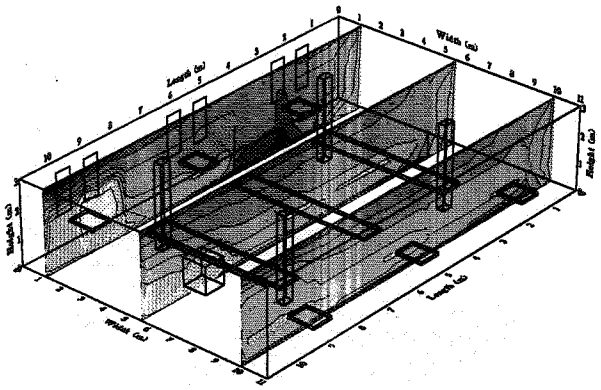


Supply air: U = 0.356 m/s ; T = 19.9 deg.C

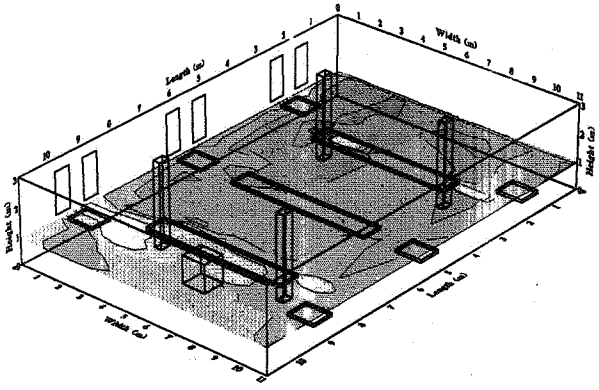
Fig. 2 Predicted velocity vectors & isotherms of air in a classroom with occupancy (case 1)



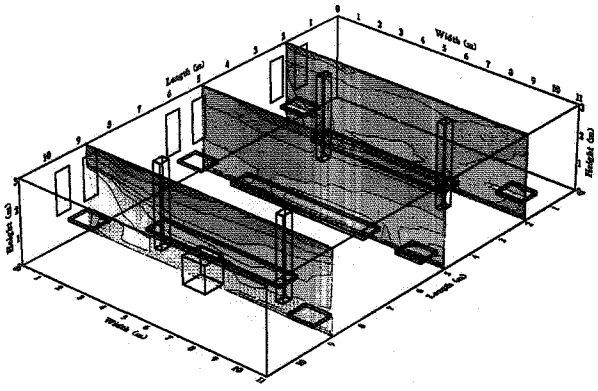
(a) Velocity vectors



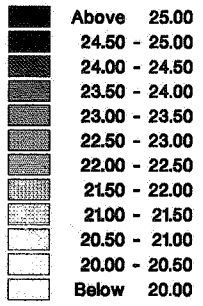
(b) Isotherms on vertical planes



(c) Isotherms on a horizontal plane

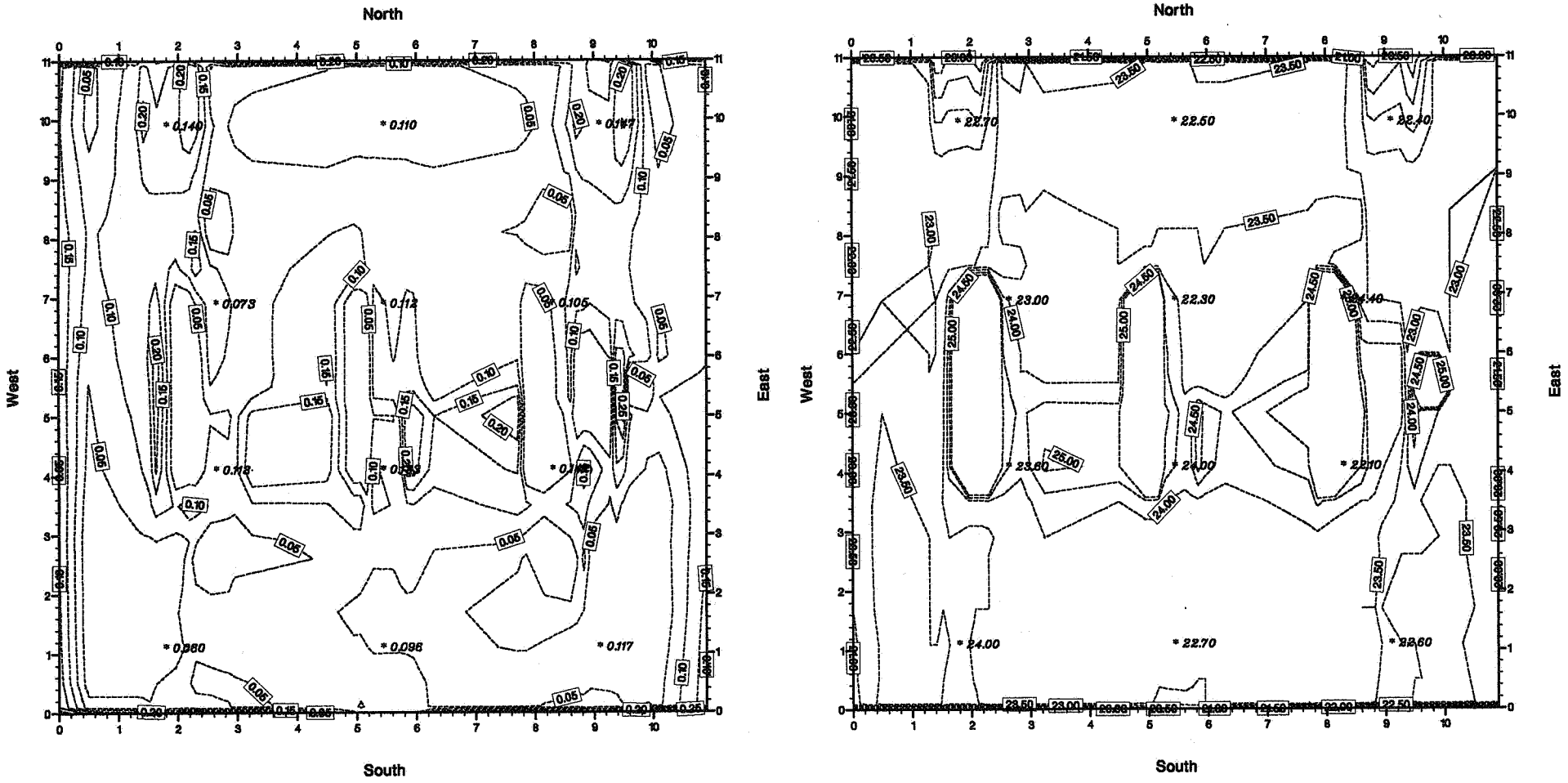


(d) Isotherms on vertical planes



Supply air: U = 0.76 m/s ; T = 19.9 deg.C

Fig. 3 Predicted velocity vectors & isotherms of air in a classroom without occupancy (case 6)

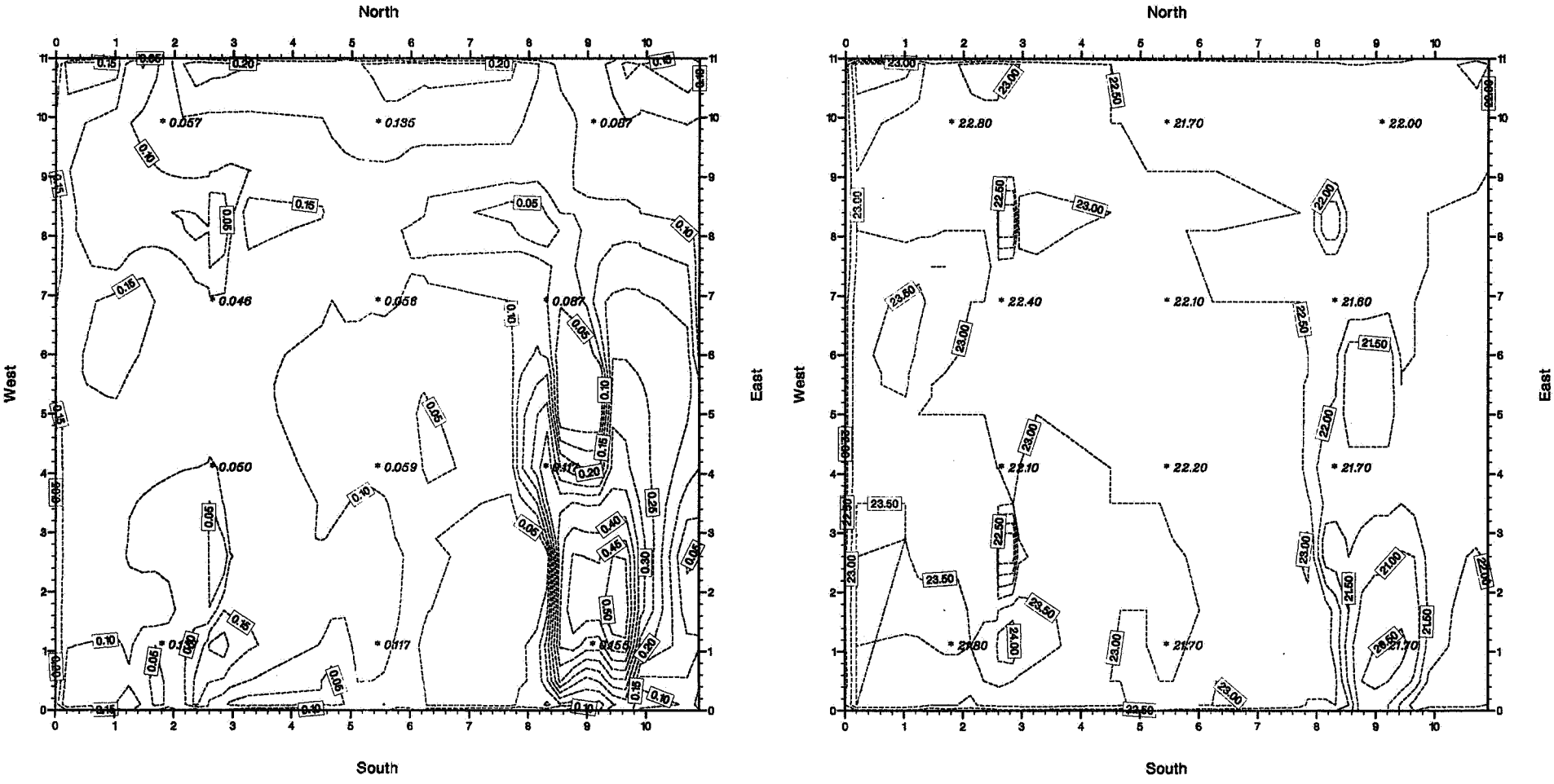


(a) Velocity (m/s)

(b) Temperature (deg.C)

Supply air: U = 0.356 m/s ; T = 19.9 deg.C

Fig. 4 Comparison of predicted isovels and isotherms with measured velocities and temperatures (*) on a horizontal plane (0.9 m above the floor) of a classroom with occupancy (case 1)

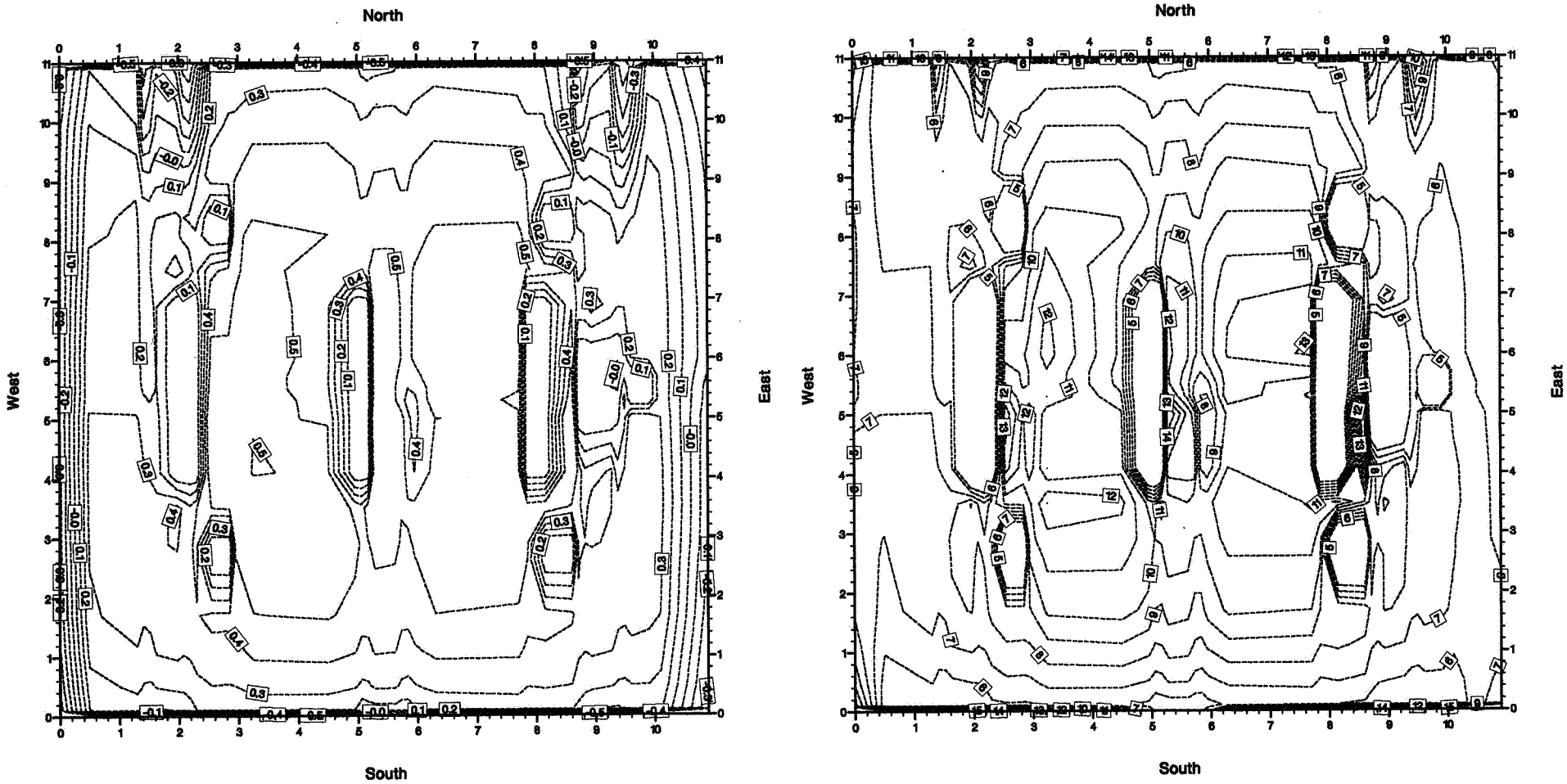


(a) Velocity (m/s)

(b) Temperature (deg.C)

Supply air: U = 0.76 m/s ; T = 19.9 deg.C

Fig. 5 Comparison of predicted isovels and isotherms with measured velocities and temperatures (*) on a horizontal plane (0.9 m above the floor) of a classroom without occupancy (case 6)

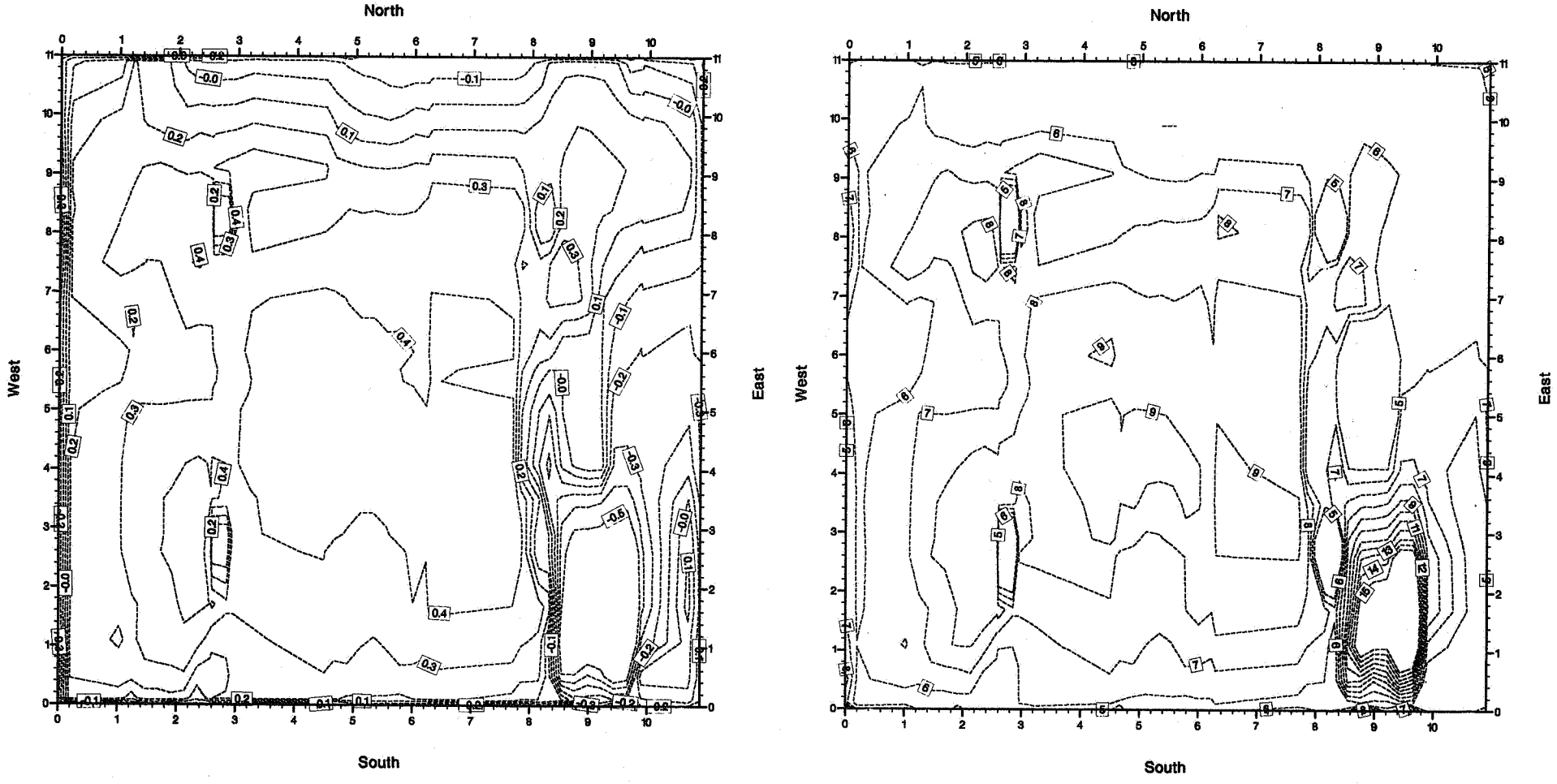


(a) Predicted mean vote

(b) Predicted percentage of dissatisfied (%)

Supply air: U = 0.356 m/s ; T = 19.9 deg.C

Fig. 6. Contours of predicted mean vote and predicted percentage of dissatisfied on a horizontal plane (0.9 m above floor) of a class room with occupancy (case 1)

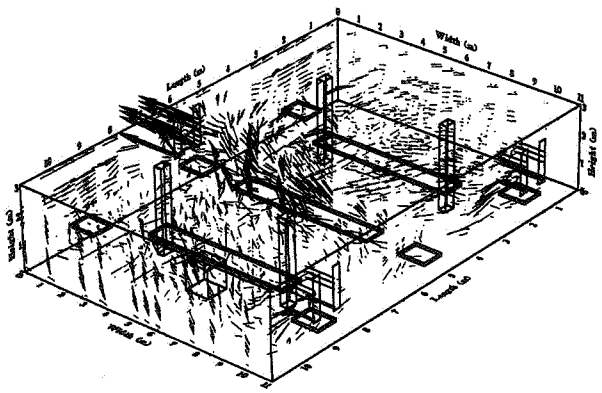


(a) Predicted mean vote

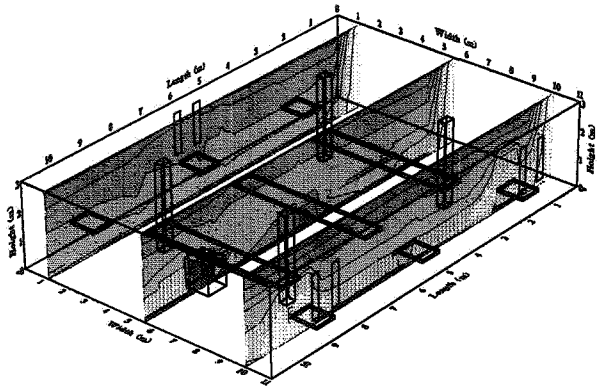
(b) Predicted percentage of dissatisfied (%)

Supply air: U = 0.76 m/s ; T = 19.9 deg.C

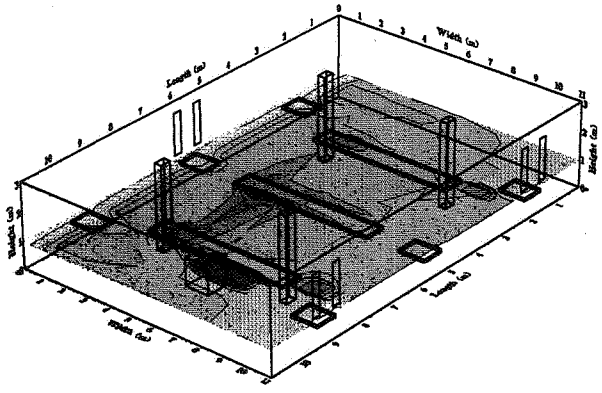
Fig. 7. Contours of predicted mean vote and predicted percentage of dissatisfied on a horizontal plane (0.9 m above floor) of a class room without occupancy (case 6)



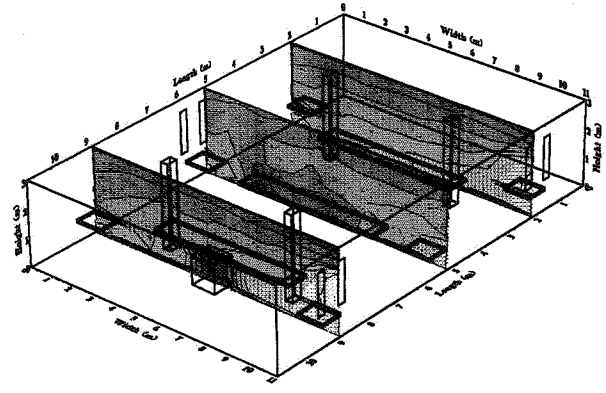
(a) Velocity vectors



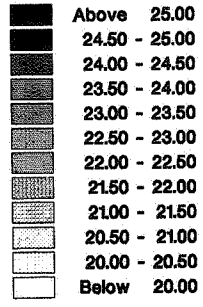
(b) Isotherms on vertical planes



(c) Isotherms on a horizontal plane



(d) Isotherms on vertical planes



Supply air: U = 0.356 m/s ; T = 19.9 deg.C

Fig. 8 Predicted velocity vectors & isotherms of air in a classroom without occupancy

AIR MOVEMENT & VENTILATION CONTROL WITHIN BUILDINGS

12th AIVC Conference, Ottawa, Canada
24-27 September, 1991

POSTER 42

Modelling of Air Flows, Temperatures and Contaminant Levels for Localized Ventilation Systems.

Richard A Grot

Lagus Applied Technology
18519 Village Mart Drive
Suite 242
Olney, MD 20832
USA

ABSTRACT

Results of 3-D computational fluid dynamic simulations of the air flows, temperature distribution and contaminant remove efficiencies for typical workstation configurations which include the option for localized supply of outdoor air will be presented. A typical office configuration including desks, partitions, localized heat and contaminant sources will be modelled. The results will be compared to similar simulations the same workstation environment using ceiling supply and return plenum configurations. The emphasis of the presentation will be on usefulness of computational fluid dynamics for the design of local ventilation systems and the accuracy required of 3-D simulations for making design decisions.

AIR MOVEMENT & VENTILATION CONTROL WITHIN BUILDINGS

12th AIVC Conference, Ottawa, Canada
24-27 September, 1991

POSTER 43

Numerical Prediction of Airflow Patterns and Ventilation Effectiveness in an Open Office Environment.

Jin B. Fang and Andrew K. Persily

Building & Fire Research Laboratory
Bldg.226/Room A313
National Institute of Standards & Technology
Gaithersburg, MD 20899
USA

ABSTRACT

Numerical modelling is performed to predict air movement, thermal comfort level and contamination distribution within an open office space. The office located in the building interior has a concentrated thermal load at its center and is conditioned by cool air delivered from a ceiling-mounted linear diffuser. the air velocity and temperature distributions and contaminant dispersion in the office are calculated for three different cooling loads and air exchange rates with a three-dimensional turbulent finite difference model. Calculations of ventilation effectiveness based on the time variations of contaminant or tracer gas concentrations in the supply, exhaust and occupied space are performed for the condition of constant injection of tracer gas into the supply air stream. The calculated values of the Air Diffusion Performance Index (ADPI) and ventilation effectiveness in the occupied zone for different supply airflow rates are presented.

AIR MOVEMENT & VENTILATION CONTROL WITHIN BUILDINGS

12th AIVC Conference, Ottawa, Canada
24-27 September, 1991

POSTER 44

Modelling Complex Inlet Geometries in CFD - Applied to Air Flow in Ventilated Rooms.

M. Skovgaard, P.V. Nielsen

University of Aalborg
Denmark

MODELLING COMPLEX INLET GEOMETRIES IN CFD - APPLIED TO AIR FLOW IN VENTILATED ROOMS

By

Skovgaard, M. and Nielsen P.V.,
The University of Aalborg, DK.

SUMMARY

Modern inlet devices applied in the field of ventilation of rooms are getting more complex in terms of geometry in order to fulfil the demand for thermal comfort of the occupants in the room and in order to decrease the energy consumption. This expresses the need for more precise calculation of the flow field. In order to apply CFD for this purpose it is essential to be able to model the inlet conditions precisely and effectively, in a way which is comprehensible to the manufacturer of inlet devices and in a way which can be coped by the computer resources.

In this paper a universal method is presented and tested. The method is based upon three dimensional - and radial wall jet theory and upon diffuser specific experimental data.

Simulations are held up against a more basic method and full scale measurements. The inlet model is evaluated in terms of result, computational effort and applicability. Promising results are obtained.

LIST OF SYMBOLS

A	Area
a	Coefficient in difference equation, area
C_1	Constant in the turbulence model
C_2	Constant in the turbulence model
C_D	Constant in the turbulence model
C_μ	Constant in the turbulence model
E	Wall roughness function in the logarithmic law
F	Force
I	Turbulence intensity
k	Turbulent kinetic energy
K	Factor in wall jet formula
n	Air change rate, normal to surface
P	Pressure
PD	Percentage Dissatisfied people due to draught
Re	Reynolds number ($\rho \underline{l} U/\mu$)
S	Source term
Tu	Turbulence intensity
u,v,w	Velocity fluctuations
U,V,W	Mean velocities
U^+	Dimensionless velocity parallel to the surface ($U_p/U\tau$)
x,y,z	Directions
y	Normal distance from wall
y+	Dimensionless wall distance ($U_\tau y_p \rho/\mu$)

Subscripts

D	Downstream point
E	East point
i,j,k	Indicators of direction
N	North point
o	Inlet
P	Centre point
r	Radial
rm	Recirculation maximum
S	Shear, south point
t	Turbulent
U	Upstream point
W	West point

Greek

δ	Kronecker delta, wall jet width, area
ϵ	Energy dissipation
θ	Angle
κ	Von Karman constant
μ	Viscosity (dynamic)
ρ	Density
τ	Shear stress
σ	Constant in the turbulence model (the turbulent Prandtl number)
ϕ	Generalized variable

INTRODUCTION

Numerical prediction of air flow patterns in mechanically ventilated rooms has been a research object for almost two decades. Up through 1970 and -80 Computational Fluid Dynamics (CFD) showed that it was possible to predict the flow field in large domains with relatively small openings (see e.g. *Nielsen 1976, Nielsen et. al. 1978* or *Gosman et. al. 1980*).

In recent years the field of ventilation engineering has started to look upon CFD as a design and analysing tool, because CFD offers a radical change in available analytical tools, by which the engineer can predict the impact of a certain design of an air condition system on the indoor climate and the energy management of real buildings. But in contrast to most test carried out with CFD, real buildings and air condition systems are often very complex in terms of building - and air supply device geometry (fig. 1), which gives arise to very complex flow phenomena such as transitional and non-developed flow regimes etc.

The aim of the work reported in the present paper is to look into the influences of a modern complex air supply terminal used in the mixing type of ventilation. The ideas about the model, however, may just as well be applied in the field of displacement ventilation.

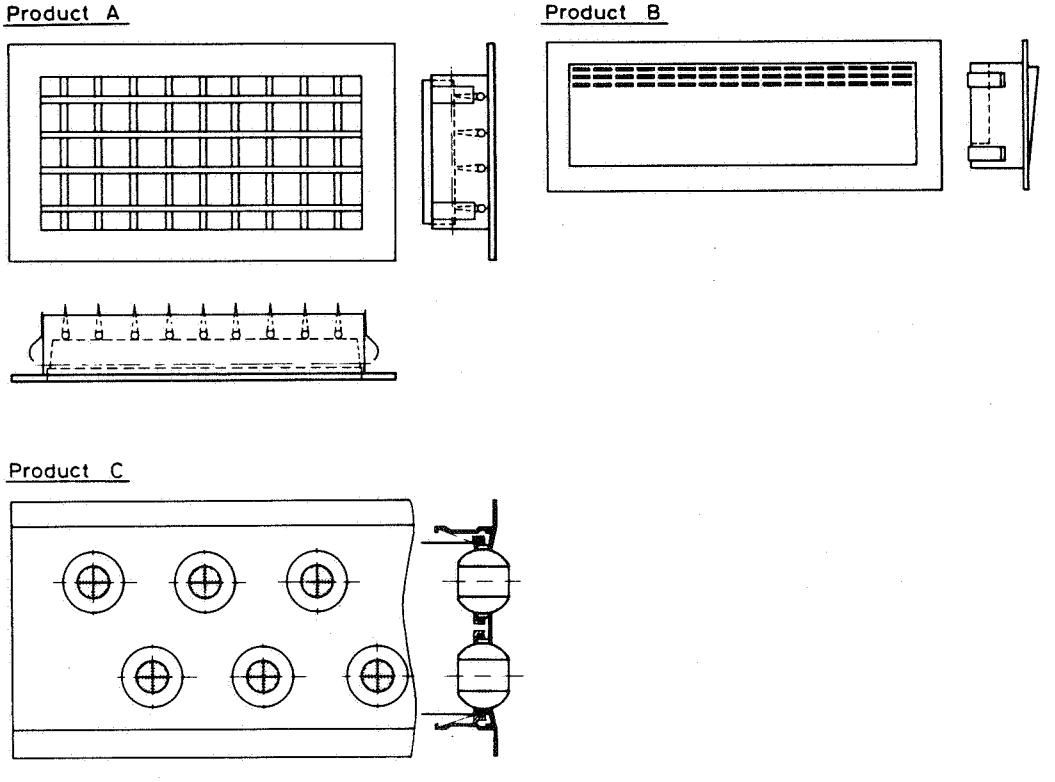


Figure 1. Different designs of air inlet devices.

It is well known that the velocity level in a room ventilated by a mixing type of ventilation is strongly influenced by the supply conditions *(Nielsen 1976)* and that it is

the momentum flow of the inlet which has the major impact of the flow pattern in the room (except maybe for very low inlet velocities). It is also known that the momentum flow in a wall jet created by the jet from the inlet diffuser is lower than the inlet momentum flow (*Mc Ree et. al. 1967*). It is therefore very important that the model of the inlet device is able to produce that wall jet momentum either directly by a model of the inlet device or by use of empirical data. In *Nielsen 1976* a method is presented which fulfils these basic requirements by use of diffuser specific data. This fact makes also the method quite universal. The model presented in the following utilizes the same basic ideas.

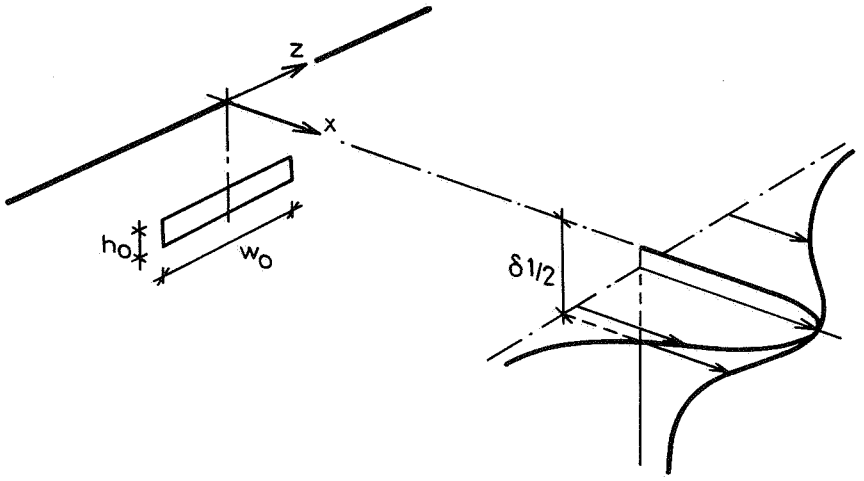


Figure 2. Typical flow from a wall mounted diffuser.

Fig. 2 shows a typical mounting of a inlet device in a wall. The flow from the inlet creates a wall jet type of flow in a certain distance from the inlet, either because the inlet flow is directed upwards or because it is influenced by the Coanda effect. An attempt to model the inlet directly would in most cases require too much computational effort to be realistic. Another more comprehensible way would be to prescribe the actual wall jet conditions in a volume where the flow has adopted this character. Such a method implies that device specific data are available.

MATHEMATICAL MODEL

The mathematical model of the flow is described by the following equations.

The continuity or mass conservation equation

$$\frac{\partial}{\partial x_i}(\rho U_i)=0 \qquad (1)$$

The momentum equations

$$\frac{\partial}{\partial x_i}(\rho U_i U_j) = -\frac{\partial P}{\partial x_i} + \frac{\partial}{\partial x_i}(-\rho\overline{u_i u_j}) + \frac{\partial}{\partial x_i}\left(\mu\left(\frac{\partial U_i}{\partial x_j}+\frac{\partial U_j}{\partial x_i}\right)\right) \quad (2)$$

where U_i is the time mean velocity of the direction x_i and u_i is the fluctuating velocity in the x_i direction.

To solve the above set of equations it is necessary to represent the fluctuating velocity by a set of turbulence equations. There are several of such models available, but the most suitable model for practical engineering is the k-ϵ model, which is a 2 equation semi-empirical model for turbulent kinetic energy and its dissipation. The k-ϵ model takes up the eddy viscosity concept by describing the Reynolds stresses in the following way

$$-\rho\overline{u_i u_j} = \mu_t\left(\frac{\partial U_i}{\partial x_j}+\frac{\partial U_j}{\partial x_i}\right) - \frac{2}{3}\rho k\delta_{ij}$$

By substituting the eddy viscosity concept into (2) we obtain the following equation for the mean flow

$$\partial(\rho U_i U_j) = -\frac{\partial P}{\partial x_i} + \frac{\partial}{\partial x_i}\left((\mu_t+\mu)\left(\frac{\partial U_i}{\partial x_j}+\frac{\partial U_j}{\partial x_i}\right)\right) - 2\rho k\delta_{ij} \quad (3)$$

$$\textit{where} \quad \mu_t = C_\mu \rho \frac{k^2}{\varepsilon} \quad (4)$$

The closure equations for k and ϵ will be transport equations of the following form

$$\frac{\partial(\rho U_i k)}{\partial x_i} = \frac{\partial}{\partial x_i}\left(\frac{\mu_t}{\sigma_k}\frac{\partial k}{\partial x_i}\right) + \mu_t\frac{\partial U_i}{\partial x_j}\left(\frac{\partial U_i}{\partial x_j}+\frac{\partial U_j}{\partial x_i}\right) - C_D\rho\varepsilon \quad (5)$$

$$\frac{\partial(\rho U_i \varepsilon)}{\partial x_i} = \frac{\partial}{\partial x_i}\left(\frac{\mu_t}{\sigma_\varepsilon}\frac{\partial \varepsilon}{\partial x_i}\right) + C_1\frac{\varepsilon}{k}\mu_t\frac{\partial U_i}{\partial x_j}\left(\frac{\partial U_i}{\partial x_j}+\frac{\partial U_j}{\partial x_i}\right) - \frac{\varepsilon}{k}C_2\rho\varepsilon \quad (6)$$

where k and ϵ has the definition

$$k = \frac{1}{2}\overline{u_i u_j}$$

$$\varepsilon = \frac{\mu}{\rho}\overline{\frac{\partial u_i}{\partial x_j}\frac{\partial u_j}{\partial x_i}}$$

For fully turbulent flow the following set of constants is assigned

C_μ=0.09; C_1=1.44; C_2=1.92; σ_k=1.0; σ_ε=1.3; C_D=1.0

NUMERICAL PROCEDURE

The computational domain is divided into a number of cells by a non-uniform, staggered and rectangular mesh in order to produce finer grid close to the walls and other areas where gradients may be expected to be large. The previous set of equations (3 + 5 + 6) are dicretised by the finite volume technique (FV) *(Patankar 1980)* and cast into following general form:

$$a_P\phi_P = a_E\phi_E + a_W\phi_W + a_N\phi_N + a_S\phi_S + a_D\phi_D + a_U\phi_U + S_\phi \qquad (7)$$

$$S_\phi = S_C + S_P\phi_P$$

The pressure is linked via the pressure correction technique and the turbulent viscosity is calculated by (4).

When a surrounding set of boundary conditions is provided a solution can be obtained. To solve the equations (7) the TMDA technique with an ADI - like procedure in the cross room planes is used.

BOUNDARY CONDITIONS

To be able to solve the discretised set of equations a full set of boundary conditions (BC) must be given because of the elliptic nature of the governing equations. However, the use of the hybrid scheme may have the effect that not all BC's are effective.

Test case

The test room is shown in fig. 3. The inlet device is of the HESCO-type (KS4W205K370) where the flow can be adjusted to any kind of three dimensional flow. For this purpose all nozzles are adjusted to an angle of 40° upwards.

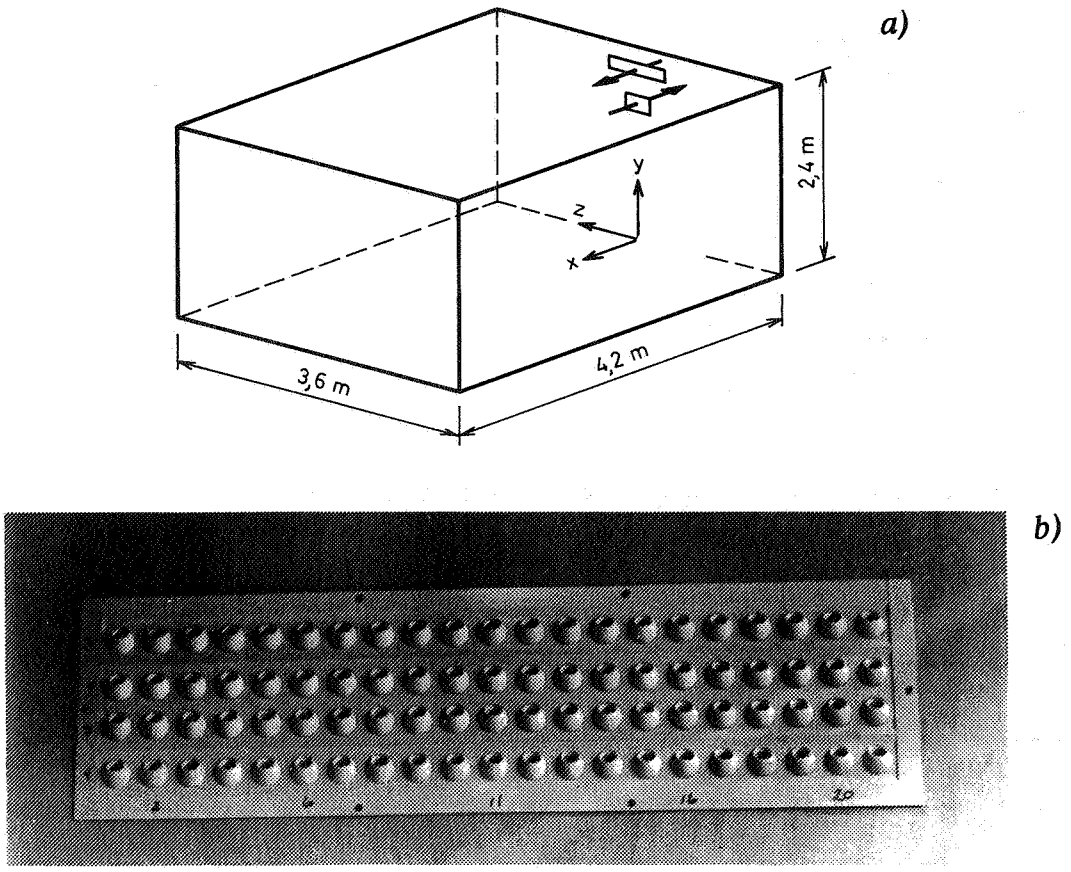


Figure 3. Sketch of the test case. a) The room geometry. b) Close up of the inlet device.

(i) Boundary conditions at surfaces

Because of the validity range of the set of equations (fully turbulent region) the no-slip boundary conditions have to be introduced indirectly by wall functions in the source term at the first gridnode (subscript p). This approach has also the advantage that it spares some gridnodes in the near wall region. However, this method can be difficult to use in areas where the maximum velocity is found close to the surface (e.g. the wall jet region).

The boundary conditions are given by the shear force at the wall (subscript s) and the velocity parallel to the surface in the first gridnode (subscript p)

$$F_s = \delta x_s \tau_s = -\delta x \mu \frac{\partial U}{\partial n}$$

If $y^+ < 11.63$:

$$F_s = -\mu \frac{(U_p - U_s)}{y_p} \delta x \tag{8}$$

If $y^+ > 11.63$:

$$F_s = -\frac{\rho C_D C_\mu^{\frac{1}{4}} k_p^{\frac{1}{2}} (U_p - U_s)}{U^+} \delta x \tag{9}$$

$$U^+ = \frac{1}{\kappa} \ln(E y^+) \; ; \quad k_p = \frac{U_\tau^2}{\sqrt{C_\mu}} \; ; \quad \kappa = 0.4187 \; ; \quad E = 9.793$$

F_s is subtracted as a source term in the near wall cell in the point p with ϕ_p equal to u_p and $u_s = 0$.
The limit 11.63 is probably not valid in three dimensional boundary layer flow and one can argue that it is already too low in the one dimensional boundary layer but it is, nevertheless, used in this two layer approach.

Turbulent kinetic energy and dissipation:

$$\frac{\partial k}{\partial n} = 0$$

$$\varepsilon = \frac{C_\mu^{\frac{3}{4}} k^{\frac{2}{3}}}{y_p \kappa}$$

(ii) Boundary conditions in the return opening

Outlet U-velocity is set to fulfil the overall continuity so

$$U_{out,uniform} = \frac{\int_{x_1}^{x_2}\int_{y_1}^{y_2} U_o(x,y)dA}{A_{out}}$$

All gradients in the outflow plane are zero as well as the pressure. Upwind boundary is assumed so exact values are not required.

(iii) Inlet boundary conditions

The inlet boundary is particularly complex because we must give an exact image of the real conditions and real conditions often mean a very complicated design of the inlet device. The complex inlet device used in present test case is chosen to give a complicated flow pattern around the inlet and therefore is a realistic test of the CFD method. The present inlet device is difficult to model directly because the many small nozzles are distributed, over a fairly large area and are directed upwards in an angle of 40°. It is therefore decided to try two approaches to represent the inlet flow conditions.

The two methods tested in the following are: a basic momentum preserving method and a development - or extension of the method outlined by *Gosman et. al. 1980*, and further explaned by *Nielsen 1989* and *Skovgaard et. al. 1990*. The latter method is developed to be general - and to be more comprehensible to the manufacturer. The ideas behind the method are not only useful in most set-ups of the mixing type but also in many displacement systems.

The basic method:

The assumptions for this method are that the momentum flow in the jet created around the inlet should be presented by a more simple model. The distributed nozzles are simulated by a single opening having the same effective inlet area, the same aspect ratio (h/w) and the flow rate equal to the measured and therefore the same momentum flow as the actual diffuser. The above mentioned assumptions give following B.C.'s.

$a_{inlet} = 0.18*0.062 = 0.011\ m^2$

$a_o = f(u_o)$
for n = 1 : 0.008 m^2
for n = 3 : 0.00855 m^2
for n = 6 : 0.009 m^2

$U_o = 3.6$ m/s : $U_{inlet} = 2.71$ m/s, $V_{inlet} = 2.27$, $W_{inlet} = 0.0$ (n = 3)

$k_{inlet} = 1.5*I^2U_{inlet}^2$, I = 0.1

$\epsilon_{inlet} = C_\mu^{3/4} k^{3/2}/l$

The "prescribed velocity" PV method:

When the PV method is used the velocity profiles for u and v are prescribed in a full volume in front of the diffuser at a location where the wall jet type of flow is established and therefore has a parabolic nature. This method requires data for the behaviour of the real flow. Test were carried out on the chosen inlet geometry by *Skovgaard et. al. 1990*. The tests showed that the maximum velocity of the wall jet is described by

$$U_r = K(\theta) U_0 \frac{\sqrt{a_0}}{x+x_0} \tag{10}$$

where the K-factor for this particular inlet is interpolated from experimental data (*Skovgaard et. al. 1990*) (fig. 4).

$$K(\theta) = 4.2 - 0.975\theta - 8.206\theta^2 + 7.828\theta^3 - 2.088\theta^4 \tag{11}$$

θ is in rad.

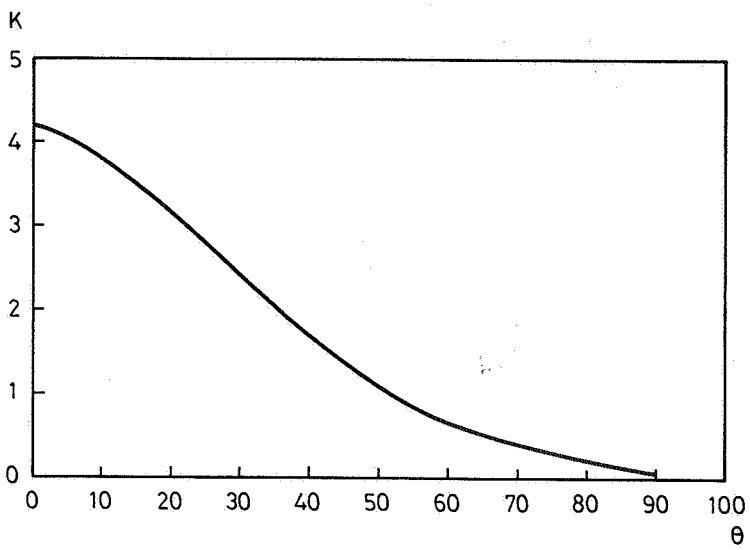


Figure 4. K(θ) interpolated from eksperimental data.

U and V are calculated from

$U = \cos\theta U_r$
$V = \sin\theta U_r$

U and V profiles are self similar up to a distance of $y/\delta_{½} = 1.0$ under the ceiling

(*Nielsen 1989*). The following wall jet profile is assumed (*Verhoff 1963*)

$$f\left(\frac{y}{\delta_{\frac{1}{2}}}\right) = 1.4794\left(\frac{y}{\delta_{\frac{1}{2}}}\right)^{\frac{1}{7}}\left[1-erf\left[0.6775\left(\frac{y}{\delta_{\frac{1}{2}}}\right)\right]\right]$$

and δ is taken from *Skovgaard et. al. 1990*:

$$\delta_{\frac{1}{2}}(x) = 0.08(x+0.45)$$

RESULTS.

Simulated results from the basic- and the PV model will in the following be compared with measured data for air change rates 1, 3 and 6 h^{-1}.

The overall flow patterns for the cases are shown in fig. 5 and 6.

Predictions in the basic model show that the radial jet below the ceiling, fig. 5g, has a component of very high velocity directed against the corners. This flow pattern may be the result of the impingement at the ceiling and it has the effect that a high velocity level is obtained in the occupied zone.

The velocity distribution below the ceiling in the case of the PV model has a characteristic "peak" along the centre line, fig. 6g. This is, in the experiments, observed as a area with parallel flow. Measurements by *Heikkinen 1991* have also shown this combination af two/three dimensional flow and radial flow. The maximum velocity in the occupied zone is close to the measured level, which shows the practical relevance of the PV model.

The area with the maximum velocity, U_{rm}, in the occupied zone is located very close to the wall opposite the supply opening (*Skovgaard et. al. 1990*). The predictions are not able to reproduce this location.

The results in fig.7 relate to the measured data by *Skovgaard et. al. 1990*. The figure depicts the decay of the centre line velocity. x_o is measured to 0.45 m behind the inlet. $a_o^{½}$ is a function of the inlet Reynolds number and is again taken from the measured data.

It is seen that discrepancies are found in both simulations due to the very complex flow structure in the real case . In the basic model case, the peak velocity decreases too rapidly caused by the flow going outwards towards the corners. If we instead focus on the PV model it is seen that although discrepancies are present the decay is

simulated with higher accuracy.

The predictions indicate that a good description of the boundary conditions is a necessary requirement for the prediction of fully turbulent flow pattern with acceptable accuracy.

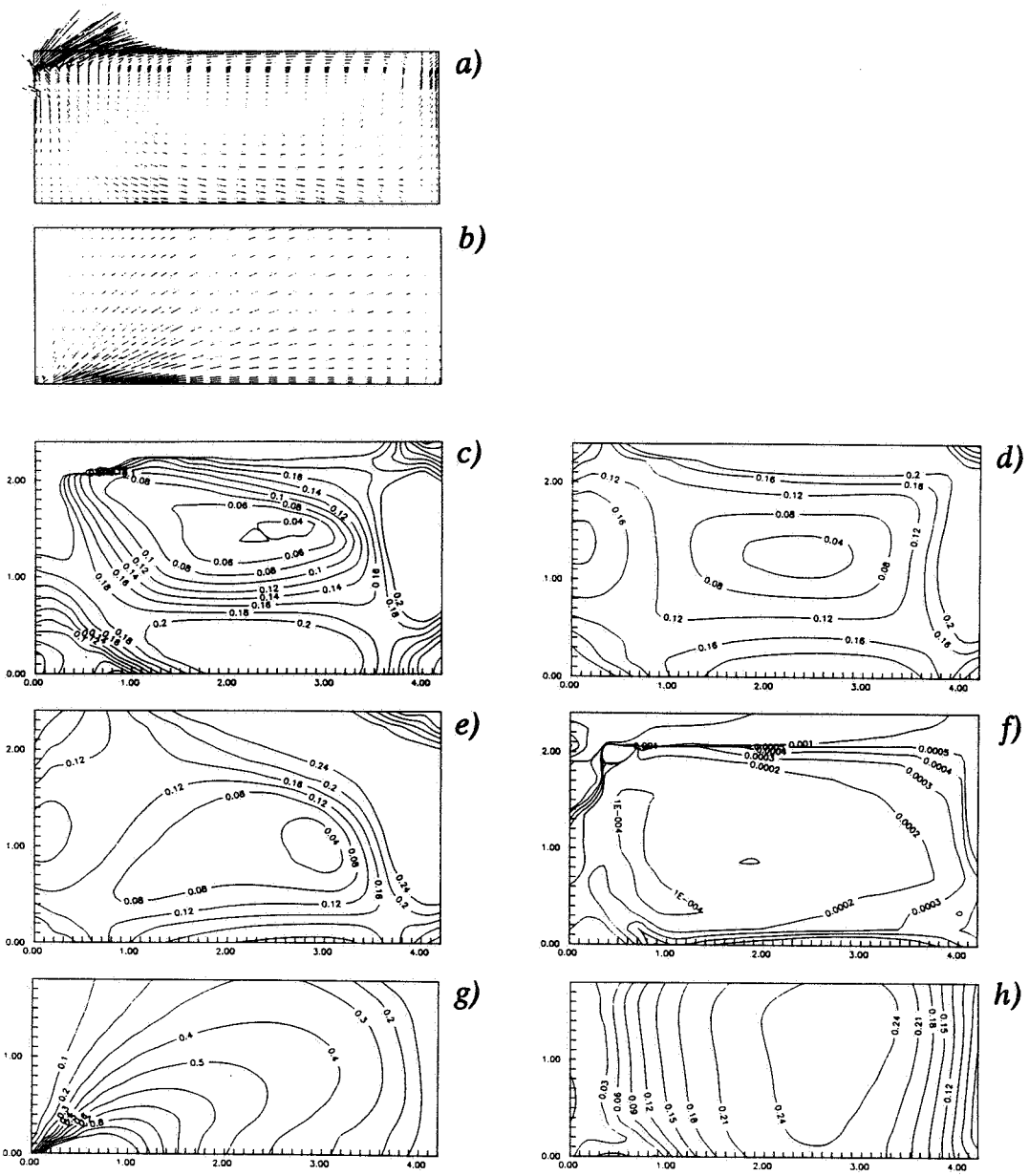


Figure 5. Air flow patterns from the basic model (n = 3h^{-1}). a) Velocity vectors in the centreline. b) Velocity vector in a plane 0.04m below the ceiling. c)-e) Speed contours in the planes z = 0.02, 1.0 and 1.7m. f) Iso - kinetic energy in plane z = 0.02. g)-h) Speed contours in y = 2.36 and y = 0.05.

The width of the jet in the centre plane, which is depicted in fig. 8, has a close connection to the results shown in fig. 5, 6 and 7. It is seen that the spread of the jet simulated by the PV boundary conditions is close to the measured values while the basic case shows some deviation.

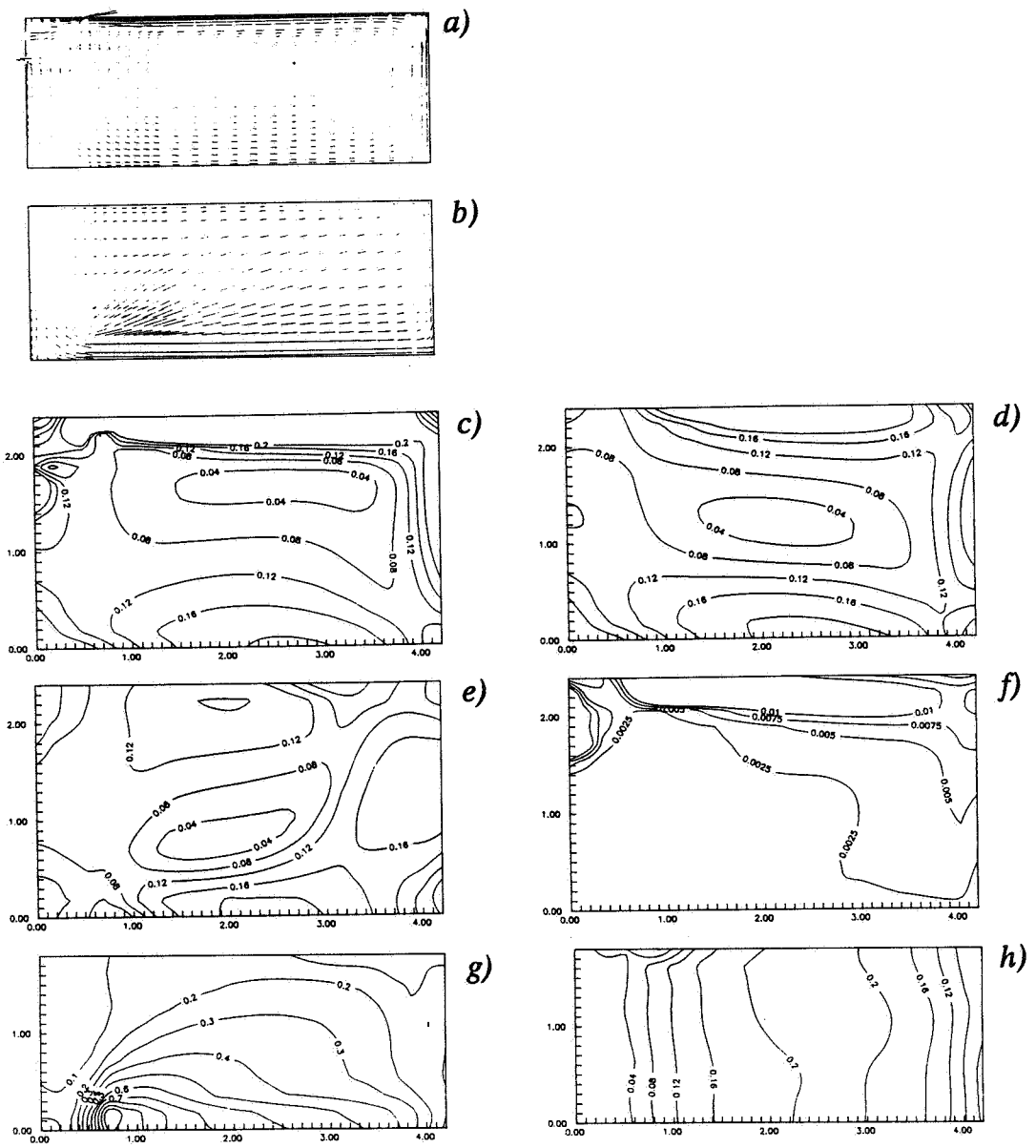


Figure 6. Air flow patterns from the PV model (n = 3h^{-1}). a) Velocity vectors in the centreline. b) Velocity vector in a plane 0.04m below the ceiling. c)-e) Speed contours in the planes z = 0.02, 1.0 and 1.7m. f) Iso - kinetic energy in plane z = 0.02. g)-h) Speed contours in y = 0.05 and y = 2.36.

One of the main purposes of a design propos is to predict the maximum velocity in the occupied zone. Fig. 9 shows the measured and the predicted maximum velocity U_{rm}. The figure shows that the PV method for description of the supply opening is giving the best estimate of U_{rm}. But it can also be seen that the performance is poor for n = 1 in both models because the low Reynolds number effect has a large impact on the flow at low velocities.

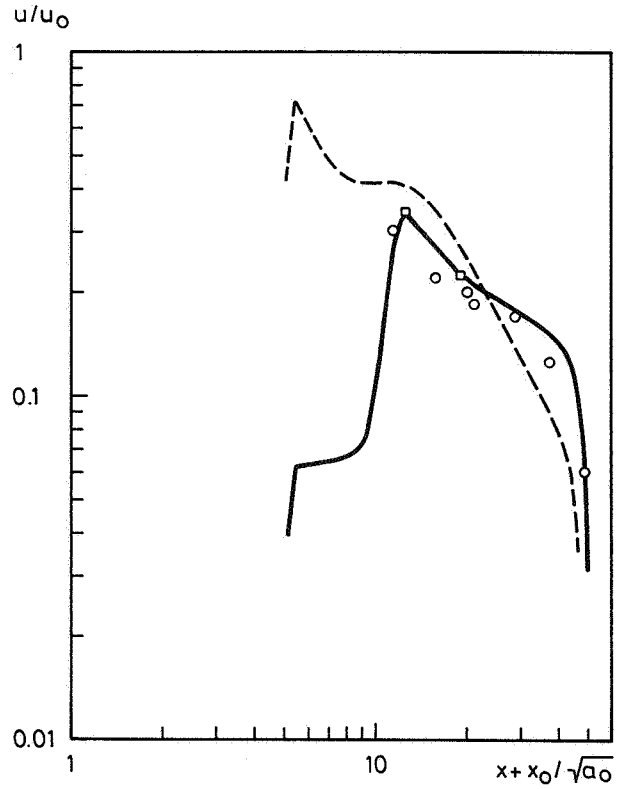


Figure 7. Measured and simulated decay of peak centreline velocity ($n = 3h^{-1}$). o - measured, dashed line - basic model and line - PV model (the PV volume in indicated by squares).

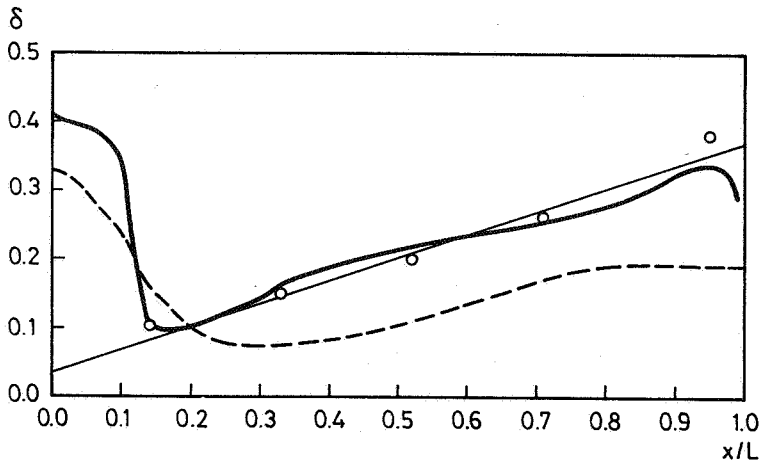


Figure 8. Spread of the wall jet in the centre plane. (o - measured, dashed line - basic model and line - PV model.)

Several authors have made studies of this phenomenon (see e.g. *Skovgaard et. al. 1990, Murakami 1983, Chen 1979* or *Restivo 1979*) but it has not led to any prediction of it because the k,ϵ model supposes a fully turbulent flow. The low Reynolds number effect i fig. 9 arises partly from the supply device and partly from the flow in the room

(*Skovgaard et. al. 1990*). The basic model can incorporate the change in the effective area, a_o and the PV model can in addition to this also include variations in the prescribed volume up to a distance of x=1.35m. The effects are not very obvious in any of the predictions. This is partly because the change in K(θ) as a function of air change rate isn't taken into account in the PV model (a mean of the measured K factors is used). But it is also because low Reynolds phenomena that are occurring inside the flow and therefore cannot be described by the boundary conditions. Further investigations in this specific area have to be done.

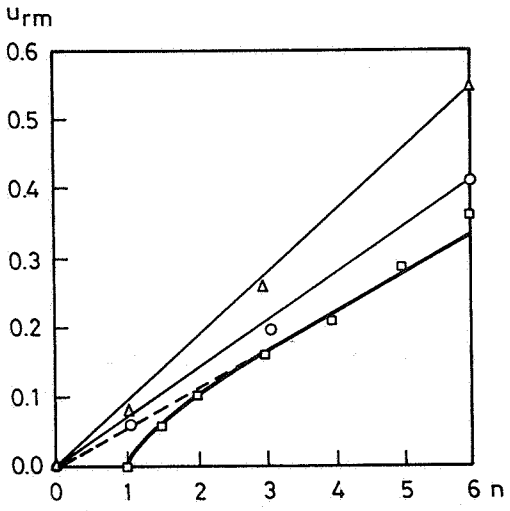


Figure 9. U_{rm} as a function of air change rate. squares - experiments, triangles - basic model, o - PV model.

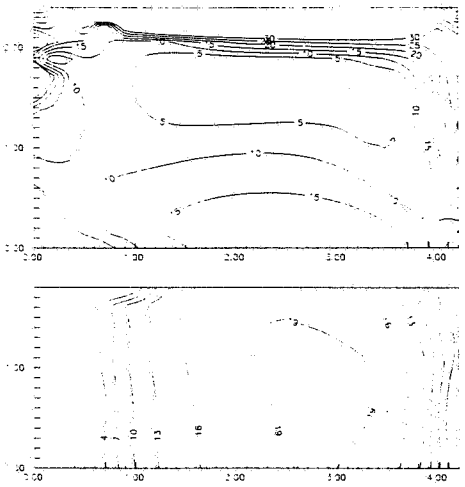
As previously mentioned one of the major forces with CFD analysis of flow fields is the very detailed knowledge of the velocity, turbulence and thermal parameters in the room. These data can be used in a comfort analysis of the room or the occupied zone. In fig 10 such an application is shown where the PD index (percent dissatisfied) is calculated (*Fanger et. el. 1989*).

The calculation is given as an example and the same equation is therefore used for the full room and for the foot level, although it is known that the draft tolerance is higher in foot level than in the average of the body. The following comfort equation is used

$$PD = (34-t_{air})(U-0.05)^{0.62}(0.37UTu+3.14)$$

where

$$Tu = \frac{\sqrt{k}}{1.1U}$$



a)

b)

Figure 10. Calculated PD index. a) z = 0.02. b) Foot height approx. 5 cm above the floor.

CONCLUSION

CFD simulations of air flow patterns in ventilated spaces give detailed information of comfort parameters and are therefore useful as a analysing and design tool.

A good representation of the boundary conditions is a necessary requirement for prediction of fully turbulent flow. Two inlet models have been tested. One which aims to model the supply device directly (basic) and one which models the resulting flow pattern in a volume in front of the diffuser (PV). The latter method, which requires diffuser specific data, has clearly the best performance. The first method fail to meet one basic requirement namely to reproduce the overall flow pattern. The second mathod gives alsothe lowest computational cost for the simulated case.

The PV model is still the best choice if low Reynolds number effects are present because it can incorporate low Reynolds number effects from the inlet device and from the resulting flow up to the border of the volume in a certain distance from the inlet.

The simulation indicates that low Reynolds number effects not only arise from the inlet device and the boundary layer but from the flow in the room. This pert of the low Reynolds number effects can therefore not be taken into account by solely modifying the boundary conditions.

LIST OF REFERENCES

Chen, Q., Suter, P. and Moser, A.
Influence of Air diffusion. Energy systems laboratory series. Federal Inst. of Tech, ETH, Zürich Switzerland *1990.*

Fanger, P.O., Melikov, A.K., Hanzawa, H. and Ring, J.
Turbulence and draft. ASHRAE journal, *1989.*

Gosman, A. D., Nielsen, P. V., Restivo, A. and Whitelaw, J. H.
The Flow Properties of Rooms with Small Ventilation Openings. ASME Journal of Fluids Eng. Vol 102 *1980.*

Heikkinen, J.
Appendix to IEA, RID no. 1.13: Specifications of Test case B. *1989.*

Heikkinen, J.
Private communication. *1991.*

Murakami, S., Tanaka, T. and Kato, S.
Numerical Simulation of Air Flow and Gas Diffusion in Room Model - Correspondance between Simulation and Model Experiments. University of Tokyo, *1983.*

Nallasamy, M.
Turbulence models and their application to the prediction of intenal flows, a review. Computers and fluids, Vol. 14 no. 2. *1987.*

Nielsen, P.V.
Flow in Air Conditioned Rooms - Model Experiments and Numerical Solutions of the Flow Equations. Revised ed. of Ph.D. - Thesis *1976.*

Nielsen, P.V, Restivo, A. and Whitelaw, J. H.
The velocity Characteristics of Ventilated Rooms. ASME Journal of Fluid Eng. Vol. 100, *1978* p.291.

Nielsen, P.V.
Representation of Boundary Conditions at Supply Openings. International Energy Agency, Annex 20, ISSN 0902 - 7513 R8902, *1989.*

Mc Ree, D.I. and Moses, H.L.
The Effect of Aspect Ratio and Offset on Nozzle Flow and Jet Reattachment. *1967* FLUIDICS symposium ASME.

Patankar, S. V.
Numerical Heat Transfer and Fluid Flow. Hemisphere Publishing Coorporation. ISBN 0-89116-522-3, *1980.*

Restivo , A.M.O.
Turbulent flow in ventilated rooms. Imp. Coll. of Science and Tech, Mech. Eng. Dept. Ph.D. - Thesis, *1979.*

Skovgaard, M., Hyldgård, C.E. and Nielsen, P.V.
High and Low Reynolds Number Measurements in a Room with an Impinging Jet.

Roomvent '90, Oslo, *1990.*

Verhoff, A.
Report N626, Princeton University, Dept. of Aeronautional Engineering, *May 1963.*

AIR MOVEMENT & VENTILATION CONTROL WITHIN BUILDINGS

12th AIVC Conference, Ottawa, Canada
24-27 September, 1991

POSTER 45

Numerical Investigation of Transient Flow Over a Backward Facing Step Using a Low Reynolds Number k-e Model.

M. Skovgaard, P.V. Nielsen

University of Aalborg
Denmark

NUMERICAL INVESTIGATION OF TRANSIENT FLOW OVER A BACWARD FACING STEP USING A LOW REYNOLDS NUMBER k-ϵ MODEL.

By

M.Skovgaard and P.V.Nielsen,
The University of Aalborg, DK

SUMMARY.

Recent full scale experiments has detected the presence of low Reynolds number effects in the flow in a ventilated room. This means that one are unable to predict the flow patterns in some geometries for air change rates - or Reynolds numbers - which are relevant for ventilation engineering by a standard model of turbulence.

In this paper it is investigated if it is possible to simulate and capture some of the low Reynolds number effects numerically using time averaged momentum equations and low Reynolds number k-ϵ model. The test case is the laminar to turbulent transistional flow over a backward facing step with expansion ratio (h/H eq. 1/6).

The results are evaluated and held up against experimental LDA data and simulation with a Reynolds stress model (RSM).

ACKNOWLEDGEMENTS.

This paper is partly made during a stay at UMIST, Manchester, UK.
The authors would like to send many thanks to the staff of UMIST, who made the stay very pleasant.
Especially we would like to thank *Dr. N. Inze* and *Prof. B. Launder* who have been very inspiring, supportive and participating thoughout the work at UMIST.

LIST OF SYMBOLS

$C_{\epsilon 1}$	Constant in the turbulence model
$C_{\epsilon 2}$	Constant in the turbulence model
$C_{\epsilon 3}$	Constant in the turbulence model
C_{μ}	Constant in the turbulence model
E	Wall roughness function in the logarithmic law
f_{μ}	Function which mimics the direct effect of the molecular viscosity on the shear stress in the turbulence model
f_1	Function to increase the dissipation near the wall in the turbulence model
f_2	Function to incorporate low Reynolds number effects in the destruction term of the ϵ equation
h	Inlet height
H	Channel height
LRN	Low Reynolds number
k	Turbulent kinetic energy
P	Pressure, generation term
R	Turbulent Reynolds number
Re	Reynolds number ($\rho \underline{l} U/\mu$)

RSM	Reynolds stress model
S	Source term
u,v,w	Velocity fluctuations
U,V,W	Mean velocities
U^+	Dimensionless velocity parallel to the surface ($U_p/U\tau$)
x,y,z	Directions
y	Normal distance from wall
y+	Dimensionless wall distance ($U_\tau y_p \rho/\mu$)

Subscripts

i,j,k	Indicators of direction
o	Inlet
RE	Recirculation
S	Shear
t	Turbulent

Greek

δ	Kronecker delta, area
ϵ	Energy dissipation
$\tilde{\epsilon}$	Energy dissipation in the Launder-Sharma k,ϵ model
κ	von Karman constant
μ	Viscosity (dynamic)
ρ	Density
τ	Shear stress
σ	Constant in the turbulence model (the turbulent Prandtl number)
ϕ	Generalized variable

INTRODUCTION

The flow patterns in mechanically ventilated rooms gives arise to many complications when one wants to predict them theoretically and/or numerically. These complications ranges from the fact that the flow is turbulent and the confined space is relatively large to the complexcities of the geometrical design of the components involved. Factors as transitional flow through inlet devices, transistional effects in the resulting jets and low Reynolds number effects in the room where the velocities are low are also very important.

The succes of numerical predictions in this area depend very much of the situation. If one or more of the above mentioned factors are involved - which is often the case - then the numerical procedure and the mathematical models must be able to capture these phenomenas.

Some studies of the complicated factors has recently been carried out - both numerically (e.g. *Skovgaard et. al. 1991a, Murakami, 1983* and *Chen 1990)* and experimentally (e.g. *Nielsen et al. 1988, Skovgaard el. al. 1990 , Heiselberg et. al. 1987* and *Restivo 1979).*

Present paper reports work done on the low Reynolds number flows near the wall and in the transitional jet regime. Both areas are important when one wish to predict flow patterns in a ventilated room because the velocity level in a room is strongly influenced by the inlet momentum flow and - at lower velocities - boundary layer flow.

In order to be able to separate the two subjects from other complexities which might

occur in a real situation a simpler geometry is adopted. The geometry of a two - dimensional single sided sudden expansion of ratio 1/6 is chosen. The simulation covers a range of Reynolds number which is typical for room air flows. This is the same range which covers the transistional regime with evidence of periodicy (flow experiments *Restivo 1979)* to the high velocity regime where the turbulent fluctuations is spread over a wide frequency range and the Reynolds number dependence is little (fully turbulent region). Comparisons with experiments are available from work done by *Restivo 1979.*

THE MODEL AND THE NUMERICAL APPROACH

The model consist of the continuity - and the momentum equations for the time averaged flow and a eddy viscosity concept for the turbulent Reynolds stresses.

The govering equations for steady flow are

$$\frac{\partial}{\partial x_i}(\rho U_i) = 0 \tag{1}$$

$$\frac{\partial}{\partial x_i}(\rho U_i U_j) = -\frac{\partial P}{\partial x_i} + \frac{\partial}{\partial x_i}\left(\mu\left(\frac{\partial U_i}{\partial x_j}+\frac{\partial U_j}{\partial x_i}\right)\right) - \rho\overline{u_i u_j} \tag{2}$$

To describe the Reynolds stresses several models can be adopted. It is here chosen to apply a low - Reynolds number (LRN) form of the k-ϵ model which is still the most used in engineering types of flow. *Patel et. al. 1985* reviewed several forms of LRN k-ϵ models and although differences were recorded several models gave similar solutions in the prediction of the flate plate boundary layer. The Launder - Sharma version of the Jones - Launder model is applied here (*Launder and Sharma 1978).*

The model takes the following form for 2D isotropic homogenious flow

$$\mu_t = \rho C_\mu f_\mu \frac{k^2}{\underline{\varepsilon}} \; ; \; \underline{\varepsilon} \approx \varepsilon - 2\frac{\mu}{\rho}\left(\frac{\partial}{\partial x_i}\left(\frac{\partial \sqrt{k}}{\partial x_j}\right)\right)^2 \tag{3}$$

$$\frac{\partial}{\partial x_i}(\rho U_i k) = \frac{\partial}{\partial x_i}\left(\left(\mu+\frac{\mu_t}{\sigma_k}\right)\frac{\partial k}{\partial x_i}\right) + P - \rho\underline{\varepsilon} \tag{4}$$

$$\frac{\partial}{\partial x_i}(\rho U_i \underline{\varepsilon}) = \frac{\partial}{\partial x_i}\left(\left(\mu+\frac{\mu_t}{\sigma_\varepsilon}\right)\frac{\partial \varepsilon}{\partial x_i}\right) + C_{\varepsilon 1} f_1 \frac{\underline{\varepsilon}}{k} P - C_{\varepsilon 2} f_2 \rho \frac{\underline{\varepsilon}^2}{k} + C_{\varepsilon 3} \frac{\mu \mu_t}{\rho}\left(\frac{\partial}{\partial x_i}\left(\frac{\partial U_i}{\partial x_j}\right)\right)^2 \quad (5)$$

Where P is the generation rate due to shear effects

$$P = -\rho \overline{u_i u_j} \frac{\partial U_i}{\partial x_i}$$

Reynolds stresses are computed from

$$-\rho \overline{u_i u_j} = \frac{2}{3}\delta_{ij}\rho k - \mu_t\left(\frac{\partial U_i}{\partial x_j}+\frac{\partial U_j}{\partial x_i}\right)$$

The model constants and functions can be seen in tabel 1.

It should be noticed that ϵ in (5) is replaced by $\underline{\varepsilon}$ which is the total dissipation rate. This is a convenient form which allows the $\underline{\varepsilon}$ wall boundary conditions to be zero. The trade - off of this substitution is the complex source term $C_{\epsilon 3}$.....

Regarding the calculations of the source terms $C_{\epsilon 1}$..... and $C_{\epsilon 2}$..... the authors found that it should be calculated as written in 5 and if any under-relaxation is needed the k-value from previous iteration can conveniently be used.

The k-ϵ model.	Fully turbulent version.	LRN version.
C_μ	0.09	0.09
$C_{\epsilon 1}$	1.44	1.44
$C_{\epsilon 2}$	1.92	1.92
$C_{\epsilon 3}$	-	2
σ_k	1.0	1.0
σ_ϵ	1.3	1.3
f_μ	1.0	$\exp(-3.4/(1+R_t/50)^2)$
f_1	1.0	1.0
f_2	1.0	$1-0.3\exp(-R_t^2)$

Tabel 1: The turbulent model constants and functions. $R_t = \rho k^2/\mu\underline{\varepsilon}$

NUMERICAL PROCEDURE

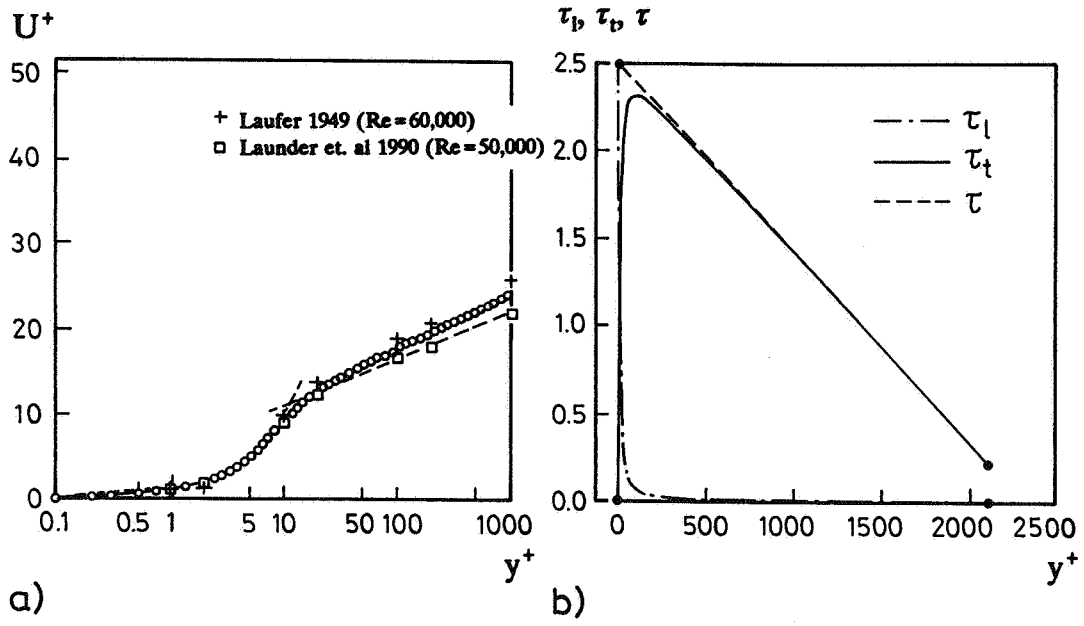
The two-dimensional elliptic flow solver TEAM *(Huang 1986)* which has been extentively used and validated was used to obtain the flow solutions. The code is using the finite volume technique to solve the equations mentioned in the previous paragraph imploying the staggered grid layout to overcome the checkerboard phenomenon. The solution scheme in SIMPLE and the differencing scheme was QUICK for convective terms in the momentum eq.s and PLDS for other terms and variables. A non uniform grid was used in order to achieve a finer grid in the near wall region and in the shear layers. In fact the solution is rather sensitive to the grid layout especially the region $5 < y^+ < 30$. The equations was solved line by line in an ADI - iterative manner. As expected the convergence is rather slow because of the slow diffusive proces in the boundary layer and because of the necessary fine grid.

TEST IN STRAIGHT CHANNEL FLOW

To validate the performance of the model it is chosen to apply it to fully developed channel flow. Primarily because a wide range of data is available for comparison and second because the fully developed u, k and $\underline{\epsilon}$ profile will serve as inlet conditions in the later application.

The case was run one-dimensional with fixed dP/dx, in the u - momentum eq. In this way it is only nessesary to solve for u, k and $\underline{\epsilon}$. 35 gridnodes was used in the crossstream direction. Boundary condition for u, k and $\underline{\epsilon}$ was set to zero on the walls.

Fig. 1a depicts the mean velocity up through the boundary layer for Re_{bulk} = 50,000. As seen are the U^+ values in the sublayer in good agreement with the RSM data (*Launder et. al. 1990*) and the experimental data of *Laufer 1949*. In the outer - fully turbulent region are the U^+ values too high compared to the log. law and the RSM data which *Patel et. al. 1985* concluded to arise from the source term $C_{\epsilon 3}$..... which



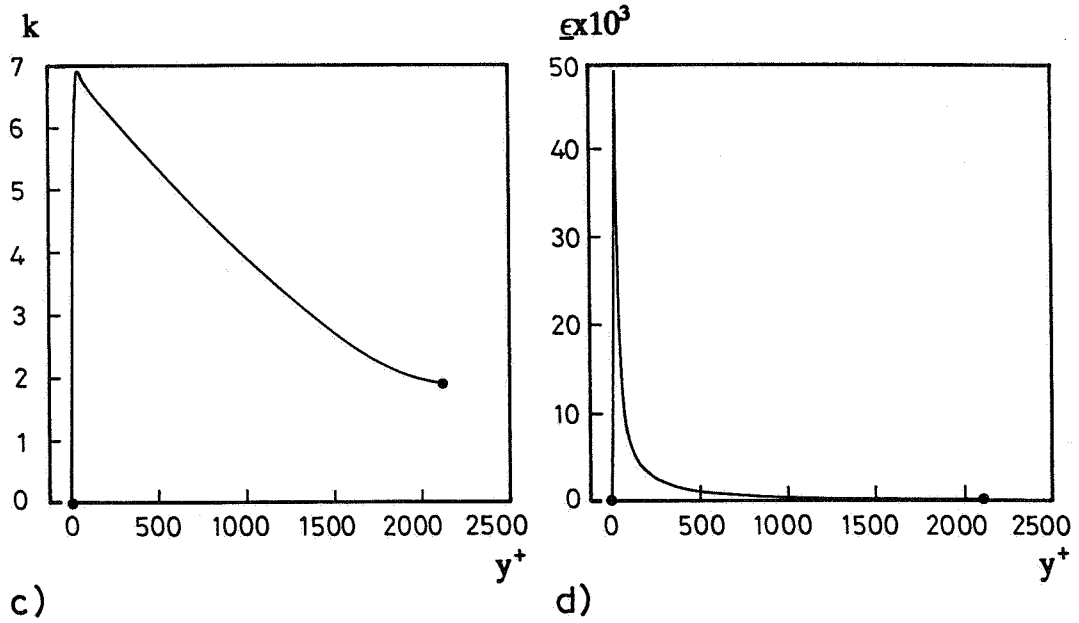


Figure 1. Simulated data from the straight channel flow (line). Experimental data by Laufer 1949 (plus). RSM data by Launder and Tselepedakis 1990 (square). a) U^+ values as a function of y^+, b) shear stress profiles, c) k profiles and d) ε profiles.

increases the dissipation level in the shear layer giving a too low k level.

TRANSIENT CALCULATION IN THE BACKWARD FACING STEP GEOMETRY

In the following paragraph the LRN model is applied in an numerical experiment to see whether it is possible to predict the transient flow over a backward facing step geometry (fig. 2) with a expansion ratio of 1/6 (h/H =1/6) in the Re_{inlet} range of 0-5050.

The interesting thing about this numerical eksperiment is to see if it possible to get a solution in the region 500 < Re < 5000 - which is very important for ventilation engineering. In this region the peak-velocity in the jet and the velocity decay are different from the fully turbulent behaviour and the turbulent viscosity in the recirculation zone is in the same order of magnitude as laminar viscosity. All those

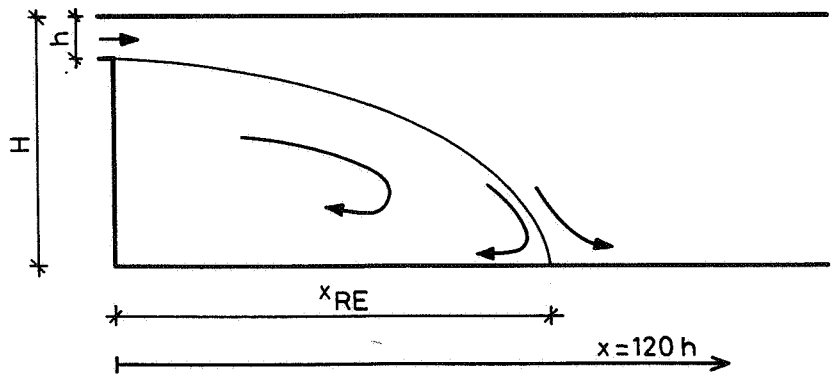


Figure 2. Sketch of backward facing step geometry. h/H = 1/6.

effects are affecting the flow in the whole domain. Another thing which affect the flow is the periodic behaviour which the flow might show. However this is not taken into account in the steady state model.

Numerical approach and boundary conditions

In addition to the numerical procedure already mentioned there are some features which may be important to bear in mind when the results of the numerical experiment are presented.

The scheme is implicit. All calculations are done with the same grid layout which means that the amount of nodes in the sub - and buffer layer is not the same. The grid used for calculation of the inlet boundary conditions (80 in the cross stream direction) is rather coarse.

The boundary conditions are as follows

inlet: u, k, $\underline{\epsilon}$ - calculated profiles by the method mentioned in the previous chapter.
v = 0

wall: $u = v = k = \underline{\epsilon} = 0$

outlet: $v = 0$; $du/dx = dk/dx = d\underline{\epsilon}/dx = 0$.
The outlet is placed 120h downstream were the flow is expected to be uniform.

RESULTS

Fig 3 shows the results from a simulation with Re_{bulk} = 5,050. As seen the inlet conditions for U - velocity is well predicted so the inlet momentum is exactly the same as recorded in the experiments. The $k^{1/2}/U_o$ values are on the other hand much higher than the experimental values. The predicted values are in the interval from 7 to 13% where the measured are from 2 to 6%. This discrepancy - which is significant may be caused by differences in inlet conditions. In present simulation the inlet condition is strictly two dimensional where the experimental setup has a contraction in the third dimension which could damp the turbulent fluctuations. It can also be seen from the values of kinetic energy in the cross section x = 5h that the inlet condition is not important compared to the dominant effect of the shear layer.

If the downstream region is observed it is seen that the mean velocities and the recirculation zone are very well predicted, but again the turbulence level is overpredicted. If f.ex. the cross section x = 30h is observed the measured values are in the range 6 to 11% and the simulated values are in the range of 8 to 15% resulting in a discrepancy of a factor of 2 in the kinetic energy. This significant difference in the turbulence level is unexpected taking the good agreement in the mean velocity into account. Also previuos calculations (*Skovgaard et. al. 1991a*) with the same Re -

number in a very similar but confined enclosure has shown that the *Launder - Sharma* model is able to predict the k - level, but one should bear in mind that the relation u eq. $k^{1/2}$ is very dependent on the turbulent flow type. *Restivo 1991* reported also that the flow was very unstable and had a periodic tendency.

The maximum value of u in a fully developed wall jet is close to $0.22U_x$, where U_x is the peak velocity in the profile at a given distance (*Nelson 1969*). If this assumption is used on the flow in fig. 3 it shows that k is underpredicted at x=10h and 15h while it is over predicted further downstream. All the measurements has a lower level of u compared to the values expected in a fully developed self-similar wall jet.

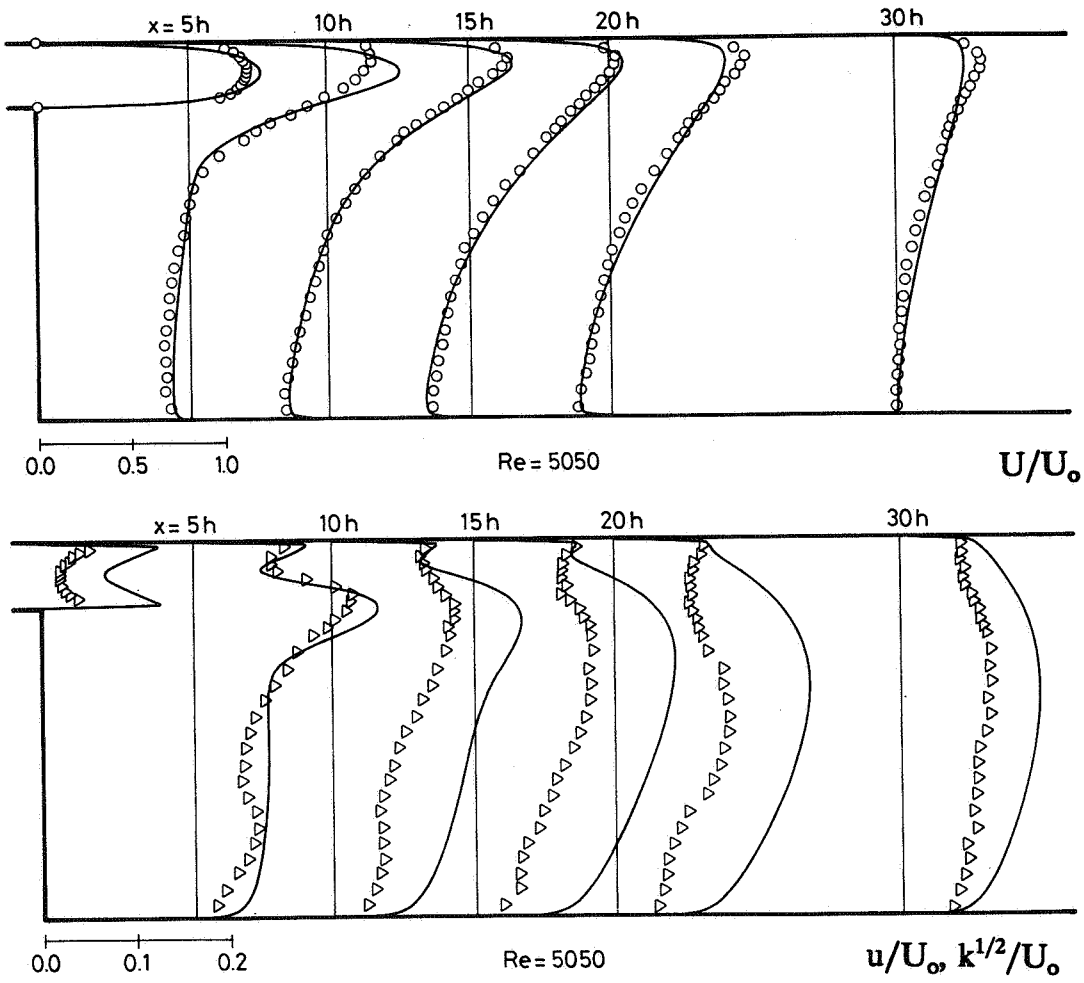


Figure 3 comparisons of present data (line) with experimental values from Restivo (marks). Re = 5,050. a) velocity profiles. b) turbulence intensity.

Figure 4 shows the recirculation length as a function of the Reynolds number. The figure indicates that the mean flow pattern in the backward facing step varies very substantially for different Re numbers. The behaviour has also been reported of several other authors in geometries with other expansion ratios.

The figur shows measured data by *Restivo 1979* compared with simulated results. It is seen that all the numerical models fails to give the same tendency as measured. If we

focus on the LRN results specificly is it seen that there is a region (below Re = 1000) where it is impossible to obtain a converged solution, because the function f_μ is close to zero and the model consequently is equal to the laminar set of equations.

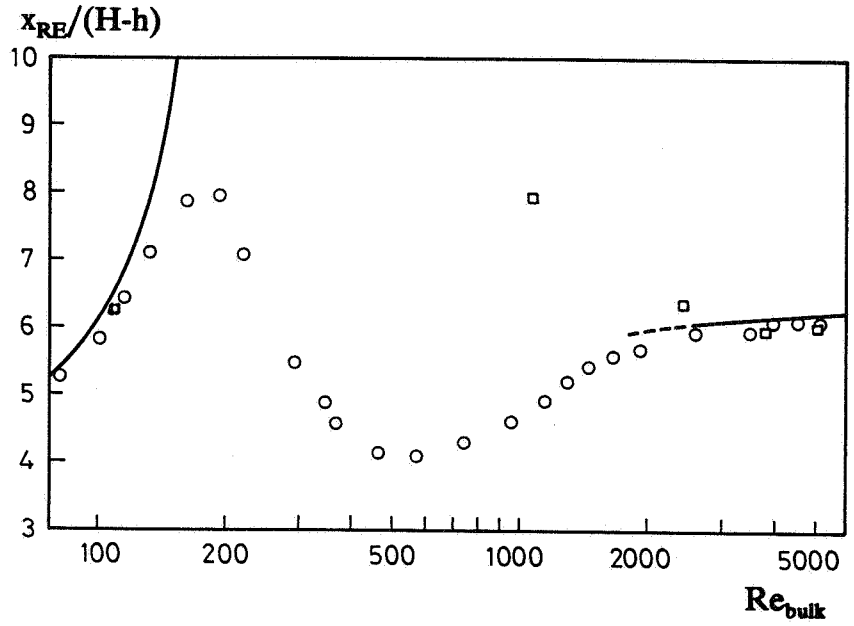


Figure 4. Recirculation length vs. Re number. (o - measured, lines / laminar and fully turbulent simulation by Restivo 1979 and squares - LRN simulation).

DISCUSSION

The performance of the LRN model in channel flow is acceptable if the necessary fine grid, which is at least 10 points in the y^+ range from 5 to 30, is applied. This again means that it can be used to predict flow close to walls or obstacles as for example to calculate heat transfer coefficients and to calculate velocity distribution in a wall jet with low Re numbers etc.

If we look at the backward facing step test we see that there is still a region in the transitional regime where the LRN model, as well as the high Re number version, fails to give converged results. The explanations of this may be many: The recorded timedependent behaviour of the flow in the transistional regime is not taken into account in the simulation which it might be required if we want to calculate transient flow (as already discussed by *Restivo 1979*). The resolution of the grid in the shear layer may have to be higher than used in present simulations where the same grid was used for all Re numbers. The reason may also be that the LRN turbulence phenomena we find in the recirculation zone has a different character than turbulence in the boundary layer, so in order to capture this, the model has to be tuned for these phenomena as well as for the near-wall behaviour of the turbulence parameters.

That LRN phenoma arising from different sources are occuring in ventilated spaces is an established fact. In order to be able to predict these some work has to be done

in the above mentioned areas so a better understanding of the different phenomenas can be obtained.

LIST OF REFERENCES

Chen, Q. Suter, P. and Moser, A.
Influence of Air Diffusion, Energy systems laboratory, series Federal Inst. of Tech. ETH, Zürich, Switzerland, *1990.*

Heiselberg, P. and Nielsen, P.V.
The Contaminant Distribution in a Ventilated Room With Different Air Terminal Devices. RoomVent '87, Sweden, *1987.*

Huang G.P.
The Computation of Elliptic Turbulent Flows with Second Moment Closure Models. Ph.D. - Thesis, UMIST, Manchester, *1986.*

Inze, N.Z. and Launder B.E.
On the computation of buoyancy - driven turbulent flows in rectangular enclosures. UMIST, Manchester, UK, *1989.*

Laufer, J.
Investigations of Turbulent Flow in a Two - Dimensional Channel, NACA report 1053, *1949.*

Launder B.E. and Sharma B.I.
Letters in Heat and Mass transfer. *1978*, 1, 129.

Launder B.E. and Tselepidakis D.P.
Directions in Second - Moment Modelling of Near - Wall Turbulence, UMIST, Manchester, UK. 29 th Aero space Sciences Mecting AIAA 91 - 0219, Nevada, *1990.*

Murakami, S., Tanaka, T. and Kato S.
Numerical Simulation of Air Flow and Gas Diffusion in Room Model - Correspondence Between Simulation and Model Experiments. University of Tokyo *1983.*

Nelson, J.L.
An experimental investigation of the turbulent and mean flow properties of a plane two-dimensional turbulent wall jet. Dissertation, University of Tennesee. Dept. of Chem. Eng. *1969.*

Nielsen, P. V. and Möller Å.T.A.
Measurements on Buoyant Jet Flows From Ceiling Mounted Slot Diffuser. III seminar on Appl. of fluid mechanics in enviromental protection, Silesion Tech. University, Gliwice, Poland, *1988.*

Patel V.C., Rodi W. and Scheurer G.

Turbulent Models for Near - Wall and Low Reynolds Number Flows: A Review AIAA Journal, Vol 23, No. 9, *1985*.

Restivo A.M.O.
Turbulent flow in ventilated rooms, Imp. Coll. of Science and Tech., Mech Eng. Dept. Ph.D. - Thesis, *1979*.

Skovgaard, M., Hyldgård, C.E. and Nielsen, P.V.
High and low Reynolds Number Measurements in a room with an Impinging isothermal Jet, Roomvent '90, Oslo, Norway, *1990*.

Skovgaard, M. and Nielsen, P.V.
Simulation of Simple Test Case, Case 2D1. IEA, Annex 20 report, *1991a*.

Skovgaard, M. and Nielsen, P.V.
Modelling complex inlet geometries in CFD - applied to air flow in ventilated rooms. 12th IAVC Annual conference, Canada, sept. *1991b*.

Tselepidakis D.P.
Private Communications, UMIST, Manchester, UK. *1991*.

AIR MOVEMENT & VENTILATION CONTROL WITHIN BUILDINGS

12th AIVC Conference, Ottawa, Canada
24-27 September, 1991

POSTER 46

MODELLING OF A SUPPLY AIR TERMINAL FOR ROOM AIR FLOW SIMULATION

Jorma Heikkinen

Technical Research Centre of Finland
Laboratory of Heating And Ventilating
Lämpömiehenkuja 3, SF-02150 Espoo, Finland

SYNOPSIS

The paper discusses methods to set boundary conditions at the air supply opening in predictions of room air flows with computational fluid dynamics. The work is a part of the International Energy Agency project "Air Flow Patterns within Buildings", Annex 20.

The air supply terminal in the Annex 20 project is a commercial diffuser which creates a stagnation region and a complicated wall jet below the ceiling.

Fairly well predictions in the wall jet region were obtained replacing the diffuser by a simple opening which has the same momentum flow as in the diffuser. The momentum flow was well known which is not usual for complicated diffusors. In the initial section of the jet, the numerical method causes unintentional and uncontrollable mixing, which resembles the diffusion properties of the actual diffuser. The simple opening case was also measured and the agreement with the diffuser case in the wall jet was found to be satisfactory.

More advanced methods as the momentum method and the prescribed velocity method allow more freedom to modify the jet flow. They should be preferred in practice.

1. INTRODUCTION

Computational fluid dynamics (CFD) is increasingly becoming a practical tool to predict air and contaminant flows in ventilated spaces. A general discussion of the method applied to the room air flows is given in reference [1]. The computational principle is simple: the room is divided into a number of volume cells, say, 20 000 cells, and the balance equations of mass, momentum and heat are solved for those cells. Nevertheless, compromises in practical computations have to be made because of limited computer capacity and incomplete turbulence models. Therefore it is important to compare the effects of different simplifying assumptions with full scale measurements. This kind of work has been done in an international project, IEA Annex 20. This paper is a part of that project and it compares different simplified ways to set boundary conditions for a commercial air diffuser.

The small details of a supply air terminal have an obvious influence on the air flow field in the mixing type of ventilation. These details cannot however be handled in most practical air flow simulations and therefore simplifying assumptions are needed. Different methods to model complicated air terminal devices are described by Nielsen [2]. In this paper various methods are used and compared with measurements.

2. TEST CASE

The test room in the IEA Annex 20 project is a small empty office room shown in figure 1. The air supply terminal is located 0.2 m below the ceiling. It consists of 84 ball nozzles which are all directed 40 degrees upwards, see figure 2. A detailed description of the test room and the diffuser is given in references [3] and [4].

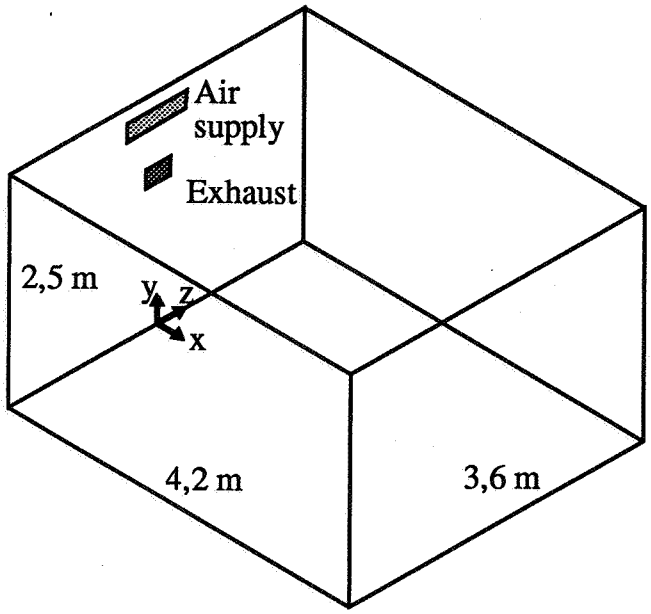


Figure 1. The test room.

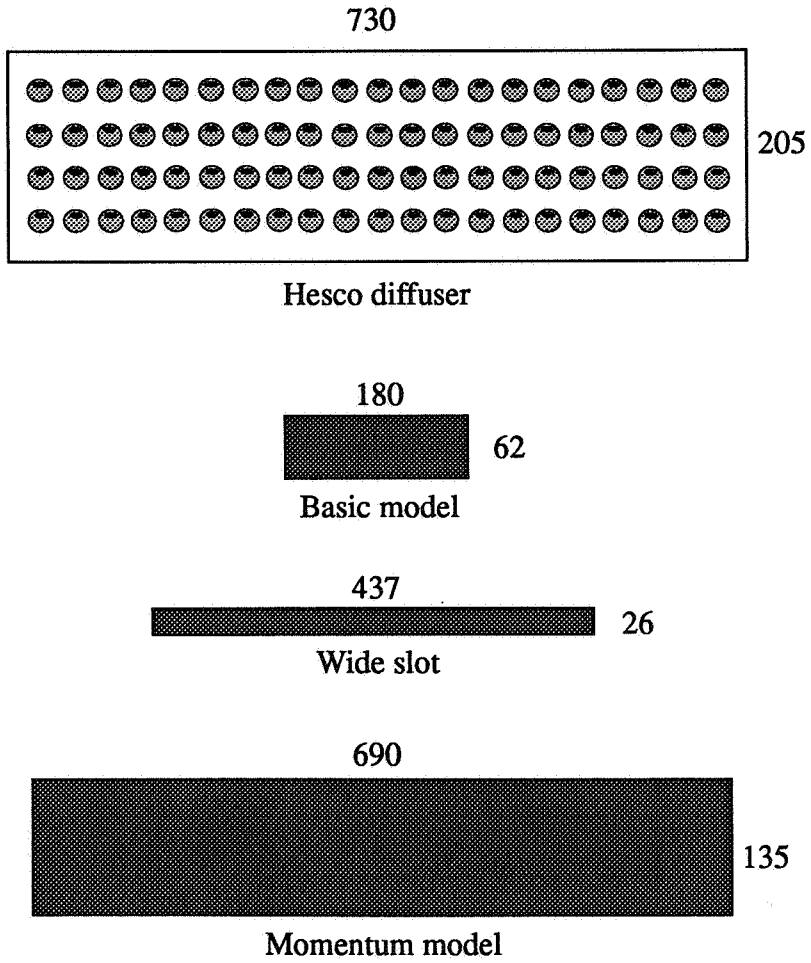


Figure 2. The 84-nozzle supply air diffuser and the methods to replace it by a simple opening. Dimensions are in millimetres.

The air change rate is 3 air changes per hour, which means an air flow 0.0315 m^3/s. Only isothermal flow in discussed in this paper. It is believed that the results can be useful also in non-isothermal simulations if buoyancy effects are small in the early stages of the jet development.

The observed flow field near the diffuser can be seen in figure 3. The velocity in the nozzles is about 3.7 m/s and it decreases quickly when the 84 small jets combine into a single jet. A maximum velocity of 1.5 m/s was measured in the combined jet at a distance of 0.1 m from the wall. The combined jet impinges on the ceiling where the upward momentum force of the jet is balanced by a pressure increase in the stagnation region. From the stagnation region the jet spreads below the ceiling to all directions, also to the left upper corner where a recirculating zone exists.

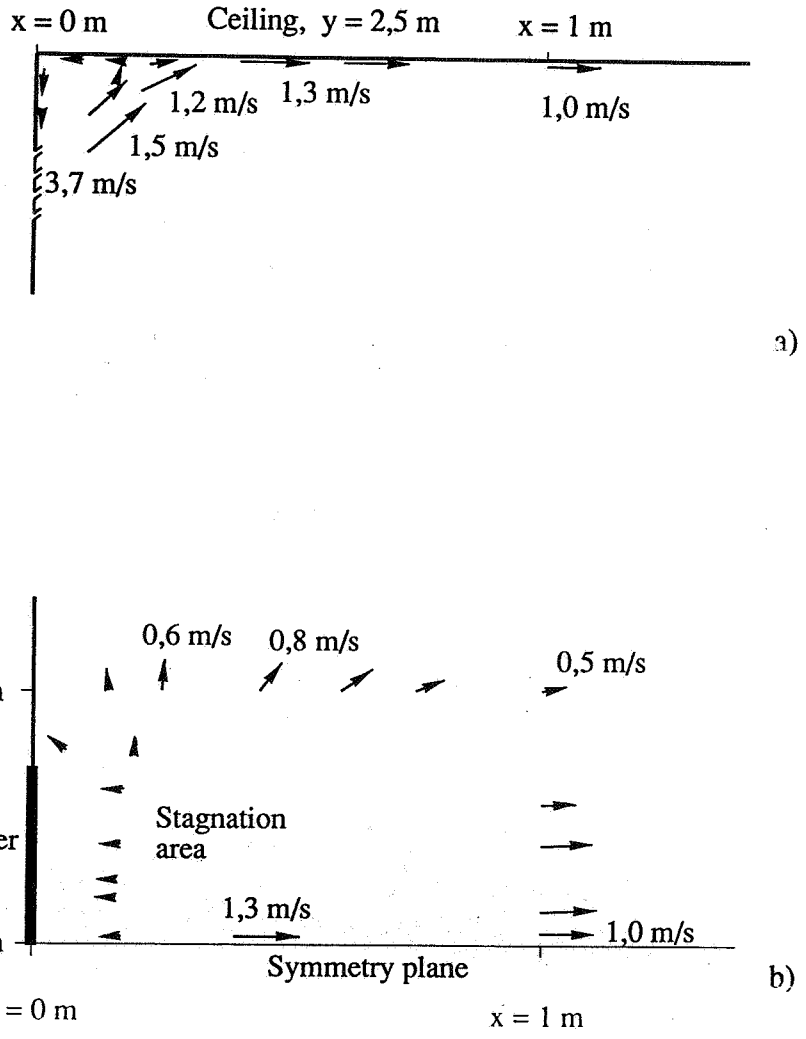


Figure 3. The observed flow field near the diffuser, at the symmetry plane (a), and just below the ceiling (b). Note that only half of the symmetrical room is shown in the figure b.

Air speeds were recorded in 560 locations in the room according to IEA Annex 20 specifications [3]. Velocity profiles in the jet were also measured and these results are mainly used in this report. Detailed measurement results of the same test case have been published already by Skovgaard et al. in reference [5].

Additional measurements were also performed for a case where the diffuser was replaced by a rectangular opening which has the same effective area as the diffuser. This corresponds to the basic model for the supply air terminal discussed in this paper.

The accurate computation of the complete flow field near the diffuser and also near the stagnation area is difficult because a fine grid is needed and standard turbulence models such as the as k-ε model are not perhaps valid. But fortunately the momentum flow of the diffuser is fairly well known and will make the task easier than in most other practical cases. A discussion of the momentum flow is given in appendix 1 after the main text.

3. SIMULATION METHOD

The main features of the simulations are the finite volume method [6], a staggered grid for the velocity components [6], the high Reynolds number k-ε turbulence model and logarithmic wall functions [7]. Fluent code [8] and Wish code [9] have been used. In Fluent, two differencing schemes can be used, namely the "power-law differencing scheme" (PLDS) recommended in reference [6] and the "quadratic upstream interpolation for convective kinematics", which is less prone to false diffusion [10]. Wish code has been used because it enables us to prescribe variables in the flow field and it constitutes an open code for modifications. The present version of the Wish code uses only an upwind differencing scheme, which is comparable with the power-law scheme.

Computations have been carried out on only half of the room because the room is symmetrical. The number of volume cells varied from 6 300 to 22 800 in different simulations. To be able to use wall functions and the high Reynolds number turbulence model, the distance from the first grid point to the wall should be selected properly. Near the ceiling the distance varied between 9 and 25 mm when using different grids.

4. MODELS FOR THE SUPPLY AIR TERMINAL

4.1 Basic model

It is possible to replace the complicated diffuser with a simple opening which has the same effective area as the small nozzles together. One has only to decide the shape of the opening and its location. IEA Annex 20 has agreed to use an opening which has the same aspect ratio as the real diffuser and is located in the middle of the diffuser, see figure 2. The supply air opening width and height are 180 mm and 62 mm respectively and the centre of the opening is 285 mm from the ceiling [11]. The supply velocity is 3.68 m/s and it is directed upwards at an angle of 40°. The turbulence kinetic energy is 0.204 m^2/s^2 and its dissipation 6.65 m^2/s^3. Turbulence energy corresponds to a 10 % turbulence intensity and the dissipation corresponds to developed channel flow. This is called a basic model.

The basic model case was also measured by replacing the diffuser by a rectangular duct which was 2 m long and aligned 40° upwards. The velocity profile at the opening thus

corresponds to a developed channel flow. The dimensions of the opening were increased by 4 mm to get the same maximum velocity at the opening as in the nozzles. The measured maximum velocity in the middle of the opening was 4.0 m/s, which corresponds to the maximum velocity found in the nozzles in the middle of the diffuser [16].

4.2 Wide slot

Making the simple opening wider is believed to result in more mixing in the early stages of jet development because the perimeter of the jet is greater than in the basic model and corresponds more closely to reality. A width of 437 mm and a height of 26 mm were selected, see figure 2. The area and the turbulence quantities are the same as in the basic model.

4.3 Momentum model

The area of a simple opening can be freely selected by using a so called momentum model which has been used earlier by Chen et al. [12] in the Phoenics program. This makes it possible to set separate boundary conditions for the continuity equation and the momentum equations. Unfortunately in the Fluent program (version 2.99) and in the Wish program the given inlet velocity determines the boundary source terms for all equations. Therefore the Wish program was modified to allow free setting of boundary source terms. The width of the opening was selected to be 690 mm and the height 135 mm, which is the area occupied by the nozzles. The inlet momentum and the turbulence quantities are the same as in the basic model.

4.4 Box model

This is a model where the boundary conditions are given at the surface of an imaginary box around the diffuser. The box was selected to be 0.4 m high, 1 m long and 1 m wide. The air speeds on all four surfaces of the box were measured with TSI 1640 omnidirectional hot film anemometer. In addition to speed measurements, flow directions also had to be detected using smoke. The anemometer was not suitable for measuring turbulence; consequently turbulence values applicable to a two-dimensional wall jet [13] were given. An example of the measured profiles is shown in figure 4.

4.5 Prescribed velocity method

In this model boundary conditions are given at a simple opening and also in the flow field as in the box model. The idea is to minimize the necessary measurements by giving only the most important variables in the most important locations in the jet and to compute the rest. In this case only the x-direction velocity was specified in a small plane at a distance of 1 m from the supply terminal. The width of the plane was 0.6 m (0.3 m on both sides of the symmetry plane) and the height was 0.13 m where the velocity is about 35 % of the maximum value, see figure 4. The present version of the method means a simplification of the method described in the reference [2], where two velocity components are given on two perpendicular planes. The idea here is to test if the flow field produced by the basic model can be easily revised.

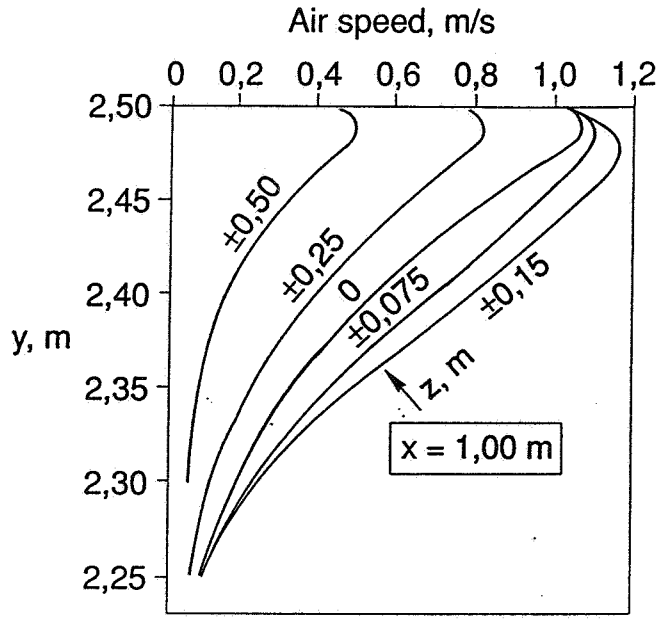


Figure 4. The air speed profiles measured at a distance of 1 m from the diffuser. These have been used in the box model and in the prescribed velocity model.

5.0 RESULTS

The supply air terminal has the most direct influence on the decay of jet velocity and also on the shape of the jet. These should be predicted correctly to be able to predict also nonisothermal cases. The discussion in this paper deals mainly with those properties. A short discussion of the maximum velocity in the occupied zone in different cases is given below before proceeding to a detailed analysis.

5.1 Maximum velocity in the occupied zone

The most interesting property for thermal comfort is the maximum velocity, which is shown in table 1 for various simulations and also for the measurements. The occupied zone has here been defined such that the volume above 1.8 m the floor and the volume closer than 0.6 m to the walls has been excluded.

From a practical viewpoint the simulated maximum velocities are fairly close to each other and also close to the measured velocities. When looking at different models for the supply air terminal it can be concluded that it is not only the diffuser model which has an effect on maximum velocity but also the number of grid points, the differencing scheme, and even the code that has been used has an effect. It is obvious that most results are not grid-independent. It will be shown later that in the early stages of the jet development numerical diffusion plays an important role.

Table 1. Maximum velocity in the occupied zone and its location in different measurements and simulations.

Case	*Velocity m/s*	*x m*	*y m*	*z m*
Measured, diffuser case	*0.19*	*3.0*	*0.03*	*0*
Measured, basic model (simple opening)	*0.20*	*2.2*	*0.05*	*0*
Basic, Fluent code, power-law scheme, 6300 points	*0.22*	*2.5*	*0.05*	*0.2*
Basic, Fluent code, QUICK scheme, 6300 points	*0.27*	*2.5*	*0.05*	*0.3*
Basic, Fluent code, power-law scheme, 22800 points	*0.23*	*2.4*	*0.16*	*0*
Basic, Fluent code, QUICK scheme, 22800 points	*0.24*	*2.6*	*0.03*	*0.6*
Basic, Wish code, 6300 points	*0.19*	*2.8*	*0.05*	*1.2*
Wide slot, Fluent code, QUICK scheme, 22800 points	*0.24*	*2.6*	*0.03*	*0.6*
Momentum model, Wish code, 8580 points	*0.16*	*2.8*	*0.05*	*1.2*
Prescribed velocity model, Wish code, 6300 points	*0.22*	*2.8*	*0.05*	*1.2*

5.2 Basic model

Computed flow field near the diffuser in figure 5 looks similar to the one observed, figure 3. There are however some differences. Near the ceiling the flow field corresponds fairly well to the observed field except near the stagnation area, which is much smaller in the z-direction in the computations because of the much narrower air inlet opening (fig. 5 b). Near the inlet (fig. 5 a), the computed jet seems to spread more in the vertical and horizontal directions than does the measured jet. One reason for this phenomenon is the staggered grid, which sets the inlet sources of x and y momentum in different locations. The other is numerical diffusion, which can be considerable because the velocity vectors are not aligned with the grid lines. Because of jet spreading, the recirculation in the left upper corner is smaller than in real conditions.

The spreading of the jet near the diffuser would be smaller if a finer computing grid could be used. Here the grid consists of 38x40x15 = 22 800 cells, which is the finest grid used because the computing time was already too long: about 4 hours on a Cray X-MP computer. The QUICK differencing scheme was used, which took twice as much computing time the power-law scheme does but reduces numerical diffusion. This can be seen in figure 6, where the decay of the jet is shown in simulations with various differencing schemes and different grids. It may be concluded that a very fine grid is needed to achieve grid-independent results, especially near the diffuser. Excessively low maximum velocity predictions were also observed in the reference [14] just beyond the supply opening owing to limited number of grid points. In the wall jet region it seems like the grid has an influence on the velocity decay. Perhaps the first grid point below the ceiling is too close to the surface (13 mm) in the fine grid and causes too high friction.

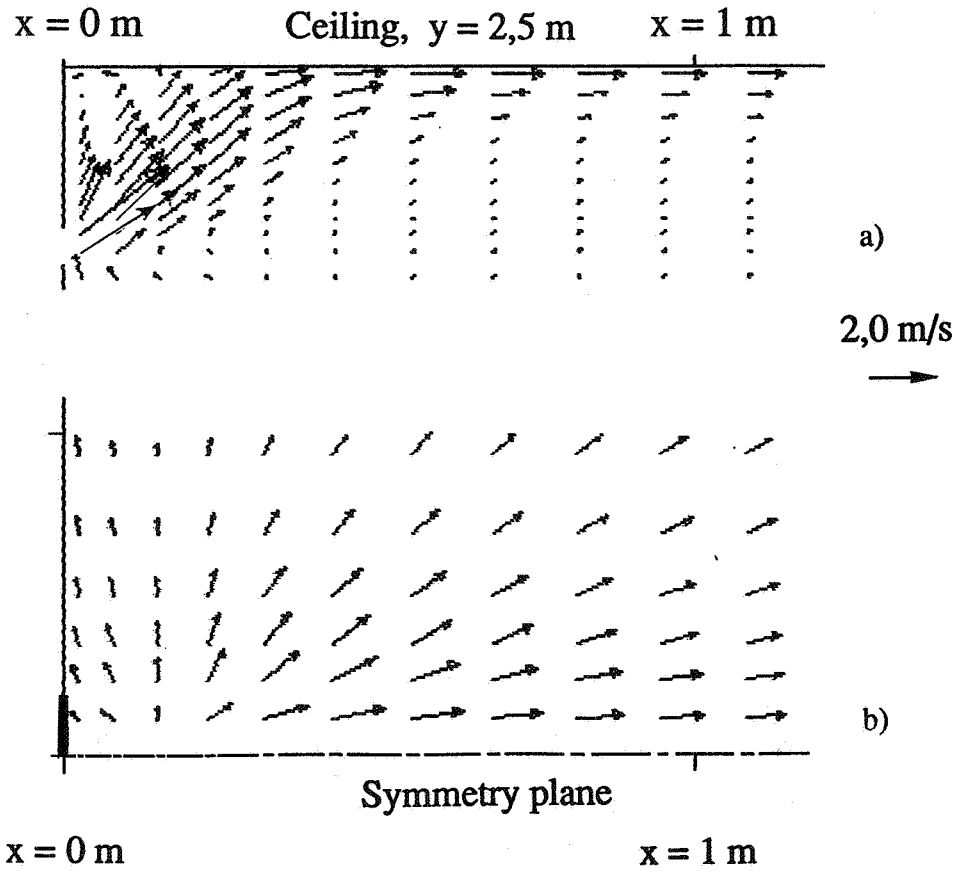


Figure 5. The flow field near the diffuser using the basic model. The symmetry plane (a) and a plane 13 mm below the ceiling (b) are shown.

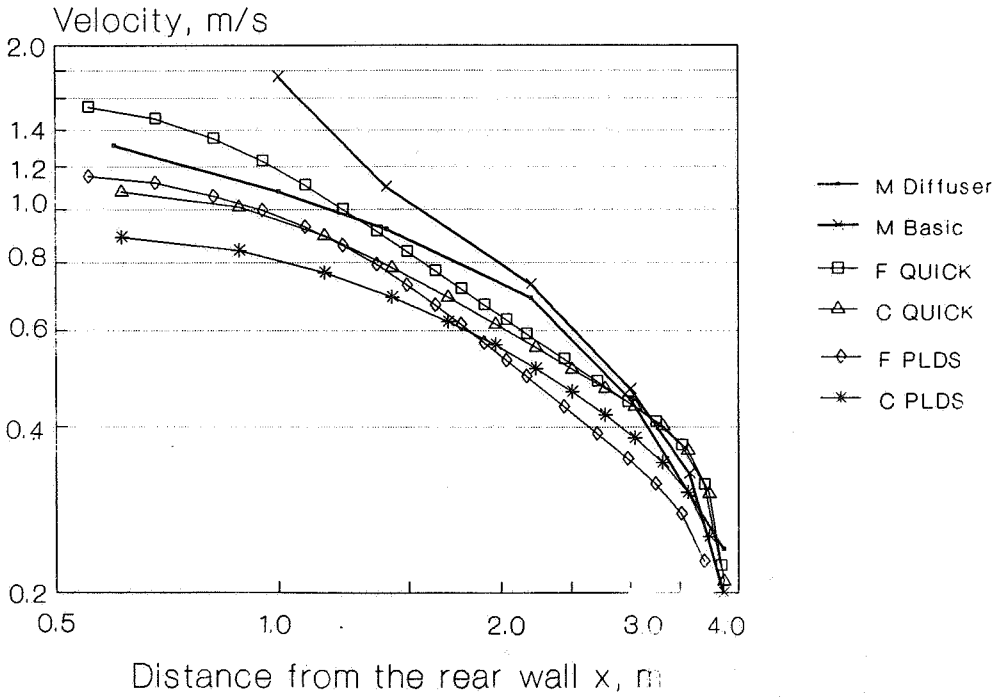


Figure 6. Measured and simulated velocity decay in the symmetry plane using the basic model. In the legend "M" refers to the measurements, "F" to the computations using the fine grid an "C" to the computations using the coarse grid.

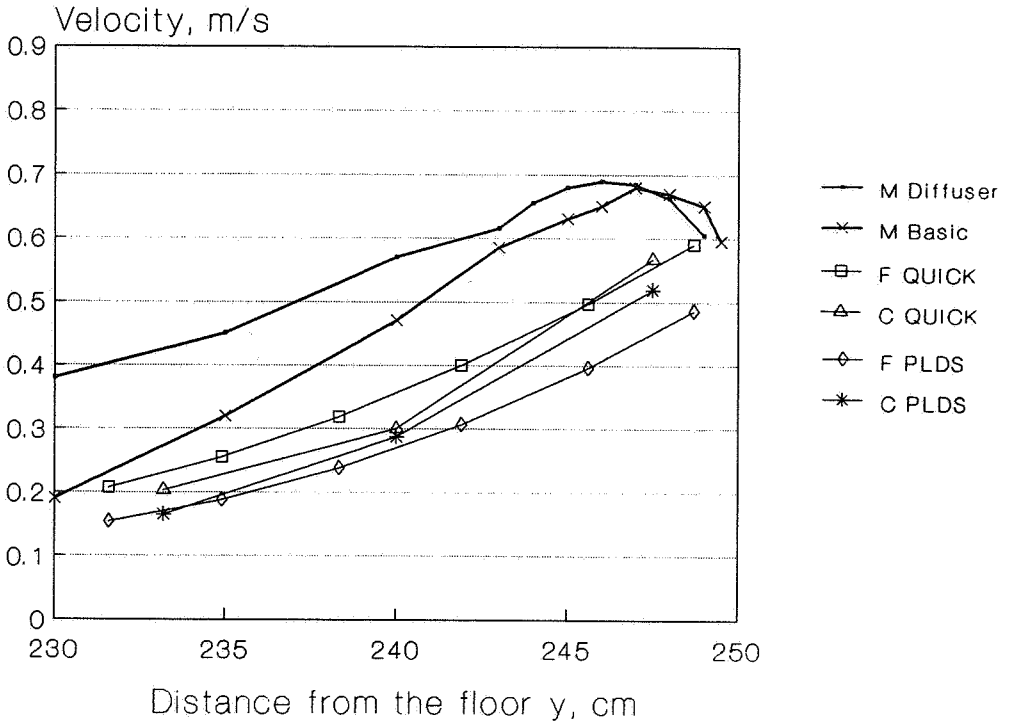


Figure 7. Measured and simulated velocity profiles in the vertical direction at 2.2 m from the diffuser in the symmetry plane using the basic model. In the legend "M" refers to the measurements, "F" to the computations using the fine grid and "C" to the computations using the coarse grid.

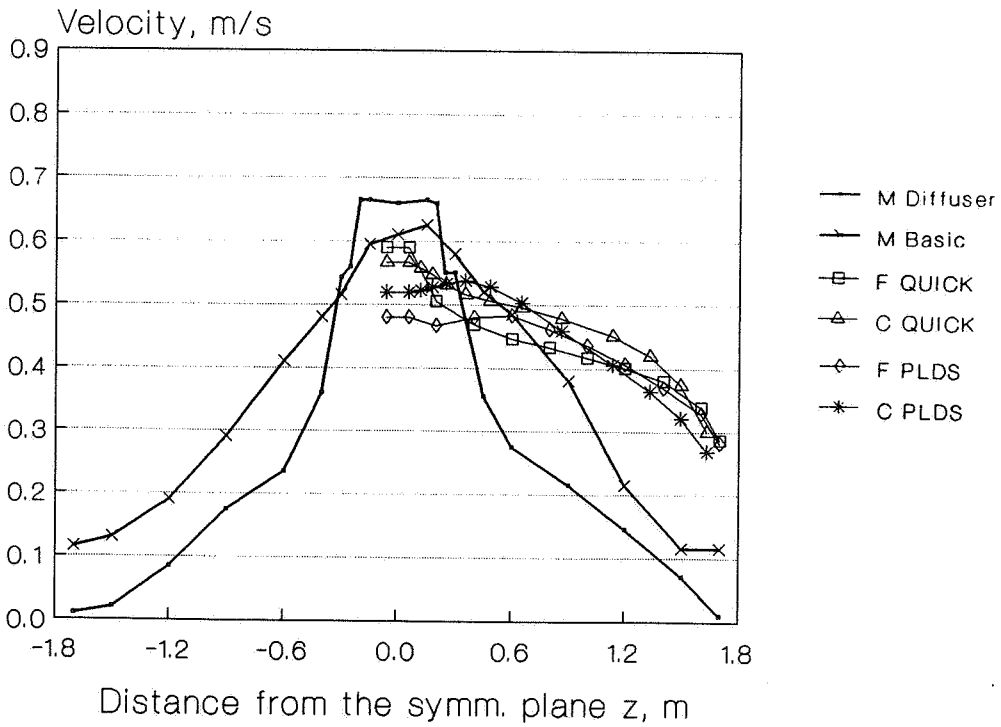


Figure 8. Measured and simulated velocity profiles in the horizontal direction at 2.2 m from the diffuser and near the ceiling using the basic model. In the legend "M" refers to the measurements, "F" to the computations using the fine grid and "C" to the computations using the coarse grid.

The velocity profiles in the wall jet near the ceiling at 2.2 m from the diffuser can be seen in figures 7 and 8 in the vertical and horizontal directions respectively. In the vertical direction the thickness of the wall jet is smaller in the computations than in the measurements. Note that the velocity maximum in the y-direction could not be predicted. In the horizontal direction the computed jet spreads more than the measured jet.

Figures from 6 to 8 also present the measured results for the basic case. The velocity is higher in the early part of the jet than in the diffuser jet. The differences become quite small during the wall jet development. This shows that from a physical viewpoint the basic model is fairly good. Apparently smaller mixing near the opening will be compensated by mixing in the wall jet region. The jet from a simple opening spreads more in the horizontal direction than the diffuser jet resembling the simulations.

5.3 Wide slot

The simulations were performed using the QUICK scheme and nearly the same fine grid as in the basic model. The decay of the jet is shown in figure 9 for various models. Using the wide slot model, at small distances mixing is increased compared with the basic model, as expected. The mixing seems to be even higher than it is in the real conditions. The decay of the jet is very slow because the jet is thick at its start near the stagnation area and therefore the characteristic decay for an axisymmetric or radial jet starts very late, at x-distances greater than 3 m.

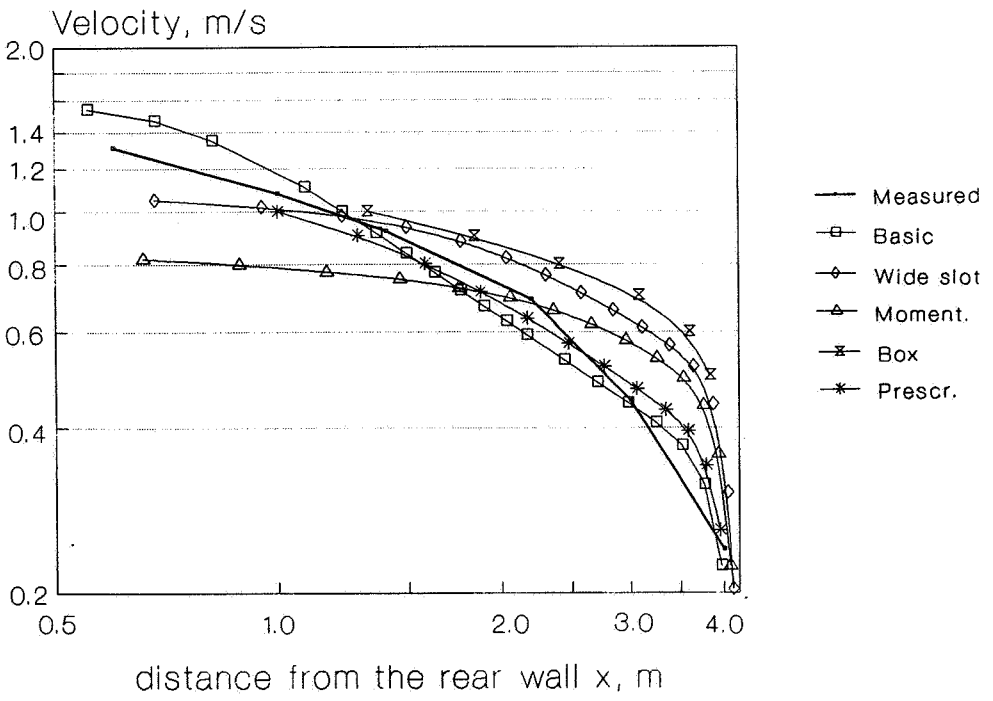


Figure 9. Measured and simulated velocity decay in the symmetry plane using various models for the supply air terminal.

Velocity profiles in the vertical direction (fig. 10) and in the horizontal direction (fig. 11) are fairly well predicted at a distance of 2.2 m from the diffuser.

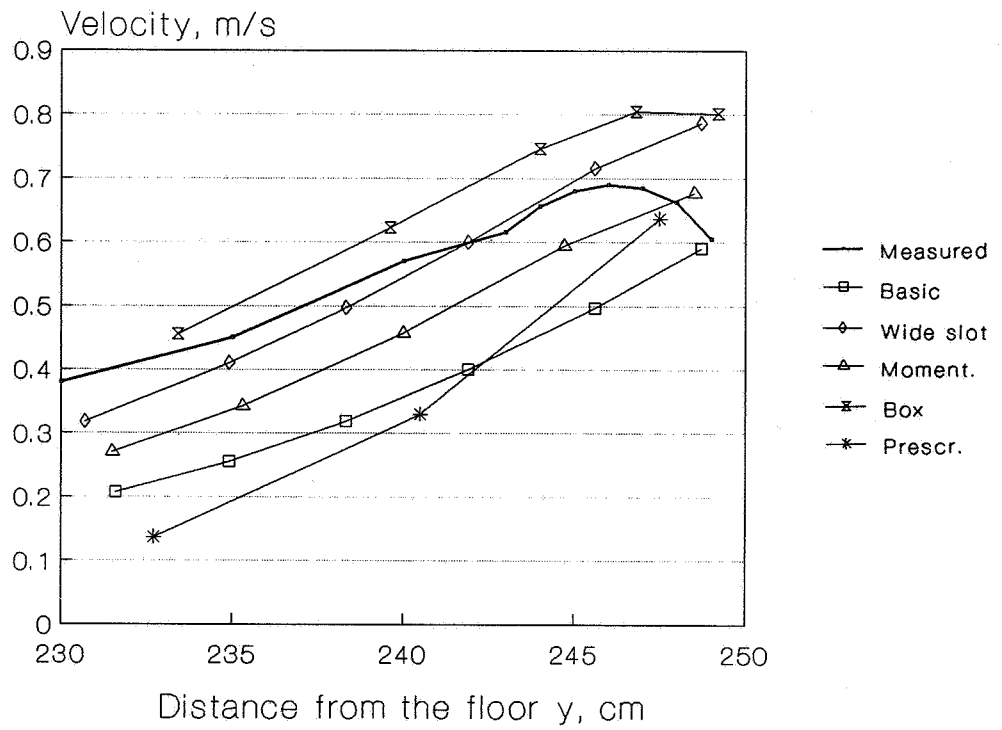


Figure 10. Measured and simulated velocity profile in the vertical direction at 2.2 m from the diffuser in the symmetry plane.

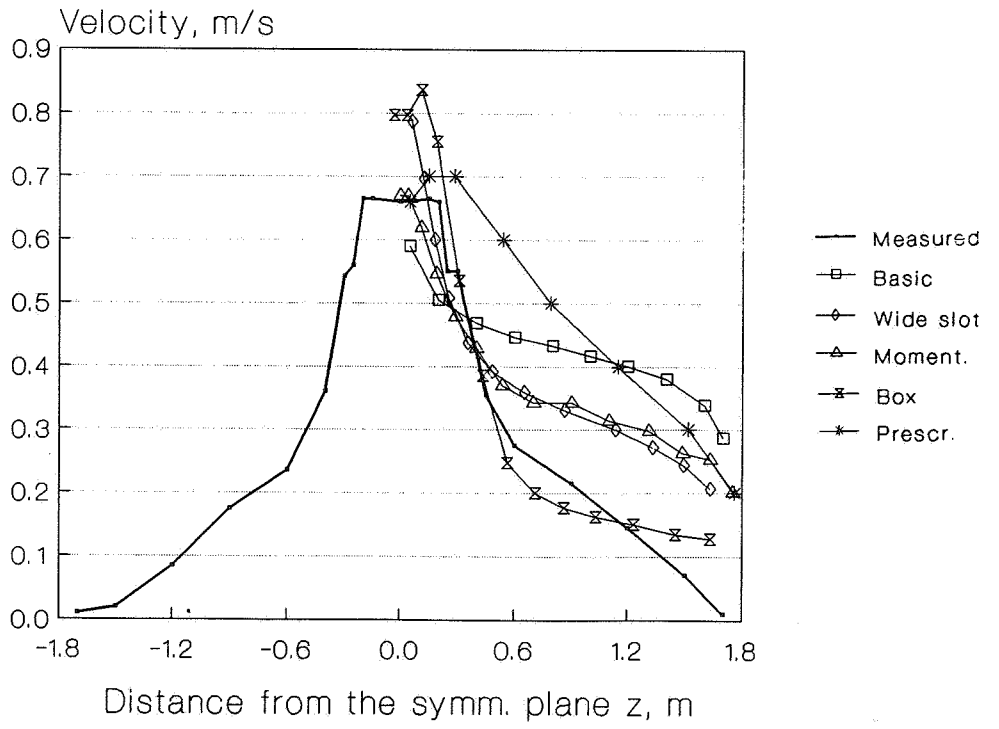


Figure 11. Measured and simulated velocity profiles in the horizontal direction at 2.2 m from the diffuser near the ceiling.

5.4 Momentum model

Velocity decay (fig. 9) is very similar to the wide slot model but there is even more mixing in the early stages of jet development. The jet is thick in the vertical direction already after the stagnation area and the thickness (defined as a distance from the ceiling where velocity reaches half the maximum) remains nearly constant in the wall jet. Velocity profiles at an x-distance of 2.2 m are also similar to the wide slot model but the maximum velocity is somewhat lower.

It seems that mixing should be reduced near the opening. This could be achieved using a smaller diffuser area in the simulation.

Part of the momentum flow of the supply air stream is lost because underpressure is formed in the area between the small nozzles. This phenomenon is well known for perforated plates as a diffuser, see the reference [15]. The underpressure was measured to be around 0.18 Pa which means about a 14 % loss of jet momentum (see appendix 1 for details) and thereby about 7 % decrease in the velocities in the room. The predicted underpressure was only slightly lower; a 10 % loss of momentum was predicted. Apparently the predicted momentum loss will depend on the grid spacing near the diffuser. In this case the length of the first volume cell in x-direction was 57 mm, which corresponds roughly to the length of the mixing zone of the small jets.

5.5 Box model

Velocity decay is again slow, corresponding to the decay of a two-dimensional wall jet. This may be due to erroneous velocity directions given as a boundary condition. Perhaps the detections of velocity directions using smoke was inaccurate. It is inconvenient to use the box model especially if the temperature or concentration profiles also have to be given as boundary conditions as explained in the reference [2]. That is why the prescribed velocity model is favoured over the box model.

5.6 Prescribed velocity model

Velocity decay is close to the measured decay. The profile in the vertical and horizontal directions is not very good: the jet does not spread enough in the vertical direction and spreads too much in the horizontal direction. A peak in the velocity profile on both sides of the symmetry plane can be clearly seen. This is partly due to the prescribed velocity profile, which has a minimum in the symmetry plane.

The way in which the method adapts the velocity field near the ceiling can be seen by comparing figure 12, where the velocity field using the basic model can be seen, and figure 13 where the velocity has been additionally prescribed. It can be clearly seen, how the method gives a kick in the x-direction at a distance of 1 m from the left wall.

The prescribed velocity method seems to be the most promising one to be used in practice when the momentum of the jet is not well known. It requires minimum amount of measured information; in this case only one velocity component was prescribed at 8 computing points. Perhaps the best combination would be to use the momentum method and the prescribed velocity method together.

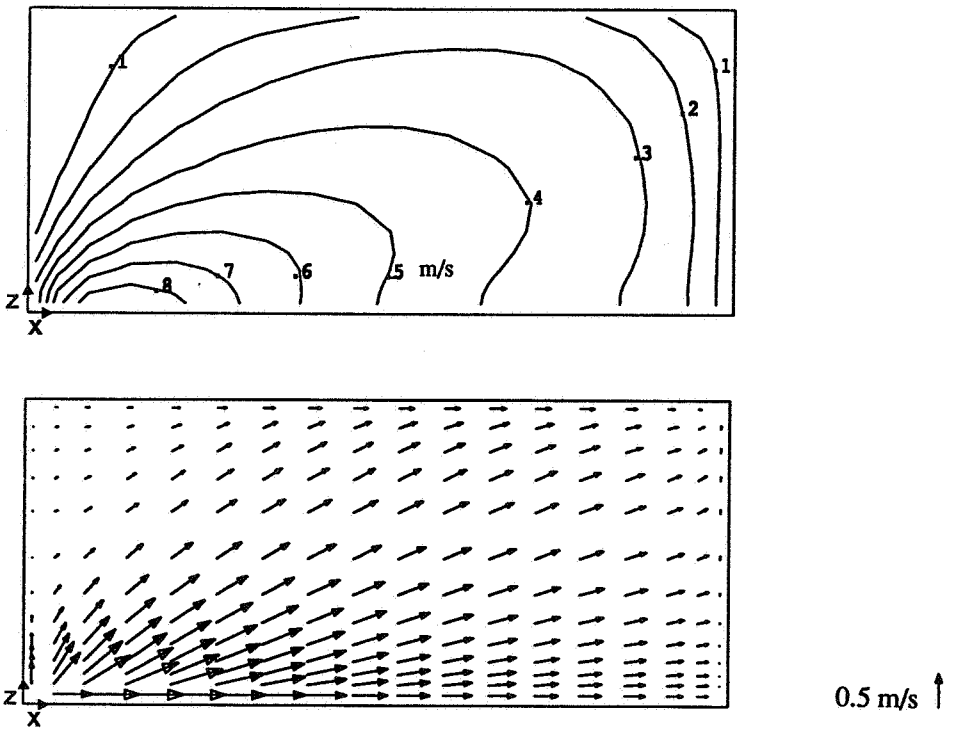


Figure 12. Velocity vectors and air speed contours using the basic model and the Wish code. Plane 25 mm below the ceiling.

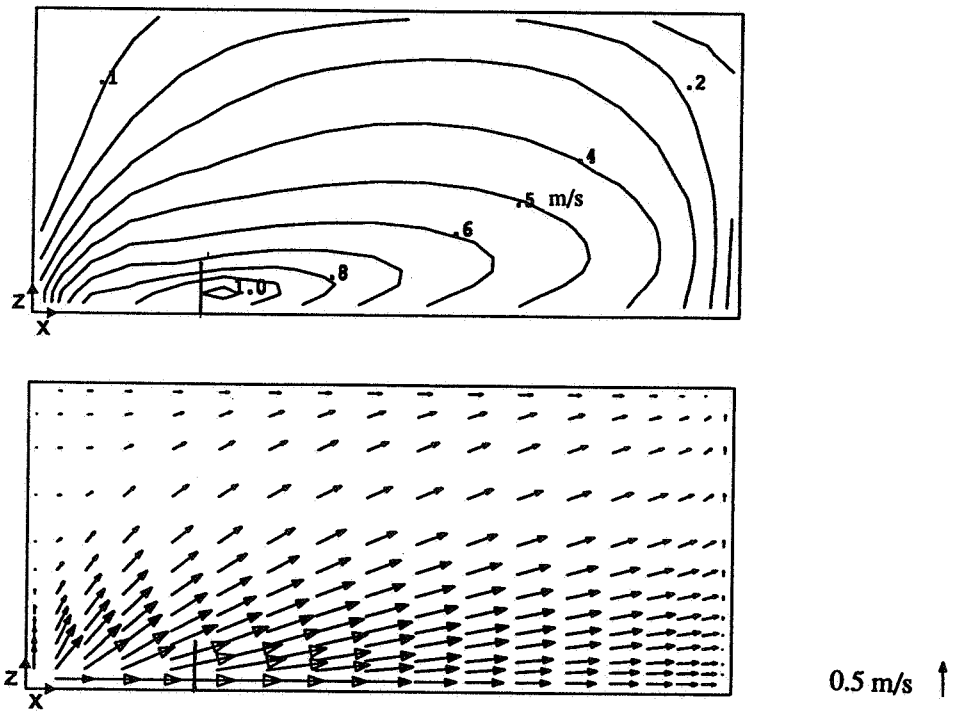


Figure 13. Velocity vectors and air speed contours using the prescribed velocity model and the Wish code. Plane 25 mm below the ceiling. The plane at x = 1 m is shown where the x-direction velocity is prescribed.

CONCLUSIONS

The jet flow including the oblique impingement on the ceiling is a complicated flow to be measured and computed.

The most important property of the supply air opening in the mixing type of ventilation is the momentum flow of the jet. In this particular case the momentum flow was fairly well known and therefore predictions of the decay of the isothermal wall jet was satisfactory with all methods. The wall jet spreads usually too little in the vertical direction and too much in the horizontal direction. The prediction of the maximum velocity in the occupied zone was satisfactory.

Modelling the diffuser by means of a simple opening seems to be a fairly good approximation according also to the measurements if the initial stage of the jet is excluded. In simulations the size of the opening has to be small compared with the room dimensions and this increases the number of grid points and the computing cost.

The numerical method causes mixing in the initial section of the jet, especially in the region where the jet flows diagonally from the inlet towards the ceiling. This unintentional diffusion resembles the diffusion properties of the real diffuser and helps to make better predictions. The problem with the unintentional diffusion is that it depends on the numerical grid and the numerical method, and is therefore not easy to control. Because of this mixing, it may in fact be more difficult to predict a flow from a simple opening where mixing is low to be predicted. This shows that the details of the supply air terminal cannot be described together with room air flow computation. New computational methods such as local grid refinement could be a solution to this problem.

The momentum method for the supply air terminal makes it possible to select the size of the simple opening and can be regarded as a generalization of the simple opening model. In this particular example there was too much mixing in the initial section of the jet. The momentum loss due to underpressure was well predicted in this particular case. It is my opinion that the momentum method is a method that could be used more generally. The method should be studied more systematically.

The prescribed velocity method has the possibility to make the best predictions, perhaps in combination with the momentum method.

MOMENTUM OF THE SUPPLY AIR STREAM

Appendix 1

Momentum flow or momentum force of the supply air stream is

$$F = \int \rho U^2 \, dA \qquad (1)$$

where

F is the momentum flow (N)
U is the velocity at the nozzle exit in the direction of flow (m/s)
ρ is air density 1.2 kg/m^3.

Integration is performed over the supply air perpendicularly to the flow. Thus we should measure the velocity profiles at the opening, or at least in one nozzle, to get the momentum flow. An approximation can be however found making use of the known mass flow

$$q_m = \int \rho U \, dA = \rho U_m A_m = 0.0378 \text{ kg/s} \qquad (2)$$

where

A_m is the area of the all 84 nozzles = 0.0092 m^2 (diameter 11.8 mm)
U_m is the mean velocity = 3.42 m/s.

We can define the effective velocity U_{eff} in such a way that following equation holds

$$F = U_{eff} \int \rho U \, dA \qquad (3)$$

The lower approximation for the momentum flow will be obtained assuming constant velocity in the opening, which means that the effective velocity is same as the mean velocity. The upper approximation for the momentum, representing the plug flow, will be found using the maximum velocity as an effective velocity. The mean value of maximum velocities in the nozzles was found to be 3.68 m/s in reference [5] (corresponding to an area 0.00855 m^2) and lately about 3.85 m/s, which is perhaps more accurate, in reference [16]. The effective velocity 3.68 m/s has been used in the simulations.

Momentum force in the free jet after the combination of small jets is smaller because pressure on the diffuser surface is lower than the ambient pressure. The pressure difference was measured by pressing a crown-formed small tube against the diffuser surface. Its mean value was about 0.18 Pa which means a loss of about 0,028 N in x-direction momentum and about 14 % loss of total momentum. If we take the momentum loss into account and use the maximum velocity 3.85 m/s, the effective velocity should be about 3.3 m/s. The direction of the supply velocity vector also changes from 40° to 48°. This is supported by visual observations.

REFERENCES

1. NIELSEN, P.V.
"Airflow Simulation Techniques - Progress and Trends"
10th AIVC Conference, Espoo, 1989.

2. NIELSEN, P.V
"Representation of Boundary Conditions At Supply Openings"
IEA Annex 20, Internal Report, University of Aalborg,
ISSN 0902-7513 R8902, 1989.

3. LEMAIRE, A.D.
"Testrooms, Identical testrooms"
IEA Annex 20 Internal Report, TNO - Institute of Applied Physics, 1989.

4. NIELSEN. P.V.
"Selection of air terminal device"
IEA Annex 20 Internal Report", University of Aalborg,
ISSN 0902-7513 R8838, 1988.

5. SKOVGAARD, M., HYLDGAARD, C.E., and NIELSEN, P.V
"High and Low Reynolds Number Measurements in a Room with an Impinging Isothermal Jet"
ROOMVENT'90, International Conference on Engineering Aero- and Thermodynamics of Ventilated Rooms, Oslo, 1990.

6. PATANKAR, S.V.
"Numerical Heat Transfer and Fluid Flow."
McGraw-Hill, New York, 1980.

7. LAUNDER, B.E and SPALDING, D.B.
"The numerical computation of turbulent flows."
Computer methods in mechanics and engineering, 3, p. 269 -289, 1974.

8. CREARE INC.
"Fluent, a general purpose computer program for modeling fluid flow, heat transfer and combustion."
Hanover NH, seminar notes, 1987.

9. LEMAIRE, A.D.
"User manual WISH."
TNO - Institute of Applied Physics, Delft, 1989.

10. HUANG, P.G, LAUNDER, B.E and LESCHZINER M.A.
"Discretization of nonlinear convection processes: a broad range comparison of four schemes."
Computer methods in applied mechanics and engineering 48 (1985), North Holland, p. 1 - 24, 1985

11. SKOVGAARD, M. and LEMAIRE, A.D.
"Representation of boundary conditions at supply opening".
Technical note on Research Item no. 1.11, IEA Annex 20 Internal Report, 1990.

12. CHEN, Q., MOSER, A., and SUTER P.,
"Indoor Air Quality and Thermal Comfort under Six Kinds of Air Diffusion."
To appear in ASHRAE Transactions, Vol. 97, part 2, 1991.

13. LAUNDER, B.E and RODI, W.
"The turbulent wall jet"
Prog. Aerospace Sci., vol. 19, pp. 81 - 128, 1981.

14. MURAKAMI, S., KATO, S. and NAKAGAVA,H.
"Numerical Prediction of Horizontal Nonisothermal 3-D Jet in Room Based on k-ε Model."
To appear in ASHRAE Transactions, Vol. 97, part 1, 1991.

15. GRIMTLIN, M.
"Zuluftvertailung in Räumen."
Luft- und Kältetechnik 1970, Nr.5, pp. 247 - 257.

16. EWERT, M. and ZELLER, M.
"Turbulence Parameters at Supply Opening (measurements)"
IEA Annex 20, Internal Report, Rheinisch-Westfälischen Technischen Hochshule, Aachen, 1991.

AIR MOVEMENT & VENTILATION CONTROL WITHIN BUILDINGS

12th AIVC Conference, Ottawa, Canada
24-27 September, 1991

POSTER 47

Definition of the Flow Parameters at the Room Inlet Device
- Measurements and Calculations -

M. Ewert, U. Renz, N. Vogl, M. Zeller
Lehrstuhl für Wärmeübertragung und Klimatechnik
RWTH Aachen
D - 5100 Aachen

Synopsis
Due to the limitations of computer storage and time the flow boundary conditions at an air inlet device have to be specified for numerical simulations of air flow patterns in rooms. With regard to this the present work gives velocity measurements near an industrial air inlet using a Laser-Doppler-Anemometer.
From the stochastic velocity data the time-averaged velocity components, standard deviation and turbulent kinetic energy are evaluated. Furthermore the dissipation rate of the turbulent kinetic energy is determined from the time scale of the autocorrelation coefficient and alternativly from the frequency spectrum of turbulence. The assumptions required for the calculations are discussed.
Finally, measured data at a distance of one meter from the air inlet are compared with the numerically predicted velocity field and turbulence parameters, which are based on boundary conditions of a simplified inlet. Comparisons of numerically predicted air flow in the occupied zone show a significant difference depending on whether measured boundary conditions or those for a simplified slit are used. In particular the predicted turbulent kinetic energy for the simplified slit boundary condition is twice that for the measured boundary condition.

1. Measurement Technique and Testcase

With a one-component Argon-Ion-Laser-System the three local velocity components are measured. The laser and data processing system, the optical sensor, connected with the laser and a Burst Spectrum Analyser (BSA) by a fiber system, and a traversing device are described in /1/.
The measurements are carried out in a testroom with an air inlet device specified in the IEA-Annex 20 work /2/, /3/. The dimensions of the testroom and location of the imaginary entrance box, where Laser-Doppler-Anemometer (LDA) measurements are carried out, and the simplified slit inlet are shown in figure 1.

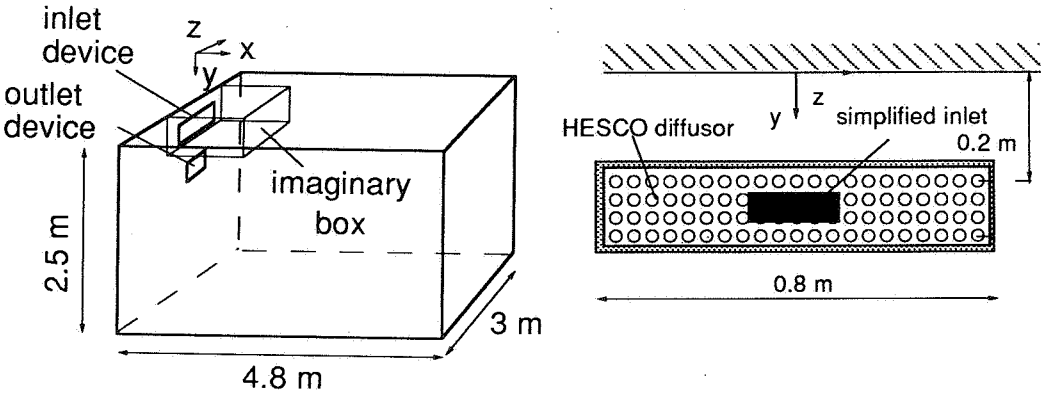


Figure 1: Dimensions of the testroom, industrial inlet device, simplified slit inlet and imaginary box

2. Determination of Turbulence Parameters

All statistical values of interest are calculated from the stochastic velocity data measured in the three directions of the testroom. The turbulent kinetic energy k is obtained from the velocity fluctuations as follows:

$$k = \frac{1}{2} \sum_{i=1}^{3} \overline{u_i'^2} \qquad (1)$$

Because the local gradients of the velocity fluctuations can not be measured simultaneously with available equipment the dissipation of turbulent kinetic energy ε can only be determined indirectly. However, different models to describe the dissipation rate as a function of known variables exist. Two suitable but rather simplifying models are found and adopted to the use of LDA measurements.
The first one is given by Rotta /4/.

$$\varepsilon = 0.165 \frac{k^{3/2}}{L} \tag{2}$$

This model relates ε with turbulent kinetic energy and length scale L. The constant depends on the definition of the length scale, which can be calculated from the spatial correlation functions and using Taylor's hypothesis from the autocorrelation function. Rotta has defined the length scale as

$$L = \frac{3}{8k} \int_0^{\infty} (R_{11}(r_2)\, \overline{u_1'^2} + R_{22}(r_2)\, \overline{u_2'^2} + R_{33}(r_2)\, \overline{u_3'^2}\,)\, dr_2 \tag{3}$$

where 1 is the main flow direction and 2 the direction of the greatest gradient. $R_{11}(r_2)$ and $R_{33}(r_2)$ are lateral and $R_{22}(r_2)$ longitudinal correlations. Assuming isotropic turbulence a relation between longitudinal and lateral correlations can be established, and with Taylor's hypothesis the spatial correlation $R_{ii}(\mathbf{r})$ and autocorrelation $R_{ii}(\tau\bar{U})$ are identical. Herein $\mathbf{r}$ is the spatial distance vector, $\bar{U}$ the mean velocity vector and τ the correlation time. The longitudinal and lateral correlation coefficients of equation (3) are found from the measured autocorrelation coefficient

$$R_{ii}(\tau) = \frac{\overline{u_i'(t)\, u_i'(t+\tau)}}{\left(\overline{u_i'(t)^2} \cdot \overline{u_i'(t+\tau)^2}\right)^{1/2}} \tag{4}$$

Figure 2 shows the measured autocorrelation function $R_{11}(\tau)$ smoothed by splines.

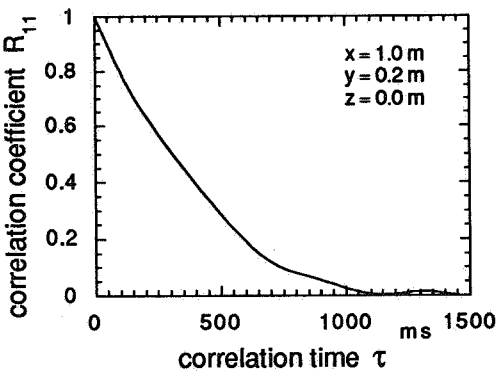


Figure 2: Measured autocorrelation function $R_{11}(\tau)$

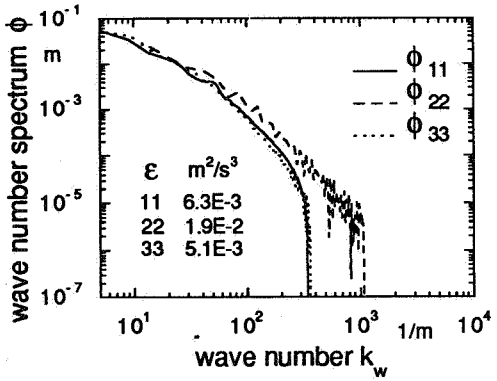


Figure 3: Wave number spectra in three directions and mean dissipation rate

The length scale, equation (3), is derived by integration of the calculated lateral autocorrelation coefficients R_{11} and R_{33} from the velocity components 1 and 3, and of the longitudinal coefficient R_{22} from the velocity component 2. More details are given in /1/, /5/.

The second model given by Hinze /6/ is based on the wave number spectrum of turbulence. If we assume isotropic turbulence the dissipation rate is given by

$$\varepsilon = 15\,\nu \int_0^\infty k_w^2 \phi_{ii}(k_w)\, dk_w, \tag{5}$$

where $\phi_{ii}(k_w)$ is the one dimensional wave number spectrum and ν the kinematic viscosity. With the following relation between the wave number k_w and the frequency ω and a simplification of the wave velocity U_c

$$k_w = \frac{\omega}{U_c} \qquad U_c = \bar{U} + \frac{\overline{ku'}}{k} \approx \bar{U} \tag{6}$$

the dissipation rate becomes

$$\varepsilon = \frac{15\nu}{\overline{U}^2} \int_0^\infty \omega^2 \phi_{ii}(\omega)\, d\omega. \tag{7}$$

The frequency spectrum $\phi_{ii}(\omega)$ is calculated from the longitudinal autocorrelation function

$$\phi_{ii}(\omega) = \frac{2\,\overline{u_i'^2}}{\pi} \int_0^\infty R_{ii}(\tau) \exp(-i\omega\tau)\, d\tau \tag{8}$$

By substituting $R_{ii}(\tau)$ with the longitudinal correlation calculated with the assumption of isotropic turbulence, we obtain three different frequency spectra and three different dissipation rates from measurements in the three directions as shown in figure 3. This indicates the nonisotropic structure of the flow. In order to get a mean value for ε which can be used as a boundary condition for the numerical simulations we introduce the following averaging

$$\varepsilon = \frac{1}{2k} \sum_{i=1}^{3} \varepsilon_{ii}\, \overline{u_i'^2} \tag{9}$$

The reason for weighting with velocity fluctuations is that the dissipation rate increases with increasing fluctuation velocities.

3. Results

3.1 Measurements and Calculations Near Air Inlet

The numerical simulations were carried out with the FLUENT code /7/ by solving the conservation equations for mass, momentum, turbulent kinetic energy and dissipation of the turbulent kinetic energy.

For the numerical simulations the real geometrical inlet conditions of experiments are simplified by a slit inlet. The mean velocity and the momentum of the slit sketched in figure 1 are the same as for the real inlet device. Comparisons of numerical predictions using different finite difference schemes and measured values of velocity, turbulent kinetic energy and dissipation rate at the symmetry plane of

the imaginary box are shown in figure 4 for an air exchange rate of 6 h^{-1} (flow rate 0,063 m^3/s).
Measurements yield higher velocities than simulations with the Power-Law (PL) and the QUICK scheme.The PL scheme results in a lower maximum velocity due to its higher numerical diffusion. A strong difference is also seen for turbulent kinetic energy. The measured values are ten times higher than calculations with PL, and two times higher than those with the QUICK scheme.
Comparison of the dissipation rate is quite difficult, because "measured" data are evaluated with simplifying models. The resulting values for the two models described above differ by more than one order of magnitude, but both curves indicate the same tendency. Results from numerical simulations are completely different. The profiles from the QUICK scheme are again closer to measurements.
Additional k- and ε-profiles calculated from the velocity magnitude as given in equation (10) are included in figure 4 for a turbulence intesity of Tu = 0.1.

$$k = 1.5\,(\bar{U}\,Tu)^2\,;\quad \varepsilon = c_\mu^{3/4} k^{1.5}/L \qquad c_\mu = 0.09; \qquad L = y \tag{10}$$

These formulas are normally used as boundary conditions if only the velocity values are available.

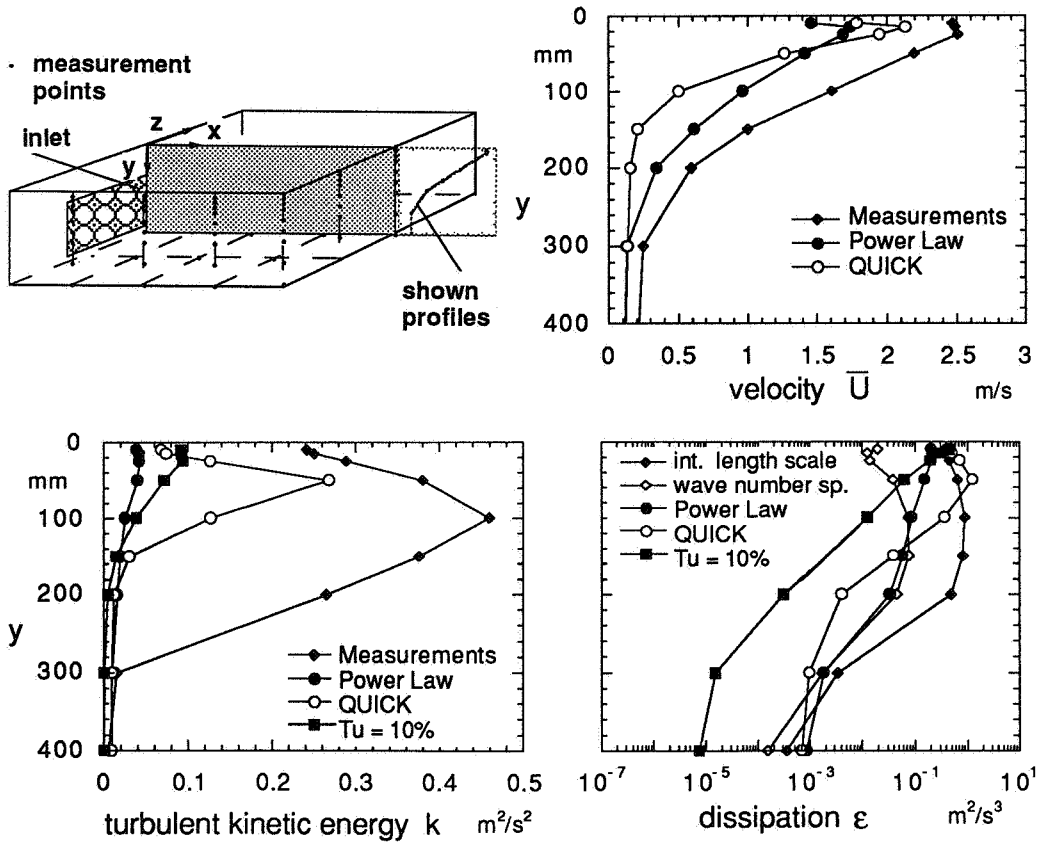


Figure 4: Comparison between measurements and numerical calculations at the symmetry plane of the imaginary box

3.2 Numerical Simulations of Room Air Flow with Different Boundary Conditions

The numerical results of air movement in rooms are compared using the four different boundary conditions as described above:

1. simplified slit and k, ε calculated from equation (10)
2. velocities, k and ε from measurements (ε calculated from integral length scale)
3. velocities, k and ε from measurements (ε calculated from turbulence spectrum)
4. velocities from measurements and k, ε calculated from equation (10).

Profiles of velocity, turbulent kinetic energy and dissipation rate near the center plane of the room are shown in figure 5 for the y-direction.
The simplified slit boundary condition yields smaller velocities in the jet area and higher velocities in the occupied zone. Velocity profiles for the other three boundary conditions look similar. The simple turbulence boundary condition (Tu = 10%) gives the highest maximum velocity because the initial turbulence intensity is much smaller than the measured one. The maximum velocity calculated with the integral length scale boundary condition is higher than that with the turbulence spectrum. This is caused by the higher initial dissipation rate (see figure 4), which results in a lower level of turbulence in the center of the room as shown in the turbulence profile. The turbulent kinetic energy and rate of dissipation again show great differences between the simplified slit and the other three boundary conditions.
The profiles in a y-plane as shown in figure 6 indicate the same tendency. It is remarkable, that the results based on measured turbulence data are very similar to the results using the simple turbulence boundary condition. Only the simplified slit results in different velocity and turbulent kinetic energy profiles. The dissipation rate at the side wall is also greater because of the larger turbulent kinetic energy gradients.

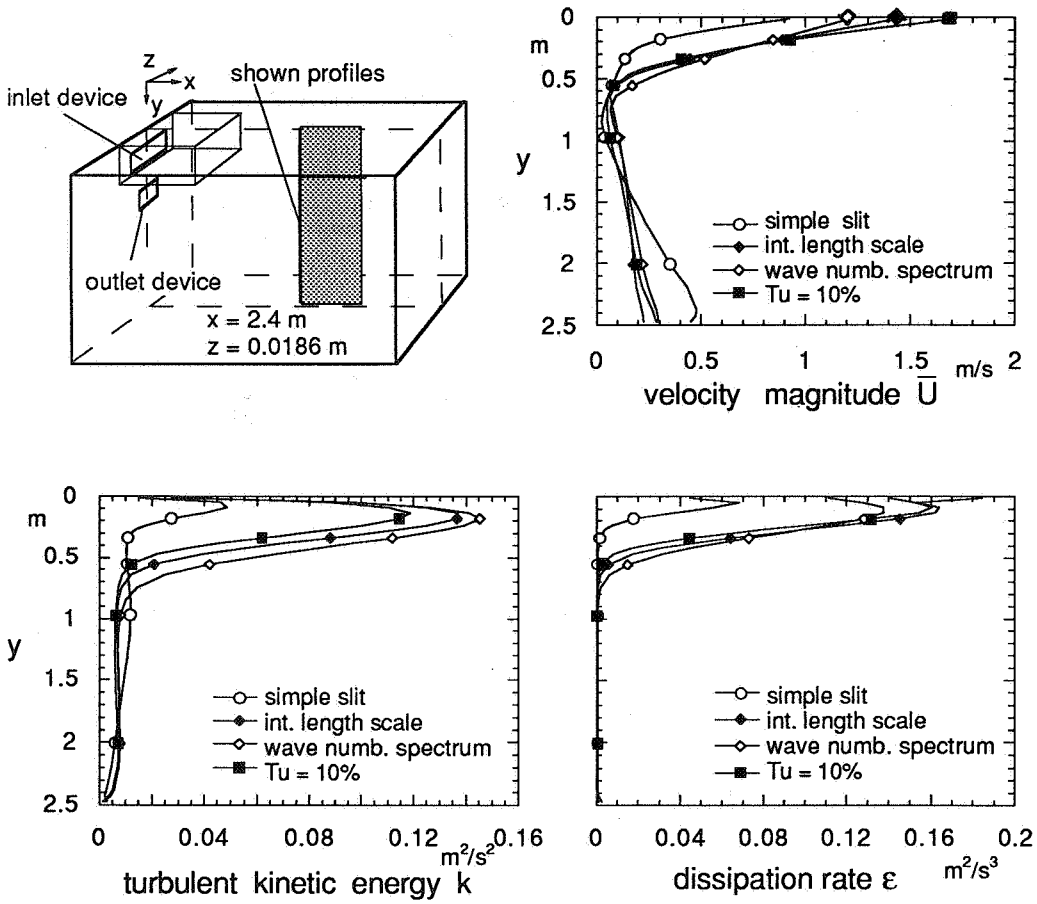


Figure 5: Profiles of velocity, k and ε from numerical simulations with different boundary conditions in a vertical plane of the room

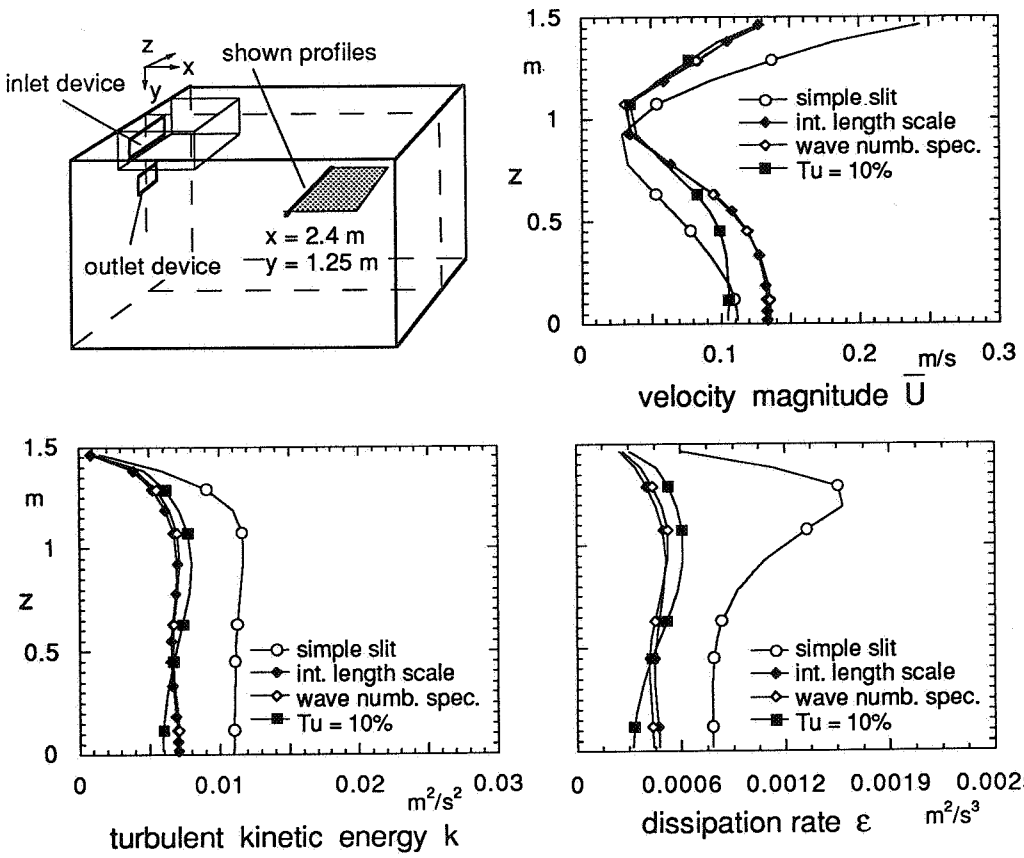


Figure 6: Profiles of velocity, k and ε from numerical simulations with different boundary conditions in a horizontal plane of the room

4. Conclusions

The evaluation of the dissipation rate of turbulent kinetic energy from measured velocities using two different models yields large quantitative differences, but the shape of the profiles is nearly the same. A general problem using the box method for the definition of boundary conditions is to determine the dimensions of the box. The box should be large enough so as to exclude the small flow structure of the real inlet from the calculation domain, but not too large, so as to avoid repercussion of the room air flow.

The comparison of numerical calculations using different boundary conditions has shown that the influence of the turbulence boundary condition is small compared with the influence of the inlet model, i.e. box method or simplified slit. The simplified slit model yields turbulent kinetic energies in the occupied zone two times larger than those resulting from the box method. The difference in these results significantly effects the PD value (percentage of dissatisfied) introduced by Fanger.

5. References

/1/ Ewert, M.; Zeller, M.; Turbulence Parameters at Supply Opening; Research Item 1.43, 1991, Annex 20 Report

/2/ Lemaire, A.D.; Testrooms, Identical Testrooms; Research Item 1.03, 1988, Annex 20 Report

/3/ Nielsen, P.; Selection of Air Terminal Device; Research Item 1.2, 1988, Annex 20 Report

/4/ Rotta, J.C.; Vollmers, H.; Ähnliche Lösungen der Differentialgleichungen für gemittelte Geschwindigkeiten, Turbulenzenergie und Turbulenzlänge; Forschungsbericht DLR (1976) 24

/5/ Rotta, J.O.; Turbulente Strömungen; B.G. Teubner Stutgart (1972)

/6/ Hinze, J.C.; Turbulence; McGraw Hill Inc.; New York and London (1975)

/7/ FLUENT. Creare Inc., PO Box 71, Hannover NH 03755 USA

AIR MOVEMENT & VENTILATION CONTROL WITHIN BUILDINGS

12th AIVC Conference, Ottawa, Canada
24-27 September, 1991

POSTER 48

BUILDING DESIGN ASSESSMENT THROUGH COUPLED HEAT AND AIR FLOW SIMULATION: TWO CASE STUDIES

J.L.M. HENSEN[1], J. HAND[2] and J.A. CLARKE[2]

[1]Eindhoven University of Technology
Group FAGO HG 11.77
P.O. Box 513
5600 MB EINDHOVEN
The Netherlands

[2]University of Strathclyde
Energy Simulation Research Unit
131 Rottenrow
GLASGOW G4 0NG
Scotland

SYNOPSIS

This paper is concerned with the application of air flow simulation in design. It describes the real world application - and the results of this with respect to building design improvement - of a building energy modelling system, *ESP*^{R†}, which supports the analysis of coupled heat and fluid flow as encountered in a building and/or plant environment.

The use of the system, and the design benefits to accrue, are demonstrated by elaborating two real world case studies. The first case study is also used to demonstrate some theoretical issues regarding coupled heat and mass flow, whereas the second case study is more concerned with practical issues.

The paper gives a brief overview of the theoretical basis of the modelling approach and it's use in a building performance evaluation context. In particular, it describes the necessary level of design abstraction, the choice of which simulations to perform, the results analysis and the design implications for the two case studies.

1 INTRODUCTION

ESP^R is a research orientated building and plant energy simulation environment. It's objective is to simulate the real world as rigorously as possible to a level which is dictated by international research efforts/ results on the matter in question. The current state of the simulation environment is the result of many years of evolutionary enhancements which seek to incorporate the latest state-of-the-art techniques to a feasible level. This means that the technique included must be more or less generally applicable and there must be a certain amount of international consensus about the technique. The program sets out to take fully into account all building & plant energy flows and their inter-connections. It also offers the possibility to assess building & plant performance in terms of thermal comfort. Thus it is specifically suited to do research on subjects in which inter-weaving of energy and mass flows plays an important role.

In order to be able to study the energy and comfort implications due to mass flows encountered in a building context, the system was recently extended so as to be capable of simulating the one-dimensional fluid (presently air and water) flow in a building and/or HVAC configuration. This involves solution of the mass balance in a nodal network in which the nodes represent either internal or boundary pressures and where the connections represent the distributed flow paths.

The system may be focussed on the fluid flow problem alone (by employing the stand-alone mass flow solver module *mfs*) or, to fuller advantage, on coupled problems (by activating the main building and plant energy simulation module *bps* and it's incorporated version of *mfs*). In the latter case, this enables energy and comfort studies of combined building and plant configurations in which the fluid flow rates may vary with time; for example due to changing boundary conditions (e.g. wind induced pressures) or as caused by changing flow path characteristics (e.g. some flow rate controller).

---

† In this context, the term *ESP*^{R} refers to the research version of the system as currently under development at various centres throughout Europe including the Universities of Strathclyde and Eindhoven. A separate version of the *ESP* system is being commercialised by a private company, ABACUS Simulations Limited.

This paper now continues with a brief outline of the approach. The use of the system, and the design benefits to accrue, will then be demonstrated by elaborating two real world case studies. The paper finishes with some conclusions towards possible future work.

2 THE APPROACH IN OUTLINE

In earlier publications a full account has been given of the internal workings of the system both with respect to energy simulation in general (Clarke 1985) and with respect to simultaneous heat and mass flow simulation (Clarke and Hensen 1991, Hensen 1991). An outline of the approach used within *ESP*^{R} could be: during each simulation time step, the mass transfer problem is constrained to the steady flow (possibly bi-directional) of an incompressible fluid along the connections which represent the building/ plant mass flow paths network when subjected to certain boundary conditions regarding pressure and/ or flow. The problem reduces therefore to the calculation of fluid flow through these connections with the nodes of the network representing certain pressures. This is achieved by an iterative mass balance approach in which the unknown nodal pressures are adjusted until the mass residual of each internal node satisfies some user-specified criterion.

Information on potential mass flows is given by a user in terms of node descriptions, fluid types, flow component types, interconnections and boundary conditions. In this way a nodal network of connecting resistances is constructed. This may then be attached, at it's boundaries, to known pressures or to pressure coefficient sets which represent the relationship between free-stream wind vectors and the building external surface pressures to result. The flow network may consist of several decoupled sub-networks and is not restricted to one type of fluid. However, all nodes and components within a sub-network must relate to the same fluid type.

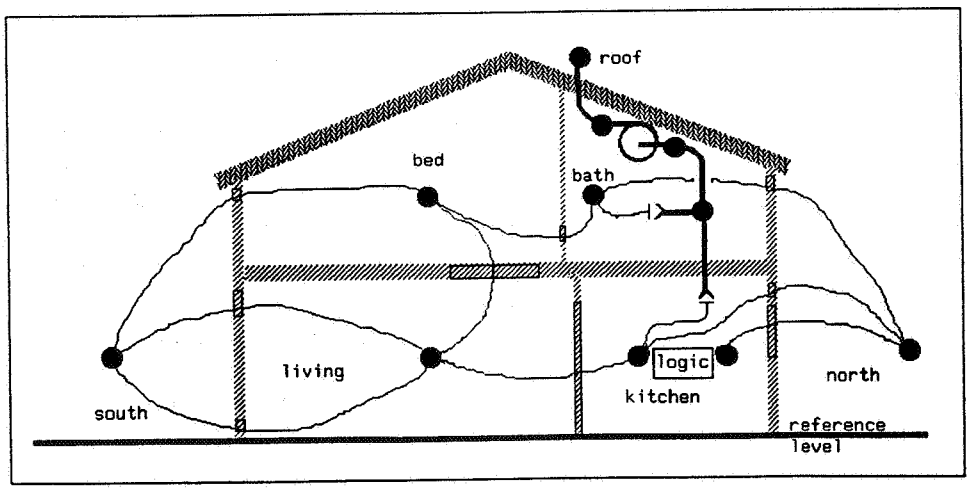


Figure 1 Example building and plant schematic

Nodes may represent rooms, parts of rooms, plant components, connection points in a duct or in a pipe, ambient conditions and so on. Fluid flow components correspond to discrete fluid flow passages such as doorways, construction cracks, ducts, pipes, fans, pumps, etc. As an example Figure 1 shows a schematic of part of a house consisting of four rooms, air flow connections between these rooms and to outside, and an exhaust-

only ventilation system. In this case the building and plant configuration contains only one mass flow network, because there is only one working fluid, ie air. One possibility with respect to the translation of this configuration into a fluid flow nodal scheme is indicated by the dots.

Coupling of building/ plant heat and mass flow in a mathematical/ numerical sense, effectively means combining the energy and flow balance matrix equations for both the building and it's plant (Clarke 1985). (Note that in the case of building-side flows and for some plant, two flow balance matrix equations will be required to represent the two fluids present; air and water vapour for example). While in principle it is possible to combine all six matrix equations into one overall 'super-matrix', this is not done within ESP^R, primarily because of the advantages which accrue from problem partitioning. The most immediate advantage is the marked reduction in matrix dimensions and degree of sparsity - indeed the program never forms a two dimensional array but instead holds matrix topology and topography as a set of vectors. A second advantage is that it is possible to easily remove partitions as a function of the problem in hand; for example when the problem incorporates building only considerations, plant only considerations, plant + flow, and so on. A third advantage is that, potentially, different partition solvers can be used which are well adapted for the equation types in question - highly non-linear, differential and so on.
It is recognised however that there are often dominating thermodynamic and/ or hydraulic couplings between the different matrix partitions. If a variable in one partition (say air temperature of a zone) depends on a variable of state solved within another partition (say the inter-zonal air flow), it is important to ensure that both values match in order to preserve the thermodynamic integrity of the system. As elaborated in the above mentioned references, ESP^R incorporates a number of mechanisms which ensure this thermodynamic integrity, such as iteration mechanisms and time-step control.

2 DEMONSTRATING APPLICATION OF AIR FLOW SIMULATION IN DESIGN

The use of the system in a building performance evaluation context, and the design benefits to accrue, will be demonstrated in the following sections. This is achieved by elaborating two case studies showing the system's real world application, and the results of this with respect to building design improvement. The first case study is also used to demonstrate some theoretical issues regarding coupled heat and mass flow, whereas the second case study is more concerned with practical issues.
Both case studies were actually performed in a real consultancy context by an energy design advisory service (Emslie and Chalmers 1988).
Apart from anything else, such real world case studies signal the need in practice and the utilization factor of the kind of simulation tool described. From the developers point of view, real world case studies are important because they increase the insight in what is necessary from a practical point of view, and they assist in developing the system and making it more robust.

2.1 Case Study 1: Environmental Assessment of Hospital Spaces

This study concerns an environmental assessment of hospital spaces located in central Scotland, where air flow rates were judged to be critical in limiting summer overheating

in zones with significant solar radiation gain (Hand 1990; Hensen 1991). Figure 2 shows the part of the hospital under consideration, which consists of a dayroom and adjoining dining room. As can be seen, the dayroom has very large glazing areas.

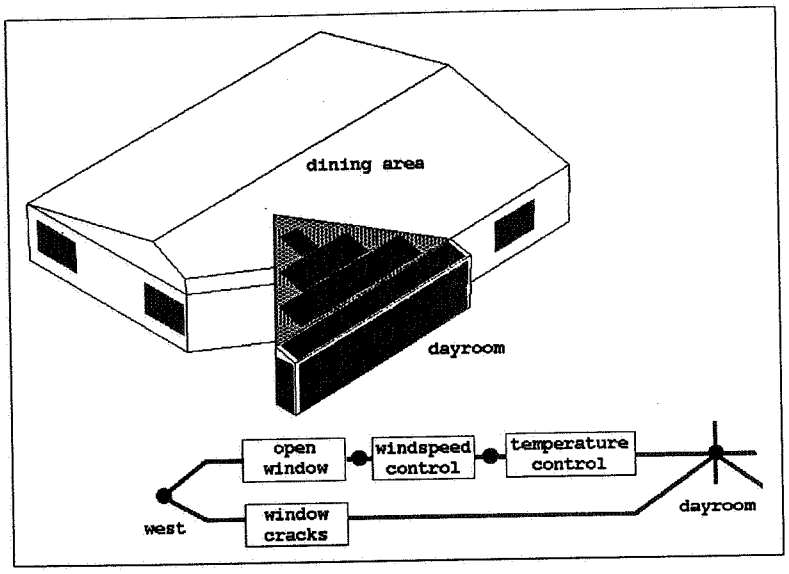


Figure 2 Schematic representation of the dayroom and adjoining dining room, when viewed from the south-west. Diagram of a fraction of the fluid flow network representing the west facade dayroom window.

It was requested to advise on useful operating strategies and/or possible modifications to the building in order to better control it's summertime indoor thermal environment. The actual case study involved a number of building thermal performance simulations regarding several aspects including shading analysis. However, here we concentrate on one issue only, namely infiltration analysis by simulation of coupled heat and mass transfer.

After reduction of solar gain, the primary means of preventing summer overheating is 'free cooling' by increasing the infiltration of ambient air. This may be achieved by, for example, opening of windows. Both the resulting cooling load by infiltration air and the indoor temperature, are influenced by the temperature difference between outside and inside, and by the actual air flow rates. In building thermal performance simulations, it has thus far been very problematic and time consuming to realistically incorporate the air flow rates. The main reason for this is that the rate of air flow depends on pressure differences which may be caused by wind or by stack effects due to temperature differences. Especially with a free floating indoor air temperature problem - like in the present case study - heat removal and air flow are closely coupled.

For the dayroom and dining area, a building thermal simulation model had been set up. In addition to this, a flow network was created with nodes representing the dayroom and the dining area on two levels to account for temperature stratification, and with nodes representing the wind induced pressures on the various facades. These nodes are inter-connected by flow components representing internal connections (doors etc), and infiltration openings (cracks etc) in the exterior envelope. The windows are also represented by flow components. In order to investigate the effects of their opening or closing, additional flow components representing logical control are incorporated in series with the window flow components, as indicated in Figure 2 for the dayroom west

window only. Incorporation of these logical controllers allows the study of occupant interactions with respect to opening and closing of windows. Various options were examined. In one case, for example, it was envisaged that the windows would be opened whenever the air temperature of either the dayroom or the dining exceeds 24°C during the period between 11:00 and 18:00 hours, and that the occupants will not open the west and south orientated windows whenever it is very windy. Therefore, for these windows additional logical controllers are incorporated to prevent window opening in case the wind speed exceeds 6 *m/s*. Of course these specific control strategies are just examples and may be changed at will.

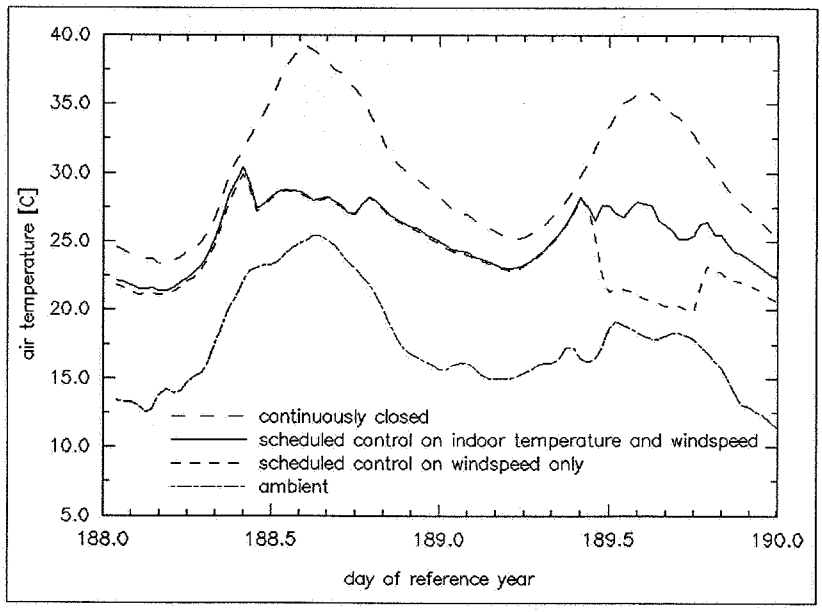


Figure 3 Predicted dayroom air temperature for July 7 and 8, assuming various window control strategies.

In order to demonstrate the effect on predicted air temperature, several simulation studies were performed. All these simulations were performed using *bps* and it's incorporated version of *mfs*, and are thus based on simultaneous and continuous simulation of heat transfer and air flow. It should be noted that this is already a more refined approach than building thermal simulation using infiltration/ventilation rates estimated by independent means which has been common practice up to now.

Figure 3 shows predicted dayroom air temperatures for July 7 and 8 of a reference year, and assuming various window control strategies. The first two (imaginary) window control strategies investigated are: (1) windows continuously closed, and (2) window opening controlled on the basis of time of day and wind speed. These two cases would have enabled prediction of at least upper and lower levels for the air temperatures to be expected, when coupled heat and mass transfer simulation would not have been possible.

With the present system the effects of more advanced controls can also be predicted. For example, a third window control strategy involved scheduled control both by wind speed and indoor temperature which is deemed to be more realistic than the previous strategies. The results for this control strategy are also shown in 2. As can be seen, the results for July 7 are almost identical to the control by wind speed only case because the indoor temperature was above 24°C throughout the period between 11:00 and 18:00 hours. For July 8 however, there are marked differences because this is a day where the

temperature control was actually activated.

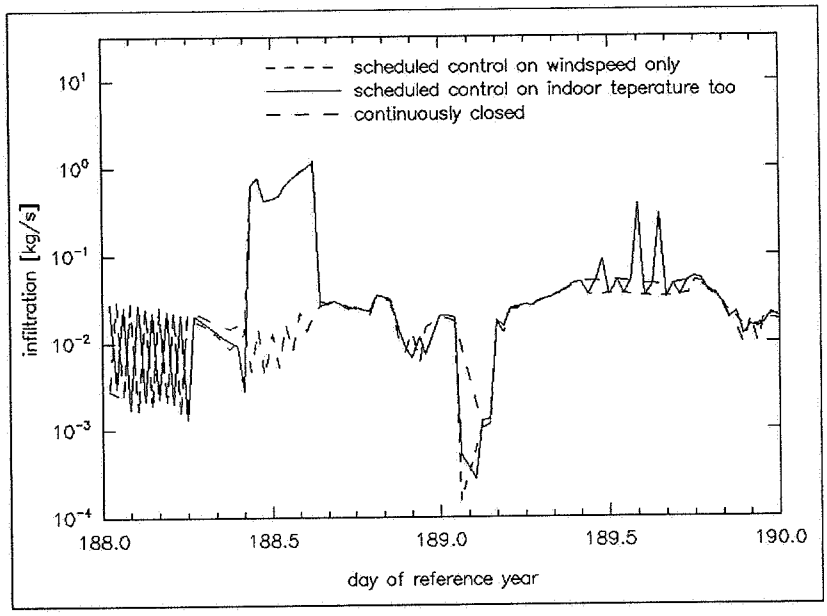


Figure 4 Predicted dayroom infiltration rates for July 7 and 8, assuming various window control strategies.

On July 8 the wind speed exceeded 6 *m/s* throughout the control period, and so the west and south orientated windows were not opened. The sharp air temperature decrease in case of the scheduled control on wind speed only, is also not due to an increase of infiltration but is caused by air flow from the dining area to the dayroom (because north and east facing windows were opened the air flow through the building changed from predominantly south-west to north-east to predominantly north to east). This is evidenced by Figure 4, which shows the predicted infiltration rates for the dayroom. Obviously as with the air temperatures, there are marked differences between the various control strategies. Infiltration is defined here as ambient air which enters the zone directly; ie in case of the dayroom excluding air flow via the dining area. Because the ambient air may enter the dayroom via the roof and the east and west window, infiltration rates may occur which seem to be out of order at first glance. For example the two peaks on July 8 (control incorporates temperature), are due to the fact that the east window is opened because of high indoor temperature. In that case air enters via this window, while at that point in time the air would leave via this window in the other two control strategy cases due to the prevailing environmental conditions.
This example may serve to illustrate the complexity of air flow paths through the building as a function of wind speed, wind direction, indoor temperatures, and control behaviour. From the analysis it was possible to define an operating regime and minimal change in equipment which would allow a zone to meet mandated environmental conditions.

In the previous cases, the air flow rates were calculated starting from the actual indoor air temperatures thus coupling heat and mass transfer. To illustrate the importance of this, some additional simulations were performed in which two cases were compared: (1) the indoor temperatures are at some fixed value, and (2) the indoor temperatures are as predicted by the thermal building simulation. So the pressure difference due to inside/outside temperature difference are accounted for in both cases, but it is only in

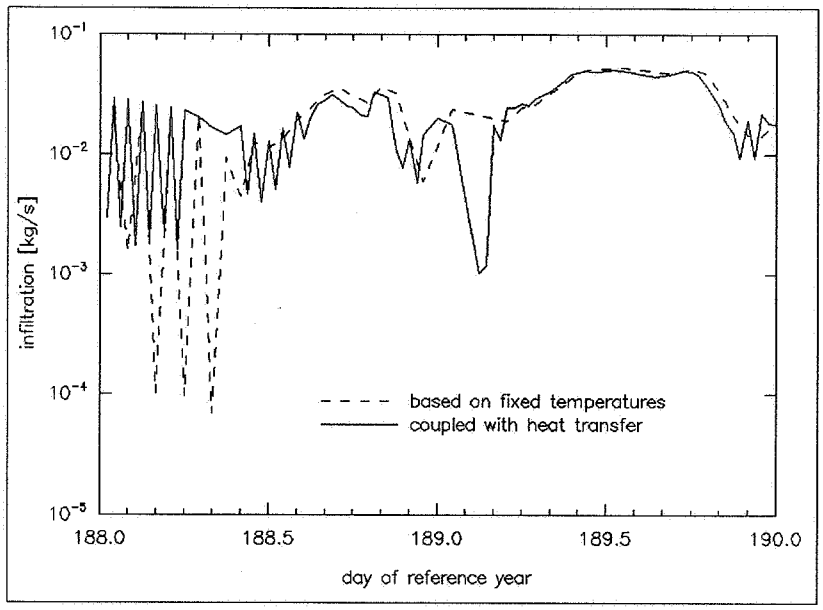


Figure 5 Effect of coupled/decoupled heat and mass transfer on predicted dayroom infiltration rates for July 7 and 8, assuming all windows closed.

the second case that varying indoor temperatures - both with respect to ambient as between the various zones - are taken into account. The first case exemplifies the case where buoyancy forces are fixed, while the second case exemplifies a case where heat and mass transfer are handled simultaneously. In both cases it was assumed that the windows are continuously closed. The corresponding indoor and ambient temperatures are shown in Figure 3. Figure 5 shows the simulation results for the dayroom infiltration rate. The differences are clear, thus stressing the importance of simulation of coupled heat and mass transfer especially when buoyancy effects play an important role or are strongly time varying.

2.2 Case Study 2: Environmental Analysis of Office Spaces

The second case study concerned a comfort and energy impact assessment of three multi-storey atria in a proposed office block. Given the time-scale and financial resources available it was decided to carry out the analysis on three section of the office building rather than attempt to model the building as a whole. Each section was abstracted from the plans and sections provided. The occupancy and casual gains were taken from documents supplied as well as interviews with office staff.
Air flows were affected by buoyancy, asymmetrical radiant and convective heat injection and the use of each atrium as an exhaust for fresh air injection. Each atrium was subdivided into thermal zones on fixed levels, each with a core and a perimeter. The flow network included one or more nodes in each atria zone as well as connections to adjacent zones and boundary conditions. The connecting elements for the atrium nodes consisted of a number of large area air flow openings which are actually based on the common orifice flow equation which assumes uni-directional turbulent flow. This is a simplification of reality, which approximates the bulk flow through the atrium. Clearly,

a CFD approach might give more detailed information, but due to practical reasons such an approach would have to be restricted to a single, fixed, moment in time and probably to just one single enclosure as well. However, in the present case the problem involved an extended period in time and a large number of enclosures. Thus, the above mentioned network approach was chosen. It is worth noting that in the immediate future a research project will start with the objective to reduce the above mentioned practical limitations (Te Velde and Hensen 1991).

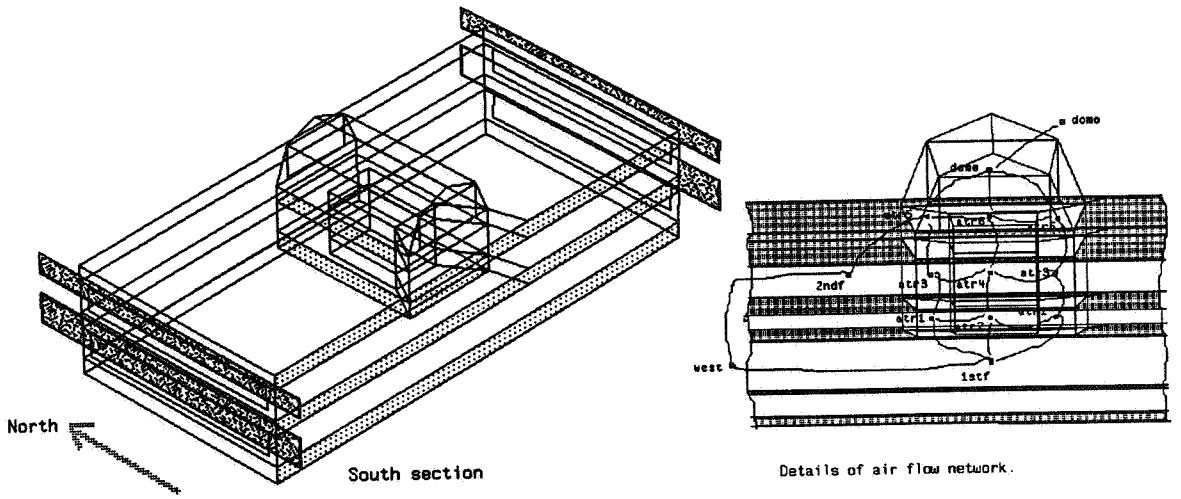


Figure 6 Schematic representation of one of the atria and the associated part of the air flow network.

Figure 6 shows the geometry of one of the atria and the associated part of the air flow network. Based on this, a combined heat and mass transfer analysis was carried out for a winter Sunday-Monday period (ie. starting up after a weekend) and for a Friday in July. The results for early in the morning and at noon are shown in Figure 7. For each branch of the network the upper value is the volume flow rate in m^3/s and the lower value is the velocity in m/s.

Beginning with the winter early morning graph, the flows at the left side are constant volume (equal to fresh air supply). Moving to the right, the four vertically stacked nodes are adjacent to the edge of the atrium while the second set of four stacked nodes represent the centre of the atrium. The diagonal at the top is adjacent to the glazing in the atrium dome and shows a downward flow of air as would be expected. This flow carries downwards until the middle of the atrium where it is met by the upwards flow from the first floor. At the base of the atrium there is a clock-wise circular flow as the unheated atrium air mixes with the first floor air.

The winter noon graph is similar in it left portion, however at this time the flow at the edge of the atrium is upwards with a strong current downwards at the centre of the atrium. Both the velocities and volume flow rates are quite high and are likely to be due to the cooler temperatures at the top of the atrium. As with the early morning there is a clock-wise mixing between the first floor and the atrium, however this time it extends to midway up the atrium. Since this analysis assumed that the only induced flow was due to the fresh air component, and this quantity was calculated based on the volume of the

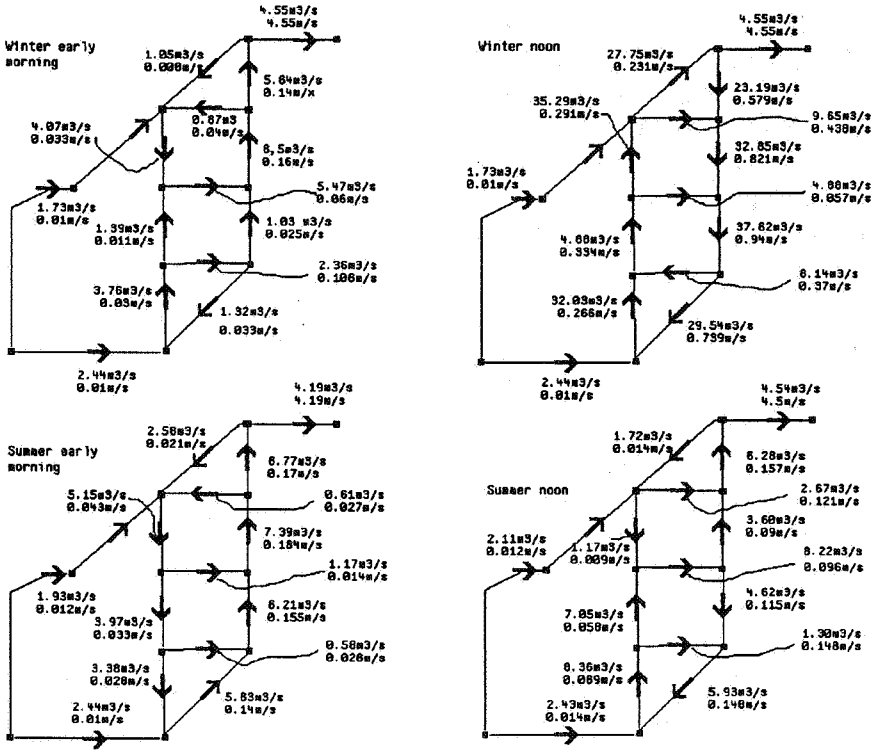


Figure 7 Predicted volume flow rates and velocities in each branch of the air flow network, for early morning and noon conditions in winter and in summer.

section, actual flows will be higher and there may be less of a temperature difference between the top and the bottom of the atrium.

The winter analysis does indicate that cold air trapped at the top of the atrium will have a tendency to flow downwards, either at the boundary of the atrium or in the centre. If care is taken to extract air so that pockets of still air are not allowed to form, then it may be possible to reduce such buoyancy driven flows.

The early morning summer flow patterns are dominated by a clear anti-clockwise flow which extends the full height of the atrium. As the high velocities are found in the centre of the atrium, the implications for thermal comfort are minimal. By noon this pattern has deteriorated into a series of circular patterns in various directions.

The analyses showed flow velocity and volume within the atria to be in the order of one magnitude greater than surrounding zones during winter start-up periods. The impact on plant capacity and comfort for occupants at the base of the atria were studied in detail and resulted in recommendations for top-up radiant heating and pre-conditioning.

3 CONCLUSIONS

By elaborating two real world case studies, this paper has demonstrated the use, and the design benefits to accrue, of a mass flow network method integrated in a building and plant energy simulation system, which is thus capable of simulating coupled heat and mass flows in buildings. The performance of the model indicates that it is practical to

solve complex building/ plant heat and mass flow problems with complex control regimes within large buildings for simulation periods of up to one year on the current generation of workstations.
It is felt that the model reflects the current state of the art in the field of network modelling approach to simulation of coupled heat and mass flows in buildings. Development and use of the model did reveal however that research is still needed in several areas. These include development of additional fluid flow component models (especially improved large opening models), modelling of intrazone effects by simplified methods and by integration with CFD modelling methods, expansion of the wind pressure database, expansion of the actual building and plant components 'database', and experimental validation of the simplifying assumptions in the flow component models and the network method.

References

Clarke, J.A. 1985. *Energy simulation in building design,* Adam Hilger Ltd, Bristol (UK).

Clarke, J.A. and J.L.M. Hensen 1991. "An approach to the simulation of coupled heat and mass flow in buildings," in *Proc. 11th AIVC Conf. Ventilation System Performance held at Belgirate (I) 1990,* vol. 2, pp. 339-354, IEA Air Infiltration and Ventilation Centre, Coventry (UK).

Emslie, S. and J. Chalmers 1988. "The RIAS Energy Design Advisory Service. Technology transfer in advanced building energy simulation," in *Proc. USER 1 working conference at Ostend,* pp. 303-309, Society for Computer Simulation International, Ghent (B).

Hand, J. 1990. "Erskine Hospital Environmental Report," ESRU project report, University of Strathclyde, Energy Simulation Research Unit, Glasgow.

Hensen, J.L.M. 1991. "On the thermal interaction of building structure and heating and ventilating system," PhD dissertation Eindhoven University of Technology (FAGO).

Velde, K. Te and J.L.M. Hensen 1991. *A hybrid network and flow field method approach to simulation of air flow in rooms,* Eindhoven University of Technology. FAGO research proposal

AIR MOVEMENT & VENTILATION CONTROL WITHIN BUILDINGS

12th AIVC Conference, Ottawa, Canada
24-27 September, 1991

POSTER 49

Estimation of Air Leakage in High-Rise Residential Buildings.

A. Parekh

Scanada Consultants Limited,
436 MacLaren Street
Ottawa, Ontario K2P 0M8
Canada

12th AIVC Conference

Air Movement and Ventilation Control within Buildings

Call for Papers

Venue: Chateau Laurier, Ottawa, Canada

Date: Tuesday 24th to Friday 27th September 1991

Proposed Paper

Title: Estimation of Air Leakage in High-Rise Residential Buildings

Author: A. Parekh

Address: Scanada Consultants Limited, 436 MacLaren Street, Ottawa, Ontario K2P 0M8 Canada

Telephone: (613) 236-71719 **FAX:** (613) 236-7202

ABSTRACT

Both infiltration and exfiltration has a predominant influence on the space heating requirements in cold climates. Good predictive design methods are required to estimate the air leakage component in buildings. This predictive methods will be useful in implementing the air leakage control strategies for reducing the problems associated with air infiltration in both new and existing high-rise buildings. The objective of this paper is to provide simple analytical methods for quantifying the air infiltration in high-rise buildings, and to present the results of field tests of two high-rise buildings to verify the estimation procedure.

A simplified air infiltration estimation procedure has been developed primarily based on equivalent air leakage area and local net pressure distribution. The pressure difference at a given location depends on the infiltration driving forces (stack, wind and mechanical ventilation) and the characteristics of the opening in the building envelope. A simplified network of air-flow paths can be established using the following information: climate and exposure, building types, building form, building dimensions, surface to volume ratios, shafts, and envelope types, windows and doors, envelope crack lengths, openings, and make-up air strategies. The algebraic sum of air-flow through these paths must always be equalled to zero. By applying the mass balance equation, component of air infiltration which would be occurring during the peak winter condition can be determined. This air-flow is responsible for the space heating load due to uncontrolled infiltration. Any reduction in this infiltration flow should decrease the heating requirements for the building.

The method has been used to predict the infiltration flows and heating loads for two high-rise residential buildings. The field tests have been conducted to verify the predictions of air leakage in these buildings, and also to assess the effects of air-sealing on overall building airtightness, indoor air quality, and power consumption before and after air-sealing.

[ ] Tick box if poster presentation preferred. (See call for papers for details.)

AIR MOVEMENT & VENTILATION CONTROL WITHIN BUILDINGS

12th AIVC Conference, Ottawa, Canada
24-27 September, 1991

POSTER 50

INFLUENCE OF RADIATIVE PARTICIPATION OF INSIDE AIR ON NATURAL CONVECTION IN A ROOM

SYNOPSIS: The bases of this study are experimental results obtained on a real scale cell in controlled climatic conditions which are used to show the potential influence of radiative participation of inside air on natural convection in a room.

In a second part, a numerical analysis of flow patterns and heat tranfer in a two dimensionnal thermally driven cavity containing a participating fluid is presented. The results obtained show the influence of the radiative coupling between the walls and the fluid, and the influence of the radiative transfer inside the fluid itself on the thermal field and flow patterns obtained in the cavity.

F. ALLARD - C.INARD - A. DRAOUI

CETHIL, URA CNRS 1372
INSA de Lyon, bât. 307
F-69621 Villeurbanne cedex, France.

Nomenclature

A	= aspect ratio ($A = Y_{max}/X_{max}$)
F_{ij}	= view factor
$F\tau_{ij}$	= view function
d_{ij}	= distance
G	= radiation intensity
J	= radiosity
L^0	= black body intensity
N_{CR}	= interaction parameter
P	= pressure
Pr	= Prandtl number
Ra	= Rayleigh number
S	= Surface area
T	= temperature
t	= time
T_C	= temperature of the cold wall
T_H	= temperature of the hot wall
T_{ref}	= reference temperature (mean temperature = $(T_H + T_C)/2.$)
X_{max}	= width of cavity
Y_{max}	= height of cavity
x, y	= coordinates
U	= x - component of the velocity
V	= y - component of the velocity

Greek symbols

β	= mean extinction coefficient
ϵ	= radiative emissivity
Δ	= Laplace's operator
λ	= thermal conductivity of the fluid
σ_o	= Stephan-Boltzmann constant
τ_o	= optical thickness of the fluid ($\tau_o = \beta.X_{max}$)
Ω_o	= scattering albedo
ν	= frequency
ϕ	= radiative flux
θ	= angle

Superscripts

*	dimensional quantity
e	emitted
t	transmited

1. - INTRODUCTION

A common assumption in building physics is to consider air as a transparent medium for long wave radiation heat transfer. In fact, looking more carefuly at the absorption spectra of air components such as water vapor or carbon dioxide, we can expect in certain cases a reasonnable radiative participation of inside air. In order to improve our knowledge about this particular point, we first carried out a serie of experiments in our MINIBAT test cell facility, then we introduced in a CFD code the radiative transfer inside the fluid itself to evaluate theoretically the influence of radiative participation of the fluid itself about flow patterns and heat transfers in a thermally driven cavity.

2. - BASIC METHOD FOR EVALUATION OF RADIATIVE PARTICIPATION OF AIR

Figure 1 shows the spectral emmisivities of water vapor and carbon dioxide

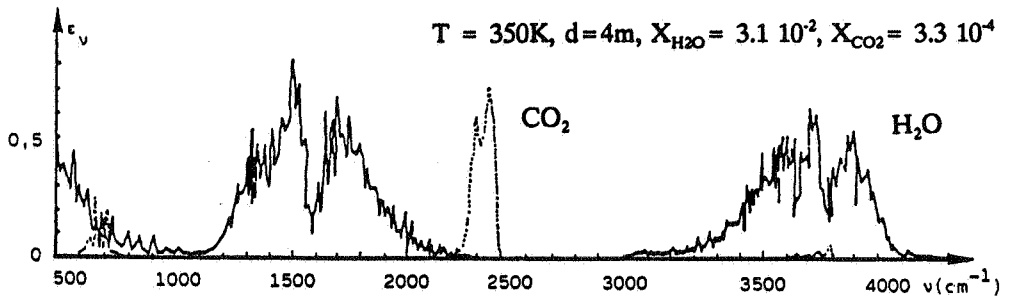


Figure 1 : Spectral emmissivities of H_2O an CO_2[1]

Even if the spectra given on Figure 1 show a significative emmissivity of water vapor, in buiding physics we used to neglect this radiative contribution of air to the energy balances considering that the overall emission of the air volume is compensated by the absorption of this same volume of the radiations coming from the surfaces of the room. That could be completely true if the surface temperatures and the air temperature were exactly similar. In fact all the experiments [2] carried out show clearly air stratification and surface temperature heterogeneousness.

Furtheremore, the heat fluxes exchanged along the walls are weak, and thus the heat balance can be very sensitive to any additionnal phenomenon.

In order to show out what could be the influence of radiative participation of air on the thermal balance of a room, we introduced in a classical spectral radiosity radiative model the effects of emission and absorption of the gas. As a first approximation we consider also that the air temperature differences inside the room will not change the absorption and emission spectra. We select as reference temperature the temperature of convective equilibrium of the air volume, this temperature is usually very close to the air temperature measured at the center of the room. In this case, the flux radiated by a surface element dS_i in a frequency domain $\Delta\nu$ centered on ν_0 and arriving on an other surface element dS_j can be written

$$d\phi^t_{i,j,\Delta\nu} = J_{i,\Delta\nu}\frac{\cos\theta_i\,\cos\theta_j dS_i dS_j e^{-K\nu_0 d_{ij}}}{\pi d_{ij}^2} \qquad (1)$$

Where K represents the monochromatic extinction coefficient. If we assume the reflection and emission of each surface to be diffuse, and integrating on each surface S_i and S_j, we will obtain the total flux radiated by S_i and arriving on S_j as:

$$\phi_{t_{i,j\Delta\nu}} = J_{i,\Delta\nu}\,F\tau_{ij}\,S_i \qquad (2)$$

We define here a new exchange function $F\tau_{ij}$ which includes in its definition both geometry characteristics and radiation transmission through the gas column. Following the same concepts, we define the proper emission of the gas column arriving on S_j.

$$\phi^e_{G,i,j,\Delta\nu} = \pi L^0_{G,\Delta\nu}\iint_{S_iS_j}\frac{\epsilon_{G,\Delta\nu}\,\cos\theta_i\,\cos\theta_j\,dS_i dS_j}{\pi d_{ij}^2} \qquad (3)$$

Or using again the above mentionned symbols:

$$\phi^e_{G,i,j,\Delta\nu} = \pi L^0_{G,\Delta\nu}(F_{ij}-F\tau_{ij})\,S_i \qquad (4)$$

Then, calling upon all the directions in the space and therefore all the elementary surfaces defined on the walls forming the room, we obtain the total monochromatic flux radiated by the gas to surface S_i.

$$\phi^e_{G,j,\Delta\nu} = \pi L^0_{G,\Delta\nu}\sum_{i=1}^{n}(F_{ij}-F\tau_{ij})\,S_i \qquad (5)$$

Writing the same expression for each surface forming the room, we finally obtain for each spectral interval a system of equations defining the spectral radiosity of each surface.

$$J_{j,\Delta\nu}-\rho_j\sum_{i=1}^{n}J_{i,\Delta\nu}F\tau_{ij}\frac{S_i}{S_j} = \epsilon_{j,\Delta\nu}M^0_{j,\Delta\nu}+\rho_j\pi L^0_{G,\Delta\nu}\sum_{i=1}^{n}F_{ij}-F\tau_{ij}\frac{S_i}{S_j} \qquad (6)$$

Integrating over all the considered spectrum (practically wavelenght from 2.5 to 70 μm), we then obtain the net fluxes of each surface and the total fluxes emitted and absorbed by the gas volume.The difference between these two quantities called net flux of the gas characterizes the overall radiative participation of air.

3. - INFLUENCE OF AIR RELATIVE HUMIDITY ON ITS RADIATIVE PARTICIPATION.

The basis of this study is a serie of experiments carried out in our Minibat Test cell [3]. In order to raise the potential effect of radiative participation of air we study the case of a convective heating of the cell. The convective power of the source is 2158W, the final air temperature obtained at the center of the room is 46.5 °C. As the extinction spectral coefficient depends directly on the relative pressure of water vapor, we can look at the influence of relative humidity of air varying this parameter in our model. Figure 2 shows this influence on the net radiative flux of the overall mass of air. We use here the surface temperature measured during the experiment as input data for our model.

The radiative deficit of air rapidly reaches 10% of the total convective power injected in the room. (.015 represents 23% of humidity at the conditions of the experiment) It is important to mention here than very low relative humidity values have a significant influence on the radiative participation of air.

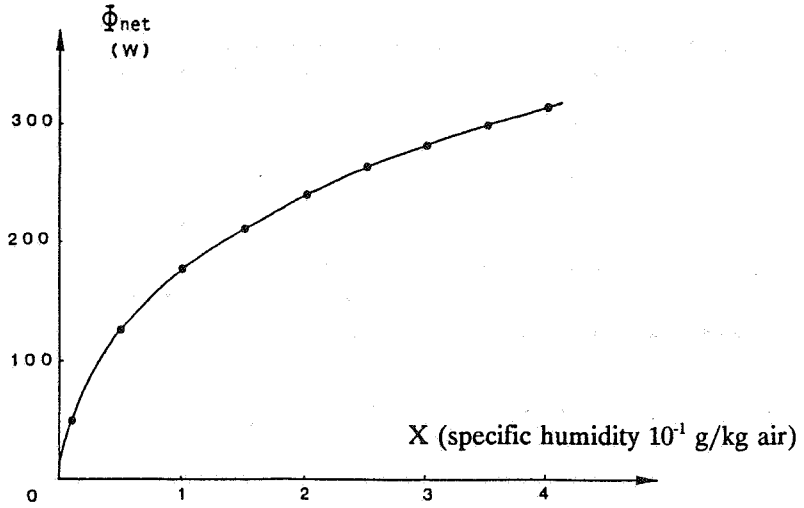


Figure 2 : Influence of specific humidity on the air radiative net flux.

If we now consider the influence of water vapor content on the heat balance of each wall surface, we see on Figure 3 that the deviation in estimating the convective heat flux at the surface of the walls is significative, it represents 25 percent of the weakest convective heat fluxes in our case.

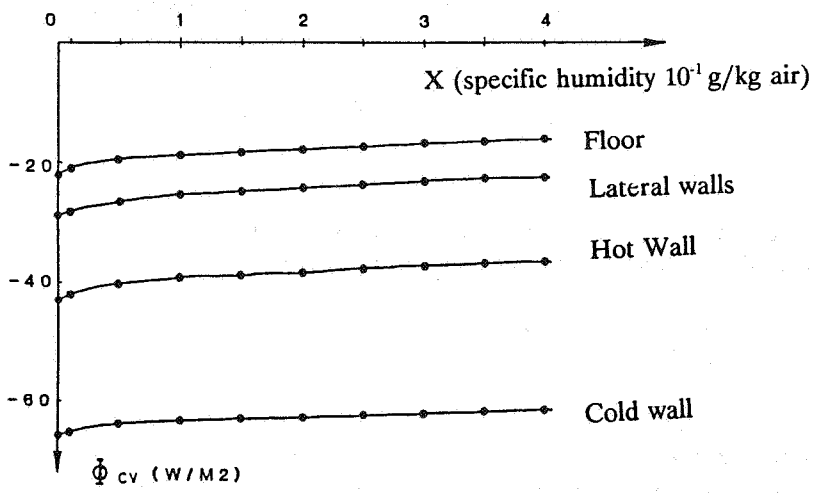


Figure 3 : Influence of the radiative participation of air on the evaluation of convective fluxes along the walls.

This first experimental study enables to show that radiative participation of air can be a significant phenomenon perturbating the energy balance of a room. Nevertheless it is limited to a convective heating situation and does not allow us to unterstand how mass and heat transfer patterns can be modify. To answer this question, we used the CONCAV code developped in our team and we coupled the Navier Stokes equations with the radiative transfer equation.

4. - NUMERICAL STUDY OF NATURAL CONVECTION IN SEMI-TRANSPARENT FLUIDS.

4.1. - MATHEMATICAL FORMULATION

The flow and heat transfer within a two-dimensional enclosure filled with a gas (absorbing, emitting, and isotropically scattering), are described by the Navier-Stokes equations in their Boussinesq-Obberbeck approximation, as the energy equation, as well as an additional equation for the radiative transfer. In our case, the P1 differential approximation [4] of the radiative transfer equation has been preferred, due to its compatibility with the governing equation system which gives the flow and heat transfer. The complete system (nondimensional) of governing equations is therefore expressed as :

* **Continuity :**

$$\frac{\partial U}{\partial x} + \frac{\partial V}{\partial y} = 0 \qquad (7)$$

* **Momentum :**

$$U\frac{\partial U}{\partial x} + V\frac{\partial U}{\partial y} = -\frac{dP}{dx} + Pr.\Delta U \qquad (8)$$

$$U\frac{\partial V}{\partial x} + V\frac{\partial V}{\partial y} = -\frac{dP}{dy} + Pr.\Delta V + Ra.Pr.(T - 0.5) \qquad (9)$$

* **Energy :**

$$U\frac{\partial T}{\partial x} + V\frac{\partial T}{\partial y} = \Delta T + \frac{1}{3N_{CR}}.\Delta G \qquad (10)$$

* **Radiative transfer :**

$$\frac{\partial^2 G}{\partial x^2} + \frac{\partial^2 G}{\partial y^2} - 3.\tau_o^2.A^2.(1 - \Omega_o).G = \qquad (11)$$

$$- 12.A^2.\tau_o^2.(1 - \Omega_o).\frac{(T_{ref} + T - 0.5)^4}{T_{ref}^4}$$

where the non-dimensional variables are defined as :
$x = x^*/Y_{max}$, $y = y^*/Y_{max}$, $A = Y_{max}/X_{max}$, $U = U^*.Y_{max}/a$, $V = V^*.Y_{max}/a$,
$T = (T^* - T^*_H)/(T^*_C - T^*_C)$, $T^*_{ref} = (T^*_H + T^*_C)/2$, $T'_{ref} = T^*_{ref}/(T^*_H - T^*_C)$
$G = G^*/(\sigma_o.T^{*4}_{ref})$, $\tau_o = \beta.X_{max}$, $N_{CR} = \lambda.\beta(T^*_H - T^*_C)/(\sigma_o.T^{*4}_{ref})$

The boundary conditions in a dimensionless form are :
U = V = 0 at all the solid surfaces; T(0,y) = 1. and T(1./A,y) = 0

$$\frac{\partial T}{\partial y} + \frac{1}{3N_{CR}} \cdot \frac{\partial G}{\partial y} = 0 \qquad aty = 0 \ \text{V} \ y = 1$$

and

$$\frac{\partial G}{\partial n_i} = \pm \frac{3 . \tau_o . A . \epsilon_i}{4 - 2\epsilon_i} . [G - 4 . (T_i + T_{ref} - 0.5)^4 / T_{ref}^4]$$

Where n_i denotes the coordinates normal to the wall, "i" denotes quantities at the wall i (i = 1, 2, 3, 4). T_i, ϵ_i are the dimensionless temperature and the emissivity of the wall i. The positive sign is taken at x = 0 or y = 0, and the negative sign at x = 1/A or y = 1. The governing equations (7)-(11) are solved by integration on elementary control volumes of all the set of differential equations including radiation transfer, and finite difference formulation. The transport-diffusion equations are expressed using a hybrid scheme. The **SIMPLER** algorithm [5], is used to obtain iteratively the solutions and by the use of a staggered grid ensures a conservative formulation.

4.3. - NUMERICAL RESULTS AND DISCUSSION

While the values of the parameters concerning natural convection are assumed to be constant, the effects of radiation on the natural convection in a square cavity are examined by decreasing the Planck number N_{CR} or by increasing the optical thickness τ_o. In the first computations, the "**Window Problem**" is treated with a Planck number decreasing from 10 to 0.05. Figure 4 shows the isotherms, streamlines and heatlines for two different Planck numbers with the same values of optical thickness (τ_o = 1) and of Rayleigh number (Ra = 10^8). It indicates that when N_{CR} decreases, the isotherms become closer near the top of the hot wall, and near the bottom of the cold wall. This phenomenon is coupled with a decrease in vertical gradient of the temperature. Furthermore, when the radiative participation becomes more important. The effect of the Planck number on the mean Nusselt number at the hot wall is presented in table 1. The effect of radiation on natural convection clearly appears with the decrease in N_{CR} [6-7]. The mean Nusselt number for convection decreases because the medium near the hot wall absorbs radiation and so makes the temperature gradient at the lower lower. However, the radiative heat transfer is so intense near the hot wall that the radiative Nusselt number increases, whereas, for the window problem, the mean Nusselt number is independent of coordinate x in the all vertical plan, and is equal to the value at the hot wall .

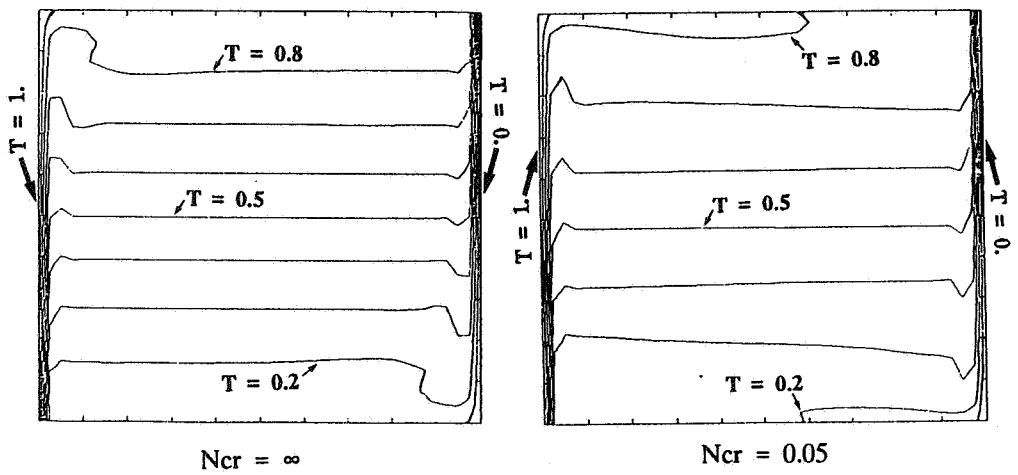


Figure 4 : Effect of parameter interaction N_{CR} on isotherms patterns, (Ra = 10^8, τ_o = 1., A = 1., Ω_o = 0., Pr = 0.71, ϵ_1 = ϵ_2 = 1., ϵ_3 = ϵ_4 = 0.).

Interaction parameter N_{CR}	Mean Nusselt number for convection	Mean Nusselt number for radiation	Mean total Nusselt number
∞	30.02	0.00	30.02
1	29.91	0.54	30.45
0.1	28.75	5.42	34.17
0.05	27.74	10.78	37.52

Table 1 : Effect of Planck number on the mean Nusselt number at the hot wall
(τ_o = 1., A = 1., Ra = 10^8, Ω_o = 0., ε_1 = ε_2 = 1., ε_3 = ε_4 = 0.)

5. - CONCLUSION

The two examples presented here are only to illustrate what can be the effect of radiative heat transfer on flow patterns and heat transfer in natural convection. In some cases, radiative participation of water vapor in air may represent around of 10% of the total heat fluxes exchanged in a room, if this phenomenon can be neglected in most applications, it can significantly perturb the evaluation of convective heat transfer at the surfaces of the walls. Furtheremore as far as scale models using water or freon are used to study natural convection in rooms, the results obtained with such fluids should be carefuly analyse before their application to building physics.

REFERENCES

[1] J. TAINE
"Spectres d'absorption à haute résolution des mélanges H_2O, $C0_2$ gaz neutres", personal comunication, Ecole Centrale des Arts et Manufactures, Paris, 1985.

[2] F. ALLARD
"Contribution à l'étude des transferts de chaleur dans les cavités thermiquement entrainées à grand nombre de Rayleigh". Thèse de Doctorat ès Sciences, INSA Lyon 1987.

[3] F. ALLARD, J. BRAU, C. INARD and J. M. PALLIER
"Thermal experiments of full scale dwelling cells in artificial climatic conditions". Energy and Buildings, N° 10, P. 49-58, 1987.

[4] M. N. ÖZISIK
" Radiative Transfer and interactions with Conduction and Convection", Wiley-Interscience, New York, (1973).

[5] S. V. PATANKAR,
"Numerical Heat Transfer and Fluid Flow", Mac Graw Hill Edit., London, (1980).

[6] A. DRAOUI, J. P. SIMONEAU, F. ALLARD,
"Combined radiation and convection in gray fluids enclosed in 2D cavities", ASME Winter Meeting, Chicago, december, Vol. 3, pp.141-146, (1988).

[7] A. DRAOUI, F. ALLARD, C. BEGHEIN,
"Numerical Analysis of Heat Transfer by Natural Convection and Radiation in Participating Fluide Enclosed in Square Cavities", **Numerical Heat Transfer**, Part A, Vol. 20, pp. 001-009, 1991.

AIR MOVEMENT & VENTILATION CONTROL WITHIN BUILDINGS

12th AIVC Conference, Ottawa, Canada
24-27 September, 1991

POSTER 51

Crack flow. A power law estimation technique.

Johnny Kronvall

Department of Building Science
Lund University
P.O. Box 118
S-221 00 LUND
Sweden

Synopsis

A set of diagrams for estimating flow coefficients and exponents in the power law flow equation for cracks are presented. The diagrams are primarily intended for those who perform infiltration calculations by hand or by using a computer program for single and multi zone infiltration and ventilation calculations.

The error introduced by the estimation technique is compensated for by means of a correction coefficient with a specific value in different pressure difference intervals. A computer program performing the calculations behind the diagrams is available for public use.

1. Introduction

For many purposes a power law approach is useful in order to describe the flow behaviour of a crack or an air gap. Many multizone infiltration and ventilation computer programs require a power law description of the flow characteristics of a crack. However, hitherto no simple ways have existed for predicting the flow coefficient and exponent in the power law by means of calculation for a given flow geometry.

2. A power law estimation technique for cracks

The power law flow equation reads:

$$q_v = a * (\text{delta } p)^b$$

where:

q_v = volumetric air flow rate, m3/s
a = flow coefficient, $m3/(s*Pa^b)$
delta p = pressure difference, Pa
b = flow exponent, -

The estimation of the coefficient a and the exponent b is made by means of running a computer program - PET - designed for this application. In the program the full hydraulic equations for duct flow, entrance-, exit-and bend effects are calculated. As these flow equations are not explicit in solving the air flow rate as a

function of the pressure difference a numerical curve fit procedure gives a power law curve fit for a number of calculated corresponding values of pressure difference and air flow rate. The fitted values of the air flow rate is compared to the exact hydraulic solution for each pressure difference. Thus a correction factor is calculated. This factor is depending on the pressure difference.

The calculations have been made for different crack widths between 0.5 and 10 mm. The bredth of the crack is always 1.00 m and the length in flow direction varies between 0 and 500 mm. For some cases a 90 deg bend is included too. The pressure difference interval chosen is 1 to 50 Pa which in most cases should be applicable for practical use.

The computer program performing the calculations behind the diagrams is available for public use by contacting the author.

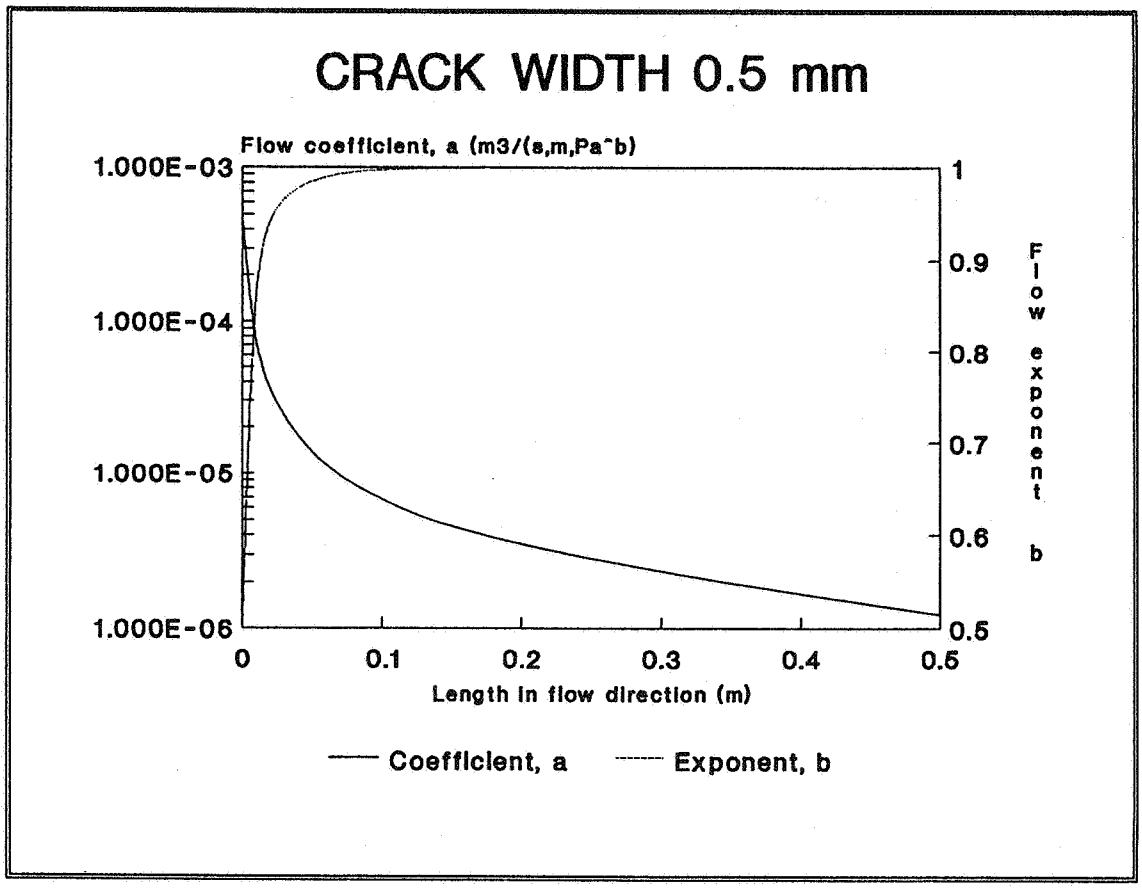
3. Results

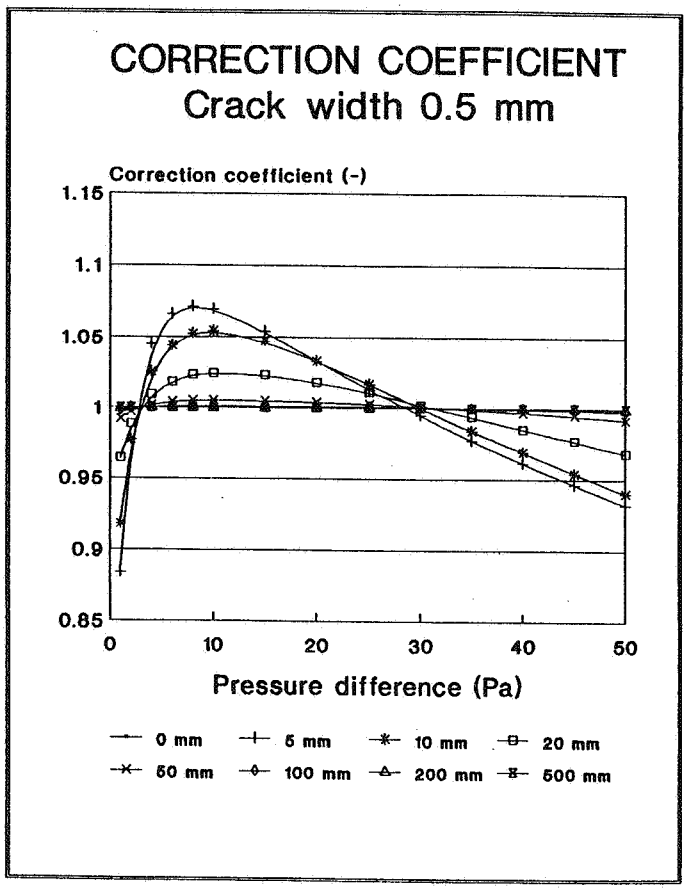
The calculations for each crack width are summarized in two diagrams, the first one showing the variation in the flow coefficient and exponent for different lengts in flow direction and the second one showing the different values a correction coefficient takes for different pressure differences. Each flow length has its own curve.

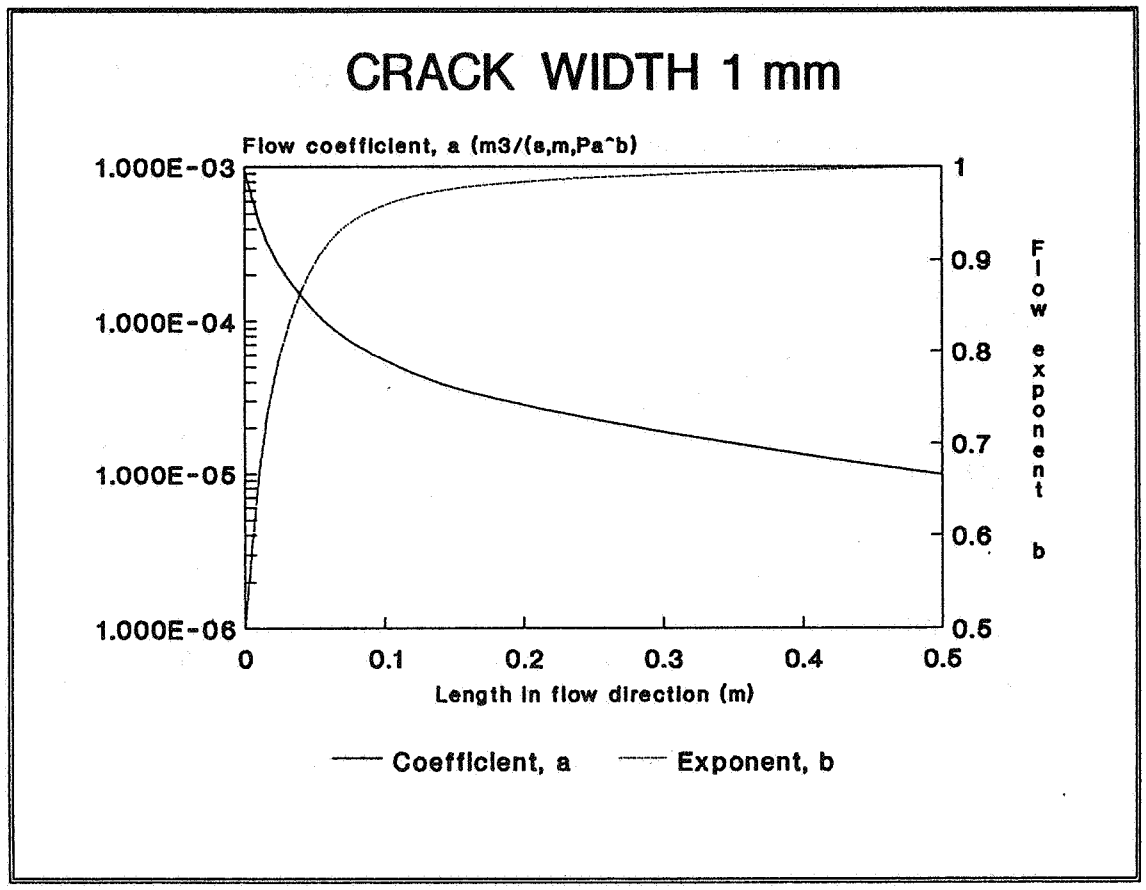
The air flow rate is eventually calculated as:

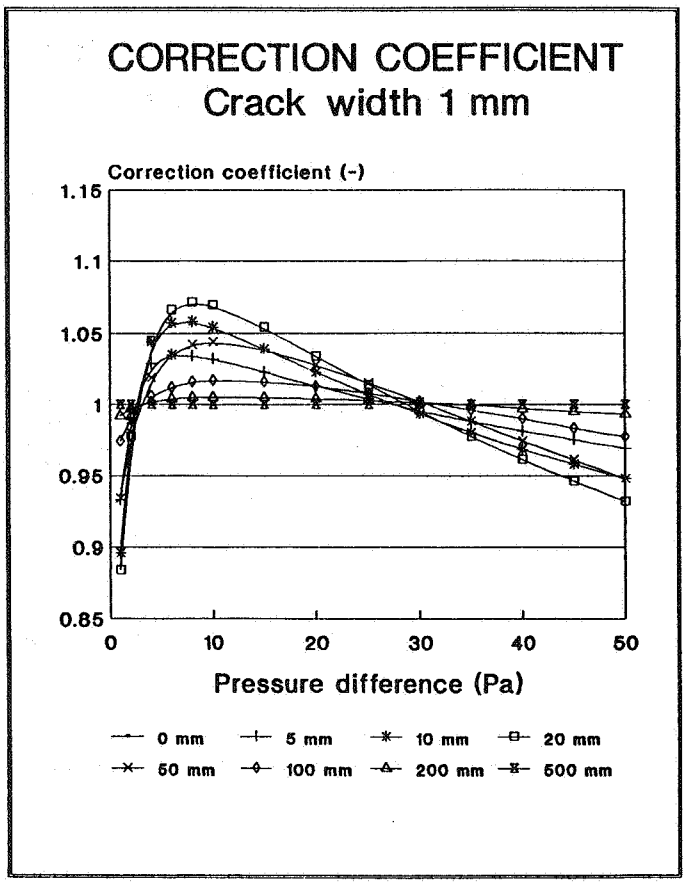
$$q_v = \text{correction coefficient} * a * (\text{delta p})^b$$

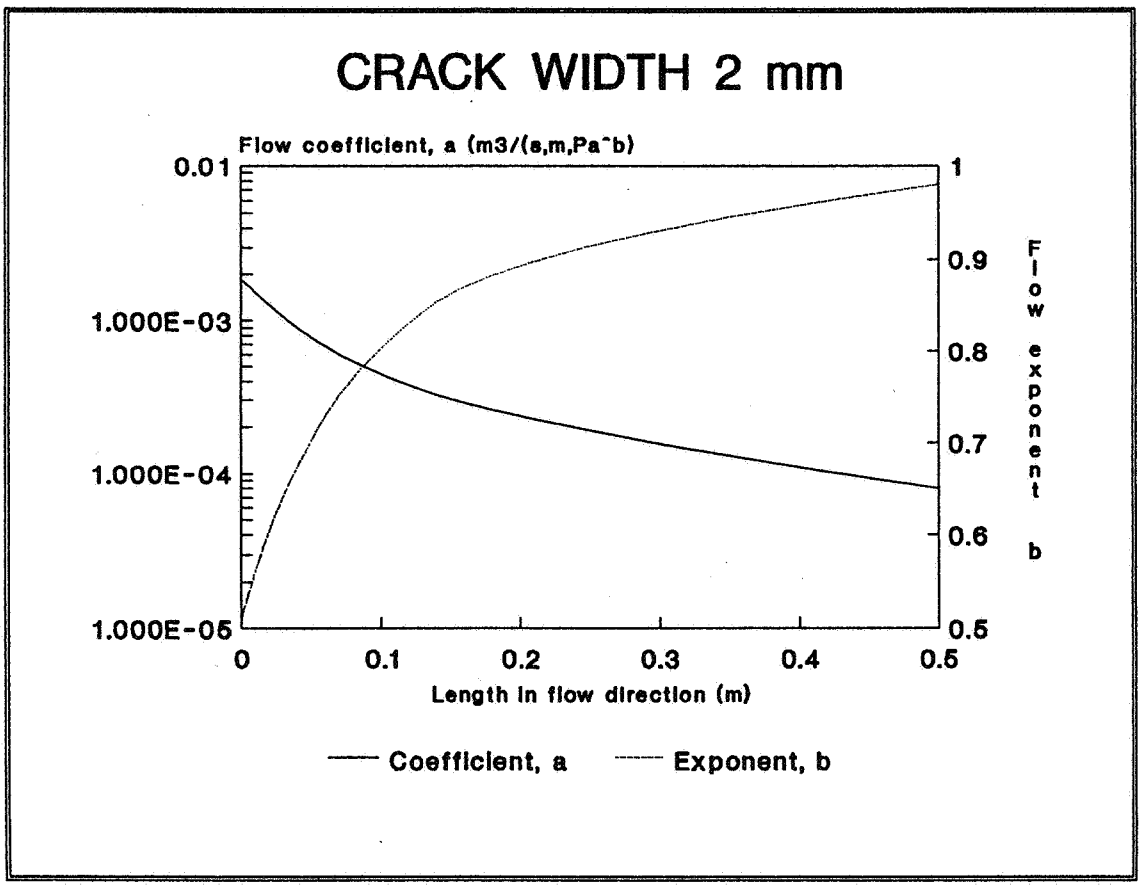
If the demands on the degree of accuracy of the calculated flow rate is less than e.g. ten percent, no correction coefficient needs to be applied at all. For many applications this is sufficient depending on the fact that other factors are determined with (far) less accuracy, by no means less the crack width.

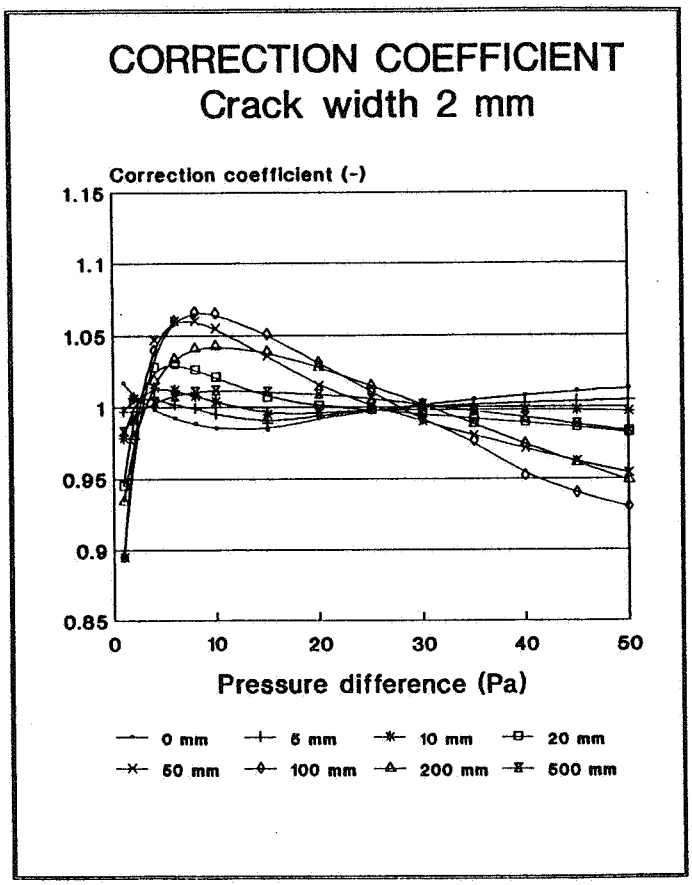

CRACK WIDTH 0.5 mm
Flow coefficient, a (m3/(s,m,Pa^b)
1.000E-03
1.000E-04
1.000E-05
1.000E-06
1
0.9
0.8
0.7
0.6
0.5
Flow exponent b
0
0.1
0.2
0.3
0.4
0.5
Length in flow direction (m)
Coefficient, a
Exponent, b

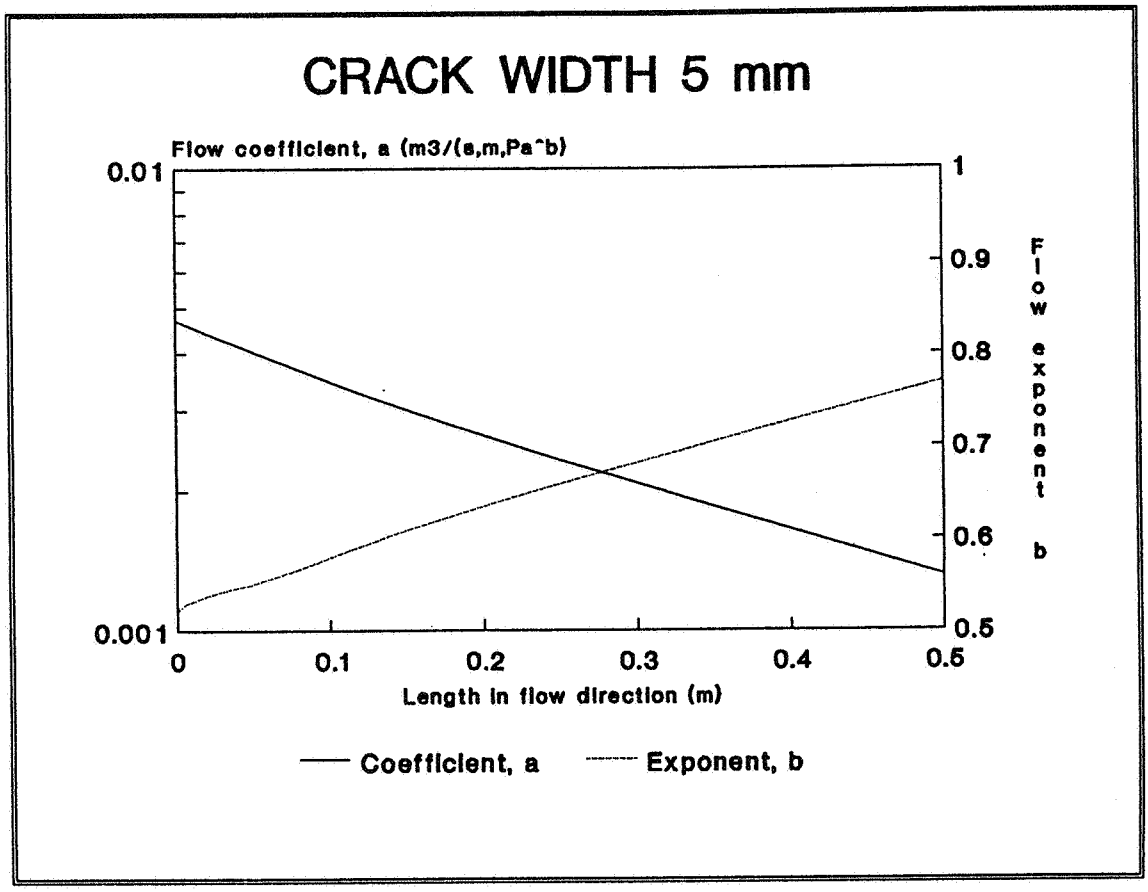

CORRECTION COEFFICIENT
Crack width 0.5 mm
Correction coefficient (-)
1.15
1.1
1.05
1
0.95
0.9
0.85
0
10
20
30
40
50
Pressure difference (Pa)
0 mm
5 mm
10 mm
20 mm
50 mm
100 mm
200 mm
500 mm

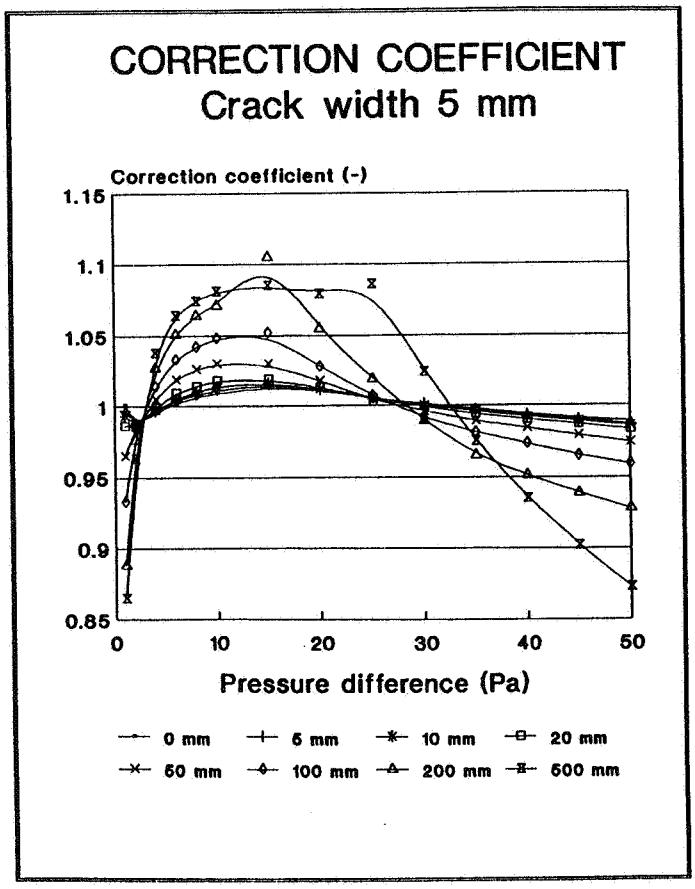

CRACK WIDTH 1 mm
Flow coefficient, a (m3/(s,m,Pa^b)
1.000E-03
1.000E-04
1.000E-05
1.000E-06
1
0.9
0.8
0.7
0.6
0.5
Flow exponent b
0
0.1
0.2
0.3
0.4
0.5
Length in flow direction (m)
Coefficient, a
Exponent, b

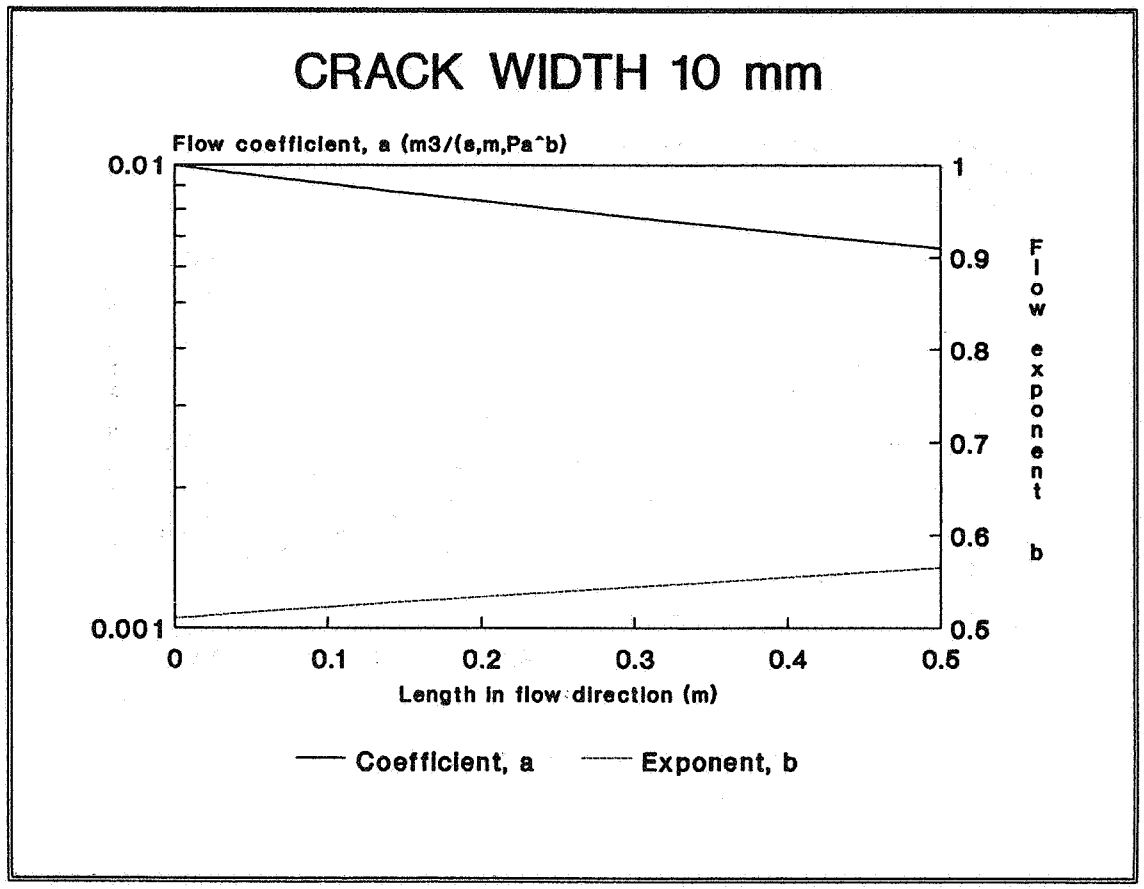

CORRECTION COEFFICIENT
Crack width 1 mm
Correction coefficient (-)
1.15
1.1
1.05
1
0.95
0.9
0.85
0
10
20
30
40
50
Pressure difference (Pa)
0 mm
5 mm
10 mm
20 mm
50 mm
100 mm
200 mm
500 mm

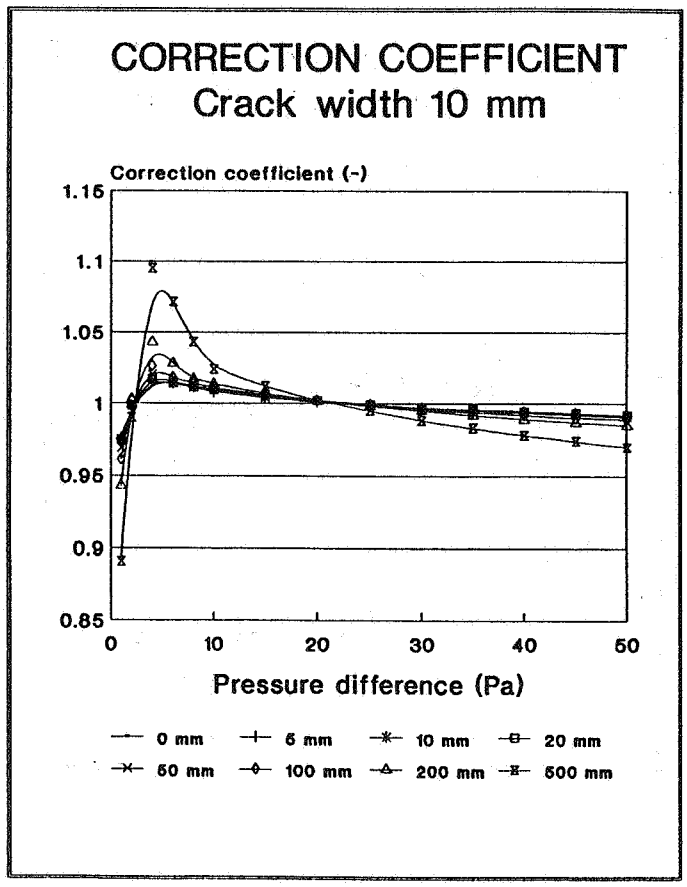

CRACK WIDTH 2 mm
Flow coefficient, a (m3/(s,m,Pa^b)
0.01
1.000E-03
1.000E-04
1.000E-05
1
0.9
0.8
0.7
0.6
0.5
Flow exponent b
0
0.1
0.2
0.3
0.4
0.5
Length in flow direction (m)
Coefficient, a
Exponent, b


CORRECTION COEFFICIENT
Crack width 2 mm
Correction coefficient (-)
1.15
1.1
1.05
1
0.95
0.9
0.85
0
10
20
30
40
50
Pressure difference (Pa)
0 mm
5 mm
10 mm
20 mm
50 mm
100 mm
200 mm
500 mm

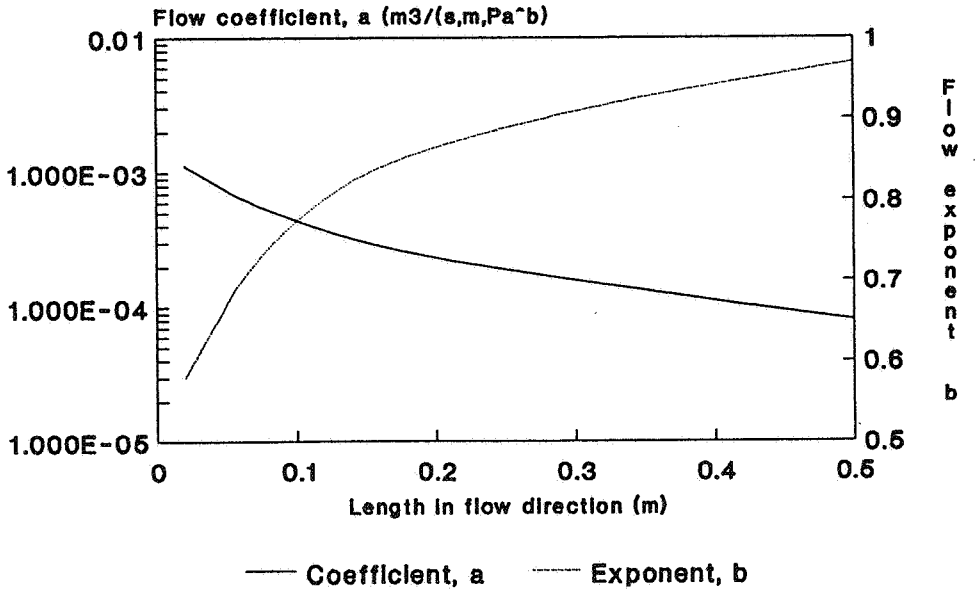

CRACK WIDTH 5 mm
Flow coefficient, a (m3/(s,m,Pa^b)
0.01
0.001
1
0.9
0.8
0.7
0.6
0.5
Flow exponent b
0
0.1
0.2
0.3
0.4
0.5
Length in flow direction (m)
Coefficient, a
Exponent, b


CORRECTION COEFFICIENT
Crack width 5 mm
Correction coefficient (-)
1.15
1.1
1.05
1
0.95
0.9
0.85
0
10
20
30
40
50
Pressure difference (Pa)
0 mm
5 mm
10 mm
20 mm
50 mm
100 mm
200 mm
500 mm

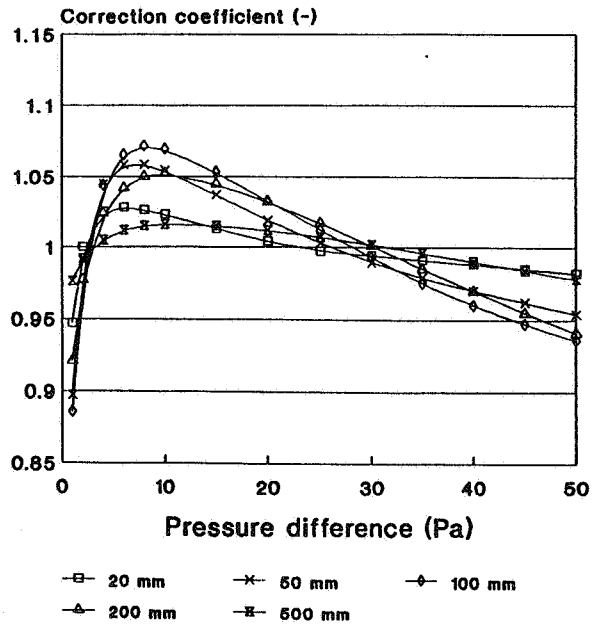

CRACK WIDTH 10 mm
Flow coefficient, a (m3/(s,m,Pa^b)
0.01
0.001
1
0.9
0.8
0.7
0.6
0.5
Flow exponent b
0
0.1
0.2
0.3
0.4
0.5
Length in flow direction (m)
Coefficient, a
Exponent, b


CORRECTION COEFFICIENT
Crack width 10 mm
Correction coefficient (-)
1.15
1.1
1.05
1
0.95
0.9
0.85
0
10
20
30
40
50
Pressure difference (Pa)
0 mm
6 mm
10 mm
20 mm
50 mm
100 mm
200 mm
500 mm

CRACK WIDTH 2 mm
1 bend



CORRECTION COEFFICIENT
Crack width 2 mm, 1 bend



AIR MOVEMENT & VENTILATION CONTROL WITHIN BUILDINGS

12th AIVC Conference, Ottawa, Canada
24-27 September, 1991

POSTER 52

USING THERMOFOIL HEATERS FOR THE EXPERIMENTAL DETERMINATION OF THE AIR FLOW PATTERNS IN A ROOM.

G. Cannistraro*, C. Giaconia*, G. Rizzo#

* Dipartimento di Energetica ed Applicazioni di Fisica, Università di Palermo, Viale delle Scienze, 90128 Palermo, Italy.

\# Istituto di Ingegneria Civile ed Energetica, Facoltà di Ingegneria, Università di Reggio Calabria, Italy.

USING THERMOFOIL HEATERS FOR THE EXPERIMENTAL DETERMINATION OF THE AIR FLOW PATTERNS IN A ROOM

Synopsis

A new simple method is here proposed for the experimental singling out of the air flow patterns in a room. It is based on the use of a series of thermofoil probes, arranged in a lattice, that can be suspended at the ceiling of the room under test.

1. Guidelines

Relative air velocity is notoriously a fundamental parameter when analyzing thermal comfort conditions inside confined environments. It is necessary for the computation of convective heat exchanges from the human body to the surroundings as well as the value of the clothing temperature. Recently researchers have found a strong dependence of the thermal conditions from the draughts induced by the turbulence of the air flowing in a room.
Usually, precise air flow measurements are performed using hot wires anemometers that, as it is well known, are high precision, high cost instruments. Moreover the stochastic characteristics of the involved physical phenomena, makes a very high instantaneous precision a less significant effort. Starting from these considerations a new simple technique is here proposed.
It is based on the use of a series of rows of thermofoil heaters, suspended at the ceiling of the room. Each probe is easily built-up by means of some inexpensive Pt-100 thermal ribbons: it should enable the evaluation of both air velocity and direction. The thermal behaviour of the probes has been tested in a little wind tunnel facility in the aim of establishing suitable relationships between the air direction and velocity in the nearby space of the probe and its heat losses. As a matter of fact, our measurements concern the electrical resistance of the probe using the four-wire method.
Through the paper some preliminary measures are presented, especially regarding the relationships between the air velocity and the temperature difference between the opposite layers of the probe, in parallel flow. Moreover, the influence of varying the incidence angle, at constant air velocity, has been also investigated.

2. Experimental facilities description

Figure 1 depicts the structure of the probe here used, along with the electrical connections. It contains four low-cost, non-matched PT-100 thermal ribbons. Each of them represents a thermofoil, that is a thin, flexible heating element, with its surface homogeneously heated. The real advantage of this feature is that two out four thermofoils can be used at the same time as a heater element and temperature sensor, when they are driven by a constant current, slightly higher than this one normally employed in the standard measurements.
This current, determining an increase in the foil surface temperature, produces also an easily measurable temperature difference between the heated elements and the elements subjected to the standard current value.
By means of the measure of this temperature, when a well known air flow is superimposed, it is possible to establish a relationship between the above cited temperature difference and the relative air velocity. The air flow can be, of course, produced by means of a suitable fan or simply generated by the natural convection movement existing in the room.
The peculiar arrangement of the probe, as illustrated in the section A-A of Figure 1, creates a strong thermal asymmetry due to the small insulation layers applied on the opposite sides of the probe in correspondence of the heated elements.
This allows the probe to have a different behaviour with respect to the air flow direction.
In order to increase the measuring precision, all the elements (heated or not), even belonging to different probes, should be connected in series, within the voltage supply capability of the current generator.

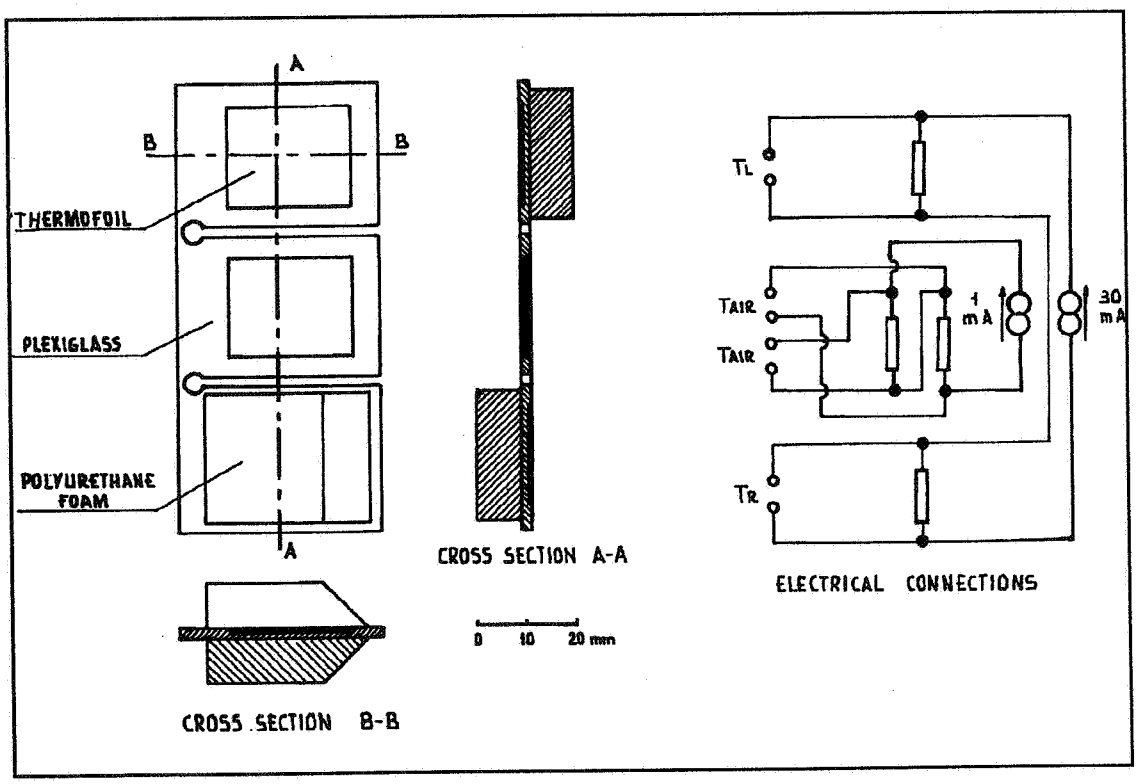


Figure 1. The sketch of the probe with the electrical connections.

As all the resistance share the same current, this turns out in the evident advantage of reducing the causes of error in the four-wire measurement.

3. Measurement methods and summary of the results.

Tests have been carried out in a wind tunnel facility where comparative measures of the air velocity have been performed using a high precision, low-response-time, laser calibrated TSI Anemometer Mod 8450/20M. Two kinds of measures have been accomplished: the first one has been conducted for several values of the air velocity, in steady-state conditions, in order to establish the relationship between the air velocity and the temperature difference between the hot and cold thermofoils, for each side of the probe.
The second has been carried out maintaining at a given value the air velocity and rotating the probe in order to vary the angle between air flux and the normal to the probe surface. This measure has been performed in the aim of finding the relationship between the direction of the air flux and the deviation between the "left" and "right" temperature difference. Because of the complexity of the probe geometry any theoretical prediction would be affected by the poor knowledge of the involved physical phenomena (local turbulence, sharp or blunt edge of the probe, heat transfer coefficients of the materials).
As a consequence we have tried to use a general formula for the heat transfer from a plate in parallel flow valid for Prandtl numbers above 0.6 and supposing that no transition occurs through the plate ($Re_{fluid} << 5 \cdot 10^5$). That is:

$$Nu = 0.664 \cdot Re_{fluid}^{1/2} \cdot Pr^{1/3} \qquad (1)$$

The logical procedure for the measurements has been the following: starting from the knowledge of each electrical resistance value, R(T), we calculate the electrical power dissipated by the heated element; moreover, by means of a trivial regression, we are able to determine the element temperature and, then, using the geometrical characteristics of the probe, we calculate the overall heat transfer coefficients and, the Nusselt number. Finally, Reynolds and Prandtl numbers are computed as a function of the thermophysical characteristics of the fluid.

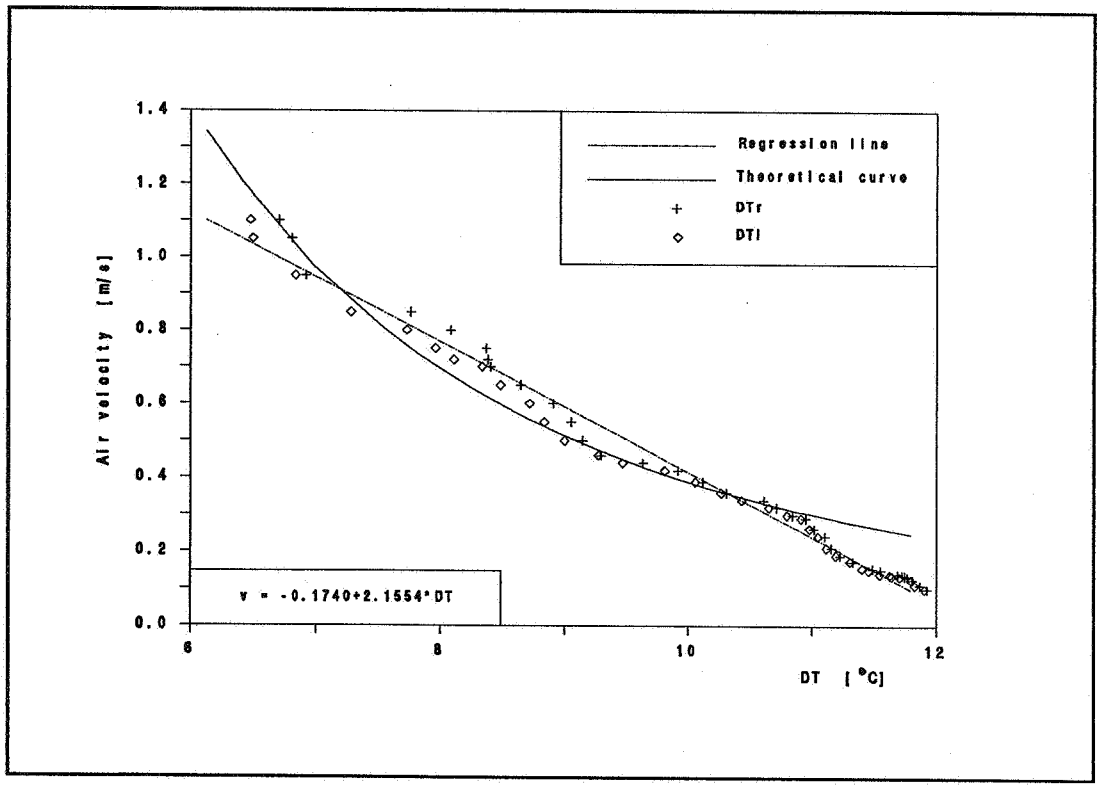


Figure 2. **Relationship between DT and the air velocity (T_{air}=25°C).**

Figure 2 shows the dependence of the temperature difference by the air velocity, both for the "left", DT_l, and "right", DT_r, side of the probe. In the same figure we have reported, in solid line, the equation 1, and, in dashed line, the first-order regression over all the experimental points. It is evident that the empirical relation doesn't apply for lower values of the air velocity, near the field of the natural convection.

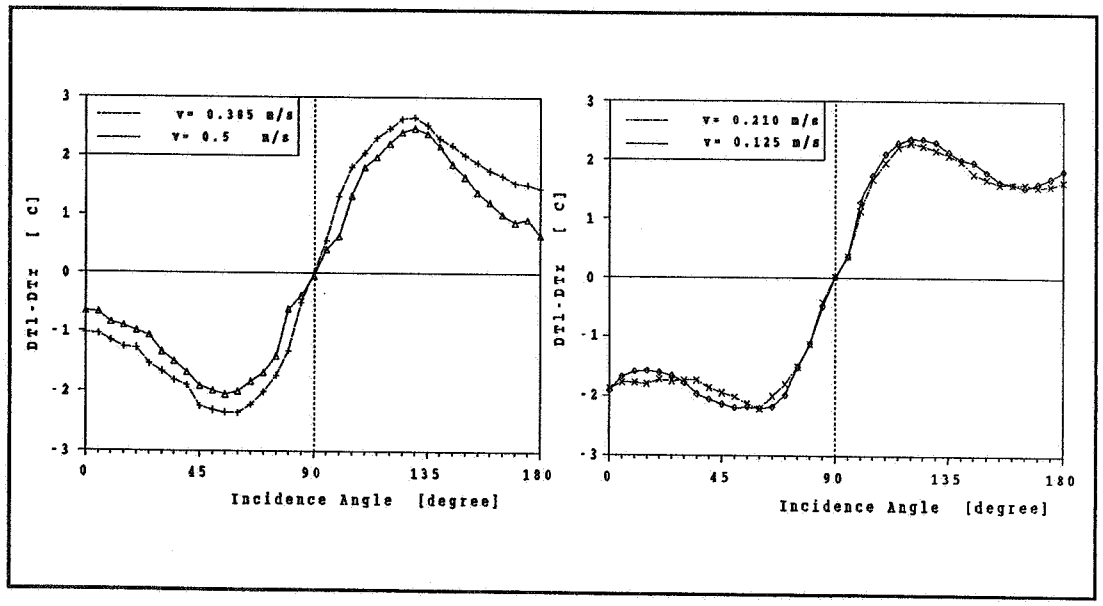


Figure 3. **Relative temperature difference as a function of the incidence angle, for two ranges of air velocity (T_{air}=25°C).**

As previously stated, we have also carried out several measures at a constant value of the air velocity, in the aim of investigating the influence of the incidence angle variations.
Figure 3 depicts some experimental results for two different velocity ranges. As it is well evident, at lower values of the air velocity the dependence of the relative temperature difference (that is DT_l-DT_r) by the incidence angle, shows a more clear relationship, and a larger zone where an univocal value of the incidence angle could be found.
Figure 4 shows all the experimental points and a tentative regression line valid for incidence angles close to 90 degrees.
Analysis of the heat loss from circular cylinders, has demonstrated that the Nu number is nearly independent of the temperature difference between the heated element and the ambient fluid. This result appears to hold when either the air temperature or the probe temperature is changed.

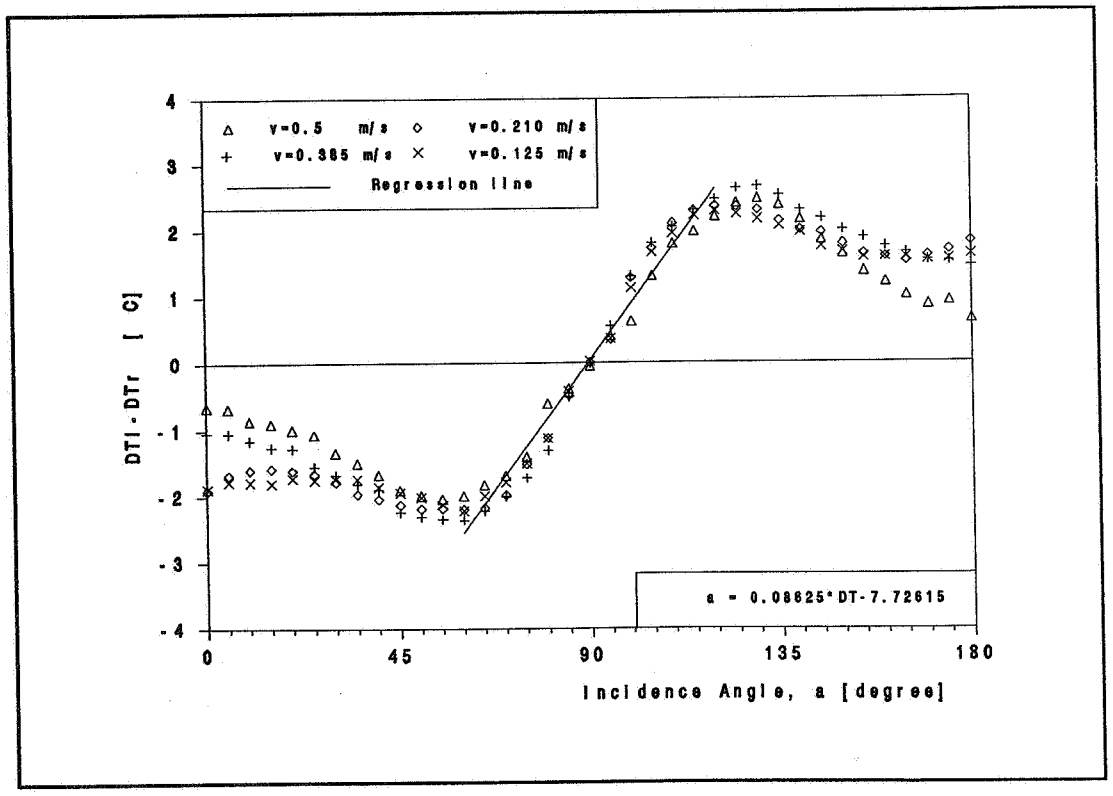


Figure 4. Sketch of the experimental points with a tentative regression line.

Some further experiments have demonstrated that this conditions could be applied even in our case.

5. Conclusions

Due to its characteristics, the proposed method candidates itself as a very suitable tool to be employed in rooms, with minor interventions. The only equipments needed are a constant current source, a series of thermofoils, a four-wires resistance meter and a high speed (or sample and hold) data logger.

6. Bibliography

INCROPERA F.P. & De WITT D.P. "Fundamentals of heat and mass transfer". J. Wiley & Sons, New York, 1990

SANDBORN V.A. "Resistance temperature transducers", Metrology Press, 1972.

AIR MOVEMENT & VENTILATION CONTROL WITHIN BUILDINGS

12th AIVC Conference, Ottawa, Canada
24-27 September, 1991

POSTER 53

HOT WIRE/FILM ANEMOMETRY FOR ROOM AIR MOTION STUDIES

J. S. Zhang, G. J. Wu and L. L. Christianson

Bioenvironmental Engineering Research Laboratory
University of Illinois at Urbana-Champaign

HOT WIRE/FILM ANEMOMETRY FOR ROOM AIR MOTION STUDIES

J.S. Zhang, G.J. Wu and L.L. Christianson

Bioenvironmental Engineering Research Laboratory
University of Illinois at Urbana-Champaign

SYNOPSIS

Application of hot wire/film anemometry in room air flows presents difficulties because: (1) the effect of natural convection due to the heated wire becomes significant for low air velocity measurements; (2) the angle sensitivity of a hot wire becomes small at low air velocities, which makes it difficult to resolve the direction of each velocity component. This study aimed at quantifying the uncertainty of the hot wire anemometry and examining the angle sensitivity of a hot wire in low air velocity measurements. Based on the experiments, it was concluded that: (1) the uncertainties due to natural convection in the velocity measurements with a single component hot wire probe operating at 200 °C wire temperature are within ±15%, ±5%, ±3%, ±1% and 0.5% for velocities of 0.05 ~ 0.1 m/s, 0.1 ~ 0.15 m/s, 0.15 ~ 0.25 m/s and 0.25 ~ 0.5 m/s, respectively, and correction can be made based on the visualization of the room air flow pattern to achieve higher accuracy; (2) air velocity components can not be measured simultaneously with multi-component hot wire probes if the air velocity is below 0.2 m/s since the angle sensitivity of the probe will be heavily contaminated by the noise signal due to the natural convection.

1. INTRODUCTION

Hot wire/film anemometers belong to the family of thermal anemometers which include hot wire, film and ball (i.e., omnidirectional) sensors. They measure the fluid velocity by sensing the changes in heat transfer from a small, electrically heated sensing element exposed to the fluid motion. This technique is most widely used in measuring room air flows because it satisfies most of the following requirements for a ideal instrument:

(1) have high sensitivity for measuring turbulent fluctuations,
(2) measure a wide velocity range,
(3) be small in size for an essentially point measurement,
(4) have high accuracy,
(5) have high resolution (low noise),
(6) create minimal flow disturbance,
(7) be unsensitive to the air temperature variation within the room,
(8) measure velocity components and detect flow reversal,
(9) be low in cost, and

(10) be easy to use.

Many researchers studying room air motion have used the omnidirectional probe (e.g., Awbi and Nemri[1], Holfman[4], Popiolek[6], and Zhang et al.[9]) which is insensitive to the velocity direction and therefore essentially measures the total speed. Special attention has been paid to the design of this type of sensor so that it is mainly for low velocity measurements (0 to 3.5 m/s). Due to the relatively large size of its sensing element (1 to 2 mm in diameter), this type of sensor typically has a time constant of about 2 seconds. Therefore, it is excellent for measuring mean velocity, but not suitable for measuring velocity fluctuations.

Hot wire/film probes have small sensing elements (typically 4 to 50 μm in diameter by 1 to 1.5 mm long) and can detect high frequency velocity fluctuations. They have been used for studying the mean and turbulent characteristics of the room air flow (e.g., Sandberg[7] and Zhang et al.[10]). The small probe size is also critical to the measurement of velocity profiles at the diffuser and within the boundary layers over surfaces of ceiling, wall, floor and internal obstructions. Sandberg[8] used a wire probe to measure the velocity profile within the boundary layer over the ceiling surface.

Multi-component sensors have also been used to detect the direction of air velocity as well as its magnitude, but applications have so far been limited to the measurements in reduced scale rooms with high air flow rates (Murakami and Komine[5]). Resolving components low air velocities is more difficult because the angle sensitivity of the hot wire/film probes decreases as velocity decreases. Studies are needed to quantify the angle sensitivity of multi-component hot wire/film probes in the low velocity range.

A difficulty involved in low air velocity measurements with the hot wire/film anemometers is to account for the effect of natural convection over the sensing element. The natural convection creates local air movement around the sensing element and causes error in the actual velocity signal. This error becomes significant when the air velocities are low (<0.25 m/s), which is typical in the occupied regions of ventilated rooms. Therefore, the uncertainty in measuring low air velocities with the hot wire/film anemometers needs to be quantified and when necessary, measured values adjusted to account for the error due to the natural convection.

Another problem with the hot wire/film anemometers is its difficulty in detecting flow reversal. A so called "flying hot wire anemometry" is developed for detecting flow reversal (Foss[3]), but the flying probe support is likely to disturb the flow field significantly since room air flows usually involve recirculations. Therefore, flow visualization techniques are usually used to complement thermal anemometers to obtain the general air flow patterns within the room.

2. OBJECTIVES

(1) Quantify the uncertainty of the hot wire/film anemometry in low air velocity measurements;

(2) Examine the angle sensitivity of a multi-component hot wire probe in low air velocity measurements.

3. FACILITY AND PROCEDURES

The experimental set up is shown in Figure 1. Air jets were generated by a commercial calibrator (TSI model 1125) of hot wire/film probes, the principles of which are described in detail by Fingerson[2]. Velocities of the jets were determined by the pressure drops across the nozzle, which were measured with a high precision pressure transducer (Valendyn model DP103). The air jet was directed either upward or downward to study the effect of thermal buoyancy on the air velocity measurement. The probe tested was a 2-D cross wire probe (TSI model 1247A) which had two tungsten wires (4 μm in diameter) perpendicular to each other. The probe can be rotated around its axis so that the angle between the wires and the jet flow direction can be varied to study the angle sensitivity of the hot wire probe.

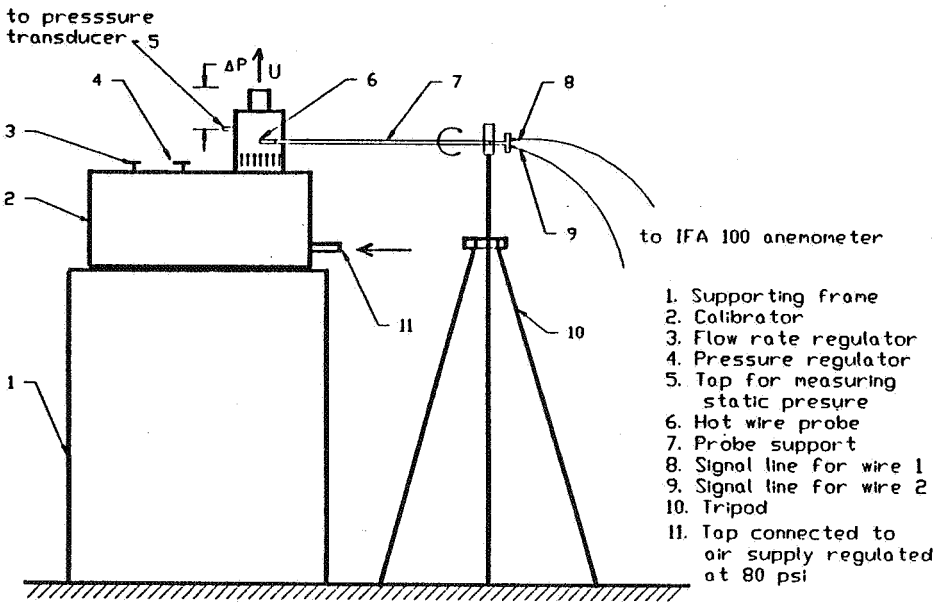


***Figure 1** Experimental set up for testing a hot wire probe*

Tests were conducted in an air conditioned laboratory which provided a constant ambient air temperature of 24$\pm$0.5 °C during the experiments. Two different wire operating temperatures (200 °C and 250 °C, respectively) were used for all the tests to study the effects of the wire operating temperature on the velocity measurements.

4. RESULTS AND DISCUSSIONS

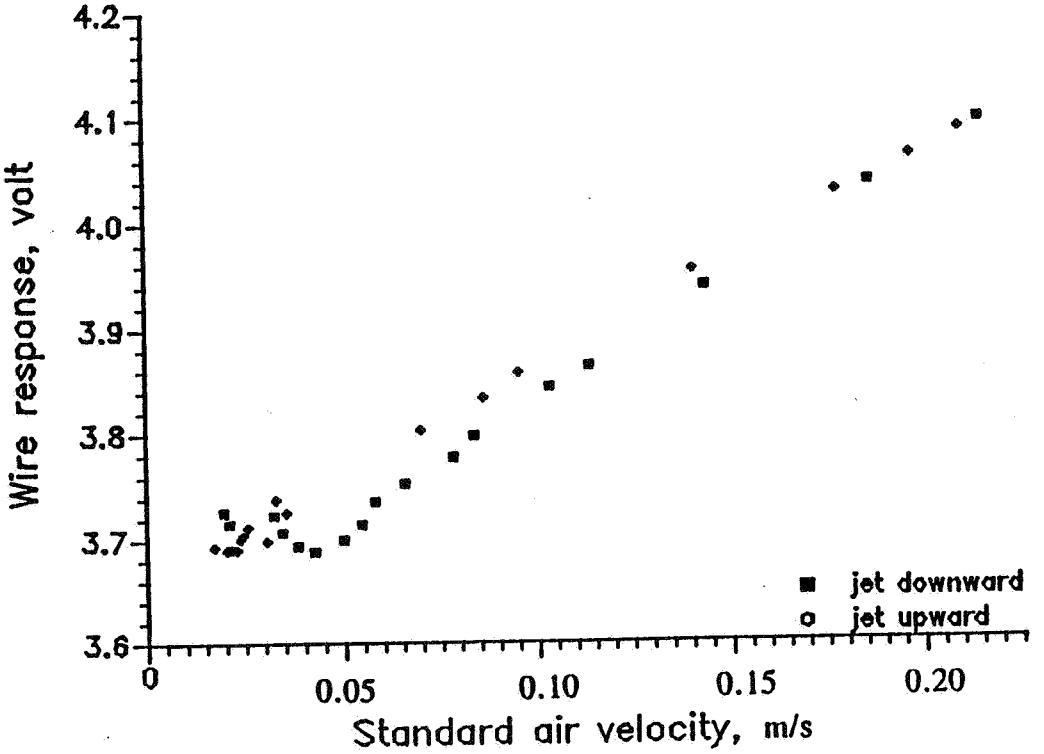
4.1 Uncertainty due to Natural Convection

Hot wire probes operate at higher temperature than the ambient air temperature. The temperature gradient between the wire and the air results in thermal buoyancy which moves air around the wire upward. The thermal buoyancy enhances the flow when the air jet is directed upward, but retards the flow when the air jet was downward. Half the difference between the two is the maximum possible uncertainty (error) due to the natural convection, assuming that the direction of the measured air flow relative to the probe orientation is unknown and that the calculation curve is selected based on horizontal flow.

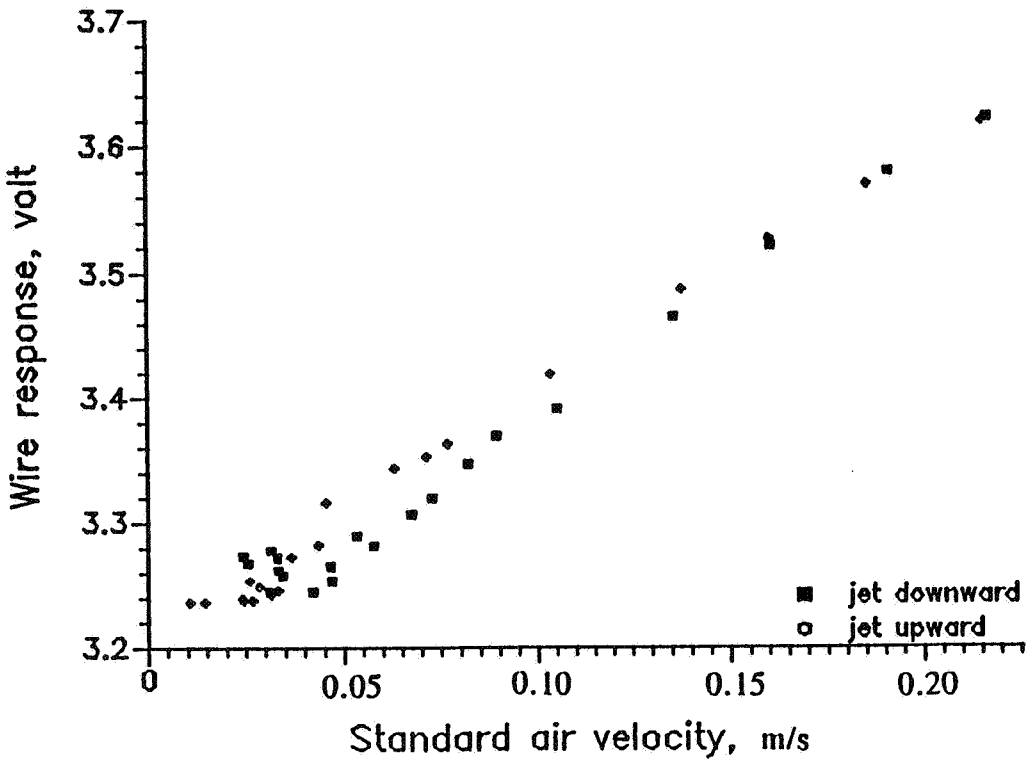
As shown in Figure 2, the difference of the wire output between the two jet orientations became larger as the air velocity decreased. The effect of thermal buoyancy was insignificant when the air velocity was higher than about 0.23 m/s. An interesting phenomena can be seen from the plots for the case when the air jet was downward, in which the wire response decreased when the air velocity increased from 0.025 m/s to about 0.046 m/s. This was because the natural convection was opposing the forced convection and natural convection had the dominating effect on the air movement around the wire when the air velocity (forced convection flow) was below 0.046 m/s.

Figure 3 was obtained by (1) fitting the data in Figures 2a and 2b for each air jet direction with a second order polynomial function using the Least Square Method; (2) calculating the wire response (volts) for a given air velocity (i.e., the X axis) with the obtained curve when the air jet is upward; (3) calculating the velocity corresponding to the wire response (volt) with the obtained curve when the air jet is downward; and (4) calculating half the difference of the two velocities in percentage (i.e., the Y axis). It can be seen that a higher operating temperature of the wire resulted in a higher uncertainty due to the natural convection. At the velocity of 0.05 m/s, the uncertainty was about $\pm 15\%$ and $\pm 20\%$ for 200 °C and 250 °C operating temperatures, respectively.

The relative uncertainty increases when the velocity decreases. Based on Figure 3, the uncertainty in measuring air velocity with 200 °C operating temperature is estimated to be $\pm 15\%$, $\pm 5\%$, $\pm 3\%$, $\pm 1\%$ and $\pm 0.5\%$ for velocities of 0.05 to 0.1 m/s, 0.1 to 0.15 m/s, 0.15 to 0.25 m/s, 0.25 to 0.5 m/s and >0.5 m/s, respectively for the probe operating at 200°C. In other words, the uncertainty due to the natural convection is within ± 0.015 m/s for velocities less than 0.5 m/s, assuming the measured air flow direction is unknown.



a. T_{op} = 250 °C



b. T_{op} = 200 °C

Figure 2 Outputs of wire #1 for two different jet orientations (T_{op} is the operating temperature of the probe)

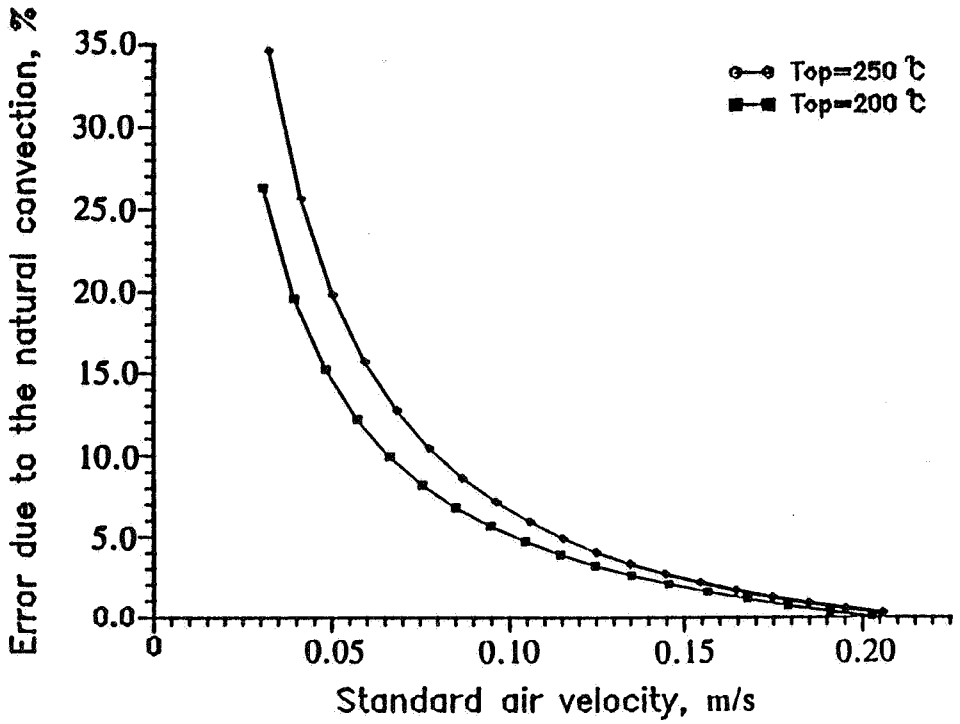


Figure 3 Error due to the natural convection (T_{op} is the operating temperature of the probe)

If one knows the direction of the measured air flow, the above uncertainty due to natural convection becomes a systematic error and can be corrected by calibrating the probe at different orientations relative to the direction of the natural convection flow (i.e., upward). In the measurements of room air ventilation flows, one can use flow visualization techniques to determine the general air flow pattern within the room. The direction of the air flow at measured points can be easily estimated within ± 15 degrees with flow visualization techniques. The systematic error due to the natural convection can then be corrected to improve the accuracy of the velocity measurements significantly.

A lower wire operating temperature would reduce the effect due to the natural convection, but at the same time would also reduce the signal to noise ratio and affect the performance of frequency response. Further studies are needed to determine the optimal wire operating temperature which minimizes the uncertainty due to the natural convection while still provides sufficient signal to noise ratio and satisfactory frequency response performance.

It should be noted that other uncertainty sources such as calibration, voltage measurement, probe positioning and alignment exist in measuring room air velocities. Zhang[11] conducted a detailed analysis of the uncertainties involved in measuring room air velocity distribution.

4.2 Angle Sensitivity of the Hot Wire Probe

The angle sensitivity of the probe was tested by measuring the wire response at different angles between the wires and the jet flow direction (Figure 4). As expected, the output from a wire decreased when the angle between the wire and the jet direction decreased. However, the difference between the outputs at the different angles also decreased as the air velocity decreased and became not appreciable when the velocity was below about 0.18 m/s.

As shown in Figure 5, the angle sensitivity may actually be overwhelmed by the uncertainty due to the natural convection when the air velocity is below 0.20 m/s. As the air velocity increased, the uncertainty decreased and the angle sensitivity increased. Additionally, for a lower wire operating temperature (i.e., 200°C), both the uncertainty due to the natural convection and the angle sensitivity were smaller, but the decrease of the angle sensitivity was much smaller than the decrease of the uncertainty. Therefore, one can use a lower wire operating temperature to reduce the uncertainty due to the natural convection while still maintain relative high angle sensitivity. Again, further studies are needed to determine the optimal wire operating temperature.

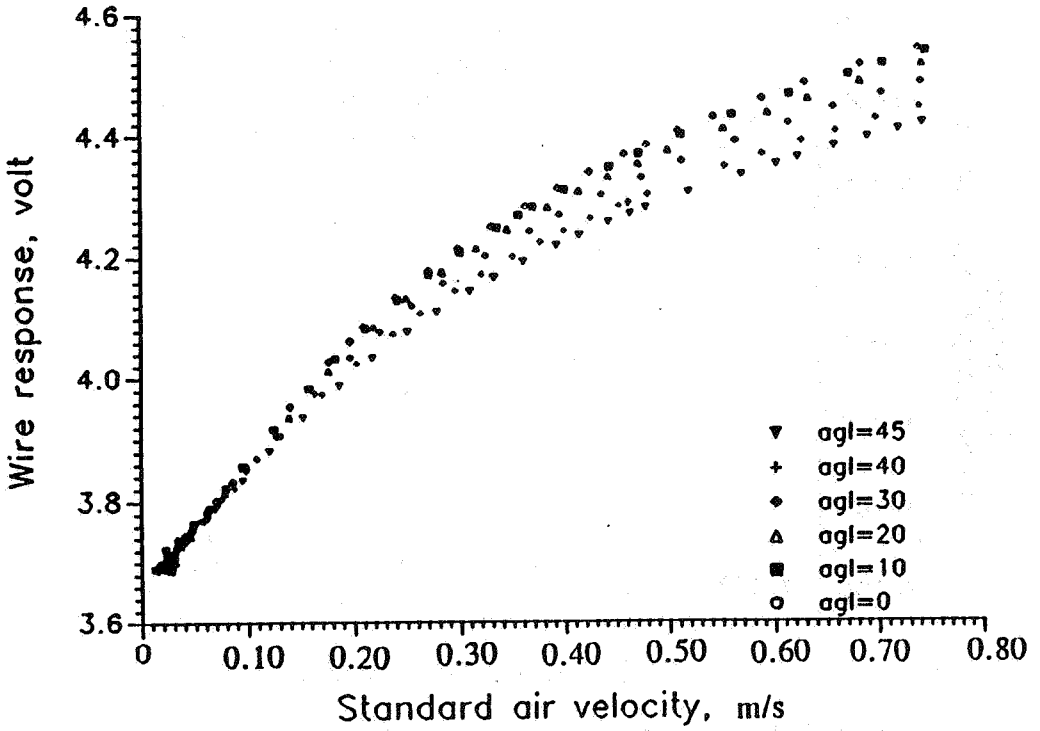
CONCLUSIONS

Based on the above analysis, the following conclusions can be made:

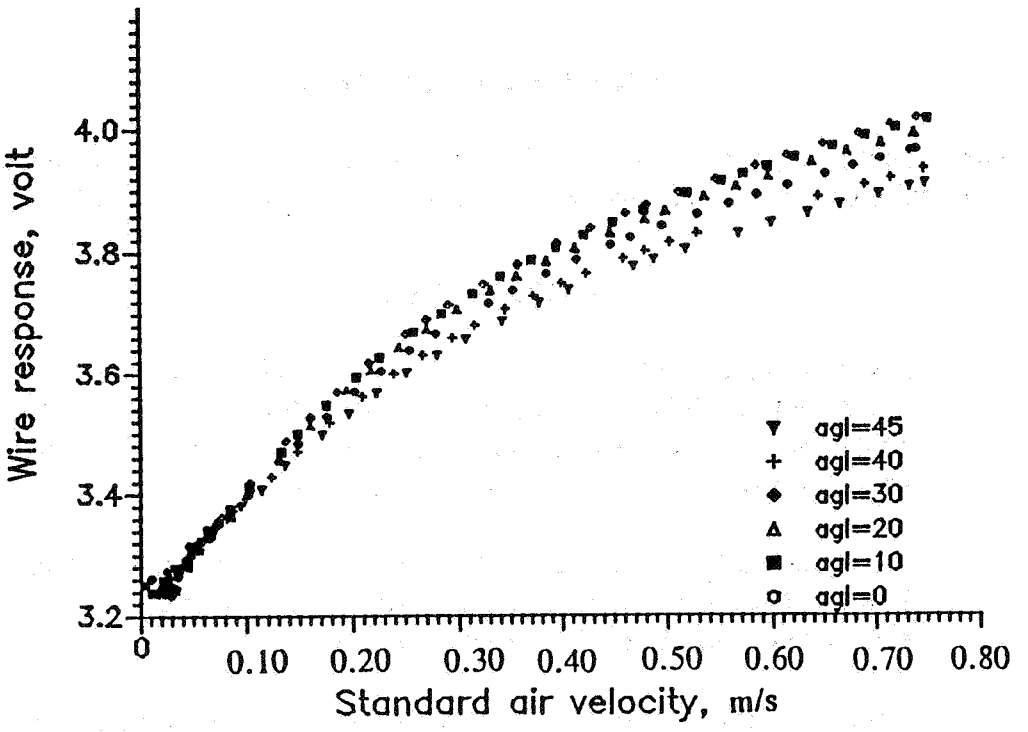
(1) The uncertainties due to natural convection in the velocity measurements with a single component hot wire probe operating at >200 °C are estimated to be ±15%, ±5%, ±3%, ±1% and 0.5% for velocities of 0.05 to 0.1 m/s, 0.1 to 0.15 m/s, 0.15 to 0.25 m/s, 0.25 to 0.5 m/s and >0.5 m/s, respectively, assuming that the direction of the measured air flow is unknown. Flow visualization techniques can be used to determine the air flow directions at the measured points within rooms approximately and improve the measurement accuracy significantly.

(2) Air velocity components should not be measured simultaneously with multi-component hot wire probes operating at >200 °C if the air velocity is below 0.2 m/s, since the angle sensitivity of the probe will be heavily contaminated by moise signal due to the natural convection.

Further studies are needed to determine an optimal probe operating temperature which minimizes uncertainty due to the natural convection while still provides sufficient signal to noise ratio and satisfactory frequency response performance.



a. T_{op} = 250 °C



b. T_{op} = 200 °C

Figure 4 Outputs of wire #1
(agl is the angle between the air jet and the normal plane of wire #1)

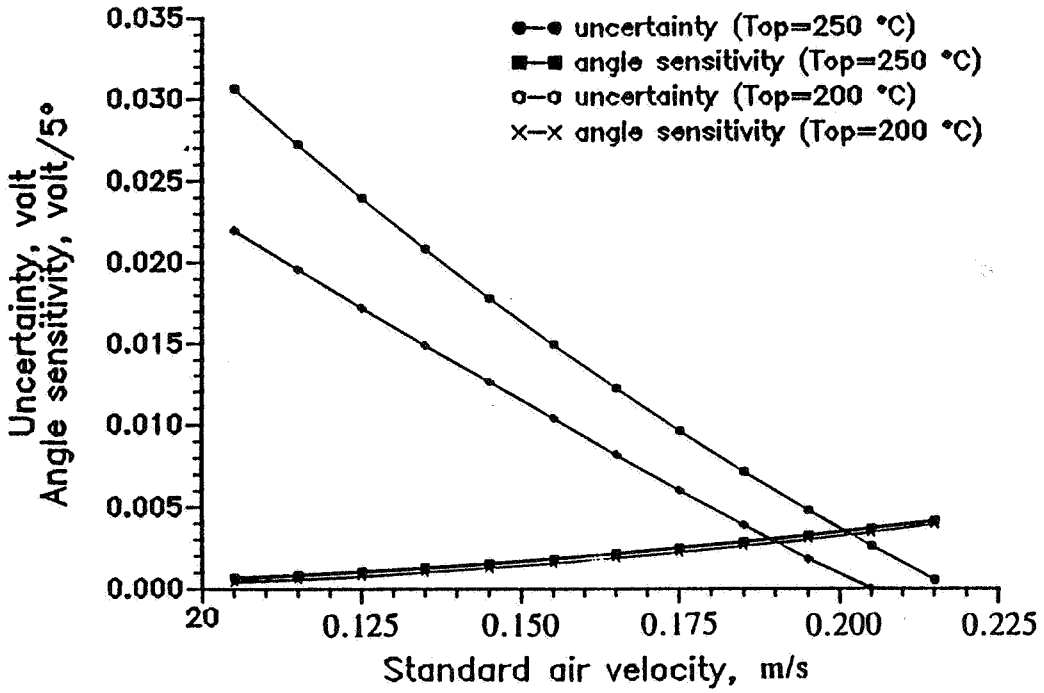


***Figure 5** Comparisons between the angle sensitivity and the measurement uncertainty of the hot wire anemometer (T_{op} is the operating temperature of the probe)*

ACKNOWLEDGEMENTS

The financial supports from the US National Science Foundation and the University of Illinois Campus Research Board are highly appreciated.

REFERENCES

1. Awbi, H.B. and M.M. Nemri. 1990. "Scale effect in room air movement modeling." Roomvent '90, Proc. 2nd international conference on engineering aero- and thermodynamics of ventilated room, session A1. Oslo, Norway, 13-15 June.

2. Fingerson, L.M. and P. Freymuth. 1983. Thermal anemometers. In Fluid Mechanics Measurements, ed. R.J. Goldstein, 99-154. Hemisphere Publishing Co., New York, NY.

3. Foss, J. 1989. Private Communication. School of Engineering, Michigan State University, East Lansing, MI.

4. Holfman, S.J., K.A. Janni and L.D. Jacobson. 1990. Modelling buoyancy affected flow. ASAE Paper No. 90-4003. St. Joseph, MI.

5. Murakami, S. and H. Komine. 1980. Measurement of three components of turbulent flow with tandem hot-wire probe. Transactions of Architectural Institute of Japan No. 297:59-69. (Japanese)

6. Popiolek, Z. 1990. Multichannel temperature and velocity measurement system with PC computer in application to room air movement tests. In Room Vent '90, Proc. 2nd international conference on engineering aero- and thermodynamics of ventilated room, session B1. Oslo, Norway, 13-15 June.

7. Sandberg, M. 1989. Velocity characteristics in mechanically ventilated office rooms. In Room Vent '87, Proc. 1st international conference of air distribution in ventilated spaces, Session 2A, Stockholm, Sweden, 10-12 June.

8. Sandberg, M. 1990. Private Communication. The National Swedish Institute for Building Research, Gavle, Sweden.

9. Zhang, J.S., L.L. Christianson and G.L. Riskowski. 1990a. Regional air flow characteristics in a mechanically ventilated room under non-isothermal conditions. ASHRAE Technical Paper No. At-90-2-3.

10. Zhang, J.S., L.L. Christianson, G.J. Wu and G.L. Riskowski. 1990b. Room air flow and turbulence characteristics in a 1/4th scale test room. In Indoor Air '90, Proc. 5th international conference on indoor air quality and climate, 4:249-254.

11. Zhang, J.S. 1991. "A fundamental study of two dimensional room ventilation flows under isothermal and non-isothermal conditions". Ph.D. Thesis. University of Illinois at Urbana-Champaign, Urbana, IL.

AIR MOVEMENT & VENTILATION CONTROL WITHIN BUILDINGS

12th AIVC Conference, Ottawa, Canada
24-27 September, 1991

POSTER 54

THEORETICAL AND EXPERIMENTAL ANALYSIS OF DIFFERENT VENTILATION STRATEGIES IN A TEST ROOM

N.Cardinale, G.V.Fracastoro, M.Mantegna*, E.Nino**

* Dipartimento di Energetica - Politecnico di Torino
Corso Duca degli Abruzzi 24, - 10100 TORINO (Italy)
**Dipartimento di Ingegneria e Fisica dell' Ambiente
Universita' della Basilicata
Via Nazario Sauro, 85- 85100 POTENZA (Italy)

ABSTRACT

The paper presents an original computer code for the analysis of contaminant diffusion in rooms developed at the Politecnico di Torino and its experimental validation by means of a test facility located at the University of Basilicata (Potenza). The velocity fields in isothermal conditions, together with local ages of the air, have been analysed and compared, with different ventilation strategies and number of air changes.

Introduction

There is a growing interest on the topic of contaminant diffusion both outdoor and indoors. Indoors, the study of this type of problem has consequences both on the hygienic and on safety sides (e.g., for the analysis of explosion risks related to gas leaks).
There are many available computer codes in this area (see, e g, Liddament, 1991), but there is still a need for further research, mainly for two reasons: firstly, these computer codes have often been created and validated for purposes different from the one considered herein; secondly, commercial codes have a wide but fixed range of possible outputs, which not always include the most interesting parameters in the ventilation studies, such as ventilation efficiency, local ages of the air, etc.
The aim of this paper is to present a new computer code, which was explicitly created for the study of the fluid dynamic field and contaminant dispersion in a room. At this preliminary stage, the concentration field is not yet computed. Therefore the programme has been experimentally validated only on the basis of velocity values.
The experimental validation has been conducted using the Controlled Ventilation Chamber of the University of Basilicata, whose description was the aim of a previous paper (Fracastoro and Nino, 1990)
Results are presented both in terms of the velocity field (although the experimental results only yield nondirectional data) and local ages of the air.

Description of the calculation procedure

The calculation method hereby described is a method which solves the fluid dynamic field for two-dimensional problems in isothermal conditions. The domain is dicretized in square cells, and to each cell the continuity equation and Navier-Stokes equations are applied.
The first set of equations is the local formulation of the continuity law:

$$\frac{\delta(\rho u)}{\delta x} + \frac{\delta(\rho v)}{\delta y} = 0$$

where u and v are the horizontal and vertical components of velocity. and ρ is the density.
For incompressible fluids the equation above is linear in u and v.
The second and third sets of equations are the scalar form in x and y of the vectorial Navier-Stokes equation in local formulation (dynamic equilibrium):

$$\rho\left(u\frac{\delta u}{\delta x} + v\frac{\delta u}{\delta y}\right) = \mu\left(\frac{\delta^2 u}{\delta x^2} + \frac{\delta^2 u}{\delta y^2}\right)$$

$$\rho\left(u\frac{\delta v}{\delta x} + v\frac{\delta v}{\delta y} + F\right) = \mu\left(\frac{\delta^2 v}{\delta x^2} + \frac{\delta^2 v}{\delta y^2}\right)$$

where F is the intensity of the force field (gravitational field) and μ is the dynamic viscosity of the fluid.
The first step for the solution of the problem, due to the low velocities involved, was to assume a hydrostatic pressure distribution.
The equation of continuity was then applied in order to make the first estimate of the scalar velocity field.
It is well known that there are two velocity potentials Φ and φ, whose equipotential lines are mutually orthogonal. These equipotential lines may be easily determined for some simple configurations, such as the flow over a flat indefinite surface (for which the Φ = constant lines are parallel to the surface). Once these equipotential lines are known for a simple domain, they may be determined for more complex domain using the theory of conformal mapping (Spiegel, 1964). This theory, illustrated in texts of complex numerical calculus , has already been usefully employed in engineering problems such as air flow around wing profiles. The transformation of a simple domain contour into a complex one (such as a poligonal contour) may be performed thanks to the Schwartz-Christoffel theory (Mantegna, 1991).
During the transformation the equipotential lines are also transformed, but due to the propriety of isogonality of conformal mapping, the new equipotential lines are still mutually orthogonal, except in the singular points of the contour. The decomposition of the domain into regions for which application of conformal mapping is possible, and the subsequent juxtaposition of the velocity fields of the various regions allows to obtain the complete velocity field for the test chamber. Once the equipotential lines in the new domain are known, the velocity field satisfying the continuity equation may be

deduced by derivation. In general this field will not, however, satisfy the Navier-Stokes equations.
This approach is different from the procedure ordinarily used in other types of solvers, such as the SIMPLE solver (Patankar, 1980). In fact, SIMPLE obtains the velocity field solving alternately the continuity equation and the dynamic balance equation, while in our case the equation of continuity is solved once for all through conformal mapping.
Now, an iterative method is needed to obtain a dynamically better balanced solution, while maintaining the mass balance. A dynamically better balanced solution means a solution in which the residuals at the right side of Navier-Stokes equation are as close as possible to zero.
The idea was to make use of a generalized version of Cross's method, widely used for plant applications (Monte, 1987). Fig. 1 shows a fragment of the square cells into which the domain has been discretized. The fictitious "elementary vortex" superimposed to the motion field in the cell will keep the mass balance, eventually causing a partial deviation of the flow. By choosing in a suitable way the intensity of such vortex, the global dynamic unbalancement may be reduced.
In such a way, the two scalar velocities sets are substituted by two new sets of unknowns: vortex intensities and pressures. It should be stressed that the algebraic equations are second degree equations only in the vortex unknowns, while they are linear in the pressures: this makes clear why it is convenient to deal differently with these two sets of unknowns. Also the SIMPLE method adopts this procedure, but the correction equations for pressure are obtained from the continuity equation, while the present method does not make any more use of mass balance equations. However, the pressure values may be corrected as if the most recent velocity values were constant.
The exact process of constructing vortex- and pressure correction equations involves a lot of details and is explained in another paper (Mantegna, 1991). Basically, two families of equations are obtained by summing and subtracting Navier-Stokes equations for horizontal and vertical balance.
Whenever no boundary condition on pressure is assigned at the walls, it may be assumed that the pressure gradient orthogonal to the wall is zero (This is equivalent to neglect the velocity component orthogonal to the wall itself).
The corrected pressure field is then substituted into another set of equations, namely the velocity correction equations (Mantegna, 1991).
For the solution of the velocity correction equations, the pressures are considered to be constant, and their best estimates, corresponding to underrelaxation of the pressure correction equations, are introduced. Also the velocities are considered to be constant, and the most recent available value is adopted: but an unknown set of

vortex intensities is superimposed to the velocity set for each cell.
By the way, there is no need to solve accurately at this stage the velocity correction equations, because the pressure values adopted are only estimates. Due to the fact that the velocity correction equations are higher than first degree equations, these can be solved by means of their gradients. In each equation, only at most 9 elementary vortex intensities (those affecting the considered cell) appear. Thus, the matrix of coefficients will be "sparse", and suitable iterative techniques may be used to solve it.
The underrelaxed values of the elementary vortex intensities are then used to correct the velocity field in each cell.
The iterative method proceeds solving alternatively the correction equations for pressure and velocity until convergence is attained. The right sides of the dynamic equilibrium equations (equal to zero for the exact solution) are taken as indicators of convergence.
When the velocities are sufficiently high the Reynolds number will surpass the maximum stability limit of laminar flow, and the regime will become turbulent. In this case the dynamic equilibrium equations valid for laminar flow are modified following the Boussinesq hypothesis, by introducing the concept of turbulent viscosity μ_t. Since turbulent viscosity is no longer a property of the fluid, the Boussinesq hypothesis has to be integrated by a "turbulence model" in order to calculate cell by cell the values of turbulent viscosity. A large number of turbulence models have been proposed, starting fron Prandtl model. Nowadays, the prevailing method is the so called k-ε method, proposed by Launder and Spalding (1972 and 1973), and subsequently modified by other authors. No model up to know is able to reproduce all the experimental results obtained on turbulence. For each type of problem there is a technique which proves itself more suitable than others.
For the case considered in this paper, one of the most important limitations is the low Reynolds number, sometimes even falling into the transition region. For this reason the k-ε turbulence model as modified by Jones and Launder (1972) was adopted. The equation of transport for k assumes the following form:

$$\rho\left(\frac{\delta k}{\delta t} + u\frac{\delta k}{\delta x} + v\frac{\delta k}{\delta \varepsilon}\right) = \frac{\delta}{\delta x}\left(\mu + \frac{\mu_t}{\sigma_k}\right)\frac{\delta k}{\delta x} + \frac{\delta}{\delta y}\left(\mu + \frac{\mu_t}{\sigma_k}\right)\frac{\delta k}{\delta y} + P_k + G_k - \rho\varepsilon + D$$

where P_k is the shear production of turbulent kinetic energy, G_k is the buoyancy production of turbulent kine-

tic energy and D is the source term , σ_k is the turbulent Prandtl number for K. (Henkes, Van der Vlugt and Hoogendoorn, 1991).
On the other side the equation of transport for ϵ takes the form:

$$\rho\left(\frac{\delta\epsilon}{\delta t} + u\frac{\delta\epsilon}{\delta x} + v\frac{\delta\epsilon}{\delta\epsilon}\right) = \frac{\delta}{\delta x}\left(\mu + \frac{\mu_t}{\sigma_\epsilon}\right)\frac{\delta\epsilon}{\delta x} + \frac{\delta}{\delta y}\left(\mu + \frac{\mu_t}{\sigma_\epsilon}\right)\frac{\delta\epsilon}{\delta y} +$$

$$+ \left(c_1 f_1 \frac{\epsilon}{k}(P_k + c_3 G_k) + c_2 \rho f_2 \frac{\epsilon^2}{k}\right) + E$$

where E is the source term, σ_ϵ is the turbulent Prandtl number for ϵ, while c_1, c_2, c_3, f_1 and f_2 are costants of method (Henkes, Van der Vlugt and Hoogendoorn, 1991).
The transport equations for the turbulent quantities are formally similar to the dynamic equilibrium equations, and may be solved adopting an identical solution technique.

Input-output of the programme AIR

The ordinary commercial codes, being totally general, need definition of the domain case by case. On the opposite, this programme is already prearranged for a rectangular domain with a variable number of immission/extraction grilles. Then we only type in the geometrical features of the room and of immission and exhaust grilles which include the number of these.
Other input data are the discretization parameters and in particular the number of cells for each side. If there are n grilles , we need to type in the module and direction of velocity for n-1 grilles and only the direction for the last grille because the module will be derived from the continuity equation.
The output data (both numerical and graphical) are the pressure, the velocity and the local mean age of air in each cell and the room mean age of air. The room mean age of air is an indicator providing a global idea of the ventilation efficiency of a room. In particular we define the local age of air as the time required by the air to move from the immission grille to a generic point in the room.
The local mean age of air in a point is the arithmetic mean of the different local ages of the air. In practice it may be calculated as the average of the local ages of the adjacent nodes weighed according to the incoming flow rates. Since air density may be considered constant the average may be obtained using as weights the local velocities.
The room mean age is the arithmetic mean of the local

mean ages in each point of the room. Since the velocity field is continuous the arithmetic mean is calculated as the volume integral of the local mean age, extended to the whole room and divided by the room volume.

The experimental facility

A concise description of the main features of the Controlled Ventilation Chamber (CVC) follows:
- Size : 3.00 (x - extensible to 4.20) x 2.40 (y) x 2.40 (z - height)
- Possible ventilation strategies: balanced, immission or extraction. Four positions of grilles on walls y-z
- Special features: one transparent x-z wall
- Range of air changes per hour: 0 to 10 ach
- Instrumentation:

Two-cell Gas Analyzer (SF_6 and NO_2), range 0 to 200 ppm
Six non-directional hot film anemometers, range 0 to 0.5 m/s
Flowmeter for the measurement of air flow rate to the CVC
An automatic system for air sampling at six different locations
An automatic system for moving the sensors around the chamber

Measurement campaigns

The CVC has already been used for many experimental campaigns which have helped to improve the performance of the instrumentation and to define its accuracy.
These include pressurisation tests, decay tests with perfect mixing, velocity at the outlets of the immission grilles, measurement of ventilation efficiencies during decay, buildup, and steady-state sequences (see, e.g., Cafaro et al., 1991).
Since it has been observed (Cafaro et al., 1991) that not only the fluid dynamic field influences the concentration field, but also the opposite thing happens (i.e., the contaminant concentration affects the velocity field), the comparison has been made only on the grounds of velocity fields, without any contaminant in the room.

Comparison between experimental and theoretical results

Many different ventilation strategies (as for grilles positioning and number of air changes) may be simulated experimentally (see Figure 2), but the comparison between theoretical and experimental results presented in this paper refers only to strategies B and C:
B) Air immission from a lower grille and extraction from the higher grille placed on the opposite wall
C) Air immission from a lower grille and extraction from

the higher wall on the same side

The experimental velocity data are known at five points simultaneously (because one of the six anemometers was excluded due to its higher range - 0 to 5 m/s). Each value is the result of 50 consecutive measurements lasting about 1'. In order to improve the detail in the knowledge of the velocity field, the five measurement points were moved along the vertical simmetry plane of the CVC.

The theoretical data are known at each cell. There was a total number of 720 cells for the cases presented.
Results are compared in terms of velocity moduli only, because the CVC is provided with non-directional anemometers.
Two cases have been compared: Strategy B with 3 ach (case B3) and strategy C with 3 ach (case C3).
For case B3 a total number of 210 measurement points is available. In the area close to the inlet grille (Figures 3 and 4), there is a moderately good agreement for both x = 270 cm and x = 280 cm axes, especially in the lower zone. Close to the ceiling there is a clear underestimate of the code. In general, the experimental values are higher than the calculated ones, and in some cases the measured value also exceeds the air velocity at the grille. This is probably due to the actual non-uniformity of inlet velocity profiles.
Proceeding towards the exhaust, in the central area (Figures 5 and 6) there is a clear agreement between calculated and measured results in the lower zone and somehow less good agreement in the upper zone. On the opposite, while the calculations clearly show only one vortex at mid height, the measurements give prominence of a double vortex, the first being just above the inlet grille, and the second at about the same height as the computed one.
Close to the exhaust grille (Fig 7 and 8), there is little resemblance between calculated and measured velocity profiles.
For case C3 there are only 90 experimental data available, and the comparison is shown in figures 9 ,10 and following. Close to the inlet/outlet grilles, the experimental data give evidence of a strong air flow closest to the grilles, increasing with height and decreasing with the distance from the grilles. All the region seems to be interested by the phenomenon, while the calculations show a marked effect at the grilles height, leaving the intermediate area practically undisturbed.
In the central area, the results are much more promising, both for the qualitative agreement and the actual values of velocity. Finally, close to the wall opposite to the grilles, there is again little agreement between experimental and theoretical results.

Future developments and conclusions

The results presented in this paper are still preliminary and require a more careful validation than it was possible to do up to this moment.
In some cases the results are encouraging, in others the model AIR seems to simplify to some extent the actual physical phenomenon. However, the work done has helped both for a better understanding of the phenomena and also to improve the experimental techniques.
The code will soon calculate also the concentration field for contaminants and a better estimate of k-ε parameters will also be available. The possibility of allowing variable size cells will also be taken into consideration.
On the experimental side it will soon be possible to make experiments with non-uniform temperature field. There are also solid hopes to make use in a short time of more powerful techniques, like laser-doppler anemometry, to define the velocity field.

Acknowledgements

The authors wish to thank Franco Mariniello for his skillfull help in the execution of measurements.

References

Cafaro, E., Fracastoro, G.V., Nino, E., Perino, M., Analisi teorico-sperimentale della diffusione degli inquinanti negli ambienti confinati. Convegno ATI, Gaeta, 1991.

Fracastoro, G.V., Nino, E., and Coretti, G., The Ventilation Chamber of the University of Basilicata, Proc. 11th AIVC Conference, Belgirate (Italy), 1990.

Fracastoro, G.V., Nino, E., La Camera a Ventilazione Controllata dell'Università della Basilicata, Convegno AICARR, Roma, 18-19 Aprile 1991.

Henkes R.A.W.M, Van der Vlugt F.F., Hoogendoorn C.J, Natural convection flow in a square cavity calculated with low-Reynolds number turbulence models, Int.J Heat Mass Transfer, vol.34, n.2, 377-388, 1991

Jones W.P., Launder B.E, The prediction of laminarization with a two-equation model of turbulence, Int.J Heat Mass Transfer, 15, 301-314, 1972

Launder B.E., Spalding D.B, Mathematical models of turbulencs, Academic Press, London, 1972

Launder B.E, Spalding D.B, The Numerical computation of Turbulent Flows, Comp. Meth.in App. Mech. and Engineering, 3, 269-289, 1974

Liddament, M.W., A Review of Building Air Flow Simulation. AIVC, Technical Note 33, March 1991.

Mantegna, M., Un metodo di calcolo della ventilazione negli ambienti (in press), 1991

Monte A., Impianti meccanici, ed.Cortina, 1987

Patankar S.V, Numerical Heat Transfer and Fluid Flow, Hemispher Publishing Co, 1980

Spiegel M.R, Theory and Problems of Complex Variables, Schaum Publishing Co., New York, 1964

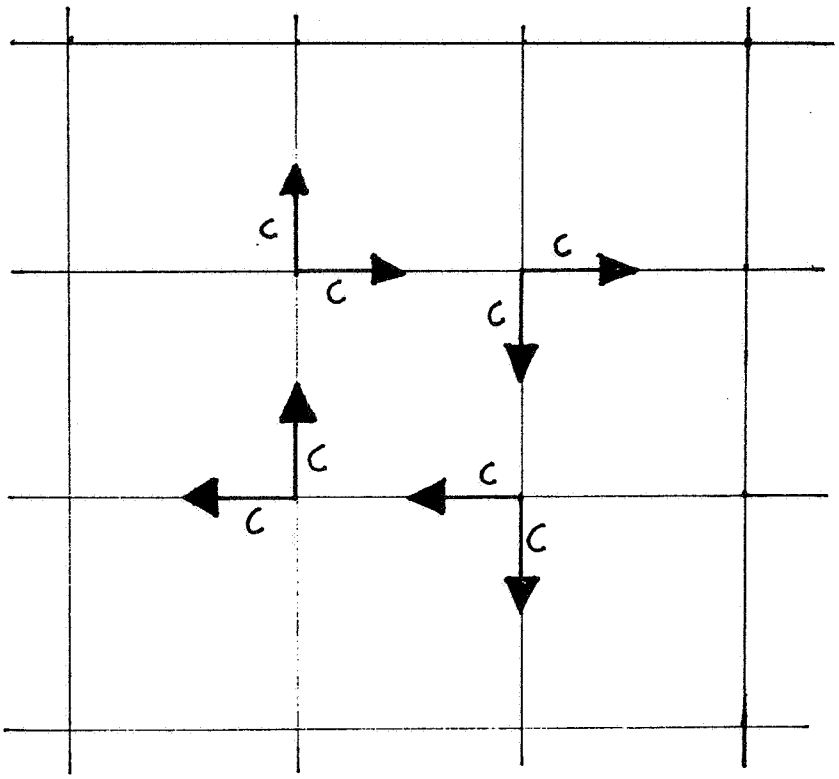


fig.1 - Fragment of the square cells of the domain with the "elementary vortex"

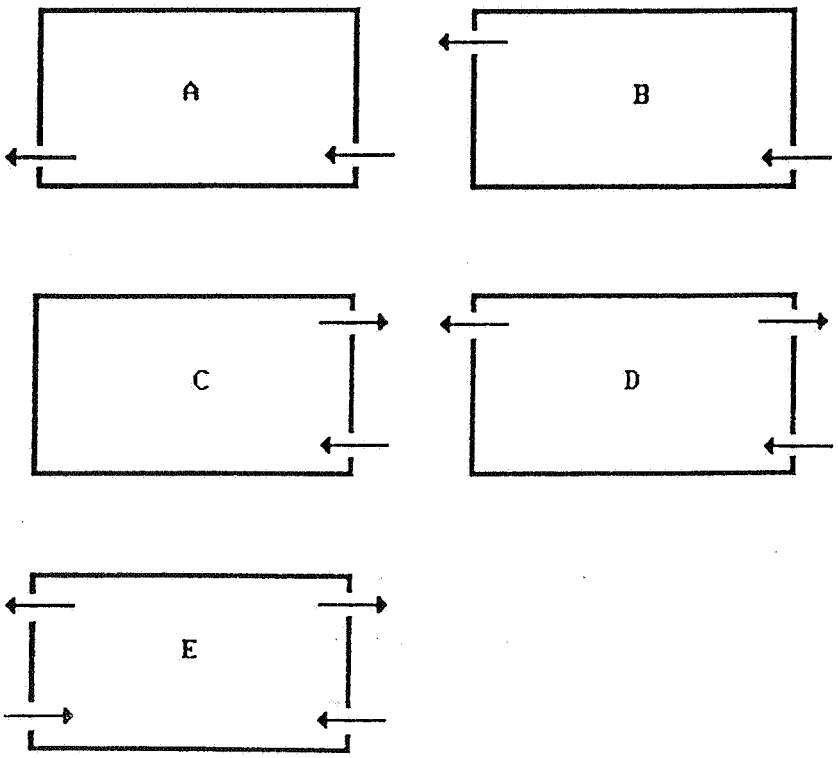


fig.2 - Ventilation strategies

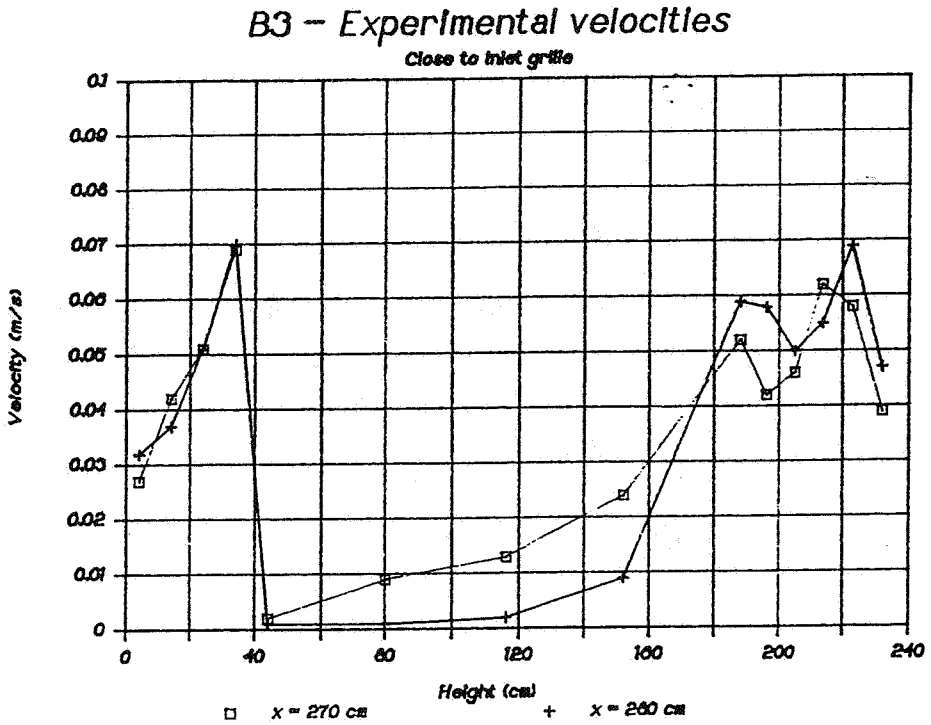


fig.3 – Experimental velocities close to inlet grille for strategy B with 3 ach

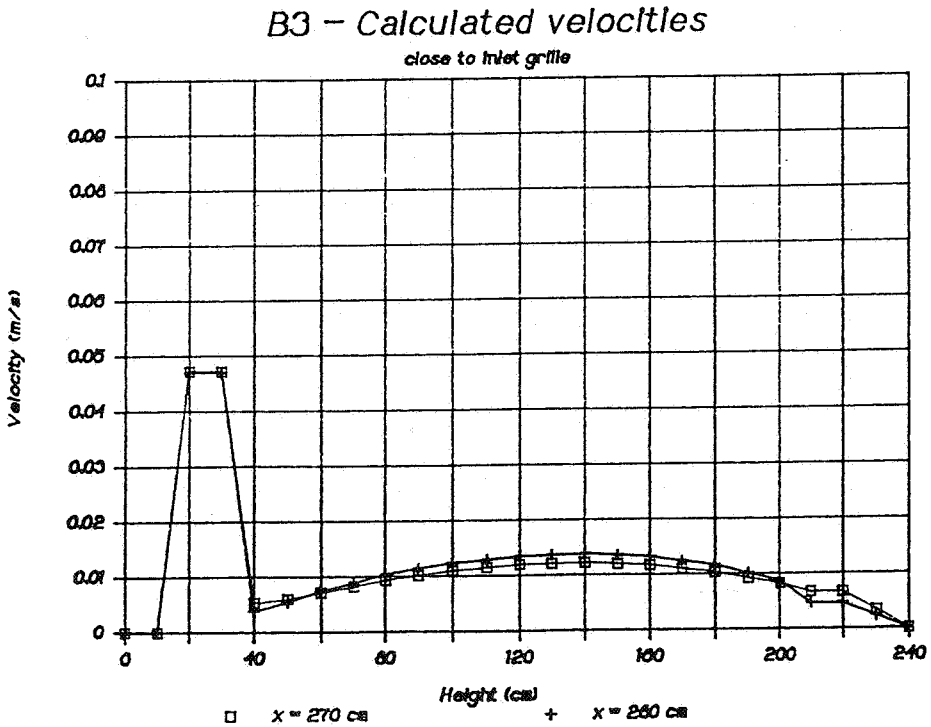


fig.4 – Calculated velocities close to inlet grille for strategy B with 3 ach

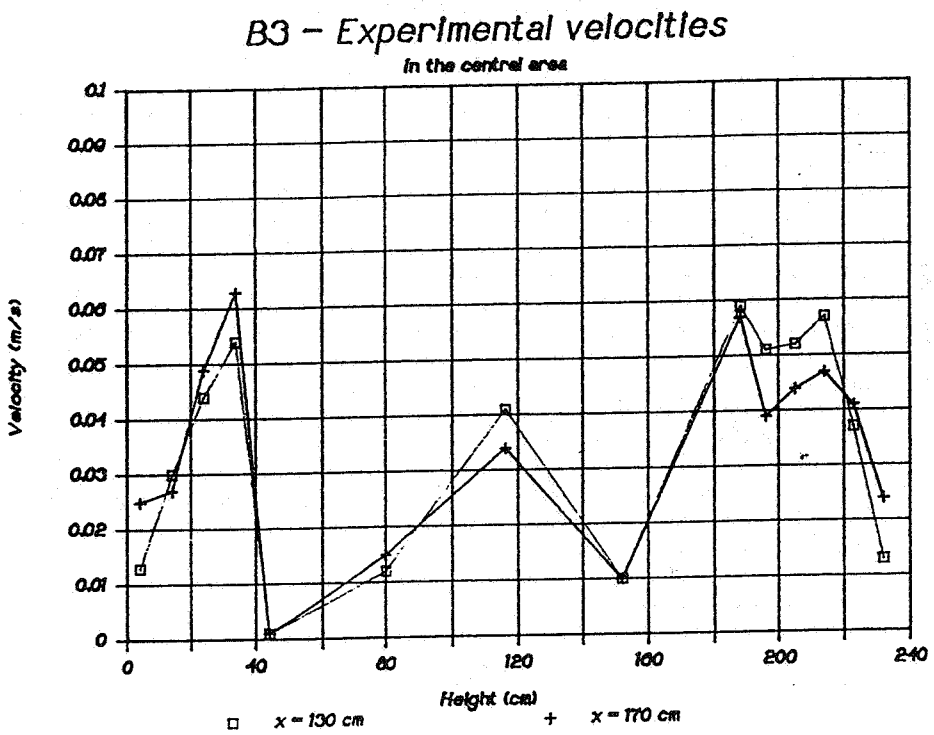


fig.5 - Experimental velocities in the central area for strategy B with 3 ach

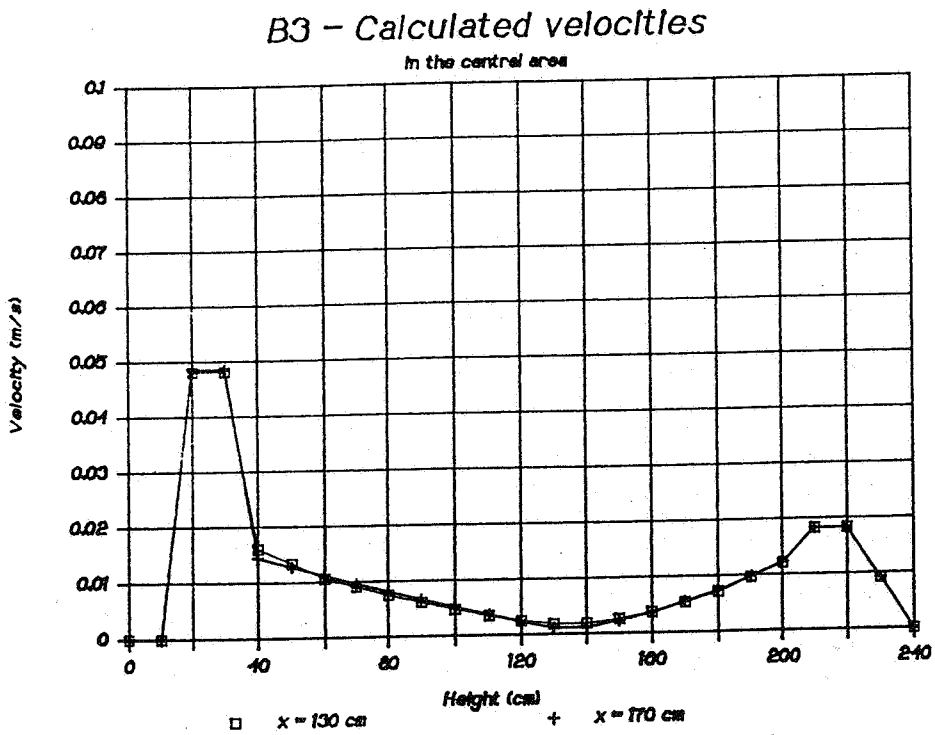


fig.6 - Calculated velocities in the central area for strategy B with 3 ach

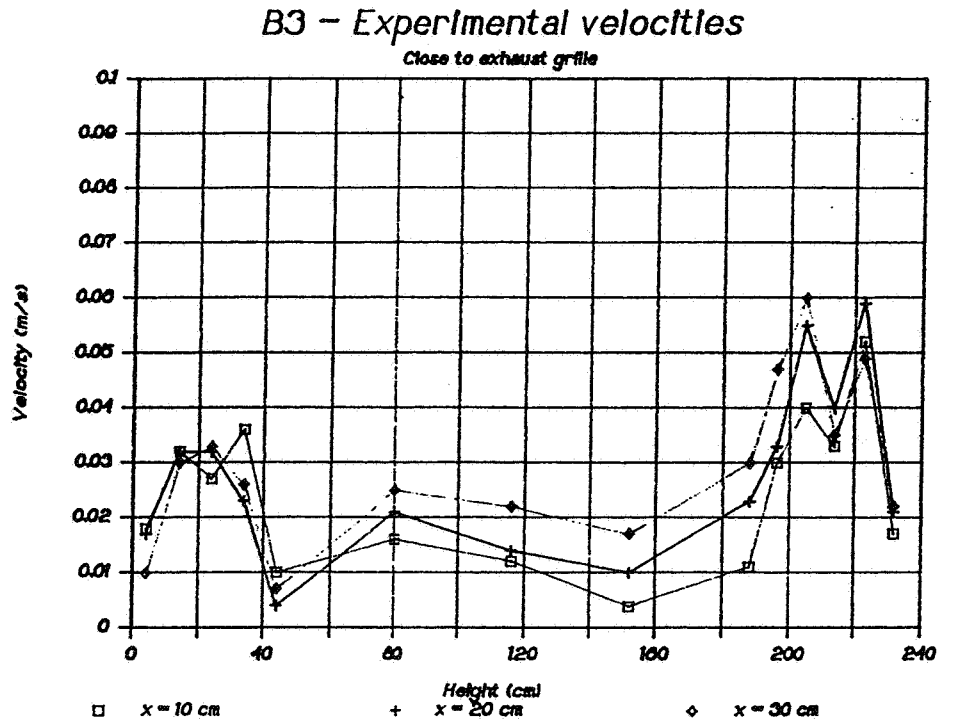


fig.7 - Experimental velocities close to exhaust grille for strategy B with 3 ach

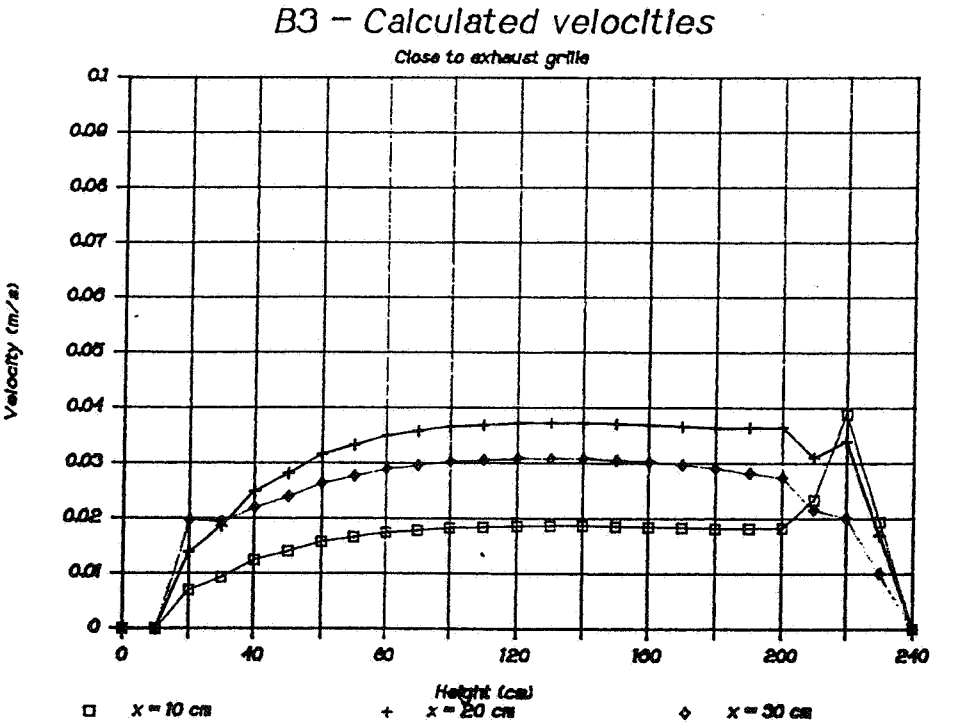


fig.8 - Calculated velocities close to exhaust grille for strategy B with 3 ach

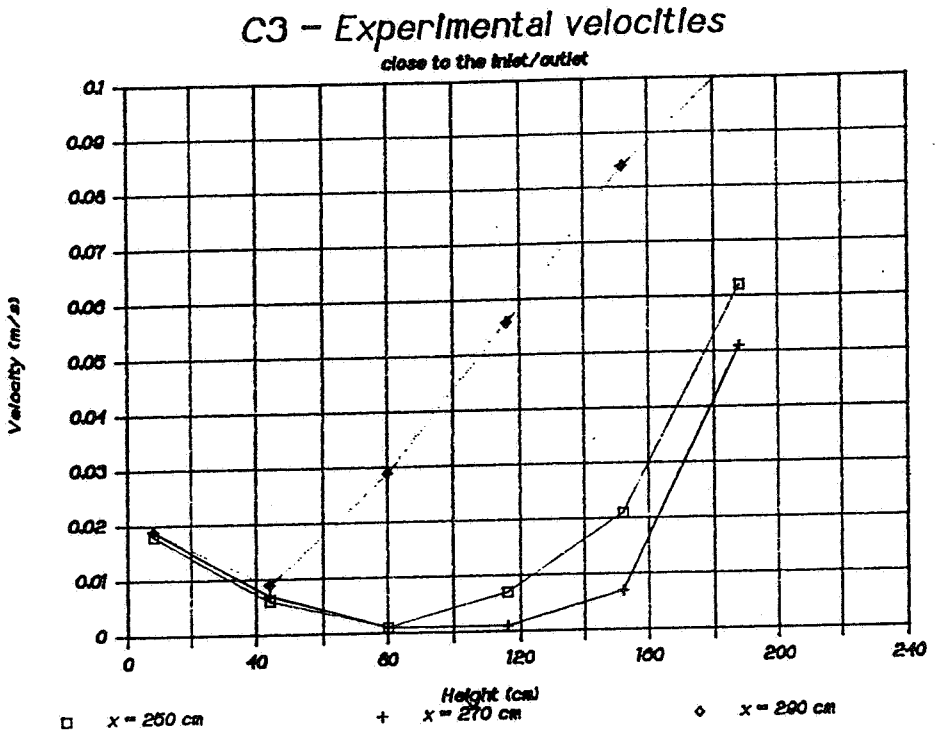


fig.9 - Experimental velocities close to inlet/outlet grilles for strategy C with 3 ach

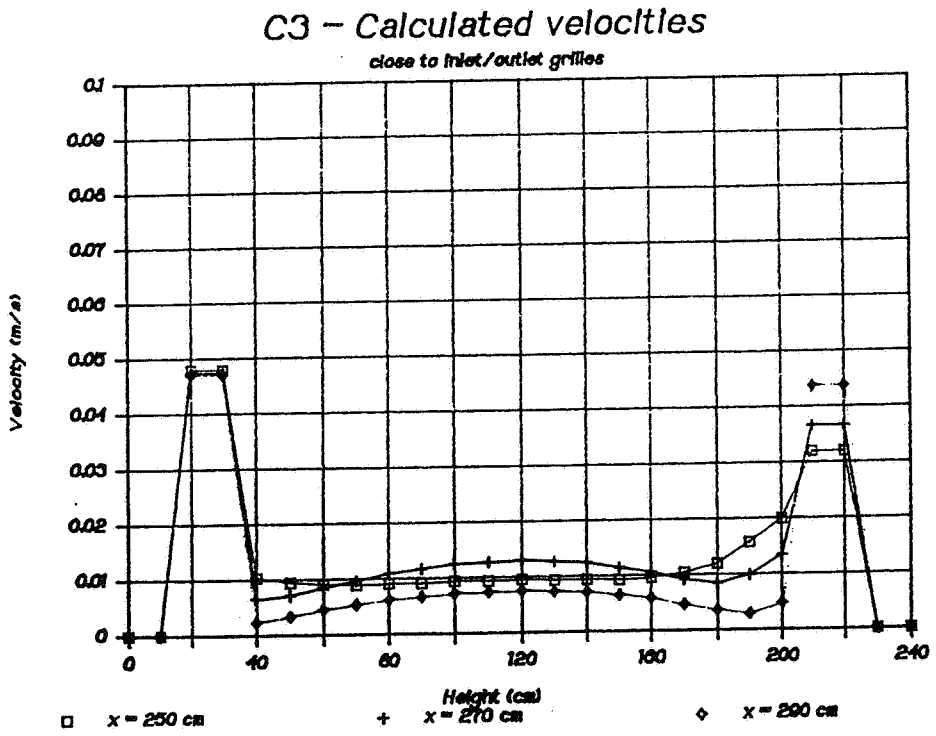


fig.10- Calculated velocities close to inlet/outlet grilles for strategy C with 3 ach

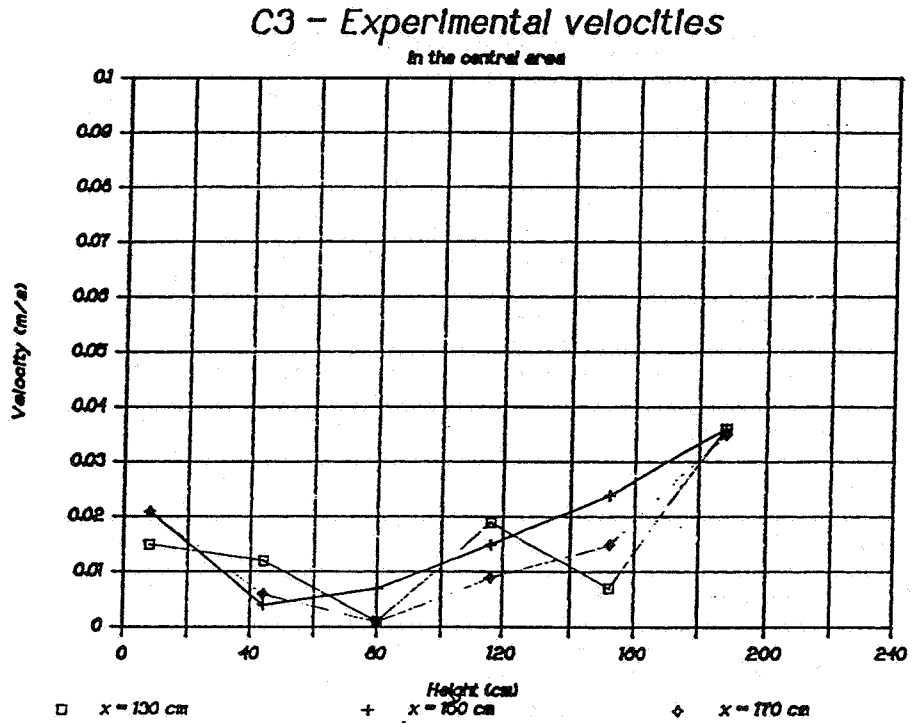


fig.11- Experimental velocities in the central area for strategy C with 3 ach

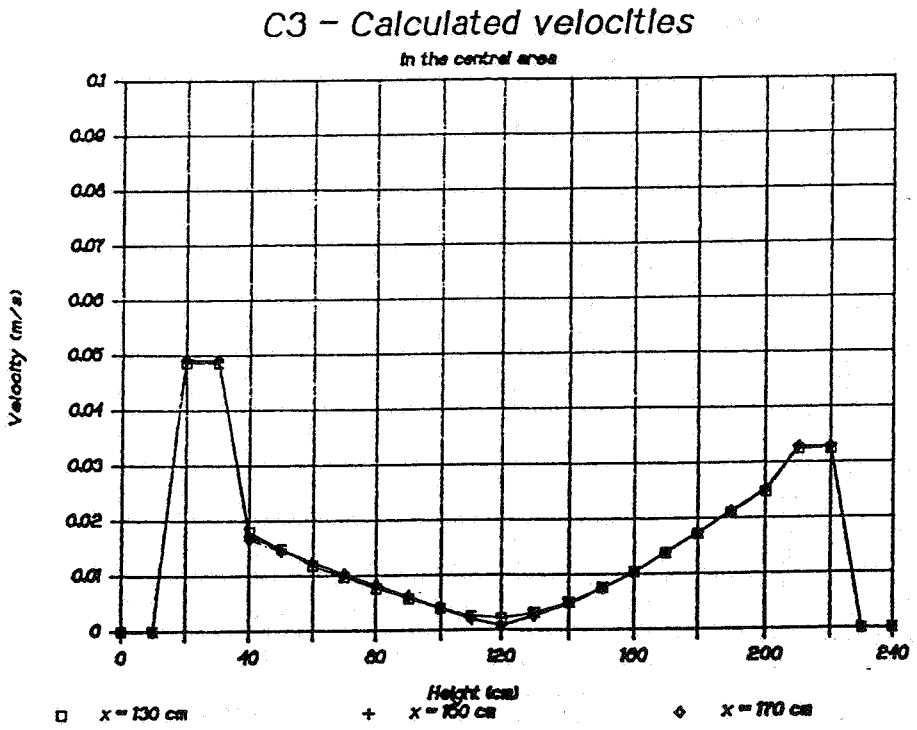


fig.12- Calculated velocities in the central area for strategy C with 3 ach

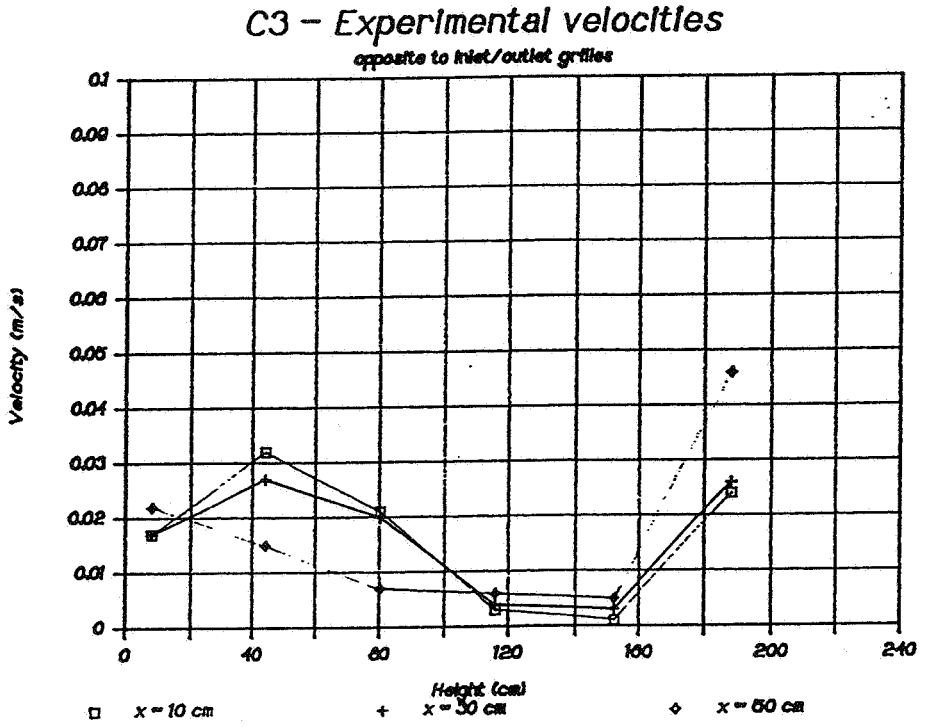


fig.13- Experimental velocities opposite to inlet/outlet grilles for strategy C with 3 ach

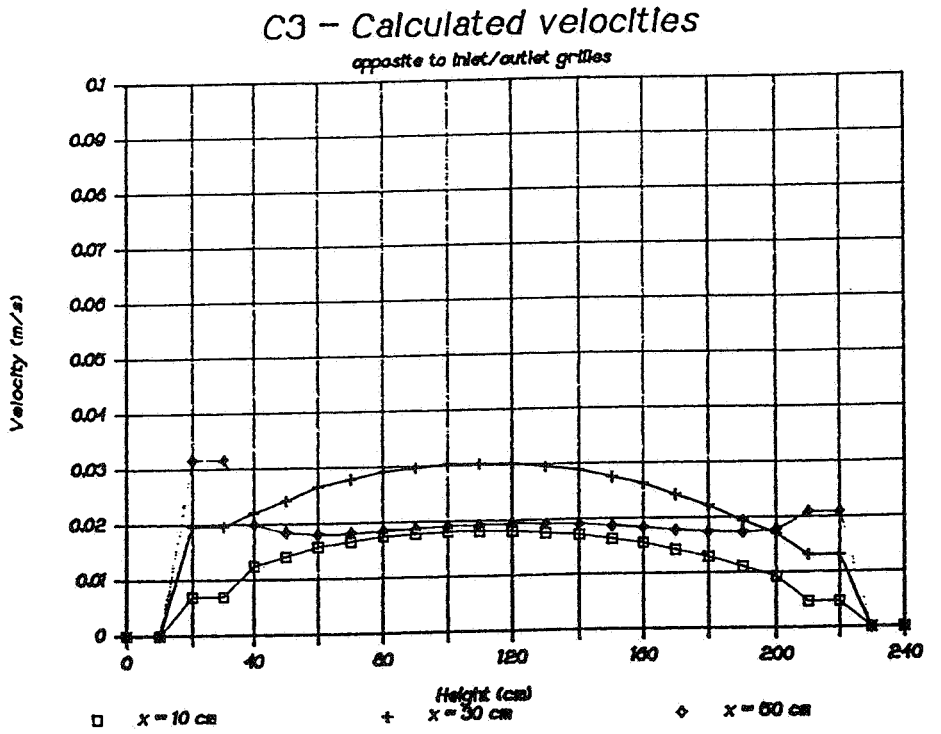


fig.14- Calculated velocities opposite to inlet/outlet grilles for strategy C with 3 ach

AIR MOVEMENT & VENTILATION CONTROL WITHIN BUILDINGS

12th AIVC Conference, Ottawa, Canada
24-27 September, 1991

POSTER 55

THE USE OF ACOUSTIC INTENSIMETRY TO SIZE AIR LEAKAGE CRACKS.

D. J. OLDHAM*, X. ZHAO+ , S. SHARPLES+ and H.G. KULA+

* School of Architecture and Building Engineering University of Liverpool Liverpool L69 3BX

+ School of Architectural Studies University of Sheffield Sheffield S10 2TN

SYNOPSIS

Reverberant sound excitation and the sound intensity technique have been used for the measurement of the sound transmission loss of narrow slits in rigid walls. A series of experiments was conducted to determine the transmission loss of slit shaped apertures. The measured transmission loss was in good agreement with existing approximate theories over their accepted ranges of validity. However, the effect of viscosity in small apertures was found to be significant and to vary systematically with the dimensions of the apertures.

As predicted by theory, the dimensions of the apertures determine the magnitudes and resonant frequencies of the sound transmission loss curves. It should thus be possible in principle to size air leakage cracks using the technique described in this paper.

SYMBOLS

A and B are constants which are functions of the crack dimensions width, w, depth, d, and length, l.
K is the product of the wave number of the incident sound, and width, w, of the slit
L is the depth-to-width ratio of the slit (d/w)
e is an end correction.
W_i is the acoustical power incident onto an aperture
W_0 is the acoustical power radiated from the aperture.
τ_c is the transmission coefficient of the aperture.
IL_r is the measured intensity level at a point distance r from the aperture on the receiving side .
SPL_i is the sound pressure level in a reverberant enclosure.

1. INTRODUCTION

Recent work on the design of energy efficient buildings has resulted in considerable attention being paid to energy losses due to air leakage via small constructional cracks. Baker Sharples and Ward [1] have carried out an investigation of air flow through cracks in walls by the method of room pressurisation. Their results show a quadratic relationship between the pressure drop, Δp, across the crack and the air flow rate Q as follows:

$$\Delta p = A\,Q + B\,Q^2 \qquad (1)$$

Where A and B in Eq.(1) are constants which are functions of the crack dimensions width, w, depth, d, and length, l.

The following expression for the sound transmission coefficient of a slit shaped aperture has been given by Gomperts and Kihlman[2]:

$$\tau_s = \frac{mK\cos^2(Ke)}{2n^2\{\frac{\sin^2K(L+2e)}{\cos^2(Ke)} + \frac{K^2}{2n^2}[1+\cos K(L+2e)\cos KL]\}} \qquad (2)$$

where K is the product of the wave number of the incident sound, and width, w, of the slit, L is the depth-to-width ratio of the slit (d/w) and e is an end correction.

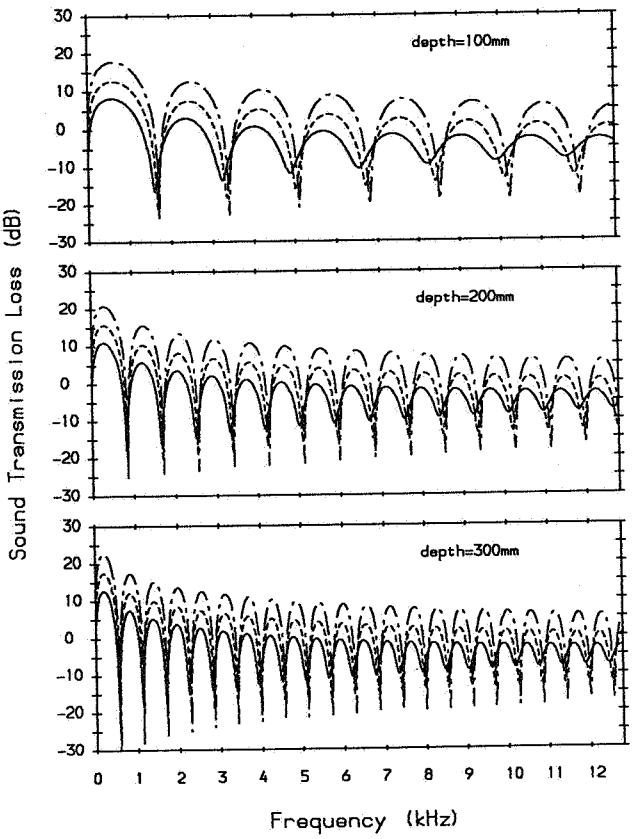


Fig.1 Predicted Transmission Loss Curves

Figure (1) shows predicted transmission loss characteristics for a number of different slits obtained from application of Equation (1). The dependance of these characteristics on slit dimensions is marked. Since the same parameters determine the air leakage characteristics, it suggests that measurement of the sound transmission loss of small cracks might be an effective indirect method of determining the air leakage characteristics of building elements.

There have been a number of previous attempts to employ acoustic techniques to locate cracks and determine their leakage characteristics. For example, Sonoda and Peterson[3] and Ringger and Hartmann[4] both used simple techniques based upon one third octave analysis of sound pressure level which were unsuccessful because they lacked both frequency resolution and sensitivity. In this paper we show how the use of a technique based upon acoustic intensimetry using a two channel Fast Fourier Transform analyser overcomes the problems associated with the earlier work.

2.THE MEASUREMENT OF TRANSMISSION LOSS

Three measurement techniques have been developed for the measurement of sound transmission loss through walls. These are sound pressure measurements which need two reverberant rooms, impulse techniques which use a short duration signal for excitation and avoid the need for reverberant chambers all together, and the sound intensity technique which requires one reverberant room to provide a diffuse exciting sound field.

In the present work the sound intensity technique was selected for the measurement of the sound transmission loss of slit shaped cracks in a rigid wall. The use of sound intensity measurement techniques for the measurement of transmission loss of partitions has been developed since the early 1980's. For example, Crocker, Raju and Forssen[5] used it to measure the sound transmission loss of panels, Minten, Cops and Wijnants[6] have reported work on the application of sound intensity to the measurement of the sound transmission of walls and Mey and Guy[7] have used it for measurement of transmission characteristics of panels.

The technique has a number of advantages over the other methods when dealing with sound transmission by very small apertures. If reverberant field excitation is employed in the experiment then only two parameters, sound pressure level in the source room and sound intensity level on the receiving side, need to be measured. Because it provides a direct measurement of sound energy propagated, there is no need to use a reverberant chamber on the receiving side. This greatly simplifies the measurement procedure and makes it possible to measure the transmission loss of small holes and narrow slits. Further, the use of an intensity measuring system based upon a two channel FFT Analyser enables the frequency

characteristics of the transmission loss to be determined with a high degree of resolution. This is essential of the resonance effects predicted by the theory of Gomperts and Kihlman are to be detected.

3. THE EXPERIMENT

The slits, which were all 500mm in length, were made using two parallel steel bars. The width of each slit was set using end spacers of known thickness and different depths of slit were obtained by employing different sizes of steel bars. Fifteen different sizes of slit were employed for these measurements.

A diffuse sound field on the source side was employed in order to simplify measurement of the sound-energy transmission . The diffusion of sound was obtained by having the walls of an enclosure containing the sound source non parallel and highly and uniformly reflective and by the use of two high-power loudspeakers and 20kHz broad-band white noise as the signal source which reduced the possibility of exciting strong individual enclosure resonances or standing waves.

For good insulation the walls of the reverberant enclosure, which had an internal volume of $3.3m^3$, were of cavity construction with mineral wool between two layers of dense chipboard. The top surface of the enclosure consisted of layers of dense 18mm thick chipboard.

The sound pressure level in the source room was measured using a standard Bruel and Kjær a quarter inch condenser microphone (B&K 4135) mounted on the end of a pipe which passed through three holes made in two walls of the enclosure. In order to provide a good acoustic seal, 'O' rings were used in the aperture through which the pipe was inserted. It was thus possible by sliding the pipe along through the different apertures to measure the sound pressure level at a number of different positions in the enclosure. The spectra of microphone were obtained using one channel of a B&K Type 2032 Dual Channel Analyser and then transferred by a standard GPIB-IEEE card to a microcomputer for recording and analysis.

The measured sound pressure level SPL_i in the source room was averaged 500 times by the analyser at each position before the data was recorded in order to eliminate random error and improve the signal-noise-ratio. At least nine positions were taken for sound pressure level measurement in the source room to obtain a uniform averaged sound pressure level. The recorded data indicated that there was very little difference between the measured sound pressure levels at the measurement points over the entire frequency range. This demonstrates that the sound field created in the source enclosure was very diffuse.

A Bruel and Kjær sound intensity probe (B&K 3520) was employed with the Analyser to measure the sound intensity radiated from the aperture. The measurement of sound intensity was carried out in a room in which absorptive material was applied to decrease the reverberant field level. The data were averaged 350 times at each point by the analyser before the record was transmitted to the computer. Eight measurement positions were employed along the slit in order to obtain an averaged sound intensity level.

4.THE MEASURED TRANSMISSION LOSS OF SLIT SHAPED APERTURES

The acoustical power, W_i, incident onto an aperture is equal to the product of incident intensity I_i and the area of the aperture i.e.

$$W_i = I_i w l \tag{3}$$

The acoustical power, W_0, radiated from the aperture will be

$$W_0 = I_i w l \tau_c \tag{4}$$

where τ_c is the transmission coefficient of the aperture.

Assuming hemi-cylindrical radiation from the slit, the intensity at a point a distance r is

$$I_r = \frac{\text{power}}{\text{area}} = \frac{W_0}{\pi r l} = \frac{I_i w \tau_c}{\pi r} \tag{5}$$

Using the relationship between sound pressure level, SPL_i, and sound intensity level, in a reverberant enclosure yields the expression

$$TL_s = -10\log\tau_s = SPL_i - IL_r - 6 + 10\log\left(\frac{w}{\pi r}\right) \tag{6}$$

Where IL_r is the measured intensity level at a point distance r from the aperture on the receiving side .

Figures (2-3) show some examples of experimental results for slit shaped apertures compared with the predicted values of transmission loss obtained using the Gomperts-Kihlman expression. Three depths (50.8mm, 76.2mm and 152.4mm) and five widths(1mm, 1.5mm 3mm, 6mm and 10mm) of slit were employed giving fifteen different aperture configurations. The measured data indicated that good agreement exists between the experimental results and the approximate theory for the wide and short slits.

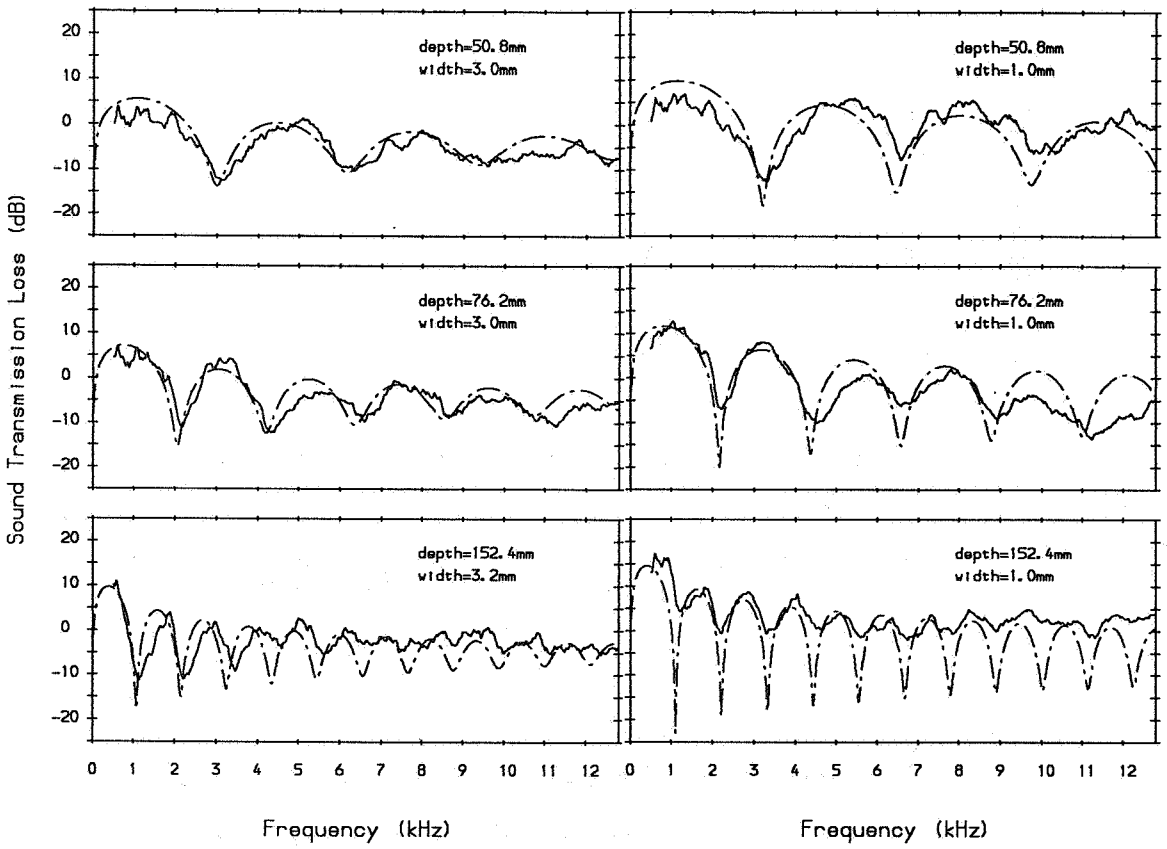


Fig.2 Transmission Loss of 3mm wide cracks.

Fig.3 Transmission Loss of 1mm wide cracks.

Two systematic trends were found from an examination of the measured transmission loss characteristics. The first is that, for a given depth, the difference between measured and theoretical values of transmission loss at the fundamental resonant frequencies become greater as the width of the aperture decreases and for a given width, the difference increases as the depth of the slit increases. This difference is plotted against the ratio of slit depth-to-width in Figure 4. It can be seen that the difference between the measured transmission loss and the theoretical value is a function of the ratio of slit depth to width.

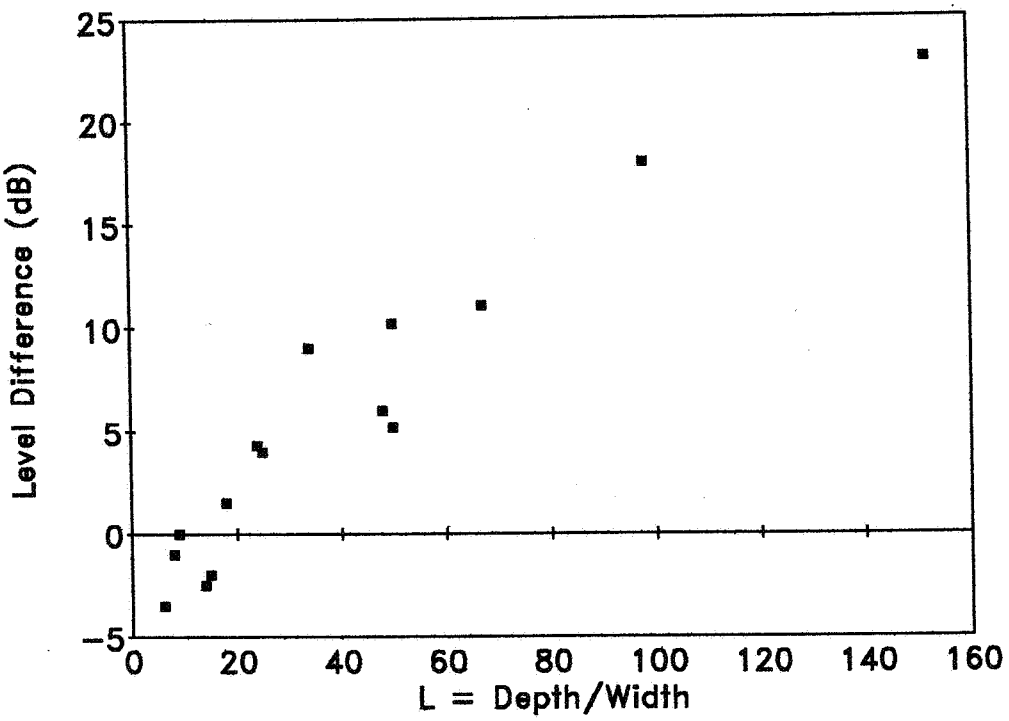


Fig.4 Difference between predicted and measured minimum transmission loss.

A possible explanation for this phenomenon is the effect of viscosity which was ignored in the derivation of Eq.(2). The theoretical transmission curves related to ideal sound propagation in the aperture without any damping. In fact, energy loss must take place in the propagation of sound waves. This loss is due to viscous effects which tend to degrade the sound energy into heat. The experimental data indicate the attenuation is a function of the ratio of depth-to-width of the aperture.

Another phenomenon which demonstrates the effects of viscosity and friction could be observed from examination of the transmission loss characteristics. The measured magnitude of transmission loss differs systematically from the theoretical predictions. The deeper the depth, the greater the difference. This again demonstrates sound energy loss due to viscous effects in a long narrow opening.

5.DETERMINATION OF CRACK DIMENSIONS

It has been shown above that the measured transmission loss characteristics of simple cracks are in good agreement with the values predicted by application of the Gomperts-Kihlman equation. In order to size air leakage cracks, however, it is necessary to be able to extract the relevant dimensions from measured transmission loss characteristics.

The measurement of crack length is relatively trivial. This parameter can be established reasonably accurately from a nearfield scan of the wall. In order to determine the depth, however, it is necessary to make use of the fact that the transmission loss characteristics are periodic with a period determined approximately by the time taken by sound to travel a distance equal to twice the crack depth. This time can be determined by performing a Fast Fourier Transform on the transmission loss characteristics.

The remaining parameter is the crack width. The most obvious approach to determining the magnitude of this parameter is by means of a simple nearfield scan. However, this method does not have sufficient resolution to determine the widths of the very narrow cracks of interest here. An alternative method has been developed based upon the fact that it is necessary to know w before the transmission loss can be calculated from the measured data.

From Figure (1) it can be seen that the transmission loss curve for a 0.3mm wide slit is "the same" as that of the 1mm wide slit but the maximum values are 10*log(1/0.3) dB higher.

Having found 1 suppose the transmission loss is predicted assuming w = 1mm and suppose the true value of w is actually 0.3mm then the predicted transmission loss curve will be shifted down relative to its true position by this value.

If the value w=1mm is also used to calculate the measured transmission loss when the true value is actually 0.3mm, then the experimentally determined transmission loss curve will be shifted up by 10*log(1/0.3)dB relative to its correct position .

If the two curves were plotted then the experimental curve would lie 2*log(1/0.3) dB above the theoretical curve.

Expressed more generally, if the predicted and measured transmission loss characteristics are calculated using a value of 1mm for the value of the width then the experimental curve would lie 2*10log(1/w) dB above the theoretical curve where w is the true width measured in mm. Therefore, if the difference between the curves is determined and substituted in the above expression it is possible to obtain a value for w.

If this value of w is then used to determine the measured and predicted transmission loss characteristics they should be very similar apart from the region of resonance (transmission loss minima) where viscosity effects become important. However, a relationship has been found between 1/w and D,the difference between the predicted minimum and the experimental minimum. Therefore, as 1 is known and D can be determined it is possible to obtain confirmation of the value of w determined above.

6.CONCLUSIONS

The sound intensity technique and reverberant sound excitation have been used for the measurement of sound transmission loss through narrow slits in rigid walls. The experimental results obtained in this study are in reasonable agreement with the Gomperts-Kihlman predictions. As predicted by the theory, the dimensions of the apertures determine the magnitudes and resonant frequencies of the sound transmission loss curves. It should thus be possible in principle to size air leakage cracks using the technique described in this paper.

Sound energy losses which were attributed to viscosity were observed in the course of this investigation. These effects were observed with narrow slits. The effect increased as the area of the apertures decreased and the depth of the opening increased. The experimental results indicated that the effect is of such magnitude that it cannot be ignored when deriving expressions for transmission loss coefficient for very small apertures. The curve of Figures 4 suggest the possibility of using the experimental data to determine an approximate relationship between the effects of viscosity and the dimensions of apertures which could be incorporated into any practical technique employed to size air leakage cracks based on acoustic intensimetry.

7. ACKNOWLEDGEMENTS

The support of the Science and Engineering Research Council of the United Kingdom for the work described in this paper is gratefully acknowledged

REFERENCES

1. BAKER,P.B., SHARPLES, S. and I. C. WARD
"Air flow through cracks."
Building and Environment 22 n4,1987, 293-304.

2. GOMPERTS, M.C. and KIHLMAN, T.
"The sound transmission loss of circular and slit shaped apertures in walls."
Acustica 18, 1967, 144-150.

3. SONADA, T. and PETERSON, F.
"A sonic method for building air leakage measurements."
Applied Energy 22, 1986, 205-224.

4. RINGGER, M. and HARTMANN, P.
"Evaluation of an acoustical method for detecting air leaks."
Air Infiltration Review 11 n1, 1989, 6-9.

5. CROCKER, M.J., RAJU, P.K. and FORSSEN, B.
"Measurement of transmission loss of panels by the direct determination of transmitted acoustic intensity."
Noise Control Engineering Journal 17 n1, 1981, 6-11.

6. MINTEN, M., COPS, A. and WIJNANTS, F.
"The sound transmission loss of a single panel measured with the two microphone and the conventional method - comparison with the statistical energy analysis model."
Applied Acoustics 22, 1987, 281-295.

7. De MAY, A. and GUY, R.W.
"Exploiting the laboratory measurement of sound transmission loss by the sound intensity technique."
Applied Acoustics 20, 1987, 219-236.

AIR MOVEMENT & VENTILATION CONTROL WITHIN BUILDINGS

12th AIVC Conference, Ottawa, Canada
24-27 September, 1991

POSTER 56

INTEGRATED FORCED-AIR HEATING AND VENTILATING SYSTEMS: EVALUATION AND DESIGN CONSIDERATIONS

Mark A. Jackson

Bonneville Power Administration
Residential Technology Section
P.O. Box 3621-RMRD
Portland, Oregon 97208 U.S.A.

SUMMARY

Mechanical systems which use common ducts for combined heating and ventilating functions are becoming popular in the Pacific Northwest (U.S.). These systems range from simple fresh-air inlets ducted to the return side of a forced air heating system to more complex heat recovery ventilation systems utilizing the heating ducts for air distribution. Typical integrated systems do not have heat recovery capability.

Several approaches to integrating and controlling non-heat recovery ventilation and forced air heating systems were evaluated as part of the Residential Construction Demonstration Project (RCDP). The houses tested for this study were built under Bonneville Power Administration sponsored energy-efficiency programs. Fan pressurization tests were performed to assess the envelope leakage characteristics, and tracer gas decay tests were used to measure infiltration and mechanical ventilation rates.

Large variations in envelope tightness and mechanical ventilation rates were encountered. In most cases, the amount of accidental air leakage through ducts and air handlers exceeds the amount of fresh air intentionally supplied to the system. Systems which are properly designed, installed, and operated work well, but the potential for problems is large.

FRESH-AIR INLET CONTROL STRATEGIES

All of the fresh-air inlets examined for this study are connected by a duct to the return side of forced-air systems. Volume limiting strategies range from simple manual balancing dampers placed in the inlet duct to motorized dampers used in conjunction with pressure-bladder type airflow regulators.

The air handlers of most forced air heating systems typically move 500 l/s of conditioned air. The fresh-air portion would be about 38 l/s. The fan energy used to move the large volume of air is typically 600 watts. Relative to a ducted system that only moves ventilation air at the required rate, the energy consumption of the integrated systems is large.

Simple Dampers:

Simple manual or barometric dampers are inexpensive and easy to install, but they provide no control over when fresh air is introduced to the system. These dampers behave much like a leak of unknown size in the return side of the system. Whenever the air handler is activated, the negative pressure created in the return duct pulls air into the system. Unless the occupant or a timing mechanism intentionally activates the air handler, the only time fresh-air is introduced into the system is when the thermostat is calling for heating or cooling. This approach provides the greatest amount of ventilation when it is least needed, during periods when infiltration is at its greatest due to stack effects.

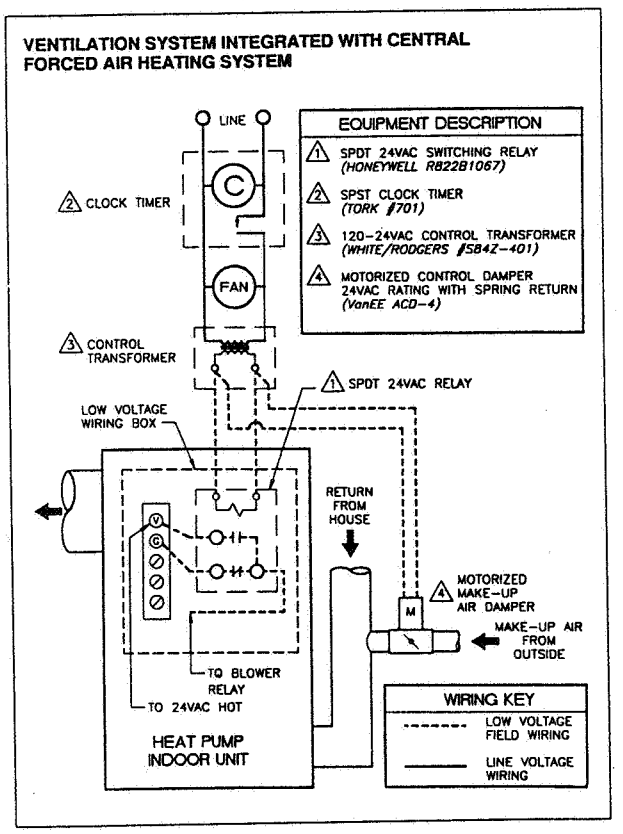
Motorized Dampers:

Motorized dampers provide a great deal of control over when fresh-air is introduced into the system. Typically, a time clock or dehumidistat opens the motorized damper and, if the system is not actively heating or cooling, activates the air handler. Since dehumidistats have proven to be an ineffective ventilation system controller in our generally leaky housing stock, time clocks have become common controllers. The major problem with using time clocks to open the damper and activate the air handler is that it assumes that the occupant knows how much mechanical ventilation is required and will set the clock according to need. We typically found the time clock set to 1 hour a day or disabled.

EXHAUST SYSTEMS

In addition to manually controlled kitchen and bathroom exhaust systems, the houses tested have one or more "dedicated" exhaust fans which are automatically controlled by a time clock or dehumidistat. Sometimes the bathroom fan serves double duty as the dedicated exhaust fan. In less sophisticated systems, the exhaust fan serves as a stand alone system and no fresh air is intentionally introduced to make up for that which is exhausted. In more sophisticated systems, the dedicated exhaust fan and a motorized damper are interlocked with the air handler. When the controller calls for ventilation, the motorized damper opens and the air handler is activated, which pulls fresh air into the systems. Simultaneously, the exhaust fan comes on to remove air from the house.

Currently, there are no manufactured devices which will simultaneously control exhaust fans, motorized dampers, and air handlers. System installers must use relays and transformers to integrate the system. The schematic shows the elements required to integrate the components.



HOUSE CHARACTERISTICS AND SYSTEM INTERACTIONS

Several factors affect the effectiveness of integrated heating and ventilating systems, such as the tightness of the building envelope, differentials pressures within the house, duct location, and duct leakage and leak distribution. The following table lists selected data acquired during site visits.

Selected Data From Site Evaluations

ACH @50 Pa	DESIGNATED FAN FLOW (l/s)	DAMPER	DUCT LEAKAGE @50 P	FRESH AIR (l/s)
2.8	21.2	Motor	31.2	30.7
2.9	27.4	Motor	0	37.8
3.6	44.4	Motor	31.2	88.3
2.5	39.6	Motor	61.4	47.2
6.1	37.8	Barometric	54.3	37.8
6.7	42.5	Manual	64.2	25.0
4.9	35.4	Manual	30.7	33.0
10.1	25.9	Barometric	66.1	0
4.9	35.4	Motor	72.7	18.9
2.5	53.8	Motor	16.5	34.0

Envelope Leakage:

The tightness of the houses ranged from fairly tight to quite leaky. As is typically found in the Northwest, houses in colder areas are significantly tighter than those in warmer coastal areas. The tightness of the building envelope determines how duct leakage, intentional fresh air supply, and exhaust fans will interact. Palmiter has shown that when unbalanced air flows from exhaust fans or duct leakage are less than twice the natural infiltration rate, one half of the unbalanced flow is additional induced ventilation, and one half is displaced infiltration.

In houses with relatively tight envelopes, virtually all of the flow induced by exhaust fans and unbalanced duct leakage results in additional infiltration. To prevent overall positive pressurization of the house, which can force moisture laden air into wall cavities and into the attic space, the use of an exhaust device to balance the flows is suggested.

Duct and Air Handler Leakage:

Duct and air handler leakage can cause unbalanced air flows and introduces thermal problems when the air handler and ducts are outside the building envelope. In the Northwest U.S. it is typical to find supply ducts located in crawlspaces and return ducts in the attic. It is also common to find the air handler located in the garage. Most air handlers examined in this study seemed to be very leaky, but it was not possible to quantify air handler leakage. Leaks in the return side of air handlers located in garages will introduce air from the garage into the house.

Fresh-Air Supply Rate:

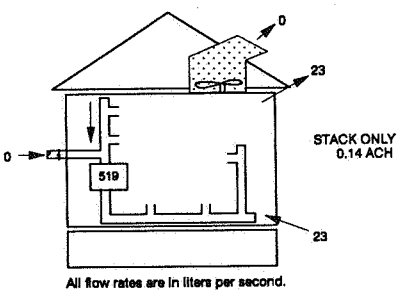
There is no way to reliably predict the quantity of fresh air that will be introduced into the system unless a pressure compensating airflow regulator is installed. it is common practice that when a simple balancing damper is installed, the damper is set to some random intake volume at the discretion of the installer. Actual airflow is rarely, if ever, measured.

Pressure compensating airflow regulators require a minimum operating pressure, typically 50 Pa. To make sure that this pressure is available, the intake duct should be kept short and should be located as close to the air handler fan as possible. In one instance, the intake duct exceeded 20 meters in length and was tied into the return grill just off the main living area. No flow was measured at the inlet.

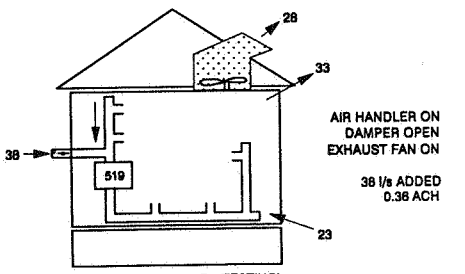
Differential Pressurization:

When the supplies and returns of a forced air heating system are separated by closable doors, large positive pressures can occur when doors are closed. The unbalanced pressures result in increased infiltration. These effects have been noted by several researchers (Cummings 1990, Palmiter 1991). In the Northwest, there are no code or programmatic requirements for pressure balancing systems or for locating both supply and return ducts in rooms with closable doors. To illustrate how the fresh-air inlet and the exhaust system interact with stack induced infiltration, the following examples are offered.

In the first example, a house with the ducts and air handler inside a fairly tight envelope (2.9 ACH @50 Pa). At a specific outside temperature (-5 C), the infiltration rate is 0.14 ACH. The combined fresh-air intake and the exhaust fan yield a total ventilation rate of 0.36 ACH. Intake and exhaust air flows were measured using a flow hood device, and overall infiltration and combined ventilation rates were measured using tracer gas decay.

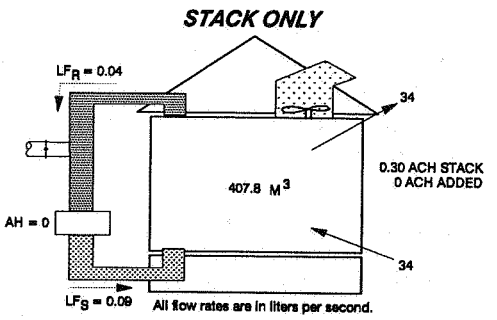


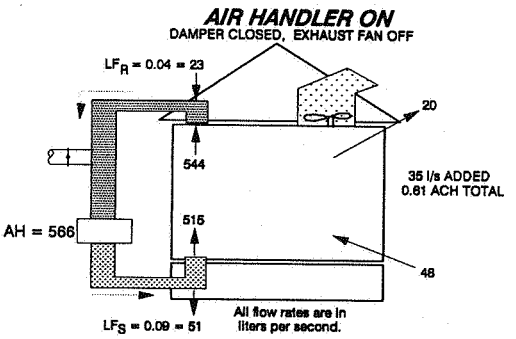
All flow rates are in liters per second.

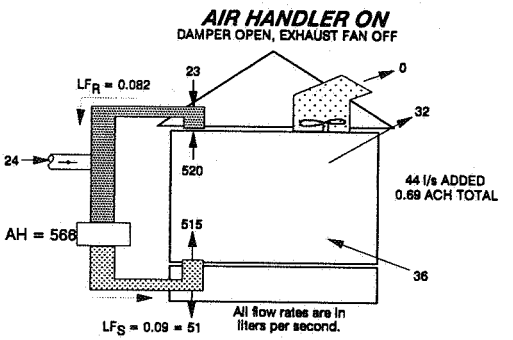


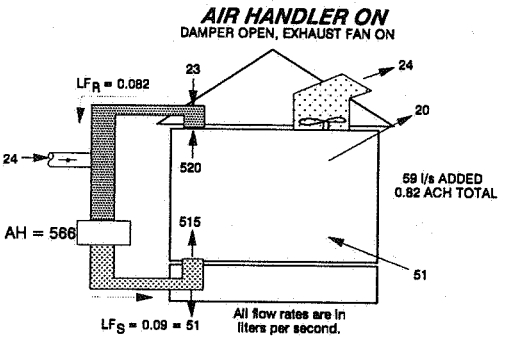
(CONFIRMED BY SF_6 TESTING)
All flow rates are in liters per second.

In this example, the ducts and air handler are located outside a leaky (10.1 ACH @ 50 Pa) envelope. The infiltration component from stack effect is shown, and then the additional infiltration induced by the duct and air handler leakage is shown. The leakage fraction on the return (LFr) is 4 percent, and the supply leakage fraction (LFs) is 9 percent. When the fresh-air damper is opened, the return leakage fraction effectively becomes 8.2 percent. The impacts of the fresh-air supply and the exhaust fan on air flows are shown, assuming that one half of the unbalanced flows result in additional infiltration.









CONCLUSIONS

Fresh-air inlets can function as an effective supply method for introducing ventilation into forced-air heating system ducts. However, it is important that both the ducts and the air handlers be as tight as possible if they are located outside the building envelope. To prevent bulk overpressurization of the house, exhaust rates should equal supply rates. Suitable controls must be used to operate the system, and this currently requires electric relays and transformers. Finally, the energy cost associated with using a large air handler to move 500 l/s of air to supply 38 l/s of fresh air is large.

REFERENCES

Jackson, M.
"Integrated Heating and Ventilating Systems Evaluated"
RCDP Technical Update, March 1991 DOE/BP-1614

Palmiter, L.
"Modeled and Measured Infiltration"
EPRI CU-7327 May 1991

Cummings, J.B et al
"Impacts of duct leakage on Infiltration Rates, Space Conditioning Energy Use, and Peak Electrical Demand in Florida Homes"
ACEE 1990 Summer Study Proceedings

Parker, D.
"Evidence of Increased Levels of Space Heat Consumption and Air Leakage Associated with Forced Air Heating Systems in Houses in the Pacific Northwest"
ASHRAE Transactions 1989

Palmiter, L., Brown, I. and Bond, T.
"Residential Construction Demonstration Project Cycle II: Infiltration and Ventilation in New Electrically Heated Homes in the Pacific Northwest"
ECOTOPE 1990

AIR MOVEMENT & VENTILATION CONTROL WITHIN BUILDINGS

12th AIVC Conference, Ottawa, Canada
24-27 September, 1991

POSTER 57

AIVC Technical Note, "Advanced Ventilation Systems".

Bas Knoll

TNO Building and Construction Research
Department of Indoor Environment
Building Physics and Systems
P O Box 29, 2600 AA Delft
The Netherlands

ABSTRACT

As part of the AIVC's technical programme, study has been performed on present and advanced ventilation systems.

The first part of the study presents a review on demands for basic ventilation of residences and major design considerations for ventilation systems.

The second part is a review on ventilation systems advanced approaches divided into:

- air movement control systems,

- flow quantity control systems,

- ventilation heat recovery systems

- alternative ventilation energy systems

Furthermore a system for the classification of ventilation systems is suggested.

Finally recommendations for future research and development are given.

AIR MOVEMENT & VENTILATION CONTROL WITHIN BUILDINGS

12th AIVC Conference, Ottawa, Canada
24-27 September, 1991

POSTER 58

Experimental Investigation of Convective Couplings Across Various Doorways Under Horizontal Temperature Gradients.

A.Baranowski*, M.Wasacz*, J.P.Eppe**

* Silesian Technical University
HVAC Institute
Pstrowskiego 5
44-101 Gliwice, Poland.

** University of Liege
Lab.de Thermodynamique
Sart Tilman
Building B49
B-4000 Liege
Belgium

12th AIVC Conference

Air Movement and Ventilation Control within Buildings

Call for Papers

Venue: Chateau Laurier, Ottawa, Canada

Date: Tuesday 24th to Friday 27th September 1991

Proposed Paper

Title: Experimental investigation of convective couplings accross various doorways under horizontal temperature gradients

Author: A.BARANOWSKI[x], M.WĄSACZ[x], J.P.EPPE[xx]

Address: [x]Silesian Technical Univ., HVAC Inst, Pstrowskiego 5, 44-101 GLIWICE, Poland

[xx]University of Liege, Lab. de Thermodynamique, SART TILMAN Building B49, B-4000 LIEGE, Belgium Country

Tel: Fax:

Abstract

(Please type in space below)

Inter-zone convection affects the general movements of air in a building and must be evaluated for accurate thermal zones heat and mass balance.

The paper presents results of an experimental study of convective heat transfers caused by temperature difference between two zones connected by an opening of height 2.05 m and varying width. Experiments were carried out in a full scale calorimetric chamber (5.5 m x 2.5 m x 2.5 m). Temperature differences were maintained by two active vertical walls located on either side of the doorway.

Convective heat transfers were deduced from energy balances and expressed in terms of Nusselt, Grashof and Prandtl numbers, i.e.:

$$Nu/Pr = C \cdot Gr^{m}$$

The C and m parameters were obtained from the analysis of approximately 30 experiments for various temperature differences and opening width.

[ ] Tick box if poster presentation preferred. (See call for papers for details.)

AIR MOVEMENT & VENTILATION CONTROL WITHIN BUILDINGS

12th AIVC Conference, Ottawa, Canada
24-27 September, 1991

POSTER 59

THERMAL PLUMES IN VENTILATED ROOMS - Vertical Volume Flux Influenced by Enclosing Walls

Peter Kofoed
Sulzer Infra Group
Winterthur, Switzerland

Peter V. Nielsen
University of Aalborg
Aalborg, Denmark

Synopsis

The flow rate in thermal plumes are influenced by many factors. Influence by enclosing walls is one of them. This article presents simple symmetry considerations to calculate the flow rate in such flows, and they are experimentally verified as regards wall plumes. When the flow takes place near to enclosing walls the entrainment is influenced and a reduction of the flow rate is observed. For displacement ventilation this means a reduction of the stipulated necessary ventilating air flow rate when an air quality based design method is used.

Symbols

C_0	Contamination concentration in the occupied zone
C_R	Contamination concentration in the return air
Q_0	Convective heat
T_F	Temperature of the floor
T_R	Temperature in the return air
V	Vertical volume flux
x	Vertical distance

1. Introduction

The main objective of ventilation is to provide good air quality for the occupants. For this purpose the necessary ventilating air change rate must be determined. Within displacement ventilation the estimation is closely related to the air flow rate in the thermal plumes when an air quality based design method is used. The vertical volume flux in a plume is influenced by many factors. Placement of the flow in relation to surrounding walls is one of them. This reduces the entrainment and is the subject of this article.

1.1 Displacement Ventilation

The qualitative behavior of displacement ventilation may be regarded as well-known due to many publications in the recent years, ref. **/1, 5, 10, 14, 15/**.

Good air quality is achieved by a separation principle where fresh air and polluted air are separated. The upward moving thermal plumes generate an upper zone with mixing flow where the contamination concentration is higher than in a lower clean zone. The characteristic layer between the two zones, the so called front, may be visualised by smoke experiments, ref. **/6 pp. 14-15, 8 pp. 75 - 78/**. The vertical contamination distribution also confirms the separation principle since a sudden step in concentration can be seen, see e.g. Heiselberg & Sandberg **/3/** or Holmberg et Al. **/4/**.

The principle of displacement ventilation appears in figure 1. The front separates the room in two zones and the level of the front depends on the relationship between the ventilating air flow rate and the flow rate in the thermal plumes. The stratification boundary will stabilize at a level where these two flow rates are equal, below there will be a clean zone. This is a result of the general upward moving air outside the plumes since they have not yet entrained all the fresh supply air. When plumes rise they continuously entrain air from the surroundings. As a consequence an increase of the ventilating air flow rate will rise the level of the front. On the other hand a too little amount will give a too low level.

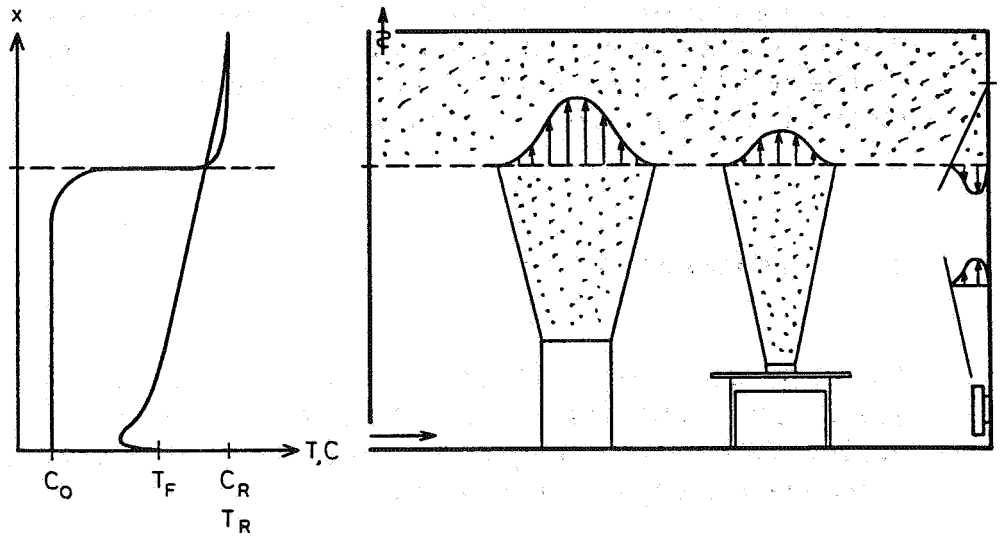


Figure 1. Displacement ventilation flow with two zones. The graphs to the left show the temperature and the contamination distributions.

1.1.1 Air Quality Based Design

One could think immediately that the ventilating air flow rate should be determined so that the clean zone includes the entire occupied zone, i.e. about up to 1.8 m height above floor level. However, such an approach leads to too high air change rates, considerably higher than usual.

Holmberg et Al. **/4/** have carried out inhalation zone air quality measurements with low normal air change rates. Their investigations still favour displacement ventilation even when the front is at a level below the inhalation zone. The clean air below is entrained and transported by the convection boundary layer around the human body from the floor level up to the inhalation zone. In this way the air quality in the inhalation zone should be better than the quality of the surrounding room air at the same level. A choice of 1 to 1.2 m as a front level height seems to give reasonable ventilating air flow rates and also to assure a good air quality in the inhalation zone.

1.2 Scope

This article presents the influence on entrainment when convective flows take place near to enclosing walls or to other thermal plumes. Simple symmetry considerations are introduced and they are experimentally verified in the case of a wall plume.

2. Theory on Plumes

Turbulent buoyant plumes have been investigated for more than 50 years. Schmidt **/13/** and Rouse et Al. **/12/** are early workers. Later Popiolek **/11/** gives an analysis. For the vertical volume flux in a free plume the following power law is found

$$V \approx Q_0^{1/3} \; x^{5/3} \qquad (1)$$

2.1 Symmetry Considerations

When the thermal flow rises near to enclosing walls the entrainment is affected, ref. **/7, 8/**. This may also be the case if two or more convection flows influence each other. Coanda effects may be present in flows near to walls so that they are no more axisymmetrical. However, the following symmetry considerations may give some idea of the vertical volume flux in such flows.

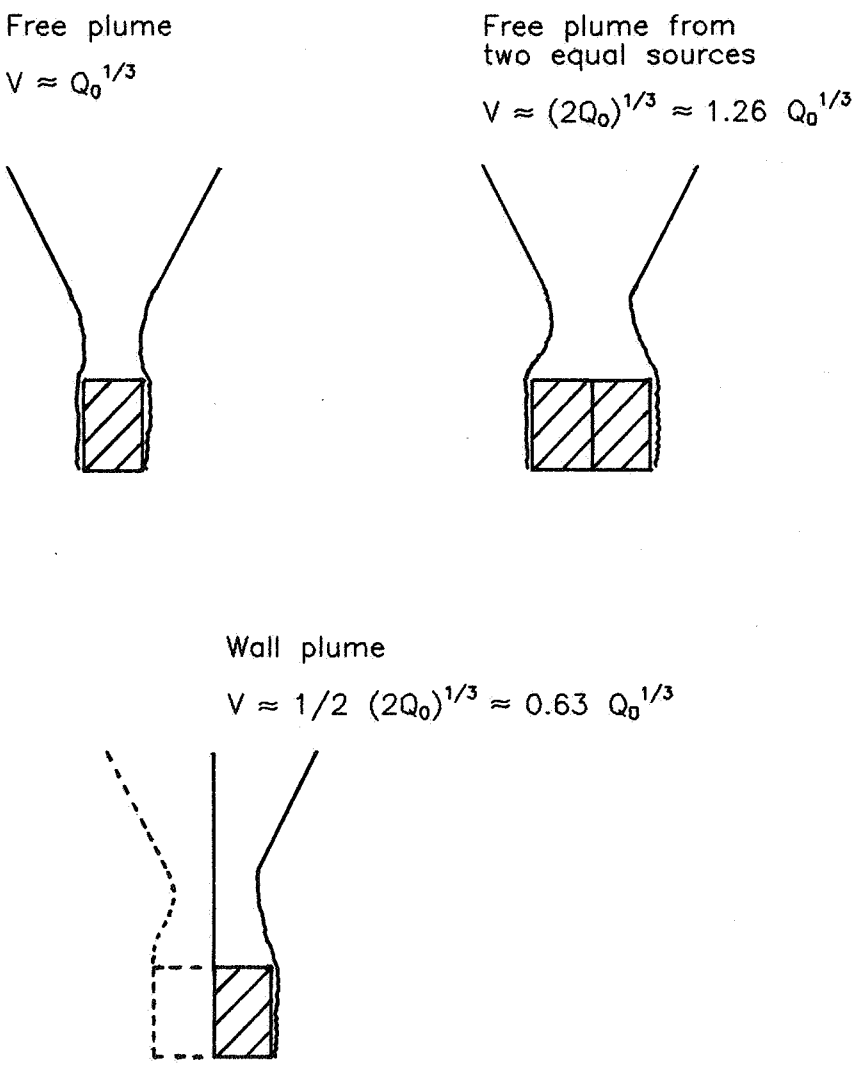


Figure 2. Symmetry considerations regarding vertical volume flux in thermal plumes are illustrated: free plume, two flows forming one plume, wall plume.

Free plume:

$$V \approx Q_0^{1/3} \quad (2)$$

Two equal sources close together forming one plume:

$$V \approx (2\,Q_0)^{1/3} \quad (3)$$

$$V \approx 1.26\,Q_0^{1/3} \quad (4)$$

Wall plume:

$$2V \approx (2\,Q_0)^{1/3} \quad (5)$$

$$V \approx 0.63\,Q_0^{1/3} \quad (6)$$

Plume in a corner:

$$4V \approx (4\,Q_0)^{1/3} \quad (7)$$

$$V \approx 0.40\,Q_0^{1/3} \quad (8)$$

The influence by the source geometry is neglected and only the heat power is taken into account. The above mentioned symmetry analysis leads to the result that the flow in a buoyant wall plume amounts to 63 % of the flow rate in the corresponding free plume, for a plume in a corner it is 40 %. Further two equal sources close to another form a flow where the vertical volume flux amounts to 126% of that from a single free source.

If the symmetry argumentation holds true, for displacement ventilation with air quality based design this means that the ventilating air flow rate may be reduced when the thermal flows take place near to walls or close to another.

3. Experimental Technique

The experimental investigations are carried out in a full-scale clima chamber at the Institute of Building Technology, University of Aalborg, Denmark. The dimensions of the room are 8x6x4.6 m. Futher a displacement ventilation system with two wall-mounted diffusers and two exhaust openings in the ceiling are installed so that the room can be ventilated and different vertical temperature gradients created, if required.

Two different circular heat sources are used to generate the convection flow. A vertical black painted closed cylinder is chosen to simulate the flow from a person. The cylinder is 1000 mm high and has a 400 mm diameter. Inside the source four electric bulbs are placed. When a power of 100 W is induced, the source has a surface temperature similar to the one of a person. During the measurements the source has been situated directly on the floor. The other source consists of a steel tube, height 150 mm and diameter 50 mm, with hot wire inside. The power is 125 W. During the measurements the source is vertically placed in mineral wool and the air is sucked through the source from below. The distance from the top of the source to the floor is 0,25 m.

3.1 Zero Method

A so called zero method has been used for the vertical volume flux measurements. First smoke visualizations by introducing smoke into the source zone have taken place to assure the vertical direction of the plume flow. Next the air is exhausted above the heat source with a circular exhaust hood. The exhausted air volume can be controlled by a helping ventilator and the air flow rate is measured with an orifice. Figure 3 shows a scheme of the set up.

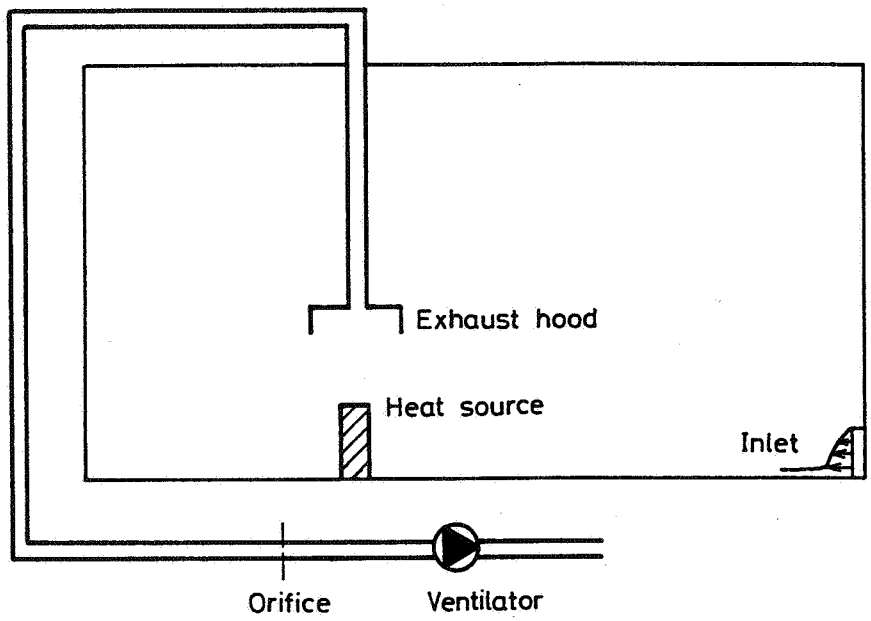


Figure 3. Scheme with the zero method set up: heat source, exhaust hood, orifice, helping ventilator, etc. The vertical temperature gradient is measured outside the flow. At the border of the hood or at the heat source smoke can be introduced.

At border of the exhaust hood from time to time small amounts of smoke are introduced, in this way it is controlled if no horizontal flow takes place. When this is the case one may assume that the same amount of air is exhausted through the hood as the vertical volume flux in the buoyant jet from the heat source at the same height.

Hoods with different widths and side heights have been investigated to improve the method. One limit is reached when the effective width of the flow (including the axis wandering) is wider than the diameter of the hood. On the other hand, the hood may not be to wide since, in this case, the horizontal velocities that determine the equilibrium between the exhaust and the air coming into the hood are very low. Practical carrying out of experiments and comparing with results of an extrapolation method, ref. **/7, 8/**, form the basis for the choice of hood diameter. A diameter of 1.60 m is convenient for measurements in 2.00 m height above the floor when the heat sources are of the type described in **/chapter 3/**. The necessary side height is dependent on the vertical velocity of the flow, high velocities giving high values. The maximum mean velocities in 2.00 m height above the floor from a heat source such as a sitting person are of the order 0.2 m/s, see Mierwinski **/9/**. A side height of 0.20 m is found suitable, in this case the flow inside the hood remains stable. If considerable higher mean velocities were present the side height should have been higher to prevent fall outs due to pressure accumulation in the hood.

3.1.1 Accuracy of the Zero Method

Since the zero method depends on individual observations by an operating person the question about accuracy soon arises. Therefore, the results of the zero method have been compared with reference results of an extrapolation method, ref. **/8 pp 123-135/**. Further, the same experiment has been carried out several times to find the spread of the results. On this basis it is concluded that the zero method gives the same result for the volume flux as the extrapolation method when investigating axisymmetrical buoyant plumes. The volume flux can be estimated with an error about of 10 % of the measured value. The zero method is easy to use and quickly it gives results. The investigated flow does not have to be axisymmetrical or fully developped. Further, flows influenced by enclosing walls, i.e. wall jets, comprise no problems since, in this case, the smoke observations become more stable.

4. Measurements Results

The heat source has been placed free, forming a free plume, or close to a wall, forming a wall plume. The measuring of vertical volume flux in the generated plume has taken place 2.00 m above the floor. Further the measurements are carried out with two different vertical temperature gradients in the surroundings and calculated between 0.10 m and 2.00 m above the floor the values are 0.3 K/m or 0.6 K/m. The measured volume fluxes appear as a table in figure 4 and grafically in figure 5.

Heat source & heat supplied	Vertical tempgrad (K/m)	Vertical volume flux	
		Free plume (m^3/h)	Wall plume (m^3/h) (% of f.pl)
Tube dia. 50 mm 125 W	≅ 0.3	238	150 (63 %)
	≅ 0.6	200	125 (63 %)
Cylinder dia. 400 mm 100 W	≅ 0.3	200	125 (63 %)
	≅ 0.6	175	112 (64 %)

Figure 4. Vertical volume flux in free plumes and corresponding wall plumes 2.00 m above the floor at two different vertical temperature gradients

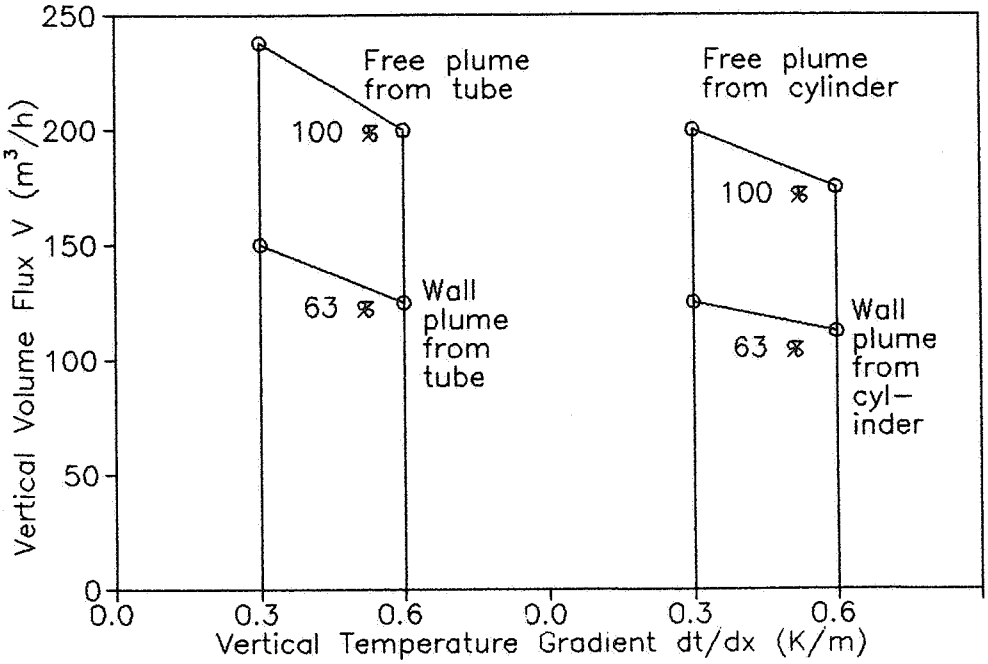


Figure 5. Vertical volume flux in free plumes and corresponding wall plumes 2.00 m above the floor. In both cases (tube left and cylinder right) an increase of stratification from 0.3 to 0.6 K/m leads to a reduction of the flow rate. Also placement plays a role, in wall plumes the flow rate is 63 % of that in the corresponding free plume.

4.1 Influence by Placement

The wall influences the entrainment in the plume, see figure 4 and 5. It looks like, that the volume flux in a wall jet amounts to around 63 % of the volume flux in the corresponding free jet. However, for each single wall plume & free plume comparison it is important that the two vertical temperature distributions are similar, that the two vertical temperature gradients have the same value and thirdly, that the temperature levels in the room are the same in the two cases. These demands are fulfilled and leaving further discussion out of account it may be concluded that:

The zero method measurement results verify symmety consideration of **/chapter 2.1/** as regards wall plumes, see equations 2 and 6. I.e. the vertical volume flux in a wall jet amounts to around 63 % of the volume flux in the corresponding free jet at the same vertical temperature gradient.

4.2 Influence by Stratification

The influence by vertical temperature gradients on the flow is discussed by several authors, ref. **/2, 7, 8, 10/**. It leads to a reduction of the flow rates.

Two different vertical temperature gradients have been present during the investigations, approximately 0.3 and 0.6 K/m. According to figure 4 and 5 an increase of the gradient involves a decrease of the volume flux as expected. Immediately it seems that the influence by the vertical temperature gradient depends on the type of heat source. Immediately it may be concluded that the relative reduction of the flow rate in a free jet and the corresponding wall jet has the same value: For the tube and cylinder a 17 and 11 % reduction, respectively, when the gradient increases from 0.3 to 0.6 K/m.

When making such conclusions it is important to take the mutual vertical temperature gradients and surface temperatures into consideration. Perhaps the vertical temperature gradient is not the only factor influencing the plume flow. Local cooling by forced convection or radiant heat exchange from the source to the surrounding surface may have a great influence too.

5. Conclusion

Several advantages of the zero method is reported: the method is very easy to use and the results are quickly produced. There is no claim on the velocity distributions, e.g. such as axisymmetrical Gaussian shaped profiles. As a result unstable flows from extensive heat sources and flows influenced by enclosing walls may be investigated, i.e. the buoyant flows that actually take place in ventilated rooms.

The method has some disadvantages too: it only gives information about the vertical volume flux in the plume and therefore it is not suitable for fluid dynamic investigations. Further the measurement results depend on the operating person who individually determines the exhausted air flow rate that estimates the vertical volume flux in the plume. However, with some experience reliable results may be produced, and the resolution is evaluated better than ± 10 %.

The experiments on wall plumes and corresponding free plumes verify a 63 % rule, i.e. the vertical volume flux in a wall plume amounts to around 63 % of the volume flux in the corresponding free plume at the same vertical temperature gradient. Thereby the symmetry considerations are verified as regards wall plumes.

The investigations further implie the statement that increasing stratification reduces the vertical volume flux in plumes. This observation is consistent with that from other authors.

Further an investigation of buoyant plumes in a corner and of the flow when two equal sources are placed close to another are suggested, and if possible to verify the symmetry considerations.

It seems reasonable to use simple symmetry argumentation to estimate the vertical volume flux when sources are placed near to walls or close to another, forming only one flow. This will reduce the stipulated necessary ventilating air flow rate when an air quality based design method for displacement ventilation is used.

References

1- Brügger, P. & B. Kegel : Displacement Ventilation for an Office Building with Triple Glaced Windows, Clima 2000, Sarajevo, Sept. 1989.

2- Fitzner, K.: Quellüftung, Forschungsbericht Nr. 522, Klimatechnisches Laboratorium Betzdorf, Heinrich Nickel GmbH, Klima- und Lufttechnik.

3- Heiselberg, P. & M. Sandberg: Convection from a Slender Cylinder in a Ventilated Room, RoomVent-90, Oslo, Norway, 1990.

4- Holmberg, R.B. et Al.: Inhalation Zone Air Quality Provided by Displacement Ventilation, RoomVent-90, Oslo, Norway, 1990.

5- Kegel, B. & U.W. Schulz: Displacement Ventilation for Office Buildlings, 10th AIVC Conference on Progress and Trends in Air Infiltration and Ventilation Research, Espoo, Findland, Sept. 25-28, 1989.

6- Kofoed, P. & P.V. Nielsen: Thermal Plumes in Ventilated Rooms - An Experimental Research Work, 3rd Seminar on Silesian Technical University, Gliwice, Poland 1988. Also published in Indoor Environmental Technology, paper no. 7, ISSN 0902-7513 R8833, 1988.

7- Kofoed, P. & P.V. Nielsen: Thermal Plumes in Ventilated Rooms - Measurements in Stratified Surroundings and Anlaysis by Use of an Extrapolation Method, RoomVent-90, Oslo, Norway, 1990.

8- Kofoed, P.: Thermal Plumes in Ventilated Rooms, Ph. D. Thesis, University of Aalborg, Denmark, 1991.

9- Mierzwinski, S.: Air Motion and Temperature Distribution Above a Human Body in Result of Natural Convection, A4-series no. 45, Dept. of Heating and Ventilating, Royal Inst. of Technology, Stockholm, Sweden, 1981.

10- Mundt, E.: Temperaturgradienter och Konvektionsflöden vid Deplacerende Ventilation, Ph.D. Thesis, KTH, Installationsteknik, Meddl. nr. 16., Sweden, 1991.

11- Popiolek, Z.: Problems of Testing and Mathematical Modelling of Plumes Above Human Body and Other Extensive Heat Sources, A4-series no. 54, Dept. of Heating and Ventilating, Royal Inst. of Technology, Stockholm, Sweden, 1981.

12- Rouse, H., C.S. Yih & H.W. Humphreys: Gravitational Convection from a Boundary Source, Tellus, 4, pp. 201-210, 1952.

13- Schmidt, W.: Turbulente Ausbreitung eines Stromes erhitzter Luft, Z. angw. Math. Mech., Bd. 21, Nr. 5 & 6, Okt. & Dez. 1941.

14- Skistad, H.: Fortrengningsventilasjon i Komfortanlegg med Lavimpuls Lufttilförsel i Oppholdssonene, Norsk VVS Teknisk Forening, 1989.

15- Skåret, E.: Ventilation by Displacement - Characterizing and Design Implications, Ventilation '85 edited by H.D. Goodfellow, Elsevier Science Publishers B.V., Amsterdam, 1986.